DOCTORAATSPROEFSCHRIFT

2012 | Faculteit Wetenschappen

Synthetic Approaches toward 4*H*-Cyclopenta[2,1-*b*:3,4-*b*']-dithiophene and 2,5-Dithienylthiazolo[5,4-*d*]thiazole Building Blocks and their Integration in Low Bandgap Copolymers for Organic Photovoltaics

Proefschrift voorgelegd tot het behalen van de graad van
Doctor in de Wetenschappen, Chemie, te verdedigen door:

Sarah VAN MIERLOO

Promotor: prof. dr. Wouter Maes
Copromotoren: prof. dr. Dirk Vanderzande
dr. Laurence Lutsen

D/2012/2451/2

universiteit hasselt

Chairman	Prof. dr. Jean Manca, UHasselt
Promoter	Prof. dr. Wouter Maes, UHasselt
Copromoters	Prof. dr. Dirk Vanderzande, UHasselt
	Dr. Laurence Lutsen, IMEC/IMOMEC
Members of the jury	Prof. dr. Frederik C. Krebs, Risø National Laboratory for Sustainable Energy, Technical University of Denmark
	Prof. dr. ir. Guy Van Assche, Vrije Universiteit Brussel
	Prof. dr. Thomas Cleij, UHasselt and Maastricht University
	Prof. dr. Peter Adriaensens, UHasselt

Table of Contents

Chapter 1

Introduction

1.1. Paramount Challenge for the 21st Century

"One problem facing humanity today, more important than any other single problem, is energy" is a famous statement by Richard Smalley,[1] who was awarded the Nobel Prize in Chemistry in 1996 for his discovery of fullerenes. New projections by the United Nations suggest the world population will exceed 10 billion by 2100.[2] The global energy consumption will probably also keep on rising exponentially, and will triple or even quadruple with respect to the current situation. Today, crude oil, coal and gas are the main natural resources for our energy supply. In recent studies it has been computed that fossil fuel reserve depletion times for oil, gas and coal are approximately 35, 37 and 107 years, respectively.[3] This means that the world is steadily running out of oil and that by 2050 coal will be the only remaining traditional energy source. Moreover, near the end of the last century, the hemispheric mean surface temperature was peaking higher than at any time during the last millennium.[4] The carbon dioxide emission, mainly originating from fossil fuel combustion, is going hand in hand with the Earth's climate change (Figure 1.1).[5] Temperatures are predicted to go off the scale in the 21st century.

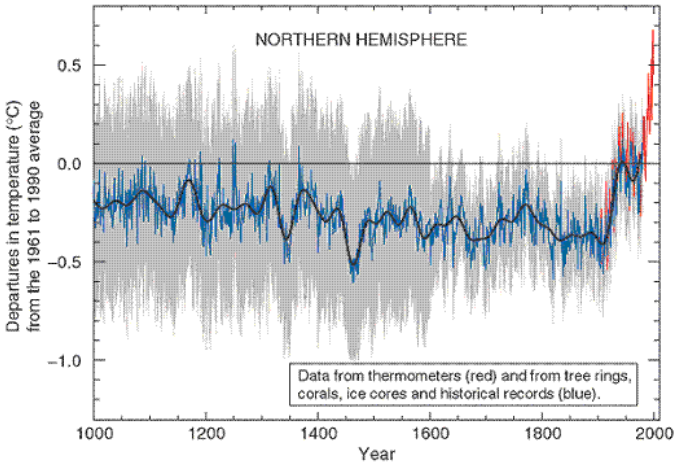

Figure 1.1. The "hockey stick" diagram: temperature reconstruction for the northern hemisphere over the past 1,000 years (Source: Intergovernmental Panel on Climate Change, 2001).

The only way to solve these problems will be to break the world's fossil-fuel addiction and to move forward with renewable energy resources.[6] Nuclear energy keeps on struggling with storage or destruction of radioactive waste, while public opinion is developing huge skepticism, especially after the nuclear accident in Fukushima earlier

this year. Of all types of renewable energy, such as hydro- and geothermal power, wind, biomass and solar energy, the energy of the sun is the most abundant one. The amount of solar irradiation incident upon Earth in one hour is equivalent to the world's annual energy demand! The sun delivers 120,000 TW of radiation, so there is clearly enough power available to cover the global energy demand (~15 TW).[7]

1.2. Photovoltaics

Over 170 years ago, Becquerel, a pioneering physicist, discovered that conductance rose with illumination during his experiments with metal electrodes and liquid electrolytes. This phenomenon was called "the photovoltaic effect" and still forms the operating principle of a present-day solar cell.[8] More than one century later, Chapin *et al.* constructed the first solar cell based on silicon, attaining 6% power conversion efficiency (PCE).[9] At present, silicon solar cells, constructed from mono- or multicrystalline Si, are considered as the **first generation** solar cell technology. Monocrystalline Si solar cells, reaching ~25% PCE,[10] cover more than 85% of the photovoltaic (PV) market, with an annual growth rate of ~40%.[11] However, production costs of crystalline Si cells are still a major drawback, limiting a wide diffusion of photovoltaic energy conversion in the absence of government incentives or special market implementation programs. With the aim to reduce production costs, a **second generation** solar cell technology has been developed over the past decade. This thin-film PV technology - comprising amorphous silicon, copper-indium-gallium-selenide (CIGS) and cadmium-telluride (CdTe) cells - has readily caught up in terms of performance and production technology is now undergoing a rapid expansion. These cell types generally show higher absorption coefficients, enabling the use of smaller material quantities (in thin films), and can be produced by a less expensive fabrication process. Inorganic thin film photovoltaics have shown laboratory efficiencies of up to 20% (CIGS).[10,12] Although the obtained efficiencies are rather satisfying, the scarcity of the required materials and their toxicity remain important obstacles. Toward high efficiency at low cost, a **third generation** of (thin film) solar cell technologies is currently explored, based on both molecular and inorganic light absorbers (including polymer blend, small molecule,[13] dye-sensitized,[14] and hybrid organic/inorganic solar cells[15]).

Compared to inorganic semiconductors, **organic materials** generally have the advantage of higher absorption coefficients, which often exceed 10^5 cm^{-1} in thin films (~1000 times higher than Si). These high absorption coefficients allow the use of very thin, semi-transparent and flexible films (generally between 50 and 200 nm), which absorb a large fraction of the incident solar light. In addition, organic materials also have much lower densities than inorganic semiconductors. This combination of high absorption coefficient and low density leads to extremely small masses of active materials applied in organic solar cells (OSCs), which reduces both weight and material costs. Moreover, the potential to produce OSCs by printing or coating techniques, compared to wafer-based production techniques for crystalline Si cells, would further reduce costs significantly. The only production technology that can achieve production rates of greater than 10,000 m^2/h at production costs as low as even 1 \$/m^2 is roll-to-roll (R2R) coating or printing. The potential low costs for a printed/coated **organic photovoltaic** (**OPV**) technology are motivating both academic and industrial research communities to develop this technology to market readiness within this decade.[16]

Figure 1.2 summarizes the efficiency roadmap of the three generations of solar cell technology over the last 35 years. Organic solar cells have grown rather spectacularly, from non-certified performances of around 1% to certified performances of over 7%, notably during the last couple of years.[17]

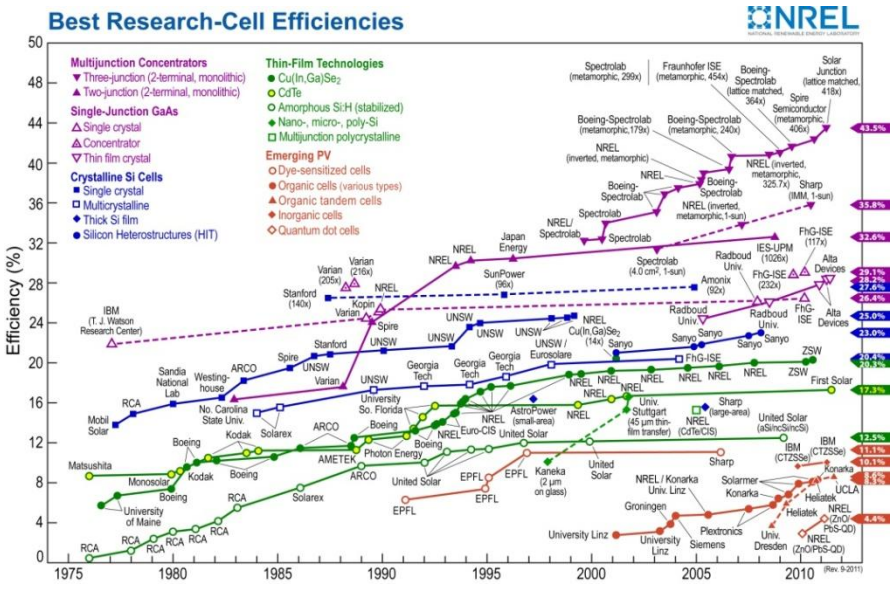

Figure 1.2. The evolution of best research-cell efficiencies over the last 35 years (source: NREL).

1.3. Organic Photovoltaics

The development of OPV technology started in the 1970s in a lab at the University of Pennsylvania. Alan Heeger, Alan MacDiarmid and Hideki Shirakawa discovered the surprisingly high conductivity of polyacetylene after treatment with chlorine, iodine or bromine. The "doped" form of polyacetylene showed a conductivity of 10^5 S/m, much higher than any other polymer, approaching the conductivity of silver or copper (10^8 S/m).[18] In 2000, these three scientists won the Nobel Prize for Chemistry for "the discovery and the development of conductive polymers".[19]

The efficiencies of the first organic solar cells reported in the 1980s, based on conducting polymers (mainly polyacetylene), were, however, rather discouraging. The situation only started to improve in 1986 when Tang *et al.* fabricated the first organic photovoltaic cell, at that time based on small molecules, with a reasonable PCE of ~1%.[20] His so-called **bilayer** device consisted of a layer of Cu-phthalocyanine as *p*-type material covered with a layer of a perylenetetracarboxylic acid derivative as *n*-type material, sandwiched between two electrodes. Both layers were deposited by thermal evaporation and the flat interface between the *p*- and *n*-type material limited the interfacial area. In 1992, Sariciftci and co-workers discovered the photoinduced electron transfer from a conducting polymer to buckminsterfullerene and thereby established the foundation for **polymer-fullerene solar cells**.[21] Due to the bad solubility of these "soccer ball" C_{60}-fullerenes, Hummelen and Wudl in 1995 synthesized a more soluble fullerene derivative, [6,6]-phenyl-C_{61}-butyric acid methyl ester (**$PC_{61}BM$**) (*vide infra*).[22] Nowadays, more than 15 years later, $PC_{61}BM$ is still the most widely applied electron acceptor material in organic solar cells. A major breakthrough for OPV was realized in the same year, when Heeger and Holmes introduced the **bulk heterojunction** (**BHJ**) concept for organic solar cells.[23] In contrast to their inorganic counterparts, achieving immediate dissociation in free charge carriers upon photoexcitation, organic materials form bound electron-hole pairs, so-called **excitons**, with a binding energy ranging from 0.4 to 0.5 eV. The dissociation of these tightly bound charge carriers is only possible after diffusion to a donor/acceptor interface, which should be within the range of 5–10 nm (the exciton diffusion length), as this is the maximum distance the exciton can travel prior to its decay back to the ground state or by radiative recombination.[24] The disadvantage of the long distances to

the donor/acceptor (D/A) interface in the bilayer heterojunction devices can be overcome with the employment of a BHJ interpenetrating network of donor and acceptor components, intermixed at a length scale less than the exciton diffusion length. The bulk heterojunction is still the most successful device architecture for polymeric photovoltaics, because exciton harvesting is near-perfect due to the highly folded architecture enabling all excitons to be formed near a heterojunction. The first BHJ architecture based on a conjugated polymer and a fullerene showed solar energy conversion efficiencies of around 1%. Although solution processed BHJ photovoltaic cells were first reported in 1995,[23] it took another 5 years before the scientific and industrial community realized the potential of this technology, and after 2000 the number of publications in the field started to rise rapidly. While the best efficiencies reported before 2000 barely reached values higher than 1%, certified efficiencies beyond 7% are state of the art today (Figure 1.2).[25]

Industrial interest in developing OPV technologies has risen strongly, especially in recent years. Large companies such as BASF and start-up companies such as Konarka Technologies, Plextronics, Solarmer Energy and Heliatek GmbH have been developing various materials and device technologies for OPV applications. Efficiencies in excess of 9% have been reported by Mitsubishi early April this year (non-certified).[26] In the mean time, the first commercial OPV product, a bag with a flexible, fully printed OPV module combined with a standard battery, was launched on the market (Figure 1.3.).[27]

Figure 1.3. Commercial solar bag (Source: Konarka).

1.4. Working Principle of an Organic Solar Cell

Figure 1.4 illustrates the mechanism by which light is converted into electrical energy in solar cell devices in a simplistic way. In a first step, upon photoabsorption by the donor material, an electron is excited from the highest occupied molecular orbital (HOMO) to the lowest unoccupied molecular orbital (LUMO), creating a Coulombically bound exciton. These strongly bound excitons must diffuse in a second step to a donor/acceptor (D/A) interface, where there is a sufficient chemical potential energy drop to drive dissociation into an electron-hole pair. As mentioned earlier, due to the small exciton diffusion length, the employment of a bulk heterojunction device is mandatory to achieve high performances. Excitons will decay when created too far from the D/A interface. In a third step, electrons will be transferred to the acceptor material with high electron affinity. After electron transfer, geminate recombination of the bound electron pair can still occur, as well as bimolecular recombination of free charge carriers during transport to the electrodes. Very important is the presence of percolated pathways in the donor and acceptor materials, which can reduce the recombination losses before collection at the electrodes occurs in a fourth step.

Empirically, the overall energetic driving force for a forward electron transfer from the donor to the acceptor material is defined by the energy difference (offset) between the LUMOs of the donor and acceptor. A minimum energy difference of ~0.3 eV is required to affect the exciton splitting and charge dissociation. On the other hand, an energy difference between the LUMOs that is larger than this minimum value results in wasted energy, not contributing to the device performance.[16,24,28–32]

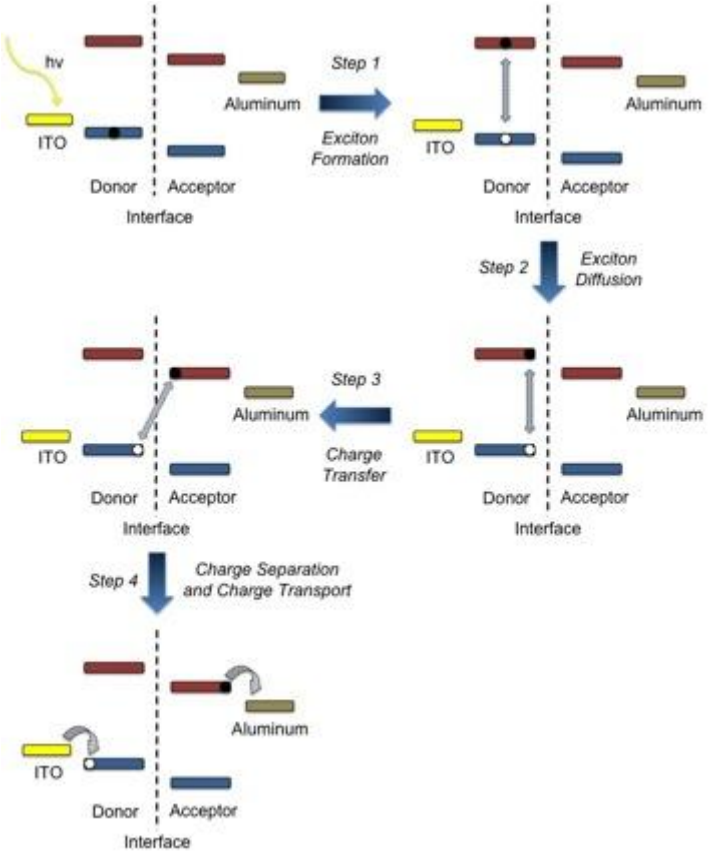

Figure 1.4. General mechanism for photoconversion in organic solar cells.

1.5. Construction and Performance Features of Organic Solar Cells

An organic solar cell, as depicted in Figure 1.5, is generally manufactured on a transparent glass substrate coated with a high work function anode material like indium tin oxide (ITO). To improve the contact properties, a hole conducting layer such as poly(3,4-ethylenedioxythiophene):poly(styrenesulfonate) (PEDOT:PSS) is deposited on top of the ITO layer. This PEDOT:PSS layer also smoothens the surface of the electrode and provides a good wettability for the active layer. Subsequently, the active layer, consisting of donor and acceptor organic materials, can be deposited from solution, e.g. by spin coating, spray coating, blade coating, gravure printing or ink jet printing, which offers cheap and rapid processing. On top of the active layer, a low work function cathode, often consisting of calcium and aluminum, is deposited by thermal evaporation.

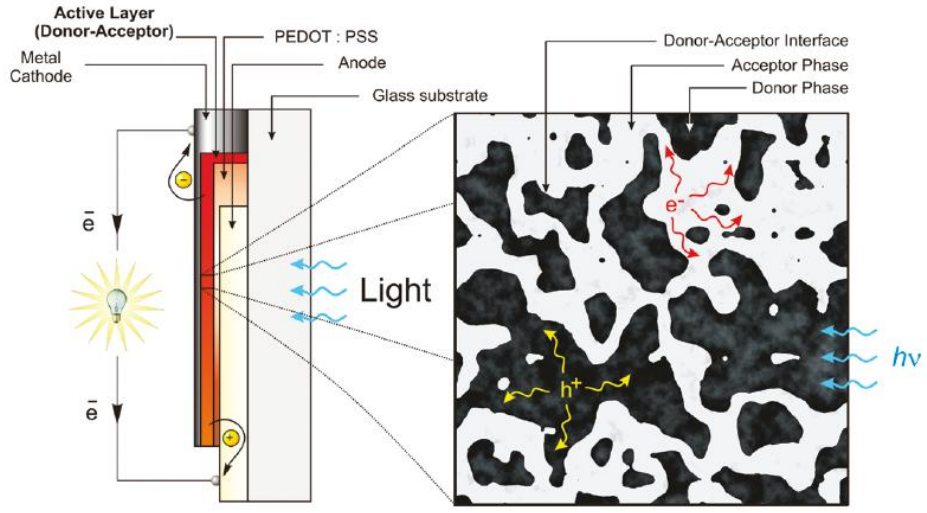

Figure 1.5. Configuration of an organic bulk heterojunction solar cell.[16k]

A solar cell under illumination can be characterized by a number of parameters, such as the short-circuit current density (J_{sc}), the open-circuit voltage (V_{oc}), the fill factor (FF) and the power conversion efficiency (PCE), as depicted in Figure 1.6. The J_{sc} is the current flowing in the illuminated device at 0 V bias. J_{sc} is the maximal current that a device is able to produce. Under external load, the current will always be less. The amount of current is determined by the overlap between the absorption spectrum of the solar cell and the solar spectrum. The current thus largely depends on the bandgap of the organic material, and also on the photoabsorption of the complete active layer, the intensity of the sunlight, the thickness of the active layer and the excitation/charge collection efficiency. The V_{oc} is the maximum voltage attainable across the cell, the voltage the device generates when no current is flowing. The V_{oc} is related to the energy difference between the HOMO level of the donor material and the LUMO level of the acceptor component.

The power delivered by a solar cell can be determined by the product between the current and the voltage. One can draw in the fourth quadrant of the classical *J*-*V* curve a rectangle with side lengths equal to a certain voltage value and its corresponding current value. This product of V_{oc} and J_{sc} then represents the theoretical maximum power point value $P_{theor\ max}$, obtained in the ideal case. During operation of the solar cell both values attain their maximum, and the power reaches the maximum power point

value P_{max} (P_{max}= V_{max} x J_{max}.) The FF represents the ratio of the organic solar cell's actual maximal power output to its theoretical maximal power output. The FF is determined by the (balanced) charge transport and recombination properties of the materials and depends in a complicated way on the charge dissociation, the charge carrier transport, and the recombination process.

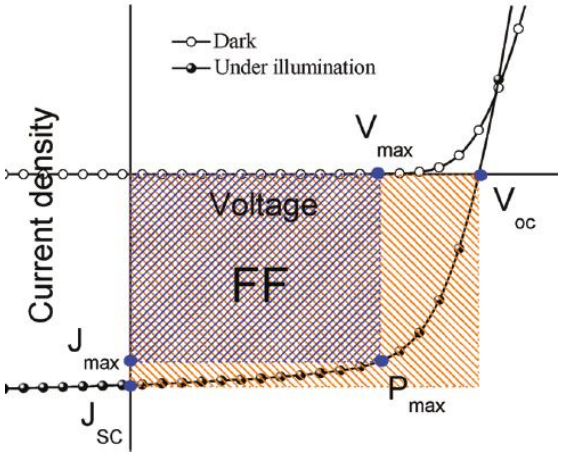

Figure 1.6. Current-voltage curve of a solar cell in the dark and under illumination with the most important parameters indicated.[16k]

$$\mathrm{FF} = \frac{Pmax}{Ptheor\ max} = \frac{Jmax\ \times Vmax}{\mathrm{Jsc}\ \times \mathrm{Voc}}$$

$$\mathrm{PCE} = \frac{Pmax}{Plight} = \frac{\mathrm{Jsc}\ \times \mathrm{Voc}\ \times \mathrm{FF}}{Plight}$$

Finally, the performance of a solar cell will be expressed by its power conversion efficiency. The PCE value represents the percentage of power converted (from absorbed light to electrical energy) and collected when a solar cell is connected to an electrical circuit. This efficiency can be calculated using the ratio of the maximum power point P_{max}, the delivered electrical power, relative to the input light irradiance (P_{light}, in W/m²) under standard test conditions. The standard test conditions specify a temperature of 25 °C and an irradiance of 1000 W/m² with an air mass 1.5 (AM1.5) spectrum. The AM 1.5 spectrum corresponds to the solar irradiance with the sun at 45° above the horizon (Figure 1.7). Narrowing the bandgap of the organic material is

required to harvest a maximum amount of photons from the solar spectrum. An ideal bandgap is situated at ~1.45 eV. Below this value the solar cell performance will be limited due to V_{oc} losses.

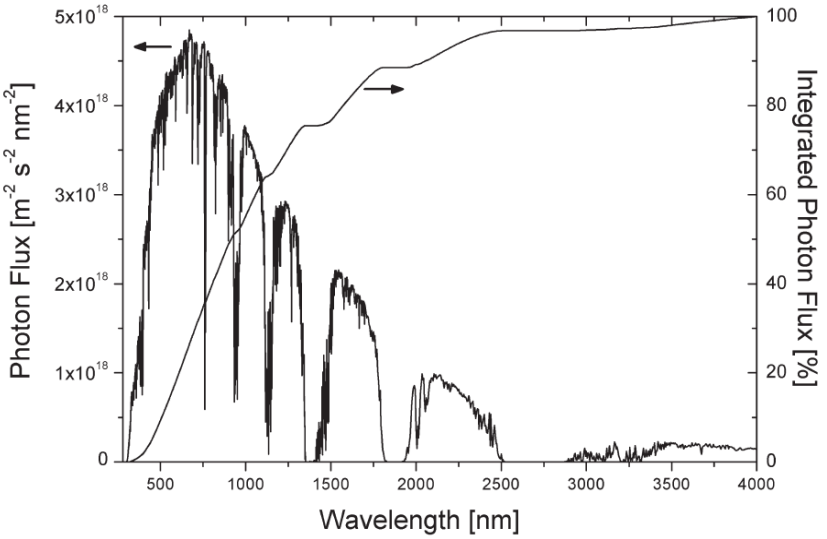

Figure 1.7. Spectrum of the solar photon flux as a function of wavelength.[24]

1.6. Literature Overview of OPV Materials[1]

The first solution-processed BHJ polymer solar cells, fabricated by Yu *et al.*, consisted of a blend of poly[2-methoxy-5-(2'-ethylhexyloxy)-1,4-phenylene vinylene] (**MEH-PPV**) (Figure 1.8) mixed with $PC_{61}BM$ (Figure 1.9).[23] Later on, Shaheen and colleagues showed that the PCE of an OPV cell based on the more processable poly[2-methoxy-5-(3',7'-dimethyloctyloxy)-1,4-phenylene vinylene] (**MDMO-PPV**) (Figure 1.8) could be increased by optimization of the blend morphology.[33] A switch in active layer processing solvent from toluene to chlorobenzene improved the self-organization of the blend components, resulting in a more intimate mixture with smaller phase-segregated methanofullerene domains. Furthermore, Pacios *et al.* demonstrated that higher hole mobilities could be achieved by an increase of the fullerene content.[34,35]

[1] In this overview we only discuss polymer donor materials, as these are most relevant for the remaining part of this PhD thesis.

For MDMO-PPV, a gradual increase of hole mobility with increasing fullerene concentration from 33 to ~70 wt% was observed. At the same time, Janssen and co-workers replaced $PC_{61}BM$ with [6,6]-phenyl-C_{71}-butyric acid methyl ester ($PC_{71}BM$),[36] because of its significant higher absorption in the visible range down to 700 nm, further enhancing the solar cell performances (Figure 1.9).

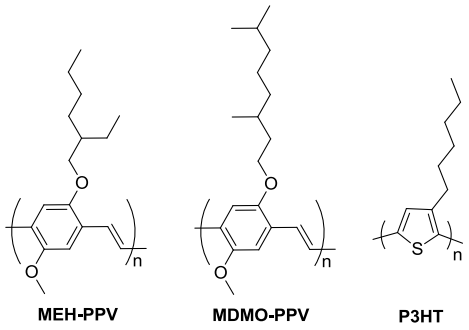

Figure 1.8. First generation polymers for PV devices.

After extensive study of PPV-based materials, interest in this material class slowly began to fade. Their large bandgap of ~2 eV and low charge tranport mobility limited power conversion efficiencies to 3% at the best. In the meantime, the interest in a new material class - poly(alkylthiophene)s, and especially poly(3-hexylthiophene) (**P3HT**) (Figure 1.8) - emerged very quickly. **P3HT** would remain the benchmark material for organic solar cells for several years and turned out to be the most studied π-conjugated polymer within the PV domain. Initial results with this material were, however, rather discouraging. In 2002, the first reasonable results for **P3HT**:$PC_{61}BM$ solar cells were published. The cells exhibited an impressive short circuit current density of 8.7 mA/cm^2, which was never reported before, resulting from a high external quantum efficiency (EQE) with a maximum value of 76% at 550 nm.[37] It was quickly demonstrated that thermal annealing of **P3HT**/$PC_{61}BM$ composites significantly enhances the photovoltaic performance due to increased charge carrier mobility.[38] Padinger *et al.* published efficiencies up to 3.5%.[39] Researchers worldwide then focused their efforts on the optimization of the **P3HT**/$PC_{61}BM$ BHJ solar cell, using the morphology of the mixed film, and in particular the crystallinity of the materials, as key parameters. Very quickly thereafter, regioregular **P3HT** was established as one of the best performing materials in organic solar cells, achieving around 5% efficiency.[40] Most significant improvements came from: *i.* increasing the regioregularity of **P3HT**,[41]

ii. optimizing the annealing temperature in combination with the molecular weight of the polymer,[40a,42] *iii.* slowing down the drying kinetics of the wet films,[40b] *iv.* using processing additives to support phase separation between **P3HT** and $PC_{61}BM$,[43] *v.* optimizing interface losses,[44] and *vi.* growing crystalline **P3HT** fibers already in solution.[45] The 5% solar cell exhibited a J_{sc} of 11.1 mA/cm^2 and a FF of 68%. The high current density resulted from a very favorable morphology of the BHJ, balanced electron and hole mobilities and, consequently, a high EQE. Unfortunately, several limitations of **P3HT** have prevented further progress. The highest V_{oc} reported for well-performing **P3HT**/$PC_{61}BM$ solar cells is around 0.66 V, due to the relatively high HOMO level of the polymer. Another disadvantage of this popular workhorse material is its relatively large bandgap of ~1.9 eV, limiting the fraction of the solar spectrum that can be harvested.[46]

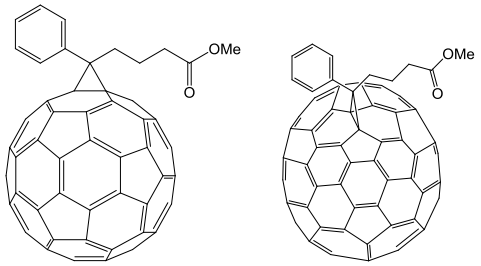

$PC_{61}BM$ **$PC_{71}BM$**

Figure 1.9. Fullerene acceptors.

Theoretical analyses of the optimum device performance achievable as a function of particular material properties have guided strategies to make further improvements in device performance beyond the **P3HT**/$PC_{61}BM$ combination. Such analyses have identified two key strategies to achieve further advances. One strategy aims at improving the voltage output of the solar cell. This voltage is limited by the energy difference between the polymer HOMO level and the $PC_{61}BM$ LUMO level. Strategies to address this limitation have typically targeted the use of polymers with larger ionization potentials (deeper HOMOs). An alternative strategy is to improve the photocurrent by enhancing light absorption by the photoactive layer. This has typically been addressed by lowering the polymer's optical bandgap to enhance the absorption of longer wavelength photons. The design and synthesis of **low bandgap polymers**, *i.e.* bandgap < 2 eV, is mainly based on the donor-acceptor approach or push-pull strategy.

The chemistry of conjugated polymers offers powerful methods to tune the HOMO and LUMO levels and to modify the bandgap of the material. In the so-called donor-acceptor approach, alternating electron-rich D and electron-poor A units are coupled together to form the polymer backbone. For such a $(\text{-D-A-})_n$ polymer, a second resonance structure $(\text{-D}^+\text{-A}^-\text{-})_n$ gains importance with respect to the neutral structure, and increases the double-bond character of the single bonds in the polymer. The consequent reduction of the bond-length alternation effectively modifies the HOMO and LUMO levels and the bandgap of the polymer.

Andersson and Inganäs have concentrated their efforts on the synthesis of polyfluorenes, thereby establishing the first class of deep HOMO (high V_{oc}) materials. Within the following years, the main focus was on the incorporation of fluorene units in alternating donor-acceptor copolymers such as poly[2,7-(9,9'-dialkylfluorene)-*alt*-5,5-(4',7'-di(2-thienyl)-2',1',3'-benzothiadiazole)] (**PFDTBT**) (Figure 1.10).[47] The pioneering work of Andersson and coworkers paved the way for other groups to optimize polyfluorene structures. High device performances were demonstrated, mainly due to the high V_{oc} of ~1 eV, resulting from the low HOMO level.[48] However, the wide bandgaps of these polymers resulted in lower J_{sc} values and consequently lower efficiencies. Yang *et al.* showed that the C-Si bonds in the dibenzosilole core are longer than the C-C bonds in a fluorene, leading to less steric hindrance and a better π-π stacking.[49] Replacing the bridging C atom by a Si atom hence had a positive impact on the charge-transport properties and efficiencies up to almost 6% were reported by Cao et *al.* for poly[2,7-(dialkylsilafluorene)-*alt*-5,5-(4',7'-di(2-thienyl)-2',1',3'-benzothiadiazole)] (**PSiFDBT**) (Figure 1.10).[50]

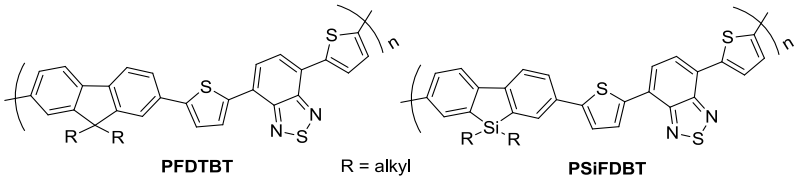

Figure 1.10. Fluorene-based photovoltaic materials.

Carbazole-based copolymers have similar electrical and optical properties as the polyfluorene class. Leclerc *et al.* synthesized poly[2,7-(*N*-9-alkyl-2,7-carbazole)-*alt*-5,5-(4',7'-di(2-thienyl)-2',1',3'-benzothiadiazole)] (**PCDTBT**) (Figure 1.11), showing solar cell performances of 3.6%.[51] Barely one year later, Heeger *et al.* set a record

efficiency of 6.1% with the same polymer, reaching an internal quantum efficiency (IQE) close to 100%, implying that essentially every absorbed photon results in a separated pair of charge carriers and that all photogenerated carriers are collected at the electrodes.[52] Despite the high V_{oc} of 0.88 V and a fill factor of 66%, the current density J_{sc} remained somewhat modest (10.6 mA/cm^2), limited by the rather wide bandgap of approximately ~1.88 eV, which restricts the portion of the solar spectrum that can be absorbed.

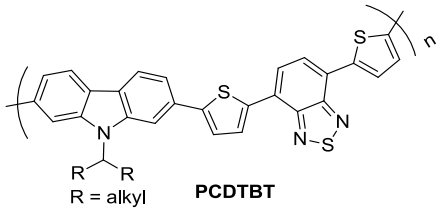

Figure 1.11. Carbazole-based copolymers.

In order to achieve their predicted full potential, the structure-property relationships of low bandgap copolymers need to be completely understood.[53] Particular attention has been directed to lower bandgap materials, for which the energy differences between the HOMO and LUMO levels didn't surpass 1.8 eV to be able to absorb a larger part of the solar spectrum (to increase J_{sc}). The first prototype polymer fulfilling the severe bandgap restriction was poly[2,6-(4,4-bis-alkyl-4*H*-cyclopenta[2,1-*b*;3,4-*b'*]-dithiophene)-*alt*-4,7-(2,1,3-benzothiadiazole)] (**PCPDTBT**) (Figure 1.12), which showed improved light harvesting in the near-infrared region due to a nearly ideal bandgap of 1.46 eV and excellent charge transport properties. Initially, PCEs of 3.2% with a V_{oc} of 0.6 eV, a J_{sc} of 11 mA/cm^2 and a FF of 47% were obtained.[54] The performance was found to be limited due to an unfavorable, very intimate nanomorphology of the blend (short carrier lifetimes and considerable recombination). To solve this problem, Bazan and Heeger added alkanedithiols upon active layer processing.[55] In this way, the blend morphology was optimized and efficiencies raised beyond 5%, with an enhanced current density of 16.2 mA/cm^2 and a fill factor of 55%. Further efficiency improvement could be observed when the bridging carbon atom was replaced by a silicon atom, affording poly[2,6-(4,4-bis-alkyl-dithieno[3,2-*b*;2',3'-*d*]silole)-*alt*-4,7-(2,1,3-benzothiadiazole)] (**PSBTBT)** (Figure 1.12). The longer Si-C bond modifies the geometry of the fused dithiophene unit, which results in a better ordering of the polymer chains and efficiencies of almost 6% were obtained.[56] A whole

series of other electron-withdrawing units (than benzothiadiazole) has been coupled with C or Si bridged bithiophenes, affording novel copolymers and their solar cell performances have been tested.[57–59] Unfortunately, the main disadvantage of this bridged thiophene class of donor constituents is its rather high-lying HOMO level, which generally doesn't allow open-circuit voltages higher than 0.6–0.7 eV when mixed with $PC_{61}BM$. As an exception, Janssen *et al.* have synthesized a copolymer with alternating 4*H*-cyclopenta[2,1-*b*:3,4-*b'*]dithiophenes (**CPDT**) and benzo-oxadiazole units, resulting in a V_{oc} of 0.78 eV. The energy loss from the bandgap (E_g) to the V_{oc} is 0.69 eV and one of the lowest values reported for BHJ solar cells to date, close to the expected minimum loss of 0.6 V.[60] Unfortunately, efficiencies of only 2.5% could be achieved for this material.

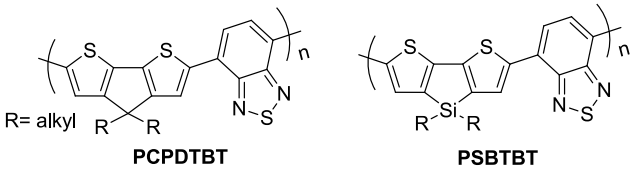

Figure 1.12. Low bandgap polymers with bridged bithiophenes as building blocks.

Summarizing all these observations, we can conclude that the ideal polymer would have a low bandgap (~1.5 eV) and simultaneously also a large V_{oc} originating from a deep-lying HOMO level. Untill now, combination of these two important features was not very successful. Either a material class with high V_{oc} and lower photocurrent (such as the **PPV**, **PF** and **PCDTBT** materials) was obtained, or polymers with smaller bandgaps (higher photocurrent) but low V_{oc} (as observed with **P3HT**, **PCPDTBT** and **PSBTBT**) were synthesized.

Further research resulted in the design of the appealing, entirely planar and symmetrical donor unit benzo[1,2-*b*:4,5-*b'*]dithiophene (**BDT**), with reasonable high oxidation potentials resulting in a high V_{oc}. Yang *et al.* combined this donor unit with the popular acceptor benzothiadiazole. Unfortunately, the best PCE reported was only 0.9%.[61] A very successful modification, however, was its combination with *N*-alkylthieno[3,4-*c*]pyrrole-4,6-dione (**TPD**). Fréchet *et al.* reported solar cell efficiencies for these poly[2,6-(4,8-bis-alkyloxybenzo[1,2-*b*:4,5-*b'*]dithiophene)-*alt*-2,8-(*N*-alkylthieno[3,4-*c*]pyrrole-4,6-dione)] (**PBDTTPD**) materials (Figure 1.13) of up to 6.8% upon addition of 1,8-diiodooctane, with a V_{oc} of 0.85 V and a J_{sc} of 11.5

mA/cm^2.[62] Yu et *al.* combined the **BDT** donor unit with thieno[3,4-*b*]thiophene (**TT**), endowed with an additional electron-withdrawing ester or ketone group (**PTB-x**; Figure 1.13). The ketone moiety seemed to have more impact on the V_{oc} value (increasing from 0.62 to 0.7 V), and efficiencies of 5.2 and 6.6%, respectively, were obtained. The subsequent introduction of a fluorine atom raised the efficiency to 7.7%, with a V_{oc} of 0.76 V, a high J_{sc} of 15.2 mA/cm^2 and a FF of 67%.[25a,63] The introduction of fluorine atoms had already been used before to increase the V_{oc} of a OPV device because of its high electron affinity.[64] Later on, You *et al.* also constructed a low bandgap polymer consisting of a benzodithiophene derivative coupled with a fluorinated benzothiadiazole, likewise affording efficiencies of 7.1%.[65] Further research via bandgap engineering will certainly drive efficiencies forward, hopefully surpassing the 10% level within a short time.

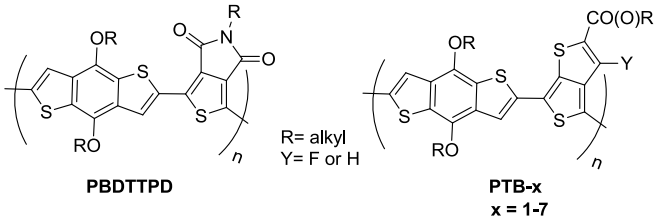

Figure 1.13. Top solar cell materials based on benzodithiophenes.

1.7. Morphology and Stability

Even if the donor and acceptor material which constitute the active layer blend have an ideal (chemical) electronic relationship, the performance of BHJ solar cells still depends on the physical interaction of the donor and acceptor components, which is manifested by the composite morphology. The ideal bulk heterojunction active layer is defined as a bicontinuous mixture of donor and acceptor, with a maximal interfacial area for exciton dissociation and a mean domain size commensurating with the exciton diffusion length (5–10 nm). The domain sizes of donor and acceptor play an important role in the actual short-circuit current measured in a device. When the domain sizes are too large, excitons will be lost due to excitonic decay. Photophysical studies can be employed to see whether all excitons are able to reach an interface. On the other hand, too small domain sizes can induce an enhanced recombination of charge carriers. The donor and acceptor domains also need to show percolating pathways toward the anode

and cathode, respectively, in order for charges to be collected. In fact, the control of this **nanomorphology** is the most difficult part of the BHJ solar cell fabrication.

At first, fine-tuning of the processing conditions (concentration, solvent, temperature, blend ratio, spin-coating speed/acceleration and time) can be considered to create an optimal morphology. Post-processing conditions such as thermal or solvent annealing can also help to improve the device performance. Thermal annealing can be applied either on the final device (post-annealing) or on the polymer film only (pre-annealing). The annealing temperature and time are the most critical parameters in this approach. The solvent-annealing approach controls the polymer nanomorphology through the solvent evaporation speed. Annealing and processing parameters have been discussed in detail for the **MDMO-PPV** and **P3HT** workhorse materials.[33,42]

More recently, the incorporation of (high boiling) additives into processing solvents has been introduced as a powerful method capable of controlling the BHJ morphology to some extent. A prominent example is **PCPDTBT**, for which the addition of a few volume percent of alkanedithiols into the blend mixture increased the efficiency from 2.8% to 5.5%.[55] The alkanedithiols selectively dissolve the fullerene phase, being a non-solvent for the polymer. The fullerenes will subsequently remain in solution for a longer time due to the high boiling temperature of the additive, providing enough time to the polymer for self-alignment and crystallization.[55b,66,67] In addition to alkanedithiols, the non-solvents nitrobenzene and 1-chloronaphtalene have also been proven successful in the case of **P3HT**.[68,69]

Once the nanomorphology is optimized there is also the challenge to preserve this nanostructure. This leads us to a final concern of critical relevance for potential commercialization of polymer-fullerene BHJ solar cells, namely the lifetime, as determined by ambient and thermal stability factors. While ambient stability may be realized through proper encapsulation to protect the devices from the action of oxygen and water, thermal stability is a critical issue that currently plagues organic BHJ solar cells. The effect of temperature on the morphological and photovoltaic stability for the model systems **MDMO-PPV**:$PC_{61}BM$ and **P3HT**:$PC_{61}BM$ has recently been studied within Hasselt University. Figure 1.14 shows the results of the *in situ* monitoring of the photocurrent-voltage characteristics of a **MDMO-PPV**:$PC_{61}BM$ layer at elevated temperatures, in combination with a systematic TEM study. Annealing at 110 °C during 25 hours resulted in a significant decay of the short circuit current with

concomitant morphology changes within the active layer due to the formation of PCBM-clusters. Upon repeating the same experiment with a "high T_g PPV":$PC_{61}BM$ active layer, the short circuit current showed much slower decay with barely observable changes in the morphology.[70] Similar results were retrieved for poly[(2-methoxy-5-(2'-phenylethoxy))-1,4-phenylene vinylene] (**MPE-PPV**), which was designed as a high T_g material within our group.[71] Increasing the glass transition temperature of the polymer materials hence defines one possible way to obtain more stable organic photovoltaic devices.

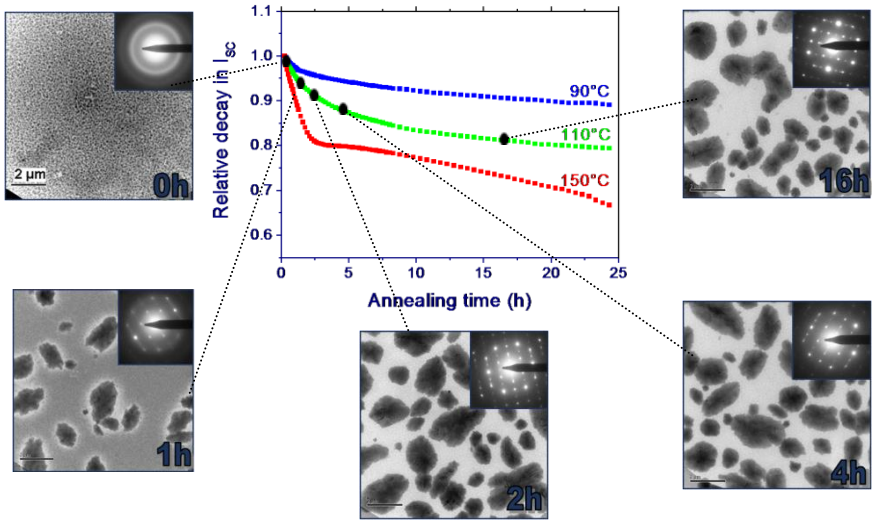

Figure 1.14. Morphology changes in the active layer of **MDMO-PPV**:$PC_{61}BM$ (1:4) after annealing at 110 °C.[70]

Another explored approach to enhance the thermal stability comprises the design of cross-linkable molecules/polymers that can 'lock' or 'kinetically freeze' the nanomorphology, preventing phase separation. Gaudiana *et al.* developed fullerene derivatives containing a glycidyl functionality.[72,73] Hashimoto and coworkers prepared a cross-linkable **P3HT** analogue, poly[3-(5-hexenyl)thiophene] (**P3HNT**), which undergoes cross-linking at the vinyl groups of the side chains upon thermal treatment.[74] Fréchet *et al.* designed **P3HT** polymers with a bromine functionality tethered to the end of the hexyl side chain. Upon photocrosslinking, improved thermal stability compared to conventional **P3HT**:PCBM blends could be observed.[75]

Some progress toward lifetime extension of organic solar cells has hence already been achieved, but tremendous efforts will still be required to enable commercialization in

the near future. As shown in Figure 1.15, OPV technology can only become a competitive market player with optimum cost, efficiency and stability parameters. Low cost and very efficient but moderately stable solar cell materials will unfortunately force this technology into a niche market, preventing successful commercialization.[16a]

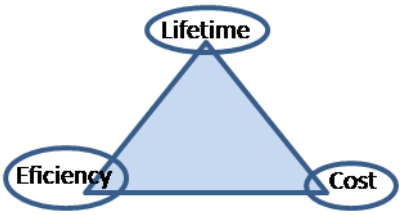

Figure 1.15. Brabec's critical triangle showing the strong interdependence of cost, solar cell efficiency and lifetime.

1.8. References

(1) Presentation of Richard Smalley at Columbia University in 2003.

(2) New York Times, 3rd May 2011.

(3) Shafiee, S.; Topal, E. *Energy Policy* **2009**, *37*, 181.

(4) Hoffert, M. I.; Caldeira, K.; Benford, G.; Criswell, D. R.; Green, C.; Herzog, H.; Jain, A. K.; Kheshgi, H. S.; Lackner, K. S.; Lewis, J. S.; Lightfoot, H. D.; Manheimer, W.; Mankins, J. C.; Manuel, M. E.; Perkins, L. J.; Schlesinger, M. E.; Volk, T.; Wigley, T. M. L. *Science* **2002**, *298*, 981.

(5) (a) Mann, M. E.; Bradley, R. S.; Hughes, M. K. *Nature* **1998**, *392*, 779; (b) Mann, M. E.; Bradley, R. S.; Hughes, M. K. *Geophys. Res. Lett.* **1999**, *26*, 759.

(6) (a) Hoffert, M. I. *Science* **2010**, *329*, 1292; (b) Davis, S. J.; Caldeira, K.; Matthews, H. D. *Science* **2010**, *329*, 1330; (c) http://www.iea.org/; (d) Delucchi, M. A.; Jacobson, M. Z. *Energy Policy* **2011**, *39*, 1154; (e) Delucchi, M. A.; Jacobson, M. Z. *Energy Policy* **2011**, *39*, 1170.

(7) McGehee, M. D.; Goh, C. *The Bridge* **2005**, *35*, 33.

(8) Becquerel, A. E. *Comptes Rendus* **1839**, *9*, 561.

(9) Chapin, D. M.; Fuller, C. S.; Pearson, G. L. *J. Appl. Phys.* **1954**, *25*, 676.

(10) Green, M. A.; Emery, K.; Hishikawa, Y.; Warta, W. *Prog. Photovoltaics Res. Appl.* **2010**, *18*, 346.

(11) Jäger-Waldau, A. PV Status Report 2011.

(12) (a) Aberle, A. G. *Thin Solid Films* **2009**, *517*, 4706; (b) Green, M. A. *J. Mater. Sci.: Mater. Electron.* **2007**, *18*, S15.

(13) Sun, Y.; Welch, G. C.; Leong, W. L.; Takacs, C. J.; Bazan, G. C.; Heeger, A. J. *Nat. Mater.* **2011**, DOI: 10.1038/nmat3160.

(14) (a) Grätzel, M. *Prog. Photovoltaics Res. Appl.* **2000**, *8*, 171; (b) Bay, Y.; Cao, Y.; Zhang, J.; Wang, M.; Li, R.; Wang, P.; Zakeeruddin, S. M.; Grätzel, M. *Nat. Mater.* **2008**, *7*, 626.

(15) Xu, T.; Qiao, Q. *Energy Environ. Sci.* **2011**, *4*, 2700.

(16) (a) Brabec, C. J. *Sol. Energy Mater. Sol. Cells* **2004**, *83*, 273; (b) Xue, J. *Polym. Rev.* **2010**, *50*, 411; (c) Deibel, C.; Dyakonov, V. *Rep. Prog. Phys.* **2010**, *73*, 096401; (d) Chidichimo, G.; Filippelli, L. *Int. J. Photoenergy* **2010**, 123534; (e) Nielsen, T. D.; Cruickshank, C.; Foged, S.; Thorsen, J.; Krebs, F. C. *Sol. Energy*

Mater. Sol. Cells **2010**, *94*, 1553; (f) Helgesen, M.; Søndergaard, R.; Krebs, F. C. *J. Mater. Chem.* **2010**, *20*, 36; (g) Bundgaard, E.; Hagemann, O.; Manceau, M.; Jørgensen, M.; Krebs, F. C. *Macromolecules* **2010**, *43*, 8115; (h) Krebs, F. C. *Polymeric Solar Cells: Material, Design, Manufacture*; DEStech Publications, Inc., Lancaster, Pennsylvania, **2010**; (i) Arias, A. C.; MacKenzie, J. D.; McCulloch, I.; Rivnay, J.; Salleo, A. *Chem. Rev.* **2010**, *110*, 3; (j) Brabec, C. J.; Gowrisanker, S.; Halls, J. J. M.; Laird, D.; Jia, S.; Williams, S. P. *Adv. Mater.* **2010**, *22*, 3839; (k) Boudreault, P.-L. T.; Najari, A.; Leclerc, M. *Chem. Mater.* **2011**, *23*, 456; (l) Hübler, A.; Trnovec, B.; Zillger, T.; Ali, M.; Wetzold, N.; Mingebach, M.; Wagenpfahl, A.; Deibel, C.; Dyakonov, V. *Adv. Energy Mater.* **2011**, *1*, 1018; (m) Teichler, A.; Eckardt, R.; Hoeppener, S.; Friebe, C.; Perelaer, J.; Senes, A.; Morana, M.; Brabec, C. J.; Schubert, U. S. *Adv. Energy Mater.* **2011**, *1*, 105.

(17) http://www.nrel.gov/ncpv/index.html.

(18) (a) Shirakawa, H.; Louis, E. J.; Macdiarmid, A. G.; Chiang, C. K.; Heeger, A. J. *J. Chem. Soc., Chem. Commun.* **1977**, 578; (b) Chiang, C. K.; Fischer, C. R.; Park, Y. W.; Heeger, A. J.; Shirakawa, H.; Louis, E. J.; Gau, S. C.; Macdiarmid, A. G. *Phys. Rev. Lett.* **1977**, *39*, 1098.

(19) Shirakawa, H. *Nobel lecture Chemistry 1996-2000*, World Scientific Publishing Co., Singapore, **2003**.

(20) Tang, C. W. *Appl. Phys. Lett.* **1986**, *48*, 183.

(21) Sariciftci, N. S.; Smilowitz, L.; Heeger, A. J.; Wudl, F. *Science* **1992**, *258*, 1474.

(22) (a) Wudl, F. *Acc. Chem. Res.* **1992**, *25*, 15716; (b) Hummelen, J. C.; Knight, B. W.; LePeq, F.; Wudl, F.; Yao, J.; Wilkins, C. L. *J. Org. Chem.* **1995**, *60*, 532.

(23) (a) Yu, G.; Gao, J.; Hummelen, J. C.; Wudl, F.; Heeger, A. J. *Science* **1995**, *270*, 1789; (b) Halls, J. J. M.; Walsh, C. A.; Greenham, N. C.; Marseglia, E. A.; Friend, R. H.; Moratti, S. C.; Holmes, A. B. *Nature* **1995**, *376*, 498.

(24) Kroon, R.; Lenes, M.; Hummelen, J. C.; Blom, P. W. M.; de Boer, B. *Polym. Rev.* **2008**, *48*, 531.

(25) (a) Chen, H.-Y.; Hou, J.; Zhang, S.; Liang, Y.; Yang, G.; Yang, Y.; Yu, L.; Wu, Y.; Li, G. *Nat. Photonics* **2009**, *3*, 649; (b) Zhou, H.; Yang, L.; Stuart, A. C.; Price, S. C.; Liu, S.; You, W. *Angew. Chem. Int. Ed.* **2011**, *50*, 2995; (c) Price, S.

C.; Stuart, A. C.; Yang, L.; Zhou, H.; You, W. *J. Am. Chem. Soc.* **2011**, *133*, 4625.

(26) Service, R. F. *Science* **2011**, *332*, 293.

(27) http://www.neubers.de/vmchk/Solar-Taschen/View-all-products.html.

(28) Mayer, A. C.; Scully, S. R.; Hardin, B. E.; Rowell, M. W.; McGehee, M. D. *Mater. Today* **2007**, *10*, 28.

(29) Bundgaard, E.; Krebs, F. C. *Sol. Energy Mater. Sol. Cells* **2007**, *91*, 954.

(30) Thompson, B. C.; Fréchet, J. M. J. *Angew. Chem. Int. Ed.* **2008**, *47*, 58.

(31) Peet, J.; Heeger, A. J.; Bazan, G. C. *Acc. Chem. Res.* **2009**, *42*, 1700.

(32) Brédas, J.-L.; Norton, J. E.; Cornil, J.; Coropceanu, V. *Acc. Chem. Res.* **2009**, *42*, 1691.

(33) Shaheen, S.; Brabec, C. J.; Sariciftci, N. S.; Padinger, F.; Fromherz, T.; Hummelen, J. C. *Appl. Phys. Lett.* **2001**, *78*, 841.

(34) Pacios, R.; Bradley, D. D. C.; Nelson, J.; Brabec, C. J. *Synth. Met.* **2003**, *137*, 1469.

(35) Pacios, R.; Bradley, D. D. C.; Nelson, J.; Brabec, C. J. *Appl. Phys. Lett.* **2003**, *83*, 4764.

(36) Wienk, M. M.; Kroon, J. M.; Verhees, W. J. H.; Knol, J.; Hummelen, J. C.; van Hal, P. A.; Janssen, R. A. J. *Angew. Chem. Int. Ed.* **2003**, *42*, 3371.

(37) Schilinsky, P.; Waldauf, C.; Brabec, C. J. *Appl. Phys. Lett.* **2002**, *81*, 3885.

(38) Mihailetchi, V. D.; Xie, H.; de Boer, B.; Koster, L. J. A.; Blom, P. W. M. *Adv. Funct. Mater.* **2005**, *15*, 1260.

(39) Padinger, F.; Rittberger, R. S.; Sariciftci, N. S. *Adv. Funct. Mater.* **2003**, *13*, 1.

(40) (a) Ma, W.; Yang, C.; Gong, X.; Lee, K.; Heeger, A. J. *Adv. Funct. Mater.* **2005**, *15*, 1617; (b) Li, G.; Shrotriya, V.; Huang, J.; Yao, Y.; Moriarty, T.; Emery, K.; Yang, Y. *Nat. Mater.* **2005**, *4*, 864.

(41) Kim, Y.; Cook, S.; Tuladhar, S. M.; Choulis, S. A.; Nelson, J.; Durrant, J. R.; Bradley, D. D. C.; Giles, M.; McCulloch, I.; Ha, C.-S.; Ree, M. *Nat. Mater.* **2006**, *5*, 197.

(42) (a) Schilinsky, P.; Asawapirom, U.; Scherf, U.; Biele, M.; Brabec, C. J. *Chem. Mater.* **2005**, *17*, 2175; (b) Kline, R. J.; McGehee, M. D.; Kadnikova, E. N.; Liu, J.; Fréchet, J. M. J. *Adv. Funct. Mater.* **2003**, *15*, 1519; (c) Zen, A.; Pflaum, J.; Hirschmann, S.; Zhuang, W.; Jaiser, F.; Asawapirom, U.; Rabe, J. P.; Scherf, U.;

Neher, D. *Adv. Funct. Mater.* **2004**, *14*, 757; (d) Kline, R. J.; McGehee, M. D.; Kadnikova, E. N.; Liu, J.; Fréchet, J. M. J.; Toney, M. F. *Macromolecules* **2005**, *38*, 3312; (e) Ma, W.; Kim, J. Y.; Lee, K.; Heeger, A. J. *Macromol. Rapid. Commun.* **2007**, *28*, 1776.

(43) (a) Peet, J.; Soci, C.; Coffin, R. C.; Nguyen, T. Q.; Mikhailovsky, A.; Moses, D.; Bazan, G. C. *Appl. Phys. Lett.* **2006**, *89*, 252105; (b) Wang, W.; Wu, H.; Yang, C.; Luo, C.; Zhang, Y.; Chen, J.; Cao, Y. *Appl. Phys. Lett.* **2007**, *90*, 183512; (c) Moulé, A. J.; Meerholz, K. *Adv. Mater.* **2008**, *20*, 240.

(44) Irwin, M. D.; Buchholz, D. B.; Hains, A. W.; Chang, R. P. H.; Marks, T. J. *Proc. Natl. Acad. Sci. U.S.A.* **2008**, *105*, 2783.

(45) (a) Mena-Osteritz, E.; Meyer, A.; Langeveld-Voss, B. M. W.; Janssen, R. A J.; Meijer, E. W.; Bäuerle, P. *Angew. Chem. Int. Ed.* **2000**, *39*, 2679; (b) Malik, S.; Nandi, A. K. *J. Polym. Sci., Part B: Polym. Phys.* **2002**, *40*, 2073; (c) Berson, S.; De Bettignies, R.; Bailly, S.; Guillerez, S. *Adv. Funct. Mater.* **2007**, *17*, 1377.

(46) Dang, M. T.; Hirsch, L.; Wantz, G. *Adv. Mater.* **2011**, *23*, 3597.

(47) (a) Svensson, M.; Zhang, F.; Veenstra, S. C.; Verhees, W. J. H.; Hummelen, J. C.; Kroon, J. M.; Inganäs, O.; Andersson, M. R. *Adv. Mater.* **2003**, *15*, 988; (b) Wang, X.; Perzon, E.; Delgado, J. L.; de la Cruz, P.; Zhang, F.; Langa, F.; Andersson, M. R.; Inganäs, O. *Appl. Phys. Lett.* **2004**, *85*, 5081; (c) Gadisa, A.; Wang, X.; Admassie, S.; Per, E.; Oswald, F.; Langa, F.; Andersson, M. R.; Inganäs, O. *Org. Electron.* **2006**, *7*, 195; (d) Zhang, F. L.; Jespersen, K. G.; Björström, C.; Svensson, M.; Andersson, M. R.; Sundström, V.; Magnusson, K.; Moons, E.; Yartsev, A.; Inganäs, O. *Adv. Funct. Mater.* **2006**, *16*, 667; (e) Zhang, F.; Mammo, W.; Andersson, L. M.; Admassie, S.; Andersson, M. R.; Inganäs, O. *Adv. Mater.* **2006**, *18*, 2169.

(48) (a) Inganäs, O.; Zhang, F.; Andersson, M. R. *Acc. Chem. Res.* **2009**, *42*, 1731; (b) Chen, M. H.; Hou, J.; Hong, Z.; Yang, G.; Sista, S.; Chen, L. M.; Yang, Y. *Adv. Mater.* **2009**, *21*, 1.

(49) Chen, H.-Y.; Hou, J.; Hayden, A. E.; Yang, H.; Houk, K. N.; Yang, Y. *Adv. Mater.* **2010**, *22*, 371.

(50) Wang, E. G.; Wang, L.; Lan, L. F.; Luo, C.; Zhuang, W. L.; Peng, J. B.; Cao, Y. *Appl. Phys. Lett.* **2008**, *92*, 033307.

(51) (a) Blouin, N.; Michaud, A.; Leclerc, M. *Adv. Mater.* **2007**, *19*, 2295; (b) Blouin, N.; Michaud, A.; Gendron, D.; Wakim, S.; Blair, E.; Neagu-Plesu, R.; Belletête, M.; Durocher, G.; Tao, Y.; Leclerc, M. *J. Am. Chem. Soc.* **2008**, *130*, 732.

(52) Park, S. H.; Roy, S.; Beaupré, S.; Cho, S.; Coates, N.; Moon, J. S.; Moses, D.; Leclerc, M.; Lee, K.; Heeger, A. J. *Nat. Photonics* **2009**, *3*, 297.

(53) Scharber, M. C.; Mühlbacher, D.; Koppe, M.; Denk, P.; Waldauf, C.; Heeger, A. J.; Brabec, C. J. *Adv. Mater.* **2006**, *18*, 789.

(54) (a) Mühlbacher, D.; Scharber, M.; Morana, M.; Zhu, Z.; Waller, D.; Gaudiana, R.; Brabec, C. *Adv. Mater.* **2006**, *18*, 2884; (b) Soci, C.; Hwang, I.-W.; Moses, D.; Zhu, Z.; Waller, D.; Gaudiana, R.; Brabec, C. J.; Heeger, A. J. *Adv. Funct. Mater.* **2007**, *17*, 632; (c) Zhang, M.; Tsao, H. N.; Pisula, W.; Yang, C.; Mishra, A. K.; Müllen, K. *J. Am. Chem. Soc.* **2007**, *129*, 3472; (d) Coffin, R. C.; Peet, J.; Rogers, J.; Bazan, G. C. *Nat. Chem.* **2009**, *1*, 657.

(55) (a) Peet, J.; Kim, J. Y.; Coates, N. E.; Ma, W. L.; Moses, D.; Heeger, A. J.; Bazan, G. C. *Nat. Mater.* **2007**, *6*, 497; (b) Lee, J. K.; Ma, W. L.; Brabec, C. J.; Yuen, J.; Moon, J. S.; Kim, J. Y.; Lee, K.; Bazan, G. C.; Heeger, A. J. *J. Am. Chem. Soc.* **2008**, *130*, 3619.

(56) (a) Hou, J.; Chen, H.-Y.; Zhang, S.; Li, G.; Yang, Y. *J. Am. Chem. Soc.* **2008**, *130*, 16144; (b) Chen, H.-Y.; Hou, J.; Hayden, A. E.; Yang, H.; Houk, K. N.; Yang, Y. *Adv. Mater.* **2010**, *22*, 371; (c) Scharber, M. C.; Koppe, M.; Gao, J.; Cordella, F.; Loi, M. A.; Denk, P.; Morana, M.; Egelhaaf, H.-J.; Forberich, K.; Dennler, G.; Gaudiana, R.; Waller, D.; Zhu, Z.; Shi, X.; Brabec, C. J. *Adv. Mater.* **2010**, *22*, 367.

(57) (a) Moulé, A. J.; Tsami, A.; Bünnagel, T. W.; Forster, M.; Kronenberg, N. M.; Scharber, M.; Koppe, M.; Morana, M.; Brabec, C. J.; Meerholz, K.; Scherf, U. *Chem. Mater.* **2008**, *20*, 4045; (b) Xiao, S.; Zhou, H.; You, W. *Macromolecules* **2008**, *41*, 5688; (c) Hou, J.; Chen, T. L.; Zhang, S.; Chen, H.-Y.; Yang, Y. *J. Phys. Chem. C.* **2009**, *113*, 1601; (d) Chen, C.-H.; Hsieh, C.-H.; Dubosc, M.; Cheng, Y.-J.; Hsu, C.-S. *Macromolecules* **2010**, *43*, 697.

(58) Jung, I. H.; Yu, J.; Jeong, E.; Kim, J.; Kwon, S.; Kong, H.; Lee, K.; Woo, H. Y.; Shim, H.-K. *Chem. Eur. J.* **2010**, *16*, 3743.

(59) (a) Peet, J.; Wen, L.; Byrne, P.; Rodman, S.; Forberich, K.; Shao, Y.; Drolet, N.; Gaudiana, R.; Dennler, G.; Waller, D. *Appl. Phys. Lett.* **2011**, *98*, 043301; (b)

Subramaniyan, S.; Xin, H.; Kim, S. F.; Shoaee, S.; Durrant, J. R.; Jenekhe, S. A. *Adv. Energy Mater.* **2011**, *1*, 854.

(60) Bijleveld, J. C.; Shahid, M.; Gilot, J.; Wienk, M. M.; Janssen, R. A. J. *Adv. Funct. Mater.* **2009**, *19*, 3262.

(61) Hou, J.; Park, M.-H.; Zhang, S.; Yao, Y.; Chen, L.-M.; Li, J.-H.; Yang, Y. *Macromolecules* **2008**, *41*, 6012.

(62) (a) Piliego, C.; Holcombe, T. W.; Douglas, J. D.; Woo, C. H.; Beaujuge, P. M., Fréchet, J. M. J. *J. Am. Chem. Soc.* **2010**, *132*, 7595; (b) Zou, Y.; Najari, A.; Berrouard, P.; Beaupré, S.; Réda Aïch, B.; Tao, Y.; Leclerc, M. *J. Am. Chem. Soc.* **2010**, *132*, 5330; (c) Zhang, Y.; Hau, S. K.; Yip, H.-L.; Sun, Y.; Acton, O.; Jen, A. K.-Y. *Chem. Mater.* **2010**, *22*, 2696; (d) Zhang, G.; Fu, Y.; Zhang, Q.; Xie, Z. *Chem. Commun.* **2010**, *46*, 4997.

(63) (a) Liang, Y.; Wu, Y.; Feng, D.; Tsai, S.-T.; Son, H.-J.; Li, G.; Yu, L. *J. Am. Chem. Soc.* **2009**, *131*, 56; (b) Hou, J.; Chen, H.-Y.; Zhang, S.; Chen, R. I.; Yang, Y.; Wu, Y.; Li, G. *J. Am. Chem. Soc.* **2009**, *131*, 15586; (c) Liang, Y.; Xu, Z.; Xia, J.; Tsai, S.-T.; Wu, Y.; Li, G.; Ray, C.; Yu, L. *Adv. Mater.* **2010**, *22*, E135; (d) Liang, Y.; Yu, L. *Acc. Chem. Res.* **2010**, *43*, 1227; (e) Szarko, J. M.; Guo, J.; Liang, Y.; Lee, B.; Rolczynski, B. S.; Strzalka, J.; Xu, T.; Loser, S.; Marks, T. J.; Yu, L.; Chen, L. X. *Adv. Mater.* **2010**, *22*, 5468; (f) Son, H. J.; Wang, W.; Xu, T.; Liang, Y.; Wu, Y.; Li, G.; Yu, L. *J. Am. Chem. Soc.* **2011**, *133*, 1885.

(64) Liang, Y.; Feng, D.; Wu, Y.; Tsai, S.-T.; Li, G.; Ray, C.; Yu, L. *J. Am. Chem. Soc.* **2009**, *131*, 7792.

(65) (a) Price, S. C.; Stuart, A. C.; Yang, L.; Zhou, H.; You, W. *J. Am. Chem. Soc.* **2011**, *133*, 4625; (b) Zhou, H.; Yang, L.; Stuart, A. C.; Price, S. C.; Liu, S.; You, W. *Angew. Chem. Int. Ed.* **2011**, *50*, 2995.

(66) Moulé, A. J.; Meerholz, K. *Adv. Funct. Mater.* **2009**, *19*, 3028.

(67) Chen, L.-M.; Hong, Z.; Li, G.; Yang, Y. *Adv. Mater.* **2009**, *21*, 1434.

(68) Moulé, A. J.; Meerholz, K. *Adv. Mater.* **2008**, *20*, 240.

(69) Chen, F.-C., Tseng, H.-C.; Ko, C.-J. *Appl. Phys. Lett.* **2008**, *92*, 103316.

(70) Bertho, S.; Janssen, G.; Cleij, T. J.; Conings, B.; Moons, W.; Gadisa, A.; D'Haen, J.; Goovaerts, E.; Lutsen, L.; Manca, J.; Vanderzande, D. *Sol. Energy Mater. Sol. Cells* **2008**, 92, 753.

(71) Vandenbergh, J.; Conings, B.; Bertho, S.; Kesters, J.; Spoltore, D.; Esiner, S.; Zhao, J.; Van Assche, G.; Wienk, M. M.; Maes, W.; Lutsen, L.; Van Mele, B.; Janssen, R. A. J.; Manca, J.; Vanderzande, D. J. M. *Macromolecules* **2011**, *44*, 8470.

(72) Zhu, Z.; Hadjikyriacou, S.; Waller, D.; Gaudiana, R. *J. Macromol. Sci., Part A: Pure Appl. Chem.* **2004**, *41*, 1467.

(73) Drees, M.; Hoppe, H.; Winder, C.; Neugebauer, H.; Sariciftci, N. S.; Schwinger, W.; Schäffler, F.; Topf, C.; Scharber, M. C.; Zhu, Z.; Gaudiana, R. *J. Mater. Chem.* **2005**, *15*, 5158.

(74) Miyanishi, S.; Tajima, K.; Hashimoto, K. *Macromolecules* **2009**, *42*, 1610.

(75) Kim, B. J.; Miyamoto, Y.; Ma, B.; Fréchet, J. M. J. *Adv. Funct. Mater.* **2009**, *19*, 2273.

Aim

Over the past ten years, organic photovoltaic (OPV) technology has made an impressive progress. To date, it holds great potential as a renewable energy source in times of rising energy costs. The research work described in this thesis was performed with the general goal to combine the urge for improvements in both the efficiency and stability of organic solar cells. It was decided to put the main focus on two specific material classes, *i.e.* 4*H*-cyclopenta[2,1-*b*:3,4-*b'*]dithiophenes (**CPDTs**) and thiazolo[5,4-*d*]thiazoles (**TzTzs**), and their possible contributions to OPV. At first, novel straightforward synthetic methods for the **CPDT** and **TzTz** building blocks had to be developed. Highly versatile and reproducible synthetic protocols, enabling fine-tuning of the material features, are desirable toward rationalized material engineering. More in particular, side chain variation for the **CPDT** derivatives, *via* an efficient method giving access to a broad range of precursors applicable in OPV, was pursued. On the other hand, introduction of suitable alkyl side chains on **TzTz** semiconducting materials, affording well-soluble compounds, was also a specific goal. For the novel monomer materials it was also intended to perform preliminary device experiments, with a focus on solution processing.

After synthesis and characterization of the required monomeric building blocks, introduction of these units in low bandgap copolymers should be performed - by combination of **CPDT** and **TzTz** or by combination with other suitable monomers - and the materials should be introduced in OPV devices, with a particular emphasis on efficiency and stability.

Outline

Chapter 2 describes the development of a convenient three-step synthetic route toward **CPDT** derivatives, which are generally synthesized by rather laborious multistep procedures affording mostly symmetrically dialkylated derivatives. Our major goals in searching for an alternative synthetic method are the ability to introduce two *identical* or *different* alkyl chains simultaneously and to enable the introduction of basic *functional groups* on these side chains. A plausible reaction pathway is proposed, supported by NMR spectroscopy and theoretical energy calculations. Finally, a broad scope of novel **CPDT** molecules is synthesized, inluding an ester-functionalized **CPDT**, representing an attractive precursor for variously functionalized cyclopentadithiophene compounds.

In **Chapter 3**, a number of **CPDT** derivatives endowed with two linear, branched or asymmetrical side chains are connected to 2,1,3-benzothiadiazole (**BT**) by Suzuki polymerization reactions, generating a new series of low bandgap **PCPDTBT** copolymers. Optical and electrochemical features of all prepared polymers are studied and preliminary solar cell results are presented. Finally, an ester-functionalized **PCPDTBT** copolymer is synthesized, which can act as a key intermediate toward the design of a variety of **PCPDTBT**-type polymers via basic functional group conversions.

In **Chapter 4**, the bis(3-hexylthiophenyl)-substituted **TzTz** core is introduced as an appealing acceptor unit. Synthesis of analogous **TzTz** molecules functionalized with additional thienyl groups is presented as well and detailed NMR structural elucidation and electrochemical properties are described. Substitution with alkyl chains leads to an improved solubility, enabling application in printable electronics. Furthermore, electropolymerization experiments afford insight in the potential low bandgap character of conjugated polymers incorporating **TzTz** building blocks.

Chapter 5 explores the design and synthesis of **TzTz** compounds in somewhat more detail and describes the synthesis of 4-cyanophenyl-, 4-fluorophenyl- and 4-trifluoromethylphenyl-functionalized derivatives. Thermal and optical material properties of all compounds are studied by thermogravimetric analysis, differential scanning calorimetry, cyclic voltammetry and UV-vis spectroscopy. Theoretical calculations of UV-vis data and HOMO-LUMO levels demonstrate the benefits of a

coordinated theoretical-experimental approach. In order to probe their suitability for printable electronics, all materials are integrated *via* solution-processing in organic field-effect transistors (FETs). X-ray diffraction, atomic force microscopy and scanning electron microscopy studies are applied to provide knowledge on the relationship between the molecular structures, film morphologies and FET performances.

In **Chapter 6** all previously mentioned **TzTz** derivatives are extensively studied by detailed 1D/2D NMR spectroscopy, providing interesting input for chemical shift prediction software. To support the NMR shift assignment, theoretical calculations are conducted, demonstrating their high potential to predict chemical shifts for protons and carbon atoms liable to the influence of different electron donating and withdrawing effects.

Finally, **Chapter 7** presents the synthesis of a solution-processable low bandgap copolymer, **PCPDT-DTTzTz**, consisting of alternating **TzTz** and **CPDT** units. Thermal, optical and electrochemical features are investigated by thermogravimetric analysis, differential scanning calorimetry, X-ray diffraction, UV-vis spectroscopy and cyclic voltammetry. As high charge carrier mobilities are required for good photovoltaic performances, the polymer is integrated in thin-film transistors. In the end, the polymer is applied as an electron donor material in polymer:$PC_{71}BM$ organic solar cells. A large effect of extensive purification (by preparative size exclusion chromatography) on the solar cell performance is identified. Morphology features are explored by atomic force and transmission electron microscopy.

Chapter 2

A Three-Step Synthetic Approach to Asymmetrically Functionalized 4*H*-Cyclopenta[2,1-*b*:3,4-*b'*]dithiophenes[†]

A convenient and efficient three-step route toward both symmetrically and asymmetrically functionalized 4*H*-cyclopenta[2,1-*b*:3,4-*b'*]dithiophenes has been developed. Using this method a broad collection of functionalized bridged bithiophenes can smoothly be accessed. Starting from 3-bromo-2,2'-bithiophene, prepared by Kumada coupling of 2-thienylmagnesium bromide with 2,3-dibromothiophene under Pd(dppf)Cl_2 catalysis, lithiation and subsequent reaction with dialkyl ketones afforded (a)symmetrically dialkylated tertiary alcohol derivatives. By means of final Friedel-Crafts dehydration cyclization in sulfuric acid medium, these derivatives were converted to 4,4-dialkyl-4*H*-cyclopenta[2,1-*b*:3,4-*b'*]dithiophenes. Upon replacement of the dialkyl ketone reagent by ethyl levulinate, an ester-functionalized 4*H*-cyclopenta[2,1-*b*:3,4-*b'*]dithiophene was prepared, representing an attractive precursor for variously functionalized cyclopentadithiophene compounds.

[†] Van Mierloo, S.; Adriaensens, P. J.; Maes, W.; Lutsen, L.; Cleij, T. J.; Botek, E.; Champagne, B.; Vanderzande, D. J. *J. Org. Chem.* **2010**, *75*, 7202.

2.1. Introduction

During the last decades cyclopentadithiophenes have emerged as attractive building blocks for the development of novel materials. These heterocycles have for example been applied in the design of polymerization catalysts and conjugated polymers with various applications.[1–7] Cyclopentadienyl ligands fused with thiophene units have been investigated as structural subunits of homogeneous metallocene catalysts for the polymerization of 1-olefins, affording enhanced control over the polymer microstructure not achievable by traditional Ziegler-Natta catalysts.[1] On the other hand, cyclopentadithiophenes have become popular rigid precursors for polymeric (semi)conducting materials.[2–7] Zotti and others have extensively studied the optical, electrochemical and conducting properties of poly(cyclopentadithiophenes), immobilized on surfaces by electrochemical polymerization.[2,3] Such polymers could be applied as sensor systems when well-established supramolecular recognition elements (calixarenes or crown ethers) were appended.[2c,h,3f] Electrochromic polymers based on cyclopentadithiophenes have also been reported recently,[4] whereas conducting cyclopentadithiophene-based matrices for electrochemically controlled (DNA) delivery systems have been developed by the group of Cougnon and Pilard.[5]

Out of the six possible cyclopentadithiophene isomers, 4*H*-cyclopenta[2,1-*b*:3,4-*b'*]dithiophene has majorly been applied for the construction of conjugated polymer materials, whereas the 7*H*-cyclopenta[1,2-*b*:4,3-*b'*]dithiophene analogue has most often been used for the development of metallocene catalysts. The vast majority of 4*H*-cyclopenta[2,1-*b*:3,4-*b'*]dithiophene (CPDT) building blocks reported to date have been synthesized by rather laborious multistep procedures affording mostly symmetrically dialkylated cyclopentadithiophenes.[8] Consequently, finding a more economic, straightforward and versatile synthetic protocol would be beneficial and could also facilitate optimization of the CPDT-based material features. In this paper, a three-step pathway toward both symmetrically and asymmetrically substituted dialkyl-CPDTs and functional derivatives thereof is reported.

2.2. Results and Discussion

The first synthetic pathway toward the 4*H*-cyclopenta[2,1-*b*:3,4-*b'*]dithiophene isomer was reported in 1968 by Wynberg and co-workers, affording the parent CPDT **5** in a low overall yield.[8a] Although some improvements to this procedure have been made over the years, synthetic progress has been rather limited.[8b–g] More recently, Reynolds and Brzezinski described a three-step synthesis - one-pot double lithiation and iodination, oxidation and Ullmann coupling - toward 4*H*-cyclopenta[2,1-*b*:3,4-*b'*]dithiophen-4-one (**4**), the ketone analogue of the rigidly bridged bithiophene unit (Scheme 2.1).[8h] This cyclic ketone could subsequently be reduced with hydrazine according to a Huang-Minlon modification of the Wolff-Kischner procedure, as reported by Turner *et al.* (Scheme 2.1).[8i,j] Dialkylation at the methylene bridge (4-position) of the planar bithiophene unit, required for processability from solution, has been performed with various alkyl halides, either employing KOH in DMSO (Scheme 2.1)[8i,j] or by stepwise lithiation and alkylation.[2a,9]

The synthetic protocol as summarized in Scheme 2.1 represents the most efficient route toward dialkylated CPDTs to date and is hence applied frequently for the construction of CPDT-based materials. This state-of-the-art synthetic procedure can, however, be regarded as comparatively laborious and more suitable for symmetrically dialkylated CPDT derivatives.[9] This encouraged us to search for an alternative synthetic method, which would be applicable toward a wide range of CPDTs. The major goals were the ability to introduce, using one single straightforward approach, two *identical or different* alkyl chains simultaneously and to enable introduction of basic functional groups on these alkyl chains.

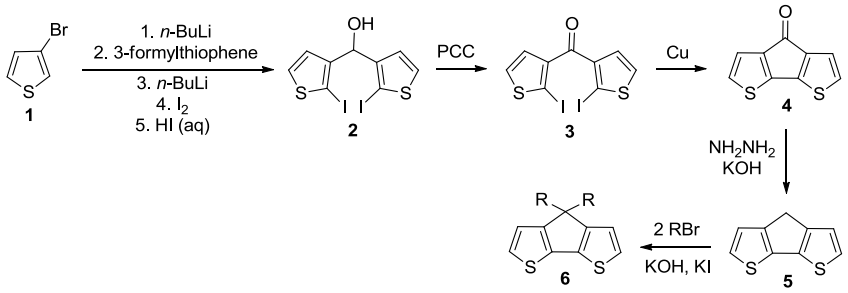

Scheme 2.1. State-of-the-art method toward dialkyl-CPDTs.[8h,i,j]

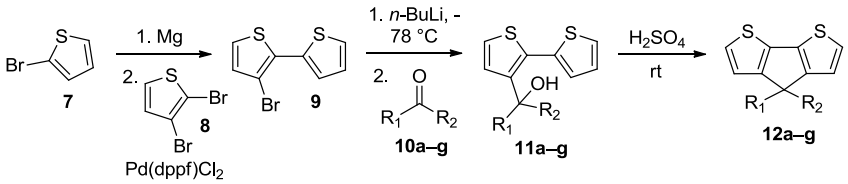

12a $R_1 = R_2$ = Et (55%), **12b** R_1 = Me, R_2 = Nonyl (16%), **12c** $R_1 = R_2$ = Isobutyl (35%), **12d** R_1 = Octyl, R_2 = 2-Ethylhexyl (57%), **12e** $R_1 = R_2$ = Pentyl (32%), **12f** $R_1 = R_2$ = Cy (40%), **12g** $R_1 = R_2$ = Octyl (53%)

Scheme 2.2. Novel synthetic route toward 4,4-dialkyl-4*H*-cyclopenta[2,1-*b*:3,4-*b'*]dithiophenes.

Our novel synthetic approach comprises three main steps, as depicted in Scheme 2.2. 4,4-Diethyl-*4H*-cyclopenta[2,1-*b*:3,4-*b'*]dithiophene (**12a**) was used as the model compound during this study, but the optimized procedures were readily extended to other (asymmetrically) dialkylated derivatives (*vide infra*). According to the reported protocol by Jüttner and co-workers,[10] 3-bromo-2,2'-bithiophene (**9**) was synthesized through a Kumada coupling of the Grignard reagent of 2-bromothiophene (**7**) with 2,3-dibromothiophene (**8**) under Pd(dppf)Cl_2 catalysis. The next step involved regiospecific formation of the lithio derivative by bromo-lithio exchange. The lithiated compound was then *in situ* reacted with 3-pentanone (1 equiv) affording tertiary alcohol derivative **11a**.[11] Subsequently, after tedious optimization of the ring closure conditions, an acid-catalyzed (H_2SO_4) cyclization reaction afforded the desired diethyl-CPDT **12a**.

To the best of our knowledge, there are no literature reports in which (Lewis) acid-catalyzed alkylative cyclization of bithiophene moieties toward 4*H*-cyclopenta[2,1-*b*:3,4-*b'*]dithiophenes has been performed.[12,13] Scherf *et al.* described a series of ring closure reactions promoted by borontrifluoride dietherate ($BF_3{\cdot}OEt_2$) toward thiophene-phenylene and thiophene-naphthalene step-ladder copolymers.[14] However, application of the same reaction conditions to tertiary alcohol derivative **11a** (Table 2.1, entry 1)

afforded majorly alkene *Z* and *E* isomers **13** and **14** by simple dehydration (Scheme 2.3). Under all tested reaction conditions (variation of the number of equiv of $BF_3{\cdot}OEt_2$ and the reaction time), formation of these alkene isomers remained dominant (Table 2.1, entries 1–4). Several attempts were carried out to perform the cyclization reaction with Brönsted acids. However, this effort did not lead to any noticeable improvement (Table 2.1, entries 5–9). Finally, efficient ring closure was achieved by means of addition of an excess of sulfuric acid (Table 2.1, entry 10). The as-formed orange solution was diluted with water and dichloromethane followed by extraction and, after purification of the crude oil by column chromatography, CPDT **12a** was obtained in a reasonable yield of 45%. A slightly higher yield (55%) could be achieved upon dilution of the reagents in *n*-octane (Table 2.1, entry 11), whereas addition of acetic acid afforded once more the alkene mixture (Table 2.1, entry 12). As an alternative Brönsted acid to promote cyclization, chromic acid could also be used (Table 2.1, entry 13).

Table 2.1. Tested (Lewis) acidic reaction conditions for the alkylative cyclization reaction toward CPDT **12a**.

entry	(Lewis) acid	equiv	reaction time (h)	solvent	*T* (°C)	**12a** (%)
1	$BF_3{\cdot}OEt_2$	159	3	CH_2Cl_2	rt	/[a]
2	$BF_3{\cdot}OEt_2$	80	2	CH_2Cl_2	rt	/[a]
3	$BF_3{\cdot}OEt_2$	80	3	CH_2Cl_2	rt	/[a]
4	$BF_3{\cdot}OEt_2$	1	12	CH_2Cl_2	rt	/[a]
5	HCl	8.5	4	AcOH	120	/[a]
6	HCl	8.5	12	AcOH	120	/[a]
7	HNO_3	12	12	/	rt	/[a]
8	*p*-TsOH	12	12	*n*-octane	rt	/[a]
9	H_3PO_4	12	12	/	rt	/[a]
10	H_2SO_4	12	12	/	rt	45[b]
11	H_2SO_4	12	12	*n*-octane	rt	55[b]
12	H_2SO_4	12	2	AcOH	80	/[a]
13	H_2CrO_4	12	12	/	rt	35[b]

[a] Mainly a mixture of **13** and **14**, sometimes accompanied by small amounts of **12a**. [b] No remaining alkene isomers.

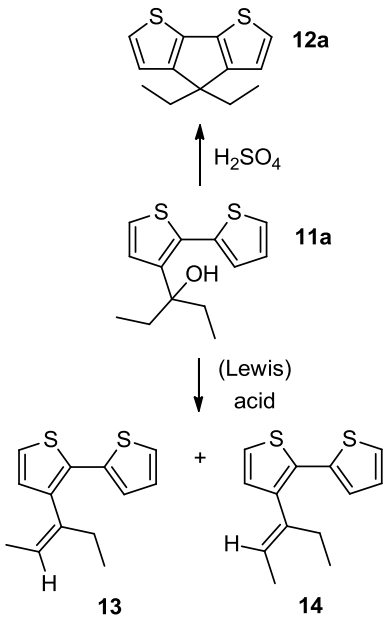

Scheme 2.3. Ring closure *vs.* alkene formation.

It can be assumed that after dehydration the formed alkene *Z* and *E* isomers **13** and **14** undergo protonation of the double bond and subsequent intramolecular alkylation (Scheme 2.3). Several test reactions indicated that immediate work-up after addition of sulfuric acid to the alcohol derivative **11a** afforded alkene isomers **13** and **14**. On the other hand, all traces of alkenes were converted into ring closed CPDT **12a** after one hour. Treatment of the isolated alkene mixture with H_2SO_4 also afforded **12a**. Summarizing these observations, the cyclization seems to be thermodynamically controlled with the CPDT as the thermodynamic sink. To support this interpretation, theoretical calculations on the alkene isomers and diethyl-CPDT **12a** were carried out. At the MP2/6–311+G** level of approximation, the ring closed structure was found to be about 8–9 kcal/mol more stable than the alkene-containing species. As shown in Figure 2.1, compound **12a** is planar whereas large deviations from planarity are observed for the alkenes. The two alkene stereoisomers **13** and **14** could not readily be separated resulting in complex NMR spectra for the alkene mixture. The intensity difference of the signals due to the ratio of the two isomers enabled the distinction of the signals for each isomer, *i.e.* one isomer was formed in 35%, whereas the other was formed in 65%.[15]

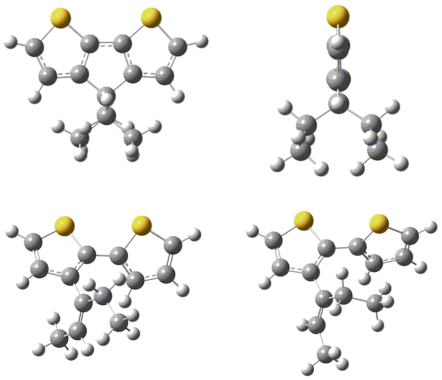

Figure 2.1. Optimized structures of CPDT **12a** (top; front and side view) and alkenes **13** and **14** (bottom).

Complete assignment of the proton and carbon resonances was accomplished by a combination of 2D-HETCOR and one dimensional NMR techniques (^{1}H, ^{13}C, DEPT and APT). All chemical shift data of both isomers could be collected, but since they were not separable, NOE(-dif) experiments were required to establish a clear distinction. Two datasets were acquired in one of which selective preirradiation was applied. In Figure 2.2 only the part of the spectra is shown which changed in intensity. Upon preirradiation at 1.47 ppm, saturating the methyl protons (H_7) of the isomer found in the biggest amount, NOE enhancement was observed for the β-thienyl proton (H_3) at 6.77 ppm (Figure 2.2). This gave a first indication that *Z* isomer **13** is formed in excess resulting in the highest peak intensities. In addition, NOE enhancement was also observed for the vinyl proton (H_6) at 5.62 ppm (Figure 2.2). Upon preirradiation at 5.57 ppm, saturating the resonance corresponding to the vinyl proton (H_6) of the isomer formed in the smallest amount, NOE enhancement was observed for the β-thienyl proton (H_3) at 6.85 ppm (Figure 2.2). This confirmed that the *Z* alkene **13** is majorly formed, whereas the *E* isomer **14** is produced in smaller amounts. In addition, NOE enhancement was also observed for the methyl protons (H_7) at 1.74 ppm. No further NOE's were observed.

Hence, *Z* alkene **13** was formed in 65%, whereas the *E* alkene **14** represented only 35%. This observation might indicate that the *Z* alkene is slightly more thermodynamically stable than the *E* alkene.

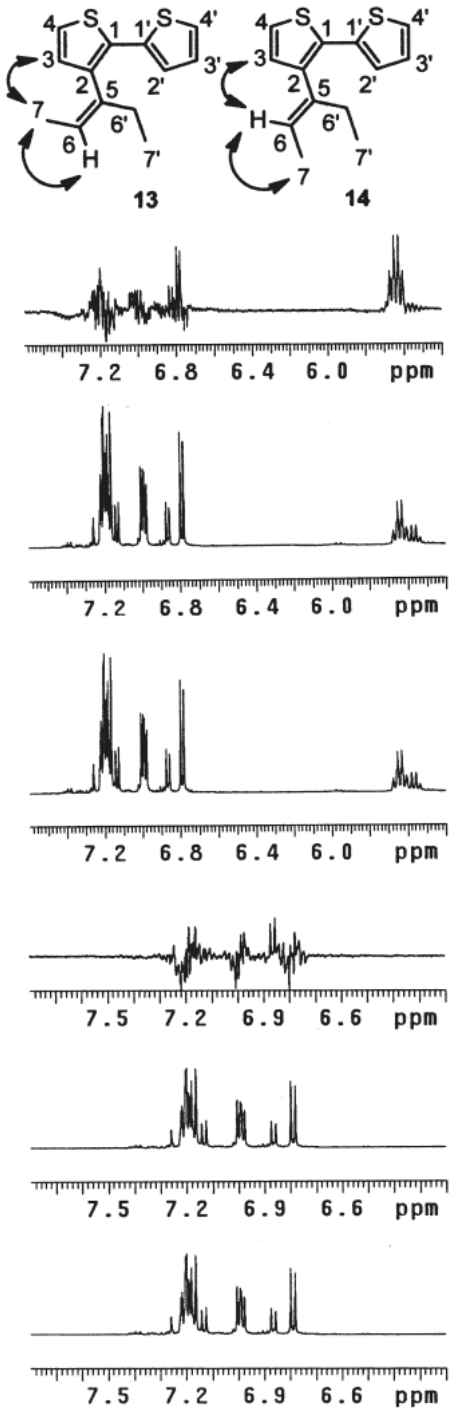

Figure 2.2. NOE spectra for the mixture of alkene isomers **13** and **14**: preirradiation at 1.47 ppm (top) and 5.57 ppm (bottom) – (control) spectrum without preirradiation (bottom), NOE spectrum (middle) and difference spectrum (top).

These results were also confirmed by theoretical ΔG calculations. Using the MP2/6–311+G** method and accounting for solvent effects (AcOH), a slightly lower energy (by 1 kcal/mol) was found for *Z* alkene **13** as compared to *E* alkene **14**. This difference in favor of the *Z* form is attributed to the important deviation from planarity, *i.e.* to the larger inter-thiophene-ring dihedral angle (S_1-C_5-C_9-S_{10}) of the *E* form and the larger distortion of its double bond planarity (C_4-C_6=C_{14}-R_{15} and C_4-C_6=C_{14}-R'_{16}), resulting in a slightly larger C_6=C_{14} bond length (Figure 2.1, Table 2.2).

Table 2.2. Selected optimized parameters for *Z* alkene **13** and *E* alkene **14**.

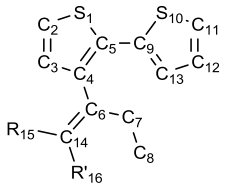

parameters	*Z*: R=Me, R'=H (**13**)	*E*: R=H, R'=Me (**14**)
bond lengths (Å)		
C_5-C_9	1.454	1.458
C_4-C_6	1.483	1.481
C_6-C_7	1.514	1.520
C_6=C_{14}	1.351	1.354
C_{14}-R_{15}	1.504	1.091
C_{14}-R'_{16}	1.089	1.502
torsion angles (°)		
S_1-C_5-C_9-S_{10}	50.6	73.4
C_6-C_4=C_5-C_9	5.0	8.7
C_3-C_4-C_6=R_{14}	67.8	56.2
C_{14}=C_6-C_7-R_8	6.0	71.0
C_4-C_6=C_{14}-R_{15}	3.6	5.1
C_4-C_6=C_{14}-R'_{16}	178.0	185.0

The main advantages of the presented route compared to the traditionally applied route are the shortened straightforward sequence and the ability to synthesize different materials simply by changing the ketone reagent applied in the formation of the tertiary alcohol. In this way a number of dialkylated CPDTs **12b–g**, both symmetrical and asymmetrical derivatives, have been prepared. Reaction with the dialkyl ketone and ring closure both proceeded in moderate to good yields (18–75% for **11a–g**, 16–57%

for **12a**–**g**). Once again, the yield for the cyclization step could be improved by dilution of the alcohol precursor in *n*-octane (from 17% to 57% for **12d**, from 30% to 53% for **12g**).[16]

The newly developed three-step procedure also readily allows introduction of functional groups on (one of) the alkyl substituents based upon a versatile ester-functionalized CPDT scaffold. Reaction of the lithio derivative of 3-bromo-2,2'-bithiophene (**9**) with ethyl levulinate (ethyl 4-oxopentanoate **15**) afforded lactone **16** by intramolecular transesterification of the intermediate tertiary alcohol with the terminal ethyl ester moiety (Scheme 2.4). Ring opening of the lactone in ethanol under acid-catalyzed conditions resulted in alkene isomers **17** and **18** (25:75 ratio), which were converted to ester-functionalized CPDT **12h** with the aid of sulfuric acid (Scheme 2.4). Starting from this ester derivative (or, alternatively, the lactone precursor), basic functional group conversions (or lactone ring opening reactions) should enable access to variously substituted CPDT building blocks.

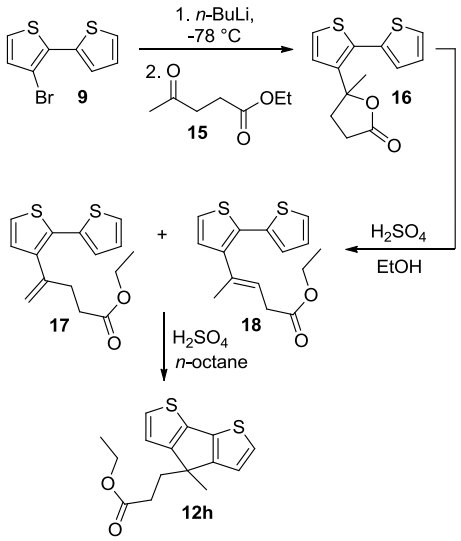

Scheme 2.4. Synthetic strategy toward ester-functionalized CPDT **12h**.

2.3. Conclusions

In summary, we have designed an elegant and convenient approach toward 4*H*-cyclopenta[2,1-*b*:3,4-*b'*]dithiophenes, shortening the currently applied route while

concomitantly extending its synthetic possibilities. Simple variation of the ketone reagent opens new perspectives in the synthesis of (asymmetrically) functionalized CPDT derivatives, and the final ring closing step was optimized. The functionalization scope can be extended further by a versatile ester-functionalized CPDT scaffold. Experimental observations on the plausible reaction pathway have been supported by detailed NMR spectroscopy and theoretical energy calculations.

2.4. Experimental Section

NMR chemical shifts (δ) in ppm were determined relative to the residual $CHCl_3$ absorption (7.26 ppm) or the ^{13}C resonance shift of $CDCl_3$ (77.16 ppm).[17] Gas chromatography-mass spectrometry (GC-MS) analyses were carried out applying Chrompack Cpsil5CB or Cpsil8CB capillary columns. Exact mass measurements were performed in the EI mode at a resolution of 10000. Solution UV-vis absorption measurements were performed with a scan rate of 600 nm/min in a continuous run from 200 to 800 nm. Infrared spectra were collected with a resolution of 4 cm^{-1} (16 scans) using films drop-casted on a NaCl disk from a $CHCl_3$ solution. Unless stated otherwise, all reagents and chemicals were obtained from commercial sources and used without further purification. Diethyl ether was dried by distillation from Na/benzophenone.

3-Bromo-2,2'-bithiophene (**9**) was synthesized according to a literature procedure.[10] Material identity and purity was confirmed by MS, IR, ^1H and ^{13}C NMR.

5-Ethylpentadecan-7-one (10d): A Grignard solution of 2-ethylhexylmagnesium bromide in dry diethyl ether (1.0 M, 110 mL, 0.11 mol) was slowly added via a syringe to a stirred mixture of *n*-octylcyanide (4.66 g, 55 mmol) in dry diethyl ether (100 mL) at 0 °C under N_2 atmosphere. After stirring for 12 h at reflux temperature, the reaction was quenched with an aqueous HCl solution (2.0 M) at 0 °C and subsequently vigorously stirred for an additional 3 h at rt. The organic phase was separated and the aqueous phase was extracted with diethyl ether. The combined organic phases were washed with a saturated bicarbonate solution and brine, dried with $MgSO_4$ and evaporated under reduced pressure to give a yellow oil. The crude oil was purified by vacuum distillation (75 °C, 10^{-2} mbar) resulting in a pure slightly yellow oil (4.51 g, 32%); GC-MS (EI) *m/z* 254 [M^+]; HRMS (EI) calcd for $C_{17}H_{34}O$: 254.2610; found: *m/z*

254.2612; ^{1}H NMR (300 MHz, $CDCl_3$) δ 2.37 (t, J = 7.5 Hz, 2H), 2.30 (d, J = 6.6 Hz, 2H), 1.89–1.81 (m, 1H), 1.60–1.53 (m, 2H), 1.26–1.18 (m, 18H), 0.91–0.81 (m, 9H); ^{13}C NMR (75 MHz, $CDCl_3$) δ 212.0 (CO), 47.6 (CH_2), 43.5 (CH_2), 35.3 (CH), 33.3 (CH_2), 32.0 (CH_2), 29.6 (CH_2), 29.4 (CH_2), 29.3 (CH_2), 29.0 (CH_2), 26.5 (CH_2), 24.0 (CH_2), 23.1 (CH_2), 22.8 (CH_2), 14.2 (CH_3), 11.0 (CH_3), 10.9 (CH_3); IR (NaCl, cm^{-1}) ν_{max} 2959/2926/2859 (s, saturated C-H), 1717 (m, CO).

3-([2,2'-Bithiophen]-3-yl)pentan-3-ol (11a): General Procedure 1: A solution of 3-bromo-2,2'-bithiophene (**9**) (3.0 g, 12 mmol) in dry diethyl ether (100 mL) was added slowly to a solution of *n*-BuLi (1.6 M in hexane, 7.5 mL, 12 mmol) in dry diethyl ether (100 mL) at -78 °C over 2 h under N_2. The mixture was stirred for 15 min at the same temperature. Freshly distilled 3-pentanone (1.29 mL, 12 mmol) was added via a syringe to the mixture at -78 °C, followed by stirring overnight at rt. The reaction was quenched with an aqueous NH_4Cl solution (2.5 M) and water at 0 °C. The organic phase was separated and the aqueous phase was extracted with diethyl ether. The combined organic phases were washed with brine, dried with $MgSO_4$ and concentrated under reduced pressure to give a crude oil. The oily residue was purified by column chromatography (silica, eluent hexane/ethyl acetate 90:10) to afford the title compound as a slightly yellow oil (1.7 g, 56%). GC-MS (EI) *m/z* 252 [M^+]; HRMS (EI) calcd for $C_{13}H_{16}OS_2$: 252.0643; found: *m/z* 252.0652; ^{1}H NMR (300 MHz, $CDCl_3$) δ 7.37 (dd, J = 5.0/1.2 Hz, 1H), 7.26 (d, J = 5.4 Hz, 1H), 7.13 (dd, J = 3.4/1.2 Hz, 1H), 7.03 (dd, J = 5.0/3.4 Hz, 1H), 6.98 (d, J = 5.4 Hz, 1H), 2.01 (s, 1H), 1.82–1.69 (m, 4H), 0.83 (t, J = 7.4 Hz, 6H); ^{13}C NMR (75 MHz, $CDCl_3$) δ 144.8, 135.6, 129.5 (CH), 129.2, 128.4 (CH), 127.3 (CH), 126.9 (CH), 125.0 (CH), 78.8 (C-OH), 35.3 (CH_2), 8.3 (CH_3); IR (NaCl, cm^{-1}) ν_{max} 3584 (w, OH), 3105/3073 (w, unsaturated C-H), 2966/2931/2877/2854 (m, saturated C-H).

2-([2,2'-Bithiophen]-3-yl)undecan-2-ol (11b): According to general procedure 1: 3-Bromo-2,2'-bithiophene (**9**) (1.00 g, 4.08 mmol), dry diethyl ether (70 mL), *n*-BuLi (1.6 M in hexane, 2.50 mL, 4.0 mmol) and 2-undecanone (0.84 mL, 4.08 mmol); eluent hexane/ethyl acetate 90:10; Yield 63% (0.86 g); GC-MS (EI) *m/z* 336 [M^+]; HRMS (EI) calcd for $C_{19}H_{28}OS_2$: 336.1582; found: *m/z* 336.1583; ^{1}H NMR (300 MHz, $CDCl_3$) δ 7.37 (dd, J = 5.1/1.1 Hz, 1H), 7.24 (d, J = 5.4 Hz, 1H), 7.14 (dd, J = 3.5/1.1 Hz, 1H), 7.07 (d, J = 5.4 Hz, 1H), 7.03 (dd, J = 5.1/3.5 Hz, 1H), 2.12 (s, 1H), 1.82–1.68 (m, 2H),

1.51 (s, 3H), 1.28–1.15 (m, 14H), 0.89 (t, *J* = 6.6 Hz, 3H); ^{13}C NMR (75 MHz, $CDCl_3$) δ 146.8, 135.6, 129.5 (CH), 129.0, 128.1 (CH), 127.2 (CH), 126.9 (CH), 124.8 (CH), 75.2 (C-OH), 44.0 (CH_2), 32.0 (CH_2), 30.4 (CH_2), 30.0 (CH_2), 29.6 (CH_2), 29.4 (CH_2), 24.3 (CH_2), 22.8 (CH_2), 14.2 (CH_3); IR (NaCl, cm^{-1}) ν_{max} 3451 (m, OH), 3105/3087/3074 (w, unsaturated C-H), 2955/2925/2854 (s, saturated C-H).

4-([2,2'-Bithiophen]-3-yl)-2,6-dimethylheptan-4-ol (11c): According to general procedure 1: 3-Bromo-2,2'-bithiophene (**9**) (3.00 g, 12 mmol), dry diethyl ether (200 mL), *n*-BuLi (1.6 M in hexane, 7.50 mL, 12 mmol), 2,6-dimethyl-4-heptanone (2.17 mL, 12 mmol); eluent hexane/ethyl acetate 90:10; Yield 18% (0.67 g); GC-MS (EI) *m/z* 308 [M^+]; HRMS (EI) calcd for $C_{17}H_{24}OS_2$: 308.1269; found: *m/z* 308.1264; ^{1}H NMR (300 MHz, $CDCl_3$) δ 7.37 (dd, *J* = 5.2/1.3 Hz, 1H), 7.25 (d, *J* = 5.3 Hz, 1H), 7.10 (dd, *J* = 3.6/1.3 Hz, 1H), 7.03 (dd, *J* = 5.2/3.6 Hz, 1H), 7.02 (d, *J* = 5.3 Hz, 1H), 1.92 (s, 1H), 1.80–1.64 (m, 4H), 1.57–1.50 (m, 2H), 0.91 (d, *J* = 6.3 Hz, 6H), 0.71 (d, *J* = 6.6 Hz, 6H); ^{13}C NMR (75 MHz, $CDCl_3$) δ 145.7, 135.6, 129.5 (CH), 128.8 (CH), 128.4, 127.3 (CH), 126.8 (CH), 124.9 (CH), 79.3 (C-OH), 52.7 (CH_2), 24.6 (CH_3), 24.4 (CH_3); IR (NaCl, cm^{-1}) ν_{max} 3587 (m, OH), 3106/3074 (w, unsaturated C-H), 2955/2928/2868 (s, saturated C-H).

7-([2,2'-Bithiophen]-3-yl)-5-ethylpentadecan-7-ol (11d): According to general procedure 1: 3-Bromo-2,2'-bithiophene (**9**) (1.00 g, 4.08 mmol), dry diethyl ether (70 mL), *n*-BuLi (1.6 M in hexane, 2.50 mL, 4.08 mmol), 5-ethylpentadecan-7-one (**10d**) (1.00 g, 4.08 mmol); eluent gradient hexane to hexane/ethyl acetate 90:10; Yield 34% (0.583 g); GC-MS (EI) *m/z* 420 [M^+]; HRMS (EI) calcd for $C_{25}H_{40}OS_2$: 420.2521; found: *m/z* 420.2492; ^{1}H NMR (300 MHz, $CDCl_3$) δ 7.37 (dd, *J* = 5.2/1.2 Hz, 1H), 7.24 (d, *J* = 5.3 Hz, 1H), 7.10 (dd, *J* = 3.5/1.2 Hz, 1H), 7.02 (dd, *J* = 5.2/3.5 Hz, 1H), 6.97 (d, *J* = 5.3 Hz, 1H), 1.93 (s, OH), 1.77–1.58 (m, 4H), 1.44–1.05 (m, 21H), 0.89–0.69 (m, 9H); ^{13}C NMR (75 MHz, $CDCl_3$) δ 145.7, 135.7, 129.5 (CH), 128.7, 128.5 (CH), 127.3 (CH), 126.8 (CH), 124.9 (CH), 78.8 (C-OH), 47.7 (CH_2), 43.4 (CH_2), 34.7 (CH), 33.9 (CH_2), 32.0 (CH_2), 29.7 (CH_2), 29.4 (CH_2), 28.7 (CH_2), 27.1 (CH_2), 23.7 (CH_2), 23.22 (CH_2), 23.16 (CH_2), 22.8 (CH_2), 14.2 (CH_3), 10.7 (CH_3), 10.6 (CH_3); IR (NaCl, cm^{-1}) ν_{max} 3589/3490 (m, OH), 3105/3073 (w, unsaturated C-H), 2956/2926/2856 (s, saturated C-H).

6-([2,2'-Bithiophen]-3-yl)undecan-6-ol (11e): According to general procedure 1: 3-Bromo-2,2'-bithiophene (**9**) (0.500 g, 2.04 mmol), dry diethyl ether (40 mL), *n*-BuLi (1.6 M in hexane, 1.25 mL, 2.04 mmol), 6-undecanone (0.42 mL, 2.04 mmol); eluent hexane/ethyl acetate 90:10; Yield 62% (0.425 g); GC-MS (EI) *m/z* 336 [M^+]; HRMS (EI) calcd for $C_{19}H_{28}OS_2$: 336.1582; found: *m/z* 336.1580; ^{1}H NMR (300 MHz, $CDCl_3$) δ 7.37 (d, *J* = 5.2/1.3 Hz, 1H), 7.25 (d, *J* = 5.4 Hz, 1H), 7.10 (dd, *J* = 3.5/1.3 Hz, 1H), 7.02 (dd, *J* = 5.2/3.5 Hz, 1H), 6.99 (d, *J* = 5.4 Hz, 1H), 1.80–1.59 (m, 4H), 1.26–1.16 (m, 12H), 0.85 (t, *J* = 7.1 Hz, 6H); ^{13}C NMR (75 MHz, $CDCl_3$) δ 145.5, 135.6, 129.4 (CH), 128.7, 128.4 (CH), 127.3 (CH), 126.8 (CH), 124.9 (CH), 78.2 (C-OH), 43.1 (CH_2), 32.3 (CH_2), 23.5 (CH_2), 22.7 (CH_2), 14.2 (CH_3); IR (NaCl, cm^{-1}) ν_{max} 3584/3474 (m, OH), 3104/3073 (w, unsaturated C-H), 2954/2929/2859 (s, saturated C-H).

1-([2,2'-Bithiophen]-3-yl)cyclohexanol (11f): According to general procedure 1: 3-Bromo-2,2'-bithiophene (**9**) (0.50 g, 2.04 mmol), dry diethyl ether (40 mL), *n*-BuLi (1.6 M in hexane, 1.25 mL, 2.04 mmol), cyclohexanone (0.21 mL, 2.04 mmol); eluent hexane/ethyl acetate 90:10; Yield 49% (0.264 g); GC-MS (EI) *m/z* 264 [M^+]; HRMS (EI) calcd for $C_{14}H_{16}OS_2$: 264.0643; found: *m/z* 264.0648; ^{1}H NMR (300 MHz, $CDCl_3$) δ 7.37 (dd, *J* = 5.2/1.2 Hz, 1H), 7.24 (d, *J* = 5.4 Hz, 1H), 7.18 (dd, *J* = 3.6/1.2 Hz, 1H), 7.11 (d, *J* = 5.4 Hz, 1H), 7.04 (dd, *J* = 5.2/3.6 Hz, 1H), 1.87–1.82 (m, 4H), 1.70-1.50 (m, 6H); ^{13}C NMR (75 MHz, $CDCl_3$) δ 147.7, 136.0, 130.0, 129.5 (CH), 127.6 (CH), 127.2 (CH), 127.0 (CH), 124.9 (CH), 73.5 (C-OH), 39.0 (CH_2), 25.5 (CH_2), 22.1 (CH_2); IR (NaCl, cm^{-1}) ν_{max} 3553/3441 (m, OH), 3104 (w, unsaturated C-H), 2932/2851 (s, saturated C-H).

9-([2,2'-Bithiophen]-3-yl)heptadecan-9-ol (11g): According to general procedure 1: 3-Bromo-2,2'-bithiophene (**9**) (5.00 g, 20 mmol), dry diethyl ether (340 mL), *n*-BuLi (1.6 M in hexane, 12.8 mL, 20 mmol), heptadecan-9-one (5.08 g, 20 mmol); eluent gradient hexane to hexane/ethyl acetate (90:10); Yield 75% (6.3 g); GC-MS (EI) *m/z* 420 [M^+]; HRMS (EI) calcd for $C_{25}H_{40}OS_2$: 420.2521; found: *m/z* 420.2521; ^{1}H NMR (300 MHz, $CDCl_3$) δ 7.37 (dd, *J* = 5.2/1.1 Hz, 1H), 7.24 (d, *J* = 5.3 Hz, 1H), 7.10 (dd, *J* = 3.5/1.1 Hz, 1H), 7.02 (dd, *J* = 5.3/3.5 Hz, 1H), 7.00 (d, *J* = 5.3 Hz, 1H), 1.98 (s, 1H), 1.78–1.63 (m, 4H) 1.31–1.14 (m, 24H), 0.87 (t, *J* = 6.6 Hz, 6H); ^{13}C NMR (75 MHz, $CDCl_3$) δ 145.6, 135.6, 129.4 (CH), 128.7, 128.4 (CH), 127.3 (CH), 126.8 (CH), 124.9 (CH), 78.2 (C-OH), 43.1 (CH_2), 32.0 (CH_2), 30.1 (CH_2), 29.7 (CH_2), 29.4 (CH_2), 23.8

(CH_2), 22.8 (CH_2), 14.3 (CH_3); IR (NaCl, cm^{-1}) ν_{max} 3588/3483 (m, OH), 3105/3073 (w, unsaturated C-H), 2954/2925/2854 (s, saturated C-H).

4,4-Diethyl-4*H*-cyclopenta[2,1-*b*:3,4-*b'*]dithiophene (12a): General Procedure 2: H_2SO_4 (0.5 mL) was added dropwise to 3-([2,2'-bithiophen]-3-yl)pentan-3-ol (**11a**) (0.193 g, 0.77 mmol) in *n*-octane (10 mL) under stirring at rt. After additional stirring for 12 h, CH_2Cl_2 and water were added. The organic layer was separated and the aqueous layer was extracted with CH_2Cl_2. The combined organic extracts were successively washed with saturated $NaHCO_3$ and brine. After drying with $MgSO_4$, the solvent was removed *in vacuo*. The crude oil was purified by column chromatography (silica, eluent hexane) to afford a pure dark yellow oil (0.10 g, 55%). GC-MS (EI) *m/z* 234 [M^+]; HRMS (EI) calcd for $C_{13}H_{14}S_2$: 234.0537; found: *m/z* 234.0546; ^{1}H NMR (300 MHz, $CDCl_3$) δ 7.17 (d, J = 5.0 Hz, 2H), 6.94 (d, J = 5.0 Hz, 2H), 1.91 (q, J = 7.7 Hz, 4H), 0.60 (t, J = 7.7 Hz, 6H); ^{13}C NMR (75 MHz, $CDCl_3$) δ 157.5, 136.9, 124.6 (CH), 121.7 (CH), 54.4, 30.3 (CH_2), 9.2 (CH_3); IR (NaCl, cm^{-1}) ν_{max} 3423 (m, OH), 3102/3070 (w, unsaturated C-H), 2964/2929/2874/2853 (s, saturated C-H); UV-vis ($CHCl_3$, nm) λ_{max} (log ε) 249 (3.880), 320 (4.115).

4-Methyl-4-nonyl-4*H*-cyclopenta[2,1-*b*:3,4-*b'*]dithiophene (12b): According to general procedure 2: H_2SO_4 (1.33 mL), 2-([2,2'-bithiophen]-3-yl)undecan-2-ol (**11b**) (0.70 g, 2.08 mmol); eluent hexane; Yield 16% (0.106 g); GC-MS (EI) *m/z* 318 [M^+]; HRMS (EI) calcd for $C_{19}H_{26}S_2$: 318.1476; found: *m/z* 318.1472; ^{1}H NMR (300 MHz, $CDCl_3$) δ 7.15 (d, J = 4.9 Hz, 2H), 6.96 (d, J = 4.9 Hz, 2H), 1.84–1.78 (m, 2H), 1.43 (s, 3H), 1.26–1.15 (m, 14H), 0.86 (t, J = 6.9 Hz, 3H); ^{13}C NMR (75 MHz, $CDCl_3$) δ 159.5, 136.0, 124.8 (CH), 121.4 (CH), 49.0, 39.2 (CH_2), 32.0 (CH_2), 30.1 (CH_2), 29.7 (CH_2), 29.6 (CH_2), 29.4 (CH_2), 25.1 (CH_2), 23.9 (CH_2), 22.8 (CH_3), 14.3 (CH_3); IR (NaCl, cm^{-1}) ν_{max} 3103/3069 (w, unsaturated C-H), 2955/2925/2854 (s, saturated C-H); UV-vis ($CHCl_3$, nm) λ_{max} (log ε) 249 (3.819), 320 (4.007).

4,4-Diisobutyl-4*H*-cyclopenta[2,1-*b*:3,4-*b'*]dithiophene (12c): According to general procedure 2: H_2SO_4 (1.45 mL), 4-([2,2'-bithiophen]-3-yl)-2,6-dimethylheptan-4-ol (**11c**) (0.688 g, 2.23 mmol); eluent hexane; Yield 35% (0.226 g); GC-MS (EI) *m/z* 290 [M^+]; HRMS (EI) calcd for $C_{17}H_{22}S_2$: 290.1163; found: *m/z* 290.1168; ^{1}H NMR (300 MHz, $CDCl_3$) δ 7.14 (d, J = 4.9 Hz, 2H), 6.93 (d, J = 4.9 Hz, 2H), 1.87 (d, J = 5.7 Hz, 4H), 1.05–0.97 (m, 2H), 0.51 (d, J = 6.8 Hz, 12H); ^{13}C NMR (75 MHz, $CDCl_3$) δ

157.9, 136.8, 124.5 (CH), 122.1 (CH), 53.2, 48.8 (CH), 24.9 (CH_2), 24.6 (CH_3); IR (NaCl, cm^{-1}) ν_{max} 3104/3067 (w, unsaturated C-H), 2954/2925/2867 (s, saturated C-H); UV-vis ($CHCl_3$, nm) λ_{max} (log ε) 249 (3.932), 320 (4.094).

4-(2-Ethylhexyl)-4-octyl-4*H*-cyclopenta[2,1-*b*:3,4-*b'*]dithiophene (12d): According to general procedure 2: H_2SO_4 (0.38 mL), 7-([2,2'-bithiophen]-3-yl)-5-ethylpentadecan-7-ol (**11d**) (0.25 g, 0.60 mmol); eluent hexane; Yield 17% (0.040 g) or H_2SO_4 (0.38 mL), 7-([2,2'-bithiophen]-3-yl)-5-ethylpentadecan-7-ol (**11d**) (0.25 g, 0.60 mmol), *n*-octane (8 mL); eluent hexane; Yield 57% (0.137 g); GC-MS (EI) *m/z* 402 [M^+]; HRMS (EI) calcd for $C_{25}H_{38}S_2$: 402.2415; found: *m/z* 402.2412; ^{1}H NMR (300 MHz, $CDCl_3$) δ 7.18 (d, *J* = 5.1 Hz, 2H), 7.02 (dd, *J* = 4.9/2.2 Hz, 2H), 2.02 (t, *J* = 7.5 Hz, 2H), 1.96–1.90 (m, 2H), 1.11–1.02 (m, 21H), 0.96 (t, *J* = 6.6 Hz, 3H), 0.87 (t, *J* = 6.9 Hz, 3H), 0.72 (t, *J* = 7.2 Hz, 3H); ^{13}C NMR (75 MHz, $CDCl_3$) δ 157.85, 157.79, 136.8, 124.3 (CH), 121.9 (CH), 53.3, 41.9 (CH), 39.7 (CH_2), 35.3 (CH_2), 34.2 (CH_2), 32.0 (CH_2), 30.2 (CH_2), 29.5 (CH_2), 29.4 (CH_2), 28.7 (CH_2), 27.4 (CH_2), 24.5 (CH_2), 22.9 (CH_2), 22.8 (CH_2), 14.3 (CH_3), 10.8 (CH_3); IR (NaCl, cm^{-1}) ν_{max} 3104/3068 (w, unsaturated C-H), 2957/2926/2855 (s, saturated C-H); UV-vis ($CHCl_3$, nm) λ_{max} (log ε) 249 (3.868), 320 (4.064).

4,4-Dipentyl-4*H*-cyclopenta[2,1-*b*:3,4-*b'*]dithiophene (12e): According to general procedure 2: H_2SO_4 (0.63 mL), 6-([2,2'-bithiophen]-3-yl)undecan-6-ol (**11e**) (0.33 g, 0.98 mmol); eluent hexane; Yield 32% (0.10 g); GC-MS (EI) *m/z* 318 [M^+]; HRMS (EI) calcd for $C_{19}H_{26}S_2$: 318.1476; found: *m/z* 318.1479; ^{1}H NMR (300 MHz, $CDCl_3$) δ 7.16 (d, *J* = 4.8 Hz, 2H), 6.96 (d, *J* = 4.8 Hz, 2H), 1.88–1.82 (m, 4H), 1.24–1.09 (m, 8H), 1.03–0.93 (m, 4H), 0.80 (t, *J* = 7.0 Hz, 6H); ^{13}C NMR (75 MHz, $CDCl_3$) δ 158.2, 136.6, 124.5 (CH), 121.7 (CH), 53.3, 37.8 (CH_2), 32.4 (CH_2), 24.3 (CH_2), 22.5 (CH_2), 14.2 (CH_3); IR (NaCl, cm^{-1}) ν_{max} 3103/3070 (w, unsaturated C-H), 2955/2929/2858 (s, saturated C-H); UV-vis ($CHCl_3$, nm) λ_{max} (log ε) 249 (3.918), 320 (4.114).

Spiro[4,5]([2,1-*b*:3,4-*b'*]dithieno)decane (12f): According to general procedure 2: H_2SO_4 (1.41 mL), 1-([2,2'-Bithiophen]-3-yl)cyclohexanol (**11f**) (0.582 g, 2.20 mmol), *n*-octane (30 mL); eluent hexane; Yield 40% (0.217 g); This compound has been prepared before by Zotti *et al.*[2g] Material identity and purity was confirmed by (HR)MS, IR, UV-vis, ^{1}H and ^{13}C NMR; HRMS (EI) calcd for $C_{14}H_{14}S_2$: 246.0537; found: *m/z* 246.0526; ^{13}C NMR (75 MHz, $CDCl_3$) δ 159.5, 135.9, 124.2 (CH), 122.8

(CH), 50.0, 34.2 (CH_2), 25.7 (CH_2), 23.8 (CH_2); IR (NaCl, cm^{-1}) ν_{max} 3102/3079 (w, unsaturated C-H), 2927/2853 (s, saturated C-H); UV-vis ($CHCl_3$, nm) λ_{max} (log ε) 249 (3.588), 320 (3.802).

4,4-Dioctyl-4*H*-cyclopenta[2,1-*b*:3,4-*b'*]dithiophene (12g): According to general procedure 2: H_2SO_4 (9.62 mL), 9-([2,2'-bithiophen]-3-yl)heptadecan-9-ol (**11g**) (6.32 g, 15 mmol); eluent hexane; Yield 30% (1.81 g) or H_2SO_4 (9.62 mL), 9-([2,2'-bithiophen]-3-yl)heptadecan-9-ol (**11g**) (6.32 g, 15 mmol), *n*-octane (200 mL); eluent hexane; Yield 53% (3.20 g). This compound has been prepared before by several groups.[2a,7i,8j] Material identity and purity was confirmed by MS, ^1H and ^{13}C NMR.

(*Z*)-3-(pent-2-en-3-yl)-2,2'-bithiophene (13): GC-MS (EI) *m/z* 234 [M^+]; HRMS (EI) calcd for $C_{13}H_{14}S_2$: 234.0537; found: *m/z* 234.0524; ^1H NMR (300 MHz, $CDCl_3$) δ 7.21 (dd, *J* = 5.1/1.3 Hz, 1H), 7.18 (dd, *J* = 3.7/1.3 Hz, 1H), 7.17 (d, *J* = 5.1 Hz, 1H), 6.99 (dd, *J* = 5.1/3.7 Hz, 1H), 6.79 (d, *J* = 5.1 Hz, 1H), 5.64 (q, *J* = 7.3 Hz, 1H), 2.28 (q, *J* = 6.9 Hz, 2H), 1.47 (d, *J* = 7.3 Hz, 3H), 1.01 (t, *J* = 6.9 Hz, 3H); ^{13}C NMR (75 MHz, $CDCl_3$) δ 138.2, 137.9, 136.7, 131.8, 130.3 (CH), 127.1 (CH), 125.1 (CH), 124.9 (CH), 123.9 (CH), 123.1 (CH), 31.2 (CH_2), 14.9 (CH_3), 13.0 (CH_3); IR (NaCl, cm^{-1}) ν_{max} 3105/3069 (w, unsaturated C-H), 2963/2926/2872/2854 (s, saturated C-H).

(*E*)-3-(pent-2-en-3-yl)-2,2'-bithiophene (14): GC-MS (EI) *m/z* 234 [M^+]; HRMS (EI) calcd for $C_{13}H_{14}S_2$: 234.0537; found: *m/z* 234.0524; ^1H NMR (300 MHz, $CDCl_3$) δ 7.21 (dd, *J* = 5.1/1.3 Hz, 1H), 7.17 (dd, *J* = 3.9/1.3 Hz, 1H), 7.13 (d, *J* = 5.2 Hz, 1H), 6.99 (dd, *J* = 5.1/3.9 Hz, 1H), 6.86 (d, *J* = 5.2 Hz, 1H), 5.57 (q, *J* = 7.0 Hz, 1H), 2.35 (q, *J* = 7.6 Hz, 2H), 1.76 (d, *J* = 7.0 Hz, 3H), 0.93 (t, *J* = 7.6 Hz, 3H); ^{13}C NMR (75 MHz, $CDCl_3$) δ 141.5, 137.4, 136.8, 131.2, 130.3 (CH), 126.9 (CH), 126.0 (CH), 125.8 (CH), 125.1 (CH), 123.0 (CH), 24.3 (CH_2), 14.3 (CH_3), 13.8 (CH_3); IR (NaCl, cm^{-1}) ν_{max} 3105/3069 (w, unsaturated C-H), 2963/2926/2872/2854 (s, saturated C-H).

5-([2,2'-Bithiophen]-3-yl)-5-methyldihydrofuran-2-(3*H*)-one (16): According to general procedure 1: 3-Bromo-2,2'-bithiophene (**9**) (1.00 g, 4.08 mmol), dry diethyl ether (70 mL), *n*-BuLi (1.6 M in hexane, 2.50 mL, 4.08 mmol), ethyl levulinate (**15**) (0.58 mL, 4.08 mmol); eluent CH_2Cl_2; Yield 36% (0.39 g); GC-MS (EI) *m/z* 264 [M^+]; HRMS (EI) calcd for $C_{13}H_{12}O_2S_2$: 264.0279; found: *m/z* 264.0255; ^1H NMR (300 MHz, $CDCl_3$) δ 7.41 (dd, *J* = 5.2/1.2 Hz, 1H), 7.28 (d, *J* = 5.4 Hz, 1H), 7.16 (d, *J* = 5.4 Hz, 1H), 7.11 (dd, *J* = 3.6/1.2 Hz, 1H), 7.06 (dd, *J* = 5.2/3.6 Hz, 1H), 2.60–2.15 (m, 4H),

1.70 (s, 3H); ^{13}C NMR (75 MHz, $CDCl_3$) δ 176.2 (CO), 142.7, 134.1, 130.0 (CH), 129.5, 127.5 (CH), 127.2 (CH), 125.6 (CH), 86.4, 35.1 (CH_2), 29.1 (CH_2), 29.0 (CH_3); IR (NaCl, cm^{-1}) ν_{max} 3106 (m, unsaturated C-H), 2977/2931 (m, saturated C-H), 1775 (s, CO-O lactone).

Ethyl 3-(4-methyl-4H-cyclopenta[2,1-*b*:3,4-*b'*]dithiophen-4-yl)propanoate (12h): H_2SO_4 (0.73 mL) was added dropwise to 5-([2,2'-bithiophen]-3-yl)-5-methyldihydrofuran-2-(3*H*)-one (**16**) (0.388 g, 1.47 mmol) in ethanol (20 mL) under stirring at rt and the reaction was continuously stirred for 12 h at rt. Work-up according to general procedure 2. The crude oily residue was purified by flash column chromatography (silica, eluent CH_2Cl_2) to afford a dark yellow oil (0.302 g, 70%). To the obtained crude alkene mixture (**17**:**18**, 25:75 ratio) (0.302 g, 1.0 mmol), H_2SO_4 (0.73 mL) and *n*-octane (15 mL) were added and the reaction was stirred for 12 h at rt. Work-up according to general procedure 2: eluent hexane/ethyl acetate 90:10; Yield 20% (60 mg); GC-MS (EI) *m/z* 292 [M^+]; HRMS (EI) calcd for $C_{15}H_{16}O_2S_2$: 292.0592; found: *m/z* 292.0572; ^{1}H NMR (300 MHz, $CDCl_3$) δ 7.16 (d, J = 5.0 Hz, 2H), 6.95 (d, J = 5.0 Hz, 2H), 3.98 (q, J = 7.2 Hz, 2H), 2.28 (t, J = 7.9 Hz, 2H), 1.80 (t, J = 7.9 Hz, 2H), 1.47 (s, 3H), 1.15 (t, J = 7.2 Hz, 3H); ^{13}C NMR (75 MHz, $CDCl_3$) δ 173.6 (CO), 157.8, 136.6, 125.3 (CH), 121.2 (CH), 60.3, 48.2 (CH_2), 33.7 (CH_2), 29.9 (CH_2), 24.2 (CH_3), 14.2 (CH_3); IR (NaCl, cm^{-1}) ν_{max} 3102/3070 (w, unsaturated C-H), 2974/2925/2869 (w, saturated C-H), 1731 (m, CO-O); UV-vis ($CHCl_3$, nm) λ_{max} (log ε) 320 (3.104).

2.5. Acknowledgments

The authors gratefully acknowledge the IWT (Institute for the Promotion of Innovation by Science and Technology in Flanders) for the financial support via the SBO-project 060843 "PolySpec". We also thank BELSPO in the frame of the IAP P6/27 network and the FWO (Fund for Scientific Research – Flanders) via the project G.0091.07N for their financial support. We further thank the EU for the FP6 Marie-Curie-RTN "SolarNtype" (MRTN-CT-2006-035533). E. B. thanks the IAP program N° P6-27 for her postdoctoral grant. The calculations were performed on the Interuniversity Scientific Computing Facility (iSCF), installed at the Facultés Universitaires Notre-Dame de la Paix (FUNDP, Belgium), for which the authors gratefully acknowledge the

financial support of the F.R.S.-FRFC for the convention n° 2.4.617.07.F and of the FUNDP.

2.6. References and Footnotes

(1) (a) Ewen, J. A.; Jones, R. L.; Elder, M. J.; Rheingold, A. L.; Liable-Sands, L. M. *J. Am. Chem. Soc.* **1998**, *120*, 10786. (b) De Rosa, C.; Auriemma, F.; Resconi, L. *Angew. Chem. Int. Ed.* **2009**, *48*, 9871. (c) Senda, T.; Hanaoka, H.; Okado, Y.; Oda, Y.; Tsurugi, H.; Mashima, K. *Organometallics* **2009**, *28*, 6915.

(2) (a) Zotti, G.; Schiavon, G.; Berlin, A.; Fontana, G.; Pagani, G. *Macromolecules* **1994**, *27*, 1938. (b) Benincori, T.; Brenna, E.; Sannicolo, F.; Trimarco, L.; Zotti, G.; Sozzani, P. *Angew. Chem. Int. Ed. Engl.* **1996**, *35*, 648. (c) Sannicolo, F.; Brenna, E.; Benincori, T.; Zotti, G.; Zecchin, S.; Schiavon, G.; Pilati, T. *Chem. Mater.* **1998**, *10*, 2167. (d) Berlin, A.; Zotti, G.; Shiavon, G.; Zecchin, S. *J. Am. Chem. Soc.* **1998**, *120*, 13453. (e) Zotti, G.; Zecchin, S.; Shiavon, G.; Berlin, A. *Macromolecules* **2001**, *34*, 3889. (f) Zotti, G.; Zecchin, S.; Berlin, A.; Shiavon, G.; Giro, G. *Chem. Mater.* **2001**, *13*, 43. (g) Benincori, T.; Consonni, V.; Gramatica, P.; Pilati, T.; Rizzo, S.; Sannicolo, F.; Todeschini, R.; Zotti, G. *Chem. Mater.* **2001**, *13*, 1665. (h) Rizzo, S.; Sannicolo, F.; Benincori, T.; Schiavon, G.; Zecchin, S.; Zotti, G. *J. Mater. Chem.* **2004**, *14*, 1804. (i) Zotti, G.; Vercelli, B.; Berlin, A. *Chem. Mater.* **2008**, *20*, 397.

(3) (a) Lambert, T. L.; Ferraris, J. P. *J. Chem. Soc., Chem. Commun.* **1991**, 752. (b) Brisset, H.; Thobie-Gautier, C.; Gorgues, A.; Jubault, M.; Roncali, J. *J. Chem. Soc., Chem. Commun.* **1994**, 1305. (c) Mills, C. A.; Taylor, D. M.; Murphy, P. J.; Dalton, C.; Jones, G. W.; Hall, L. M.; Hughes, A. V. *Synth. Met.* **1999**, *102*, 1000. (d) Kalaji, M.; Murphy, P. J.; Williams, G. O. *Synth. Met.* **1999**, *101*, 123. (e) Taylor, D. M.; William, S. *Synth. Met.* **2006**, *156*, 752. (f) Schmittel, M.; Lin, H. *J. Mater. Chem.* **2008**, *18*, 333.

(4) (a) Ko, H. C; Yom, J.; Moon, B.; Lee, H. *Electrochim. Acta* **2003**, *48*, 4127. (b) Wu, C.-G.; Lu, M.-I.; Chang, S.-J.; Wei, C.-S. *Adv. Funct. Mater.* **2007**, *17*, 1063. (c) Hou, J.; Zhang, S.; Chen, T. L.; Yang, Y. *Chem. Commun.* **2008**, 6034. (d) Wu, C.-G.; Lu, M.-I.; Tsai, P.-F. *Macromol. Chem. Phys.* **2009**, *210*, 1851.

(5) (a) Pilard, J.-F.; Cougnon, C.; Rault-Berthelot, J.; Berthelot, A.; Hubert, C.; Tran, K. *J. Electroanal. Chem.* **2004**, *568*, 195. (b) Gautier, C.; Cougnon, C.; Pilard, J.-F. *Electrochem. Commun.* **2006**, *8*, 1045. (c) Gautier, C.; Cougnon, C.; Pilard, J.-F.; Casse, N.; Chénais, B. *Anal. Chem.* **2007**, *79*, 7920. (d) Cougnon, C.; Gautier,

C.; Pilard, J.-F.; Casse, N.; Chénais, B. *Biosens. Bioelectron.* **2008**, *23*, 1171.

(6) A recent review article summarizes the wide variety of cyclopentadithiophene based electroactive materials: Coppo, P.; Turner, M. L. *J. Mater. Chem.* **2005**, *15*, 1123.

(7) (a) Asawapirom, U.; Scherf, U. *Macromol. Rapid Commun.* **2001**, *22*, 746. (b) Wu, C.-G.; Hsieh, C.-W.; Chen, D.-C.; Chang, S.-J.; Chen, K.-Y. *Synth. Met.* **2005**, *155*, 618. (c) Mühlbacher, D.; Scharber, M.; Morana, M.; Zhu, Z.; Waller, D.; Gaudiana, R.; Brabec, C. *Adv. Mater.* **2006**, *18*, 2884. (d) Zhang, M.; Tsao, H. N.; Pisula, W.; Yang, C.; Mishra, A. K.; Müllen, K. *J. Am. Chem. Soc.* **2007**, *129*, 3472. (e) Peet, J.; Kim, J. Y.; Coates, N. E.; Ma, W. L.; Moses, D.; Heeger, A. J.; Bazan, G. C. *Nat. Mater.* **2007**, *6*, 497. (f) De Cremer, L.; Vandeleene, S.; Maesen, M.; Verbiest, T.; Koeckelberghs, G. *Macromolecules* **2008**, *41*, 591. (g) Hou, J.; Chen, H.-Y.; Zhang, S.; Li, G.; Yang, Y. *J. Am. Chem. Soc.* **2008**, *130*, 16144. (h) Bijleveld, J. C.; Shahid, M.; Gilot, J.; Wienk, M. M.; Janssen, R. A. J. *Adv. Funct. Mater.* **2009**, *19*, 3262. (i) Jung, I. H.; Yu, J.; Jeong, E.; Kim, J.; Kwon, S.; Kong, H.; Lee, K.; Woo, H. Y.; Shim, H.-K. *Chem. Eur. J.* **2010**, *16*, 3743. (j) Horie, M.; Majewski, L. A.; Fearn, M. J.; Yu, C.-Y.; Luo, Y.; Song, A.; Saunders, B. R.; Turner, M. L. *J. Mater. Chem.* **2010**, *20*, 4347.

(8) Synthetic procedures toward CPDTs: (a) Kraak, A.; Wiersema, A. K.; Jordens, P.; Wynberg, H. *Tetrahedron* **1968**, *24*, 3381. (b) Jordens, P.; Rawson, G.; Wynberg, H. *J. Chem. Soc. C* **1970**, 273. (c) Wiersema, A.; Gronowitz, S. *Acta Chem. Scand.* **1970**, *24*, 2593. (d) Jeffries, A. T.; Moore, K. C.; Ondeyka, D. M.; Springsteen, A. W.; MacDowell, D. W. H. *J. Org. Chem.* **1981**, *46*, 2885. (e) Kozaki, M.; Tanaka, S.; Yamashita, Y. *J. Org. Chem.* **1994**, *59*, 442. (f) Beyer, R.; Kalaji, M.; Kingscote-Burton, G.; Murphy, P. J.; Pereira, V. M. S. C.; Taylor, D. M.; Williams, G. O. *Synth. Met.* **1998**, *92*, 25. (g) Lucas, P.; El Mehdi, N.; Ho, H. A.; Bélanger, D.; Breau, L. *Synthesis* **2000**, *9*, 1253. (h) Reynolds, J. R.; Brzezinski, J. Z. *Synthesis* **2002**, *8*, 1053. (i) Coppo, P.; Cupertino, D. C.; Yeates, S. G.; Turner, M. L. *J. Mater. Chem.* **2002**, *12*, 2597. (j) Coppo, P.; Cupertino, D. C.; Yeates, S. G.; Turner, M. L. *Macromolecules* **2003**, *36*, 2705. (k) Park, J. H.; Lee, B. Y. *Bull. Korean Chem. Soc.* **2010**, *31*, 1064.

(9) A few asymmetrically dialkylated CPDTs have been reported by Zotti *et al.* (ref. 2e,f,i).

(10) Harm, U.; Bürgler, R.; Fürbeth, W.; Mangold, K.-M.; Jüttner, K. *Macromol. Symp.* **2002**, *187*, 65.

(11) Abarca, B.; Asensio, G.; Ballesteros, R.; Varea, T. *J. Org. Chem.* **1991**, *56*, 3224.

(12) A spirodithiophenefluorene derivative in which the 7*H*-cyclopenta[1,2-*b*:4,3-*b'*]dithiophene isomeric structure can be recognized has been synthesized by Friedel-Crafts dehydration cyclization in a mixture of HCl and AcOH: Xie, L.-H.; Hou, X.-Y.; Hua, Y.-R.; Huang, Y.-Q.; Zhao, B.-M.; Liu, F.; Peng, B.; Wei, W.; Huang, W. *Org. Lett.* **2007**, *9*, 1619.

(13) (a) Qiu, S.; Lu, P.; Liu, X.; Shen, F.; Liu, L.; Ma, Y.; Shen, J. *Macromolecules* **2003**, *36*, 9823. (b) Wong, K.-T.; Chao, T.-C.; Chi, L.-C.; Chu, Y.-Y.; Balaiah, A.; Chiu, S.-F.; Liu, Y.-H.; Wang, Y. *Org. Lett.* **2006**, *8*, 5033.

(14) (a) Scherf, U.; Müllen, K. *Makromol. Chem., Rapid Commun.* **1991**, *12*, 489. (b) Scherf, U.; Bohnen, A.; Müllen, K. *Makromol. Chem.* **1992**, *193*, 1127. (c) Bünnagel, T. W.; Nehls, B. S.; Galbrecht, F.; Schottler, K.; Kudla, C. J.; Volk, M.; Pina, J.; Seixas de Melo, J. S.; Burrows, H. D.; Scherf, U. *J. Polym. Sci., Part A: Polym. Chem.* **2008**, *46*, 7342.

(15) The studied alkene mixture was obtained from the attempt to perform the cyclization with HCl in AcOH (Table 2.1, entry 6).

(16) Intermolecular reaction (oligomer formation) was observed as a minor side reaction by ESI-MS (less pronounced upon dilution).

(17) Gottlieb, H. E.; Kotlyar, V.; Nudelman, A. *J. Org. Chem.* **1997**, *62*, 7512.

2.7. Supporting Information

^{1}H and ^{13}C NMR spectra for all novel CPDTs and precursors, and complete NMR assignment of the proton and carbon resonances of alkene isomers **13** and **14** are available free of charge via the Internet at http://pubs.acs.org.

Details on the Computational Procedures

Quantum chemical calculations were carried out in a three-step procedure. First, geometry optimizations were carried out at the DFT level using the B3LYP exchange-correlation functional and the 6-311+G** basis set. The vibrational normal modes and frequencies were then determined to perform a thermodynamics analysis and in particular to evaluate the Gibbs enthalpies at 298.15 K. For each system, all the vibrational frequencies are real, demonstrating that the structures correspond to global minima. Single-point calculations were further performed at the second-order Möller-Plesset (MP2) level with the same basis set to refine the relative energies of the stationary points. Solvent (AcOH) effects were accounted for using the polarizable continuum model with the integral equation formalism.[1] All calculations were carried out using the GAUSSIAN09 package.[2]

[1] (a) Tomasi, J.; Persico, M. *Chem. Rev.* **1994**, *94*, 2027. (b) Tomasi, J.; Mennucci, B.; Cammi, R. *Chem. Rev*. **2005**, *105*, 2999.

[2] Gaussian 09, Revision A.1, Frisch, M. J.; Trucks, G. W.; Schlegel, H. B.; Scuseria, G. E.; Robb, M. A.; Cheeseman, J. R.; Scalmani, G.; Barone, V.; Mennucci, B.; Petersson, G. A.; Nakatsuji, H.; Caricato, M.; Li, X.; Hratchian, H. P.; Izmaylov, A. F.; Bloino, J.; Zheng, G.; Sonnenberg, J. L.; Hada, M.; Ehara, M.; Toyota, K.; Fukuda, R.; Hasegawa, J.; Ishida, M.; Nakajima, T.; Honda, Y.; Kitao, O.; Nakai, H.; Vreven, T.; Montgomery, Jr. J. A.; Peralta, Jr., J. E.; Ogliaro, F.; Bearpark, M.; Heyd, J. J.; Brothers, E.; Kudin, K. N.; Staroverov, V. N.; Kobayashi, R.; Normand, J.; Raghavachari, K.; Rendell, A.; Burant, J. C.; Iyengar, S. S.; Tomasi, J.; Cossi, M.; Rega, N.; Millam, J. M.; Klene, M.; Knox, J. E.; Cross, J. B.; Bakken, V.; Adamo, C.; Jaramillo, J.; Gomperts, R.; Stratmann, R. E.; Yazyev, O.; Austin, A. J.; Cammi, R.; Pomelli, C.; Ochterski, J. W.; Martin, R. L.; Morokuma, K.; Zakrzewski, V. G.; Voth, G. A.; Salvador, P.; Dannenberg, J. J.; Dapprich, S.; Daniels, A. D.; Farkas, Ö.; Foresman, J. B.; Ortiz, J. V.; Cioslowski, J.; Fox, D. J. Gaussian, Inc., Wallingford CT **2009**.

TABLE S1. Overview of atom coordinates for *Z* alkene 13, *E* alkene 14 and CPDT 12a

Z alkene **13**

6	1.467756	2.865750	-0.373170
6	2.099155	1.635951	-0.421506
6	1.210717	0.546378	-0.208862
6	-0.100914	0.980106	0.005019
16	-0.206890	2.703482	-0.044761
1	1.901106	3.847717	-0.516138
1	3.159091	1.512529	-0.621222
6	-1.290024	-0.938441	1.183987
6	-2.542688	-1.600210	1.183168
6	-3.444869	-1.024044	0.304846
16	-2.755361	0.306138	-0.529347
6	-1.246561	0.134886	0.299207
1	-2.787141	-2.453575	1.806694
1	-4.471503	-1.311060	0.115618
1	-0.438017	-1.211765	1.797366
6	1.591476	-0.885111	-0.267749
6	2.411416	-1.428551	0.658018
1	2.687776	-2.476656	0.552046
6	2.958707	-0.711604	1.860848
1	2.776270	-1.298825	2.768510
1	4.044377	-0.575958	1.782028
1	2.499223	0.272237	1.986077
6	1.016869	-1.641477	-1.446742
1	1.392923	-1.169084	-2.365341
1	-0.068810	-1.475304	-1.449736
6	1.301237	-3.140756	-1.477401
1	0.827798	-3.595714	-2.352581
1	2.375107	-3.344215	-1.532526
1	0.904149	-3.631499	-0.583058

E alkene **14**

6	1.128171	3.190677	-0.074105
6	1.913333	2.054546	-0.153346
6	1.161125	0.849293	-0.077817
6	-0.205154	1.102491	0.065798
16	-0.528617	2.797113	0.111654
1	1.440267	4.225783	-0.135601
1	2.989018	2.076548	-0.295705
6	-1.381097	-0.696002	1.424882
6	-2.482917	-1.582865	1.336044

6	-3.179144	-1.439480	0.146846
16	-2.485517	-0.231134	-0.851922
6	-1.249156	0.113696	0.303734
1	-2.764545	-2.295259	2.104099
1	-4.058927	-1.978589	-0.181483
1	-0.692300	-0.632367	2.260950
6	1.754684	-0.503007	-0.193303
6	2.749299	-0.847647	0.657706
1	3.005800	-0.136903	1.444431
6	3.539713	-2.124736	0.623514
1	4.604807	-1.915353	0.770248
1	3.231687	-2.803587	1.428290
1	3.423137	-2.653840	-0.325393
6	1.285405	-1.395392	-1.331091
1	2.162123	-1.706023	-1.915968
1	0.660156	-0.801413	-2.006513
6	0.511392	-2.645585	-0.889214
1	0.264855	-3.265670	-1.758346
1	1.104689	-3.250386	-0.197163
1	-0.418561	-2.374545	-0.385452

CPDT **12a**

6	-0.999801	-3.160568	0.237897
6	0.258836	-2.578639	0.165653
6	0.175655	-1.173154	0.014992
6	-1.149116	-0.721435	-0.000640
16	-2.276431	-1.999369	0.151093
1	-1.243767	-4.213276	0.310840
1	1.172556	-3.161194	0.219326
6	1.141771	-0.000172	0.000001
6	0.175968	1.173054	-0.015020
6	0.259568	2.578507	-0.165716
6	-0.998879	3.160829	-0.237936
16	-2.275866	2.000026	-0.151089
6	-1.148944	0.721750	0.000648
1	1.173461	3.160789	-0.219420
1	-1.242522	4.213612	-0.310878
6	1.987963	0.041005	-1.291465
6	2.981989	-1.110263	-1.443042
1	2.521611	0.999633	-1.326614
1	1.289000	0.042749	-2.137816
1	3.530205	-1.014213	-2.385849

1	3.716246	-1.120254	-0.631426
1	2.465885	-2.074519	-1.455060
6	1.987915	-0.041556	1.291489
6	2.982188	1.109493	1.443106
1	2.521347	-1.000305	1.326644
1	1.288928	-0.043150	2.137820
1	3.530371	1.013302	2.385918
1	3.716460	1.119355	0.631501
1	2.466289	2.073859	1.455143

Chapter 3

Design and Synthesis of a Series of PCPDTBT Polymers for Organic Photovoltaics

Four differently substituted 4*H*-cyclopenta[2,1-*b*:3,4-*b*']dithiophene derivatives have been synthesized by a convenient three-step protocol. These donor units have been combined with 2,1,3-benzothiadiazole as an acceptor moiety by Suzuki polycondensation reactions, affording PCPDTBT-type alternating copolymers, among which a versatile ester-functionalized polymer that can be applied as a key intermediate toward a wide collection of functionalized low bandgap materials. All PCPDTBT polymers have been characterized by cyclic voltammetry and UV-vis spectroscopy, illustrating their low bandgap character with absorption bands extending into the near-IR region. The photovoltaic performances of some of the novel polymers have been investigated. Preliminary results illustrated the high potential of these materials, although (morphology) optimization is still required for most of them, as the side chains have a huge influence on the processing parameters and blend morphology.

3.1. Introduction

Polymer solar cells have been attracting considerable attention due to their unique (potential) advantages of being low in cost and lightweight, as well as their possible application in flexible large-area devices.[1] Research efforts in this field have been concentrated on P3HT (poly(3-hexylthiophene)), the so-called "workhorse" polymer material of organic solar cells, for a long time. Unfortunately, due to its mismatch with the terrestrial solar spectrum and the inherent low open-circuit voltage (V_{oc}), interest in this material class began to fade, especially since other families of conjugated polymers showed higher potential.[2–4] Research groups worldwide nowadays focus on low bandgap polymer materials, designed by implementing donor and acceptor (heterocyclic) units in an alternating fashion in the polymer backbone. Narrowing the bandgap has proven to be particularly efficient for harvesting more solar energy to enhance the solar cell performance.

4*H*-Cyclopenta[2,1-*b*:3,4-*b*']dithiophene (CPDT) has emerged as a potential candidate toward low bandgap copolymers due to its fully coplanar structure, altering the intrinsic properties of bithiophene and leading to more extended conjugation, smaller HOMO/LUMO energy gap and stronger intermolecular interactions.[5] PCPDTBT, combining CPDT with 2,1,3-benzothiadiazole (BT) in an alternating fashion, has been proven to be one of the most efficient low bandgap photovoltaic materials to date.[6,7] Heeger *et al.* integrated this material together with $PC_{71}BM$ in bulk heterojunction solar cells and exceeded 5% power conversion efficiency (PCE) after the addition of 1,8-octanedithiol (ODT) as an additive.[7]

For the design of new polymers, considerations on non-energetic parameters such as those that influence the physical interaction between the bulk polymer and fullerene materials are also important. In particular, the choice of solubilizing groups is a critical factor determining photovoltaic properties. To date, only a limited amount of studies have been directed toward the understanding of the subtle effects of the side chains on the properties of the active layer material blend and photovoltaic efficiencies.[8]

We have previously developed a versatile three-step synthetic route enabling the preparation of a variety of 4*H*-cyclopenta[2,1-*b*:3,4-*b*']dithiophene units with asymmetrically functionalized side chains.[9] In this paper, we present the synthesis of a series of four different PCPDTBT-type polymers: two symmetrical variants **P1** and **P2**,

substituted with either two 2-ethylhexyl or two octyl chains, respectively, one asymmetrical polymer **P3**, endowed with one octyl and one 2-ethylhexyl chain, and an asymmetrical ester-functionalized polymer **P4** (Figure 3.1). The latter polymer can give access to a broad range of functionalized copolymers *via* postpolymerization reactions, considerably enlarging the scope of possibilities for material engineering.

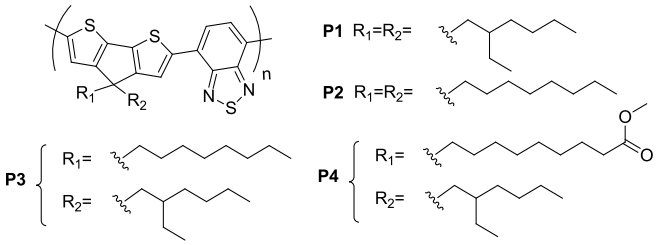

Figure 3.1. Synthesized PCPDTBT polymers.

3.2. Results and Discussion

3.2.1. Synthesis and Characterization of PCPDTBT Polymers P1–P3

The possibility of straightforward side chain variation in the 4*H*-cyclopenta[2,1-*b*:3,4-*b*']dithiophene unit was achieved by applying the three-step synthetic protocol (Scheme 3.1) recently developed in our group.[9] The ketone precursor used in the second step of this route plays an important role as a powerful synthetic tool for variation of the substitution pattern of the CPDT.

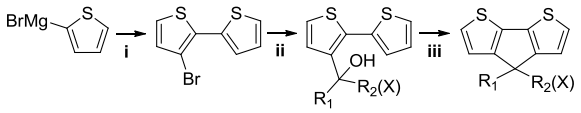

i. 2,3-dibromothiophene, $Pd(dppf)Cl_2$; **ii**. *n*-BuLi, ketone; **iii**. H_2SO_4

Scheme 3.1. Three-step synthetic approach to asymmetrically functionalized 4*H*-cyclopenta[2,1-*b*:3,4-*b'*]dithiophenes.

Toward polymer **P1**, the required symmetrical bis(2-ethylhexyl)ketone has been prepared *via* a Grignard reaction between 2-ethylhexylmagesium bromide and ethyl formiate (**1**), followed by subsequent oxidation with pyridinium chlorochromate (PCC), affording 5,9-diethyltridecan-7-one (**3**) after purification by column chromatography (Scheme 3.2).[10]

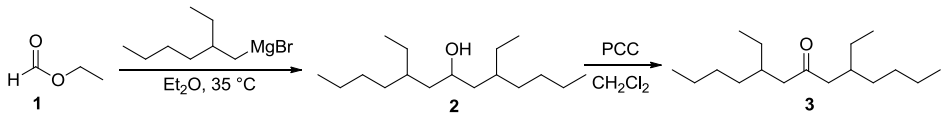

Scheme 3.2. Synthesis of the symmetrical 5,9-diethyltridecan-7-one (**3**).

This ketone was then reacted with the lithio derivative of 3-bromo-2,2'-bithiophene (**4**), yielding the tertiary alcohol derivative **5**, as depicted in Scheme 3.3. Subsequently, the alcohol was readily converted to the analogous alkene-bithiophene derivative **6**. Dehydration spontaneously occurred during purification of **5** by vacuum distillation at an elevated temperature of 190 °C. In the final step, ring closure was achieved upon addition of an excess of sulfuric acid, affording 4,4-bis(2-ethylhexyl)-4*H*-cyclopenta[2,1-*b*:3,4-*b'*]dithiophene (**7**). The dibrominated CPDT monomer **8**, required for Suzuki copolymerization, was prepared by dibromination of **7** with *N*-bromosuccinimide (NBS).

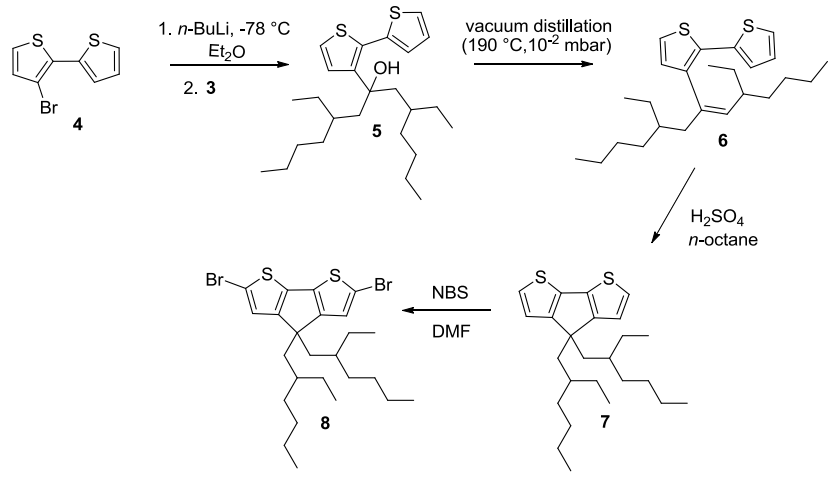

Scheme 3.3. Synthesis of the symmetrical 2,6-dibromo-4,4-bis(2-ethylhexyl)-4*H*-cyclopenta[2,1-*b*:3,4-*b'*]-dithiophene monomer (**8**).

The electron deficient coupling partner, 2,1,3-benzothiadiazole-4,7-bis(boronic acid pinacol ester) (**9**), was purchased from commercial sources and used without further purification. Polymer **P1** was then synthesized by Suzuki copolymerization,[11] combining monomers **8** and **9** with $Pd(PPh_3)_4$ as a catalyst and K_2CO_3 as a base in a toluene/water mixture with addition of phase transfer catalyst Aliquat 336 at 80 °C for 3 days, according to the polymerization procedure previously published by Müllen *et al*. (Scheme 3.4).[6d] End-capping was carried out by sequential addition of

phenylboronic acid and bromobenzene. The polymer was purified by repetitive Soxhlet extraction (with methanol, acetone, *n*-hexane and $CHCl_3$, respectively) and finally precipitated from methanol as a dark (almost black) powder.

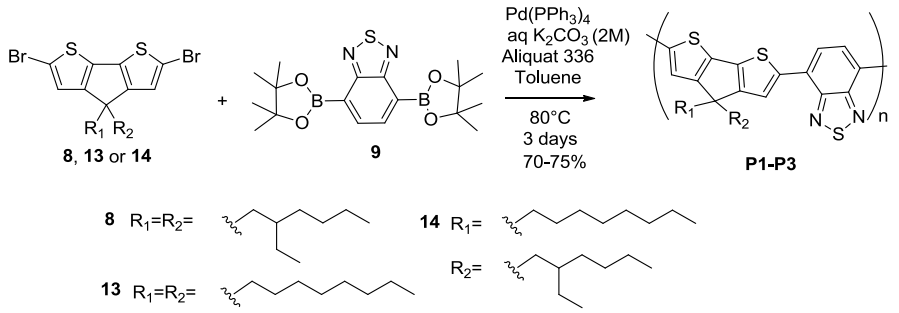

Scheme 3.4. Suzuki copolymerizations affording PCPDTBT materials **P1–P3**.

For PCPDTBT polymers **P2** and **P3** the CPDT monomers were prepared in the same way, except for the appropriate ketones **11** and **12**, which were obtained through reaction of *n*-octylcyanide (**10**) with *n*-octyl- or 2-ethylhexylmagnesium bromide, respectively (Scheme 3.5).[9]

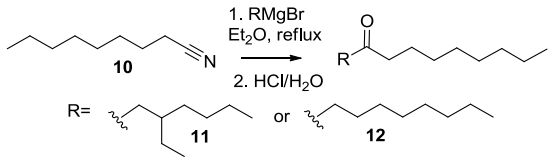

Scheme 3.5. Synthesis of 5-ethylpentadecan-7-one (**11**) and heptadecan-9-one (**12**).

Upon inserting these ketones in the three-step synthetic procedure, and subsequent dibromination of the obtained CPDTs, monomers **13** and **14** were obtained.[9] These building blocks were again coupled to the bisboronate of benzothiadiazole through Suzuki polymerization, resulting in PCPDTBT copolymers **P2** and **P3** (Scheme 3.4). The same end-capping and purification procedures as for polymer **P1** were maintained, except for **P2**, for which final Soxhlet extraction with chlorobenzene was required due to the decreased solubility in chloroform. The introduction of two linear octyl side chains introduced apparently diminished solubility. After precipitation from methanol, the polymers were isolated again as dark (almost black) powders.

The three polymers were synthesized in reasonable yields of 70–75% and their molecular weights, as evaluated by gel permeation chromatography (GPC) in chlorobenzene (for **P2**) or tetrahydrofuran (for **P1** and **P3**) (Table 3.1), were within the same range (M_n 9.000–18.000). Only the symmetrical bisoctyl derivative **P2** showed

somewhat lower molecular weights, probably due to its poor solubility in the reaction mixture, inducing precipitation during polymerization.[11] Upon repetition of the synthetic procedure for PCPDTBT **P1**, a polymer with a slightly higher M_n (and M_w) was obtained (denoted as **P1'**, Table 3.1).

Table 3.1. Analytical GPC data of the synthesized PCPDTBT polymers **P1**–**P3**.

	M_n (g/mol)	M_w (g/mol)	PDI
P1	1.1×10^4	2.3×10^4	2.1
P1'[a]	1.8×10^4	3.6×10^4	2.0
P2	8.9×10^3	1.4×10^4	1.6
P3	1.3×10^4	4.1×10^4	3.3

[a] **P1'** is the same polymer from a different polymerization batch.

The absorption spectra of PCPDTBT polymers **P1–P3** in solution and film are displayed in Figure 3.2. Through the push-pull interaction, inherent to low bandgap polymers, efficient photoinduced intramolecular charge transfer (ICT) occurs from the donor to the acceptor part upon photoexcitation, generating an absorption band at lower energy. The spectra for all three polymers **P1–P3** showed a dominating ICT absorption band located at *ca*. 700 nm in the near-infrared region, together with an absorption from the localized π-π* transitions in the visible region from 400–500 nm.[12] The absorption maxima were rather similar in solution. In film, the symmetrical bisoctyl-PCPDTBT **P2** and asymmetrically substituted PCPDTBT **P3** showed a modest red-shift, which might be attributed to enhanced π-π stacking due to the reduction of the side-chain bulkiness compared to **P1**. Broader shoulders observed for **P2** and **P3** can tentatively be explained by aggregation or light scattering issues.

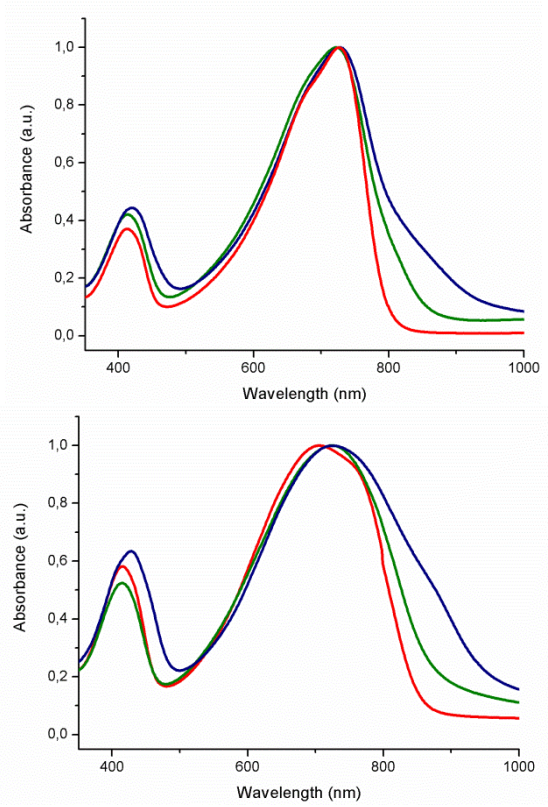

Figure 3.2. UV-vis absorption spectra of PCPDTBT polymers **P1** (red), **P2** (blue) and **P3** (green) in *o*-dichlorobenzene solution (top) and in film (bottom).

The HOMO and LUMO energy levels of the polymers, as determined by cyclic voltammetry data combined with the optical band gaps (Table 3.2), are close to the values reported by Brabec *et al.* for bis(2-ethylhexyl)-PCPDTBT (-5.3 and -3.57 eV).[6a]

Table 3.2. Cyclic voltammetry data of synthesized PCPDTBT polymers **P1**–**P3**.

	E_{onset}^{ox} (V)	E_{onset}^{red} (V)	HOMO (eV)	LUMO (eV)	E_g^{EC} (eV)	E_g^{OP} (eV)[a]
P1	0.19	-1.25	-5.18	-3.68	1.50	1.45
P2	0.05	-1.50	-4.98	-3.43	1.55	1.31
P3	0.26	-1.45	-5.19	-3.48	1.71	1.44

[a]In film

3.2.2. Bulk Heterojunction Organic Solar Cells

Polymer solar cells (PSCs) were fabricated with a layered structure ITO/hole-transporting layer (HTL)/polymer:$PC_{71}BM$/Yb/Ag and measured under air mass 1.5 global illumination conditions (AM 1.5G 100 mW/cm^2).

Table 3.3. PV characteristics of polymer:$PC_{71}BM$ solar cells.

Blend mixture	Processing solvent	Co-solvent	HTL	V_{oc} (V)	J_{sc} (mA/cm^2)	FF	PCE (%)
P1:PC$_{71}$BM[a]	CB[b]	-	PEDOT:PSS	0.45	4.83	0.29	0.63
P1:PC$_{71}$BM[a]	CB	ODT[c]	PEDOT:PSS	0.57	7.13	0.34	1.37
P1':PC$_{71}$BM[a]	CB	-	PEDOT:PSS	0.64	9.49	0.45	2.71
P3:PC$_{71}$BM	CB:$CHCl_3$[d]	ODT	PEDOT:PSS	0.61	5.06	0.33	1.03
P3:PC$_{71}$BM	CB:$CHCl_3$[d]	-	MoO_3	0.60	5.46	0.38	1.25
P3:PC$_{71}$BM	CB:$CHCl_3$[d]	ODT	MoO_3	0.56	6.10	0.39	1.34
P3:PC$_{71}$BM	ODCB[e]	ODT	PEDOT:PSS	0.64	7.44	0.38	1.81

[a] Instead of Yb/Ag, Ca/Ag was used as the top electrode. [b] CB = chlorobenzene. [c] ODT = 1,8-octanedithiol. [d] CB:$CHCl_3$ in 3:2 ratio. [e] ODCB = *ortho*-dichlorobenzene.

For the two first solar cells of the bulky branched bis(2-ethylhexyl)-substituted PCPDTBT polymer **P1**, structurally identical to the popular PCPDTBT material from literature,[6] the efficiency was more than doubled (0.63% → 1.37%) upon addition of ODT. Heeger *et al.* previously reported the influence of 1,8-octanedithiol toward an optimal morphology and attained efficiencies up to 5.5%.[7] The third solar cell was fabricated with the slightly higher molecular weight batch **P1'** and efficiencies were improved considerably to 2.71% (Figure 3.3). These preliminary results are promising, although further optimization is still required to reach literature efficiencies.

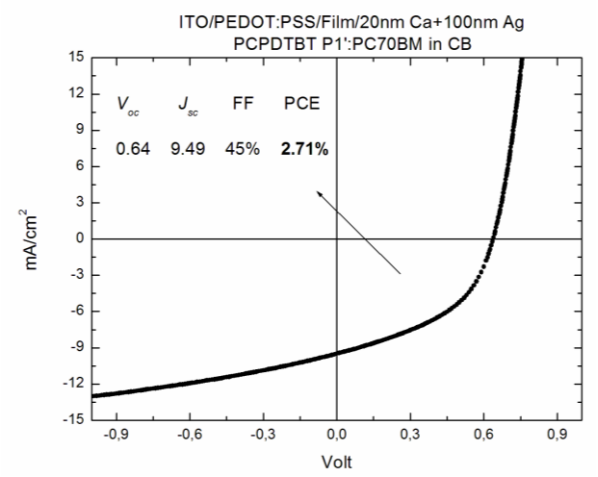

Figure 3.3. *J-V* curve of the polymer bulk heterojunction solar cell with a **PCPDTBT P1'**:$PC_{71}BM$ active layer spin-coated from CB with PEDOT:PSS as HTL (without ODT).

The elimination of the branching on the side chains in polymer **P2** promotes crystallization, which is known to lead to higher charge-carrier mobilities. Unfortunately, in first attempts no homogeneous film could be made from this material due to solubility issues. Brabec *et al.* synthesized an analogous symmetrical PCPDTBT polymer with two linear hexyl side chains.[6b] Due to low solubility in common organic solvents, this material could not even be characterized. Apparently, linear alkyl chains with 8 carbon atoms (4 carbon atoms more than Brabec's example) significantly enhance solubility, but there are still large difficulties in processing. An extension to 12 or 16 carbon atoms, as reported by Müllen *et al.*,[6d] might solve this problem.

Solar cells made from the asymmetrically substituted PCPDTBT polymer **P3** - balancing a good tendency for crystallization and high mobility (due to the linear side chain), with good solubility (due to the bulkier 2-ethylhexyl side chain) - showed moderate solar cell performances, with an efficiency of 1.03% in unoptimized solar cell devices (Table 3.3, Figure 3.4a). Efficiencies could be slightly improved (1.03→1.25%) by changing the hole transport layer (HTL) from PEDOT:PSS to MoO_3 (Table 3.3, Figure 3.4b). The enhanced efficiency might be related to the reduced thickness of the MoO_3 layer or improved interface properties.[13] Upon addition of ODT the performance was slightly improved to 1.34% (Table 3.3, Figure 3.4c).

The optimum film thickness of an active layer depends (among others) on the mobility of the electrons and holes. When an active layer has a higher mobility, the optimum

thickness will be higher. In the case of the well-performing literature PCPDTBT material, the optimum thickness is between 150 and 250 nm.[6a] In our case (lower molecular weight and probably lower mobility), the optimum thickness was ~90 nm (using 2000–2200 rpm as spin-coating speed, see SI: Table 3.4). By using 1,2-dichlorobenzene (ODCB) instead of chlorobenzene (CB) as the spin-coating solvent, the film stays soft for a much longer time and becomes thinner and thinner by spinning. This is why for the ODCB case, a lower spin speed of 800 rpm was used, compared to CB, to obtain the same thickness of ~90 nm. Modification of the solvent from a $CHCl_3$:CB mixture to ODCB improved the J_{sc} significantly (5.06 → 7.44), affording efficiencies of up to 1.81% (Table 3.3, Figure 3.5). Unfortunately, FFs are still not satisfying, suggesting unfavorable morphologies. Further work on solar cell optimization is still required.

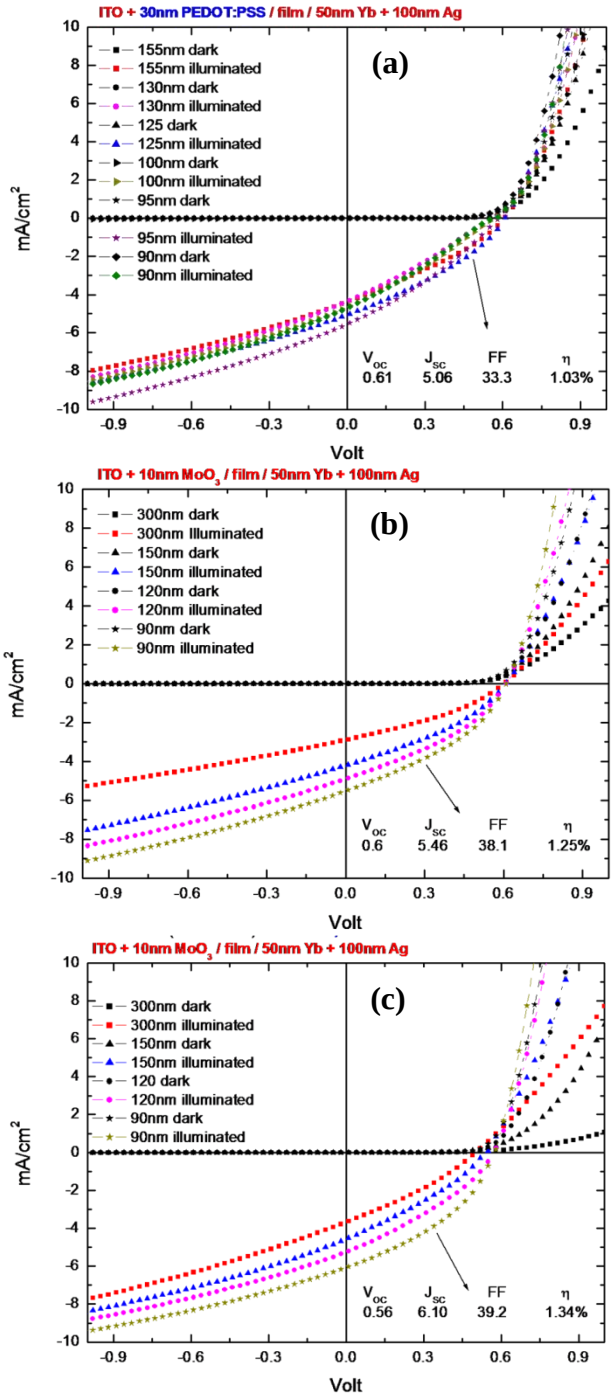

Figure 3.4. *J-V* curves of polymer bulk heterojunction solar cells with a **PCPDTBT P3**:$PC_{71}BM$ active layer spin-coated from a CB:$CHCl_3$ (3:2) mixture with PEDOT:PSS as HTL and ODT (a), with MoO_3 as HTL without ODT (b), and with MoO_3 as HTL with addition of ODT (c).

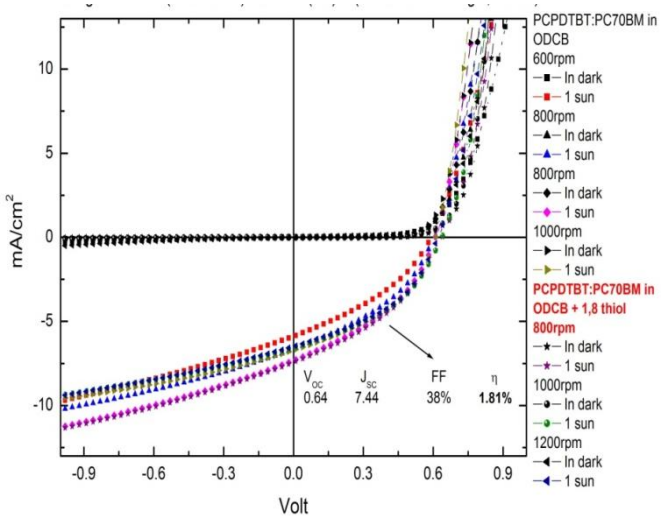

Figure 3.5. *J-V* curves of polymer bulk heterojunction solar cells with a **PCPDTBT P3**:$PC_{71}BM$ active layer spin-coated from ODCB with PEDOT:PSS as HTL and addition of ODT.

3.2.3. Synthesis and Characterization of Ester-PCPDTBT Polymer P4

After spin-coating the polymer-fullerene blend solution on substrates, control and optimization of the donor-acceptor blend morphology is extremely difficult since the blend components are kinetically trapped in a non-equilibrium state. There will be a tendency for each of the components to phase-separate to a more thermodynamically favored state. In this case, however, the desirable intimate intermixing donor-acceptor network will be lost, with a detrimental effect on the solar cell efficiency. High temperatures, as can be reached on application of the solar cells, will even speed up this solar cell degradation. Improving the stability of the film morphology in solar cells is one of the remaining challenges in the OPV domain. One particular approach to improve the thermal stability of an active layer blend morphology is the design of cross-linkable polymers. Hashimoto *et al.* focused on the synthesis of cross-linkable P3HT. After prolonged annealing times, solar cells comprised of P3HT with cross-linked vinyl functionalities showed slower deterioration of the solar cell performances compared to solar cells made from pristine P3HT.[14] Fréchet *et al.* prepared P3HT with terminal bromine groups on the alkyl side chains, which upon exposure to UV light underwent cross-linking, resulting in an improved solar cell stability.[15] In the next section, the synthesis and characterization of a new ester-functionalized PCPDTBT

material is described. This polymer can be applied as a versatile starting material for the synthesis of cross-linkable PCPDTBT polymers.

If one intends to fabricate ester-functionalized CPDTs using the three-step protocol as depicted in Scheme 3.1, the ketone precursors have to be replaced by keto esters. Punzi *et al.* proposed an elegant, simple and straightforward method toward the synthesis of keto esters by coupling organocopper reagents and monoesters of a dicarboxylic acid.[16] Two keto esters **17** and **18**, with a different number of carbon atoms between the two functionalities, were prepared in high yields of 81% and 92%, respectively (Scheme 3.6).

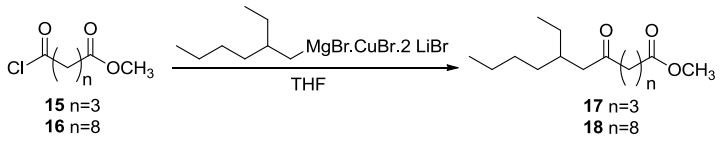

Scheme 3.6. Synthesis of methyl 7-ethyl-5-oxoundecanoate (**17**) and methyl 12-ethyl-10-oxohexadecanoate (**18**).

As previously observed for ethyl levulinate,[9] application of the short keto ester **17** in the three-step protocol mainly yielded lactone intermediate **19** by intramolecular transesterification of the tertiary alcohol intermediate with the terminal ethyl ester moiety (Scheme 3.7). Lactone ring opening was achieved with methanol under sulfuric acid-catalyzed conditions. As it was observed that the terminal ester moiety was partly hydrolyzed by the water molecules released as a side product, two different alkenes **20** and **20'** were isolated. In a final step, the ester-functionalized bithiophene **20** was converted to the ring-closed ester-CPDT **21** with the aid of sulfuric acid.

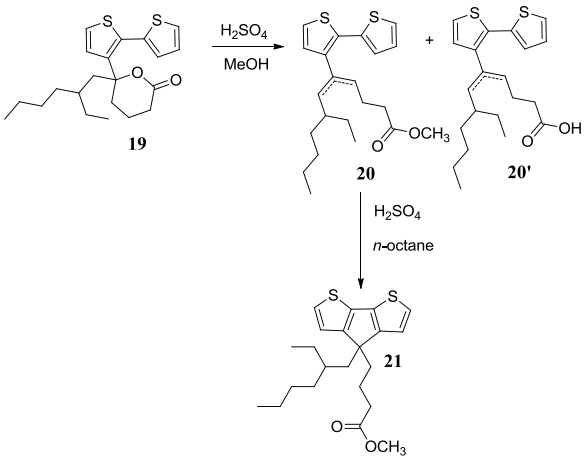

Scheme 3.7. Synthetic route toward ester-functionalized CPDT **21**.

On the other hand, keto ester **18** reacted with the lithiated derivative of 3-bromo-2,2'-bithiophene resulting in alcohol derivative **22** without subsequent lactone formation (Scheme 3.8), due to the lower tendency to form larger rings. Upon reaction with sulfuric acid, ester- and carboxylic acid functionalized CPDT derivatives **23** and **24** were obtained. The mixture was treated with sulfuric acid and methanol, transforming all carboxylic acid groups in ester functionalities through Fischer esterification.[17] In order to generate nicely soluble polymers, the ester-CPDT **25** with long aliphatic side chains was dibrominated using NBS in DMF (Scheme 3.8). After subsequent purification by column chromatography, ester-CPDT monomer **26** was available for incorporation as a donor unit in a low bandgap polymer with benzothiadiazole as the acceptor moiety, PCPDTBT (**P4**).

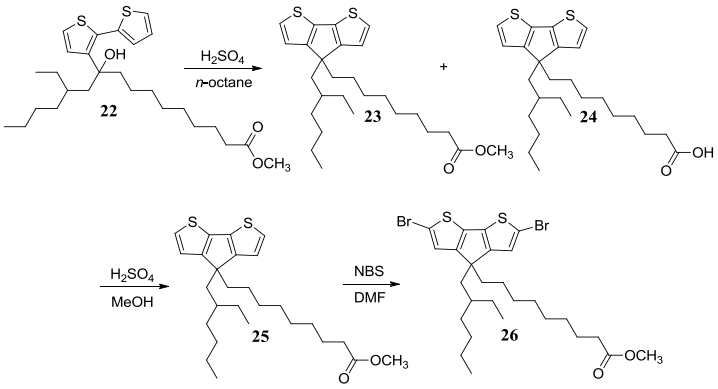

Scheme 3.8. Preparation of the dibrominated ester-CPDT monomer **26**.

The traditional Suzuki copolymerization uses basic reagents to activate the boronic acid/ester. The ester-functionalized monomer **26** will hydrolyze under comparable conditions. However, previous work on Suzuki cross-coupling reactions for small molecules illustrated that anhydrous fluoride salts such as cesium fluoride and tetrabutylammonium fluoride also have the ability to activate boronic esters.[18] For the coupling of the dibrominated ester-CPDT monomer **26** with the bisboronate of benzothiadiazole, a water-free Suzuki polymerization, using cesiumfluoride for monomer activation and DME as a solvent, was applied (Scheme 3.9).[19] After conventional thermal heating at 80 °C during three days, the ester-PCPDTBT polymer **P4** was formed in a reasonable yield of 81%. End-capping, work-up and Soxhlet-purification were performed in a similar way as for the other three polymers **P1–P3**. **P4** showed a moderate molecular weigth (M_n = 1.4 x 10^4 g/mol, M_w = 5.2 x 10^4 g/mol, PDI = 3.7), in the same range as polymers **P1** and **P3**, and the UV-vis spectra displayed once again an ICT absorption band in the near-IR region (Figure 3.6). In film, a significant red-shift could be observed, probably due to enhanced ordering or aggregation. The cyclic voltammetry data, with a HOMO of -4.98 eV and a LUMO of -3.50 eV (E_g^{EC}= 1.48 eV and E_g^{OP}= 1.42 eV), are again rather similar to the PCPDTBT literature data.[6a]

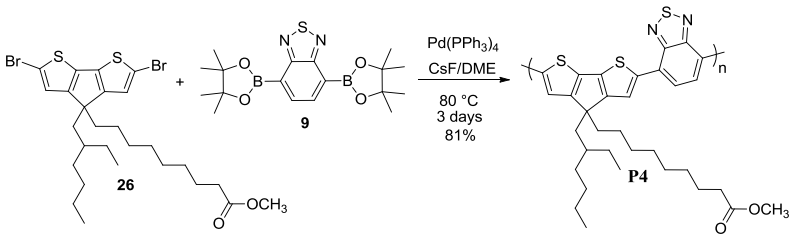

Scheme 3.9. Suzuki copolymerization yielding ester-PCPDTBT **P4**.

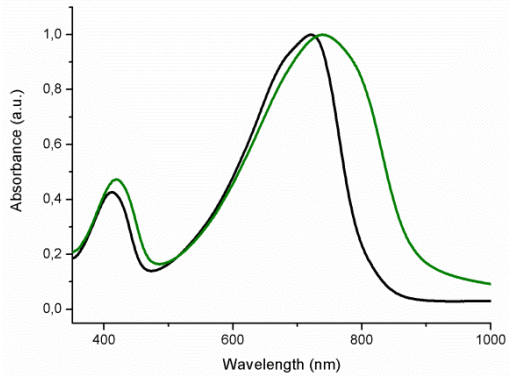

Figure 3.6. UV-vis absorption spectra of PCPDTBT **P4**.

3.3. Conclusions

Improved synthetic strategies capable of rapidly accessing structurally diverse low bandgap polymers are certainly still needed to establish solid structure-function relationships that integrate the influence of pendant groups on the solar cell performance. In this paper, we have applied the recently reported three-step protocol toward asymmetrically substituted CPDTs to synthesize PCPDTBT polymers with slightly different substitution patterns. Optical properties were quite similar for all polymers, although a slight red-shift has been observed by reduction of the side chain bulkiness. Preliminary solar cell results were disclosed, attaining a maximum efficiency of 2.71% with the symmetrical bis(ethylhexyl)-substituted PCPDTBT **P1'** and 1.81% with the asymmetrically substituted PCPDTBT polymer **P3**. Replacing the shorter and bulkier 2-ethylhexyl side chains with longer, but less bulky linear octyl side chains diminished the polymer solubility considerably, creating processing difficulties. In future work, these polymers will be used to probe the impact of backbone substituents on the solar cell performance. Of particular interest is the synthesis of the ester-PCPDTBT polymer **P4**. Starting from this material, a whole series of functionalized PCPDTBTs can be accessed by basic functional group conversions. The pioneering work on backbone modification of this class of low bandgap polymers has paved the way toward the design of functional or even cross-linkable PCPDTBT polymers.

3.4. Experimental Section

Materials and Methods

NMR chemical shifts (δ, in ppm) were determined relative to the residual $CHCl_3$ absorption (7.26 ppm) or the ^{13}C resonance shift of $CDCl_3$ (77.16 ppm). Gas chromatography-mass spectrometry (GC-MS) analyses were carried out applying Chrompack Cpsil5CB or Cpsil8CB capillary columns. Molecular weights and molecular weight distributions were determined relative to polystyrene standards (Polymer Labs) by size exclusion chromatography (SEC). Chromatograms were recorded on a Spectra Series P100 (Spectra Physics) equiped with two mixed-B columns (10 µm, 0.75 cm x 30 cm, Polymer Labs) and a refractive index detector (Shodex) at 40 °C. THF was used as the eluent at a flow rate of 1.0 mL/min. If chlorobenzene was used as the eluent, the temperature was raised to 60 °C. Solution UV-vis absorption measurements were performed with a scan rate of 600 nm/min in a continuous run from 200 to 800 nm. Thin film electrochemical measurements were performed with an Eco Chemie Autolab PGSTAT 30 Potentiostat/Galvanostat using a conventional three-electrode cell under N_2 atmosphere (electrolyte: 0.1 mol/L $TBAPF_6$ in anhydrous CH_3CN). For the measurements, a $Ag/AgNO_3$ reference electrode (0.01 mol/L $AgNO_3$ and 0.1 mol/L $TBAPF_6$ in anhydrous CH_3CN), a platinum counter electrode and an indium tin oxide (ITO) coated glass substrate as working electrode were used. The polymers were deposited by drop-casting directly onto the ITO substrates. Cyclic voltammograms were recorded at 50 mV/s. From the onset potentials of the oxidation and reduction the position of the energy levels could be estimated. All potentials were referenced using a known standard, ferrocene/ferrocenium, which in CH_3CN solution is estimated to have an oxidation potential of -4.98 eV *vs.* vacuum.
Polymer solar cells were fabricated by spin-coating a PCPDTBT:$PC_{71}BM$ (Solenne) blend in a 1:3 w/w ratio with or without co-solvent 1,8-octanedithiol (24 mg/mL) (Sigma Aldrich), sandwiched between a transparent anode and an evaporated metal cathode. The transparent anode was an ITO covered glass substrate which was coated with a 30 nm poly(3,4-ethylenedioxy thiophene)/poly(styrene sulfonic acid) PEDOT/PSS (CLEVIOS P VP.AI 4083) layer applied by spin-coating or a molybdene(VI)oxide (Sigma Aldrich) layer applied by thermal evaporation. The ITO glass substrate was cleaned by ultrasonification (sequentially) in soap solution,

deionized water, acetone and isopropanol. The cathode, a bilayer of 50 nm Ca or Yb and 100 nm Ag, was thermally evaporated. PCPDTBT and $PC_{71}BM$ (1:3 w/w ratio) were dissolved together in chlorobenzene to give an overall 40 mg/mL solution, which was stirred overnight at 80 °C inside a glovebox. Solar cell efficiencies were characterized under simulated 100 mW/cm^2 AM 1.5 G irradiation from a Xe arc lamp with an AM 1.5 global filter.

Synthesis

Unless stated otherwise, all reagents and chemicals were obtained from commercial sources and used without further purification. 2,1,3-Benzothiadiazole-4,7-bis(boronic acid pinacol ester) (95%) (**9**) was purchased from Sigma Aldrich and used without further purification.

5,9-Diethyltridecan-7-one (3). Ethyl formiate (0.066 mol, 5.36 mL) was, at rt and under an inert atmosphere, dissolved in dry diethyl ether (650 mL). Subsequently, 2-ethylhexylmagnesium bromide (200 mL, 1.0 M in diethyl ether) was added *via* a syringe to the stirred mixture at 0 °C. After stirring for 12 h at reflux temperature, the reaction was quenched with an aqueous HCl solution (0.5 M) at 0 °C. The organic phase was separated and the aqueous phase was extracted with diethyl ether (3 x 50 mL). The combined organic phases were washed with a saturated $NaHCO_3$ solution and brine, dried with $MgSO_4$, filtered and evaporated under reduced pressure to give a slightly yellow oil of pure product **2**. MS (CI) *m/z* 239 [MH^+]; ^{1}H NMR (300 MHz, $CDCl_3$) δ 3.78–3.70 (m, 1H), 1.34–1.23 (m, 22H), 0.88–0.81 (m, 12H); IR (NaCl, cm^{-1}) ν_{max} 3342 (m, OH), 2959/2927/2873/2859 (s, saturated C-H).

Subsequently, pyridinium chlorochromate (0.127 mol, 27.4 g) was added to a stirring solution of 5,9-diethyltridecan-7-ol (**2**) (0.085 mol, 21.707 g) in dichloromethane (700 mL) at rt. The reaction mixture was stirred for 12 h and then concentrated by evaporation *in vacuo*. The obtained product was dissolved in diethyl ether (3 x 300 mL) and subjected to a filtration over silica. The resulting filtrate was concentrated under reduced pressure and the residue was purified by gradient column chromatography (silica, eluent hexane - hexane/$CHCl_3$ 50:50) to afford the title compound as a slightly yellow oil (11.7 g, 70%). GC-MS (EI) *m/z* 254 [M^+]; ^{1}H NMR (300 MHz, $CDCl_3$) δ 2.24 (d, J = 6.9 Hz, 4H), 1.84–1.76 (m, 2H), 1.31–1.10 (m, 16H), 0.81 (t, J = 6.9 Hz,

6H), 0.78 (t, *J* = 7.4 Hz, 6H); ^{13}C NMR (75 MHz, $CDCl_3$) δ 211.4 (CO), 47.9, 35.1, 33.2, 28.9, 26.4, 23.0, 14.1, 10.8; IR (NaCl, cm^{-1}) ν_{max} 2959/2927/2873/2859 (m, saturated C-H), 1715 (m, CO).

3-Bromo-2,2'-bithiophene (4) was synthesized according to a literature procedure.[20] Material identity and purity were confirmed by MS, IR, ^{1}H and ^{13}C NMR.

3-(5,9-Diethyltridec-6-ene-7-yl)-2,2'-bithiophene (6). General procedure 1: A solution of 3-bromo-2,2'-bithiophene (0.041 mol, 9.92 g) in dry diethyl ether (230 mL) was added slowly to a solution of *n*-BuLi (25.3 mL, 1.6 M in hexaan) in dry diethyl ether (230 mL) at -78 °C over 2 h under N_2. The mixture was stirred for 30 min at the same temperature. 5,9-Diethyltridecan-7-one (**3**) (0.045 mol, 11.315 g) was added *via* a syringe to the mixture at -78 °C, followed by stirring overnight at rt. The reaction was quenched with an aqueous NH_4Cl solution (2.5 M) and water at 0 °C. The organic phase was separated and the aqueous phase was extracted with diethyl ether (3 x 100 mL). The combined organic phases were washed with brine, dried with $MgSO_4$, filtered and concentrated under reduced pressure to give a crude oil. The oily residue was purified by gradient column chromatography (silica, eluent hexane - hexane/ethyl acetate 90:10) and vacuum distillation (190 °C, 10^{-2} mbar), yielding a yellow oil (3.40 g, 21%). MS (CI) *m/z* 403 [MH^+]; ^{1}H NMR (300 MHz, $CDCl_3$) δ 7.27 (dd, *J* = 5.1/1.2 Hz, 1H), 7.16 (d, *J* = 5.1 Hz, 1H), 7.13 (dd, *J* = 3.6/1.2 Hz, 1H), 7.01 (dd, *J* = 5.1/3.6 Hz, 1H), 6.90 (d, *J* = 5.1 Hz, 1H), 5.36 (d, *J* = 10.2 Hz, 1H), 2.39–2.20 (m, 2H), 1.54–1.14 (m, 18H), 0.95–0.83 (m, 9H), 0.72 (t, *J* = 6.9 Hz, 3H); ^{13}C NMR (75 MHz, $CDCl_3$) δ 142.6, 138.7, 136.4, 134.7, 130.8, 129.7, 127.1, 126.8, 126.0, 123.5, 39.7, 38.2, 35.4, 35.3, 35.0, 32.8, 29.9, 28.9, 28.6, 25.9, 23.2, 14.3, 14.2, 12.1, 10.8; IR (NaCl, cm^{-1}) ν_{max} 3105/3071 (w, unsaturated C-H), 2957/2927/2872/2856 (s, saturated C-H).

4,4-Bis(2-ethylhexyl)-4*H*-cyclopenta[2,1-*b*:3,4-*b'*]dithiophene (7). General procedure 2: H_2SO_4 (5.41 mL) was added dropwise to 3-(5,9-diethyltridec-6-ene-7-yl)-2,2'-bithiophene (**6**) (8.46 mmol, 3.40 g) in degassed *n*-octane (113 mL) under stirring at rt under an inert atmosphere. After additional stirring for 12 h, ethyl acetate and water were added. The organic layer was separated and the aqueous layer was extracted with ethyl acetate (3 x 100 mL). The combined organic extracts were successively washed with saturated $NaHCO_3$ and brine. After drying with $MgSO_4$ and

filtration of the drying agent, the solvent was removed *in vacuo*. The crude oil was purified by column chromatography (silica, eluent hexane) to afford a slightly yellow oil (1.184 g, 35%). GC-MS (EI) *m/z* 402 [M^+]; ^{1}H NMR (300 MHz, $CDCl_3$) δ 7.13 (d, J = 4.8 Hz, 2H), 6.98–6.95 (m, 2H), 1.98–1.86 (m, 4H), 1.39–0.93 (m, 18H), 0.80 (t, J = 6.8 Hz, 6H), 0.63 (t, J = 7.2 Hz, 6H); ^{13}C NMR (75 MHz, $CDCl_3$) δ 157.6, 137.0, 124.1, 122.4, 53.3, 43.4, 35.1, 34.3, 28.7, 27.4, 22.9, 14.3, 10.8; IR (NaCl, cm^{-1}) ν_{max} 3105/3068 (w, unsaturated C-H), 2957/2924/2871/2856 (m, saturated C-H); UV-vis ($CHCl_3$, nm) λ_{max} (log ε) 250 (3.828), 320 (4.042).

2,6-Dibromo-4,4-bis(2-ethylhexyl)-4*H*-cyclopenta[2,1-*b*:3,4-*b'*]dithiophene (8). General procedure 3: NBS (0.334 mmol, 0.059 g) was added to a solution of 4,4-bis(2-ethylhexyl)-4*H*-cyclopenta[2,1-*b*:3,4-*b'*]dithiophene (**7**) (0.157 mmol, 0.063 g) in degassed DMF (4 mL). The reaction mixture was stirred for 3 h at rt. Subsequently, the mixture was poured onto ice and extracted with diethyl ether (3 x 100 mL). The combined organic layers were washed with saturated $NaHCO_3$ and brine, dried over $MgSO_4$, filtered and concentrated by evaporation *in vacuo*. The crude product was purified by column chromatography (silica, eluent *n*-hexane). The compound was obtained as a yellow oil (0.068 g, 78%). GC-MS (EI) *m/z* 558/562 [M^+]; ^{1}H NMR (300 MHz, $CDCl_3$) δ 6.94/6.93/6.92 (3 x s, 2H), 1.86–1.74 (m, 4H), 1.05–0.86 (m, 18H), 0.78 (t, J = 6.9 Hz, 6H), 0.62 (t, J = 7.4 Hz, 6H); ^{13}C NMR (75 MHz, $CDCl_3$) δ 155.7, 136.7, 125.3, 110.8, 55.1, 43.1, 35.2, 34.2, 28.7, 27.5, 22.9, 14.2, 10.8; IR (NaCl, cm^{-1}) ν_{max} 3082 (w, unsaturated C-H), 2958/2925/2871/2856 (s, saturated C-H); UV-vis ($CHCl_3$, nm) λ_{max} (log ε) 251 (3.905), 339 (4.315).

Poly[2,6-(4,4-bis-(2-ethylhexyl)-4*H*-cyclopenta[2,1-*b*:3,4-*b'*]-dithiophene)-*alt*-4,7-(2,1,3-benzothiadiazole)] (PCPDTBT) (P1). Polymerization procedure 1: 2,6-Dibromo-4,4-bis(2-ethylhexyl)-4*H*-cyclopenta[2,1-*b*:3,4-*b'*]dithiophene (**8**) (0.237 mmol, 0.133 g) and 2,1,3-benzothiadiazole-4,7-bis(boronic acid pinacol ester) (**9**) (0.237 mmol, 0.092 g) were dissolved in toluene (4.56 mL) under an inert atmosphere. To this stirring solution, K_2CO_3 (2.3 mL, 2 M), water (1.15 mL) and one droplet of aliquat 336 (0.2–0.5 mL) were added. The solution was purged with argon for 30 min, and then $Pd(PPh_3)_4$ (23.4 µmol, 0.027 g, 10 mol%) was added. The reaction was stirred at 80 °C for 3 days. Subsequently, a toluene solution of phenylboronic acid (0.26 mmol, 0.032 g) was added, followed by the addition of bromobenzene (0.26 mmol,

0.028 mL), and the mixture was stirred overnight at 80 °C. The resulting mixture was then poured into a mixture of methanol and water (2:1, 200 mL) and stirred overnight. The precipitated dark solid was recovered by filtration, redissolved in $CHCl_3$ (20 mL) and added dropwise to methanol (200 mL). The resulting solid was filtered off (PTFE membrane 47 mm/0.45 µm) and subjected to Soxhlet extraction for 24 h with methanol, *n*-hexane, acetone and $CHCl_3$, respectively. After evaporation of the $CHCl_3$ fraction, the polymer residue was redissolved in $CHCl_3$ and precipitated again from methanol, filtered, washed with methanol and dried, affording **P1** as a black powder (0.097 g, 72%). ^{1}H NMR (300 MHz, $CDCl_3$) δ 8.14 (br, 2H), 7.88 (br, 2H), 2.08 (br, 4H), 1.03 (br, 18H), 0.68 (br, 12H); UV-vis (ODCB, nm) λ_{max} 414, 727; UV-vis (film, nm) λ_{max} 416, 707; GPC (THF, PS standards) M_n = 1.1 x 10^4 g/mol, M_w = 2.3 x 10^4, PDI = 2.1.

4,4-Dioctyl-4*H*-cyclopenta[2,1-*b*:3,4-*b'*]dithiophene was synthesized according to our previously reported procedure.[9] Material identity and purity were confirmed by MS, IR, ^{1}H and ^{13}C NMR.

2,6-Dibromo-4,4-dioctyl-4*H*-cyclopenta[2,1-*b*:3,4-*b'*]dithiophene (13). According to general procedure 3: NBS (1.41 g, 7.96 mmol), DMF (100 mL), 4,4-dioctyl-4*H*-cyclopenta[2,1-*b*:3,4-*b'*]dithiophene (1.00 g, 2.49 mmol), eluent *n*-hexane; Yield 55% (0.77 g); ^{1}H NMR (300 MHz, $CDCl_3$) δ 6.93 (s, 2H), 1.78–1.72 (m, 4H), 1.27–1.13 (m, 24H), 0.86 (t, J = 6.9 Hz, 6H); ^{13}C NMR (75 MHz, $CDCl_3$) δ 156.0, 136.4, 124.6, 111.2, 55.1, 37.7, 31.9, 31.7, 30.1, 29.4, 24.6, 22.8, 14.3; GC-MS (EI) *m/z* 558/562 [M^+]; IR (NaCl, cm^{-1}) ν_{max} 3083 (w, unsaturated C-H), 2954/2926/2854 (s, saturated C-H); UV-vis ($CHCl_3$, nm) λ_{max} (log ε) 261 (4.230), 340 (4.346).

4-(2-Ethylhexyl)-4-octyl-4*H*-cyclopenta[2,1-*b*:3,4-*b'*]dithiophene was synthesized according to our previously reported procedure.[9] Material identity and purity were confirmed by MS, IR, ^{1}H and ^{13}C NMR.

2,6-Dibromo-4-(2-ethylhexyl)-4-octyl-4*H*-cyclopenta[2,1-*b*:3,4-*b'*]dithiophene (14). According to general procedure 3: NBS (1.41 g, 7.96 mmol), DMF (100 mL), 4-(2-ethylhexyl)-4-octyl-4*H*-cyclopenta[2,1-*b*:3,4-*b'*]dithiophene (1.00 g, 2.49 mmol), eluent *n*-hexane; Yield 65% (0.90 g); GC-MS (EI) *m/z* 558/562 [M^+]; ^{1}H NMR (300 MHz, $CDCl_3$) δ 6.94 (s, 1H), 6.93 (s, 1H), 1.83 (t, J = 4.8 Hz, 2H), 1.78–1.72 (m, 2H), 1.27–0.89 (m, 21H), 0.86 (t, J = 7.1 Hz, 3H), 0.79 (t, J = 6.9 Hz, 3H), 0.64 (t, J = 7.4

Hz, 3H); ^{13}C NMR (75 MHz, $CDCl_3$) δ 155.9/155.8, 136.6/136.5, 125.0/124.9, 111.1/111.0, 55.1, 41.6, 39.4, 35.5, 34.1, 31.9, 30.0, 29.43, 29.40, 28.6, 27.4, 24.4, 22.9, 22.8, 14.3, 14.2, 10.8; IR (NaCl, cm^{-1}) ν_{max} 3082 (w, unsaturated C-H), 2957/2926/2855 (s, saturated C-H); UV-vis ($CHCl_3$, nm) λ_{max} (log ε) 250 (3.984), 339 (4.282).

Poly[2,6-(4,4-dioctyl-4*H*-cyclopenta[2,1-*b*:3,4-*b'*]dithiophene)-*alt*-4,7-(2,1,3-benzothiadiazole)] (PCPDTBT) (P2). According to polymerization procedure 1: 2,6-Dibromo-4,4-dioctyl-4*H*-cyclopenta[2,1-*b*:3,4-*b'*]dithiophene (**13**) (0.100 g, 0.179 mmol), 2,1,3-benzothiadiazole-4,7-bis(boronic acid pinacol ester) (**9**) (0.070 g, 0.179 mmol), K_2CO_3 (2 mL, 2 M), 1 drop of aliquat 336 (0.2–0.5 mL), toluene (4 mL), water (1 mL), tetrakis(triphenylphosphine)palladium (0.020 g, 17.3 μmol), phenylboronic acid (0.20 mmol, 0.024 g), bromobenzene (0.20 mmol, 0.02 mL); Soxhlet extraction in methanol, *n*-hexane, acetone, chloroform and chlorobenzene, respectively; Yield 72% (0.073 g); ^{1}H NMR (300 MHz, $CDCl_3$) δ 8.10 (br, 2H), 7.88 (br, 2H), 2.04 (br, 4H), 1.56 (br, 6H), 1.19 (br, 16H), 0.81 (br, 6H); UV-vis (ODCB, nm) λ_{max} 417, 720; UV-vis (film, nm) λ_{max} 430, 726; GPC (CB, PS standards) M_n = 8.9 x 10^3 g/mol, M_w = 1.4 x 10^4 g/mol, PDI = 1.6.

Poly[2,6-(4-(2-ethylhexyl)-4-octyl-4*H*-cyclopenta[2,1-*b*:3,4-*b'*]dithiophene)-*alt*-4,7-(2,1,3-benzothiadiazole)] (PCPDTBT) (P3). According to polymerization procedure 1: 2,6-Dibromo-4-(2-ethylhexyl)-4-octyl-4*H*-cyclopenta[2,1-*b*:3,4-*b'*]dithiophene (**14**) (0.198 g, 0.355 mmol), 2,1,3-benzothiadiazole-4,7-bis(boronic acid pinacol ester) (**9**) (0.138 g, 0.355 mmol), K_2CO_3 (3.5 mL, 2 M), 1 drop of aliquat 336 (0.2–0.5 mL), toluene (7 mL), water (1.75 mL), tetrakis(triphenylphosphine)palladium (0.041 g, 35.5 μmol), phenylboronic acid (0.39 mmol, 0.048 g), bromobenzene (0.39 mmol, 0.041 mL); Yield 71% (0.142 g); ^{1}H NMR (300 MHz, $CDCl_3$) δ 8.11 (br, 2H), 7.87 (br, 2H), 2.09 (br, 4H), 1.56 (br, 4H), 1.18 (br, 5H), 1.05 (br, 6H), 0.80 (br, 4H), 0.69 (br, 9H); UV-vis (ODCB, nm) λ_{max} 412, 716; UV-vis (film, nm) λ_{max} 416, 727; GPC (THF, PS standards) M_n = 1.3 x 10^4 g/mol, M_w = 4.1 x 10^4 g/mol, PDI = 3.3.

Methyl 7-ethyl-5-oxoundecanoate (17). General procedure 4: A solution of anhydrous LiBr (0.073 mol, 6.35 g) in anhydrous THF (200 mL) under nitrogen and at rt was added to a stirred suspension of CuBr (0.037 mol, 5.25 g) in anhydrous THF (200 mL). The resulting mixture was stirred at rt until it became homogeneous.

Subsequently, a solution of 2-ethylhexylmagnesium bromide (36.6 mL, 1.0 M in diethyl ether) and (soon afterwards) methyl 5-chloro-5-oxopentanoate (**15**) (0.030 mol, 4.20 mL) were quickly added to the stirred solution. The mixture was then stirred for 30 min, quenched with saturated aqueous NH_4Cl and extracted with ethyl acetate (3 x 300 mL). The organic extracts were dried over $MgSO_4$, filtered and concentrated by evaporation *in vacuo*. The residue was purified by gradient column chromatography (silica, eluent hexane - hexane/ethyl acetate 50:50) to afford a slightly brown oil (5.90 g, 81%). GC-MS (EI) *m/z* 211 [M^+]; ^{1}H NMR (300 MHz, $CDCl_3$) δ 3.58 (s, 3H), 2.39 (t, *J* = 7.2 Hz, 2H), 2.28–2.22 (m, 4H), 1.85–1.76 (m, 3H), 1.21–1.10 (m, 8H), 0.82–0.73 (m, 6H); ^{13}C NMR (75 MHz, $CDCl_3$) δ 210.1 (CO), 173.4 (CO-O), 51.3, 47.2, 41.8, 35.0, 33.0, 32.8, 28.7, 26.2, 22.8, 18.7, 13.9, 10.7; IR (NaCl, cm^{-1}) ν_{max} 2959/2929/2874/2860 (s, saturated C-H), 1740 (s, CO-O), 1715 (s, CO).

Methyl 12-ethyl-10-oxohexadecanoate (18). According to general procedure 4: LiBr (51.1 mmol, 4.44 g), THF (284 mL), CuBr (25.6 mmol, 3.67 g), 2-ethylhexylmagnesium bromide (25.6 mL, 1.0 M in diethyl ether), methyl 10-chloro-10-oxodecanoate (**16**) (21.3 mmol, 4.20 mL), eluent hexane/$CHCl_3$ 80:20 - hexane/$CHCl_3$ 50:50), vacuum distillation (137 °C, 10^{-2} mbar); Yield 92% (6.14 g); MS (CI) *m/z* 313 [MH^+]; ^{1}H NMR (300 MHz, $CDCl_3$) δ 3.63 (s, 3H), 2.34 (t, *J* = 7.5 Hz, 2H), 2.29–2.24 (m, 4H), 1.87–1.78 (m, 1H), 1.60–1.50 (m, 4H), 1.29–1.19 (m, 16H), 0.85 (t, *J* = 6.9 Hz, 3H), 0.81 (t, *J* = 7.5 Hz, 3H); ^{13}C NMR (75 MHz, $CDCl_3$) δ 211.7 (CO), 174.3 (CO-O), 51.5, 47.5, 43.4, 35.2, 34.1, 33.3, 29.3, 29.24, 29.15, 28.9, 26.5, 25.0, 23.9, 23.0, 14.2, 10.9; IR (NaCl, cm^{-1}) ν_{max} 2956/2929/2857 (m, saturated C-H), 1742 (m, CO-O), 1714 (m, CO).

6-([2,2'-Bithiophene]-3-yl)-6-(2-ethylhexyl)tetrahydro-2*H*-pyran-2-one (19). According to general procedure 1: 3-bromo-2,2'-bithiophene (4.08 mmol, 1.00 g), dry diethyl ether (70 mL), *n*-BuLi (2.55 mL, 1.6 M in hexane), methyl 7-ethyl-5-oxoundecanoate (**17**) (4.08 mmol, 0.99 g), eluent dichloromethane; Yield 53% (0.83 g); MS (CI) *m/z* 377 [MH^+]; ^{1}H NMR (300 MHz, $CDCl_3$) δ 7.34 (dd, *J* = 5.1/1.3 Hz, 1H), 7.24 (d, *J* = 5.4 Hz, 1H), 7.06–7.03 (m, 2H), 7.01–6.98 (m, 1H), 2.45–2.03 (m, 4H), 1.85–1.60 (m, 4H), 1.32–1.04 (m, 9H), 0.83–0.68 (m, 6H); IR (NaCl, cm^{-1}) ν_{max} 3105/3088 (w, unsaturated C-H), 2957/2928/2872/2858 (m, saturated C-H), 1737 (s, CO-O).

Methyl 4-(4-(2-ethylhexyl)-4*H*-cyclopenta[2,1-*b*:3,4-*b'*]dithiophene-4-yl)butanoate (21). H_2SO_4 (1.28 mL) was added dropwise to a solution of 6-([2,2'-bithiophene]-3-yl)-6-(2-ethylhexyl)tetrahydro-2*H*-pyran-2-one (**19**) (2.00 mmol, 0.753 g) in methanol (27 mL) under stirring at rt and the reaction was continuously stirred for 12 h at rt. Work-up according to general procedure 2. The products **20** and **20'** were separated *via* column chromatography (silica, eluent hexane/ethyl acetate 90:10 - hexane/ethyl acetate 50:50) affording a dark yellow oil of **20** (0.510 g, 65%). Further cyclization according to general procedure **2**: ester-functionalized bithiophene **20** (1.31 mmol, 0.510 g), *n*-octane (17.44 mL), H_2SO_4 (0.84 mL), eluent hexane/ethyl acetate 90:10; Yield 23% (0.115 g); MS (CI) *m/z* 391 [MH^+]; ^{1}H NMR (300 MHz, $CDCl_3$) δ 7.14 (d, *J* = 4.8 Hz, 2H), 6.93 (2 x d, *J* = 4.8 Hz, 2H), 3.59 (s, 3H), 2.10 (t, *J* = 7.5 Hz, 2H), 1.92–1.85 (m, 4H), 1.25–1.14 (m, 2H), 1.05–0.84 (m, 9H), 0.75 (t, *J* = 6.8 Hz, 3H), 0.59 (t, *J* = 7.4 Hz, 3H); ^{13}C NMR (75 MHz, $CDCl_3$) δ 173.9 (CO-O), 157.2, 136.9, 124.6, 121.9, 53.0, 51.5, 41.8, 38.9, 35.2, 34.2, 34.1, 28.6, 27.3, 22.8, 20.0, 14.2, 10.7; IR (NaCl, cm^{-1}) ν_{max} 3104/3069 (w, unsaturated C-H), 2956/2926/2871/2856 (m, saturated C-H), 1739 (s, CO-O); UV-vis ($CHCl_3$, nm) λ_{max} (log ε) 250 (3.941), 319 (4.149).

Methyl 10-([2,2'-bithiophene]-3-yl)-12-ethyl-10-hydroxyhexadecanoate (22). According to general procedure 1: 3-bromo-2,2'-bithiophene (0.016 mol, 3.92 g), dry diethyl ether (275 mL), *n*-BuLi (10 mL, 1.6 M in hexane), methyl 12-ethyl-10-oxohexadecanoate (**18**) (0.019 mol, 5.933 g), eluent dichloromethane; Yield 40% (3.06 g); MS (CI) *m/z* 461 [MH^+]; ^{1}H NMR (300 MHz, $CDCl_3$) δ 7.35 (dd, *J* = 5.1/1.2 Hz, 1H), 7.22 (d, *J* = 5.4 Hz, 1H), 7.09 (dd, *J* = 3.6/1.2 Hz, 1H), 7.00 (dd, *J* = 5.1/3.6 Hz, 1H), 6.97 (d, *J* = 5.4 Hz, 1H), 3.64 (s, 3H), 2.28 (t, *J* = 7.5 Hz, 2H), 1.97/1.80 (2 x s, OH), 1.76–1.56 (m, 5H), 1.43–1.05 (m, 20H), 0.87–0.69 (m, 6H); ^{13}C NMR (75 MHz, $CDCl_3$) δ 174.3 (CO-O), 145.6, 135.6, 129.4, 128.6, 128.5, 127.2, 126.7, 124.9, 78.68/78.63, 51.5, 47.6, 43.2, 34.6, 34.1, 33.9, 29.9, 29.4, 29.3, 29.2, 28.7, 27.1, 25.0, 23.6, 23.1, 14.2, 10.6; IR (NaCl, cm^{-1}) ν_{max} 3521 (w, OH), 3106/3073 (w, unsaturated C-H), 2953/2928/2856 (m, saturated C-H), 1739 (m, CO-O).

Methyl 9-(4-(2-ethylhexyl)-4*H*-cyclopenta[2,1-*b*:3,4-*b'*]dithiophene-4-yl)nonanoate (25). According to general procedure 2: H_2SO_4 (3.10 mL), methyl 10-([2,2'-bithiophene]-3-yl)-12-ethyl-10-hydroxyhexadecanoate (**22**) (4.84 mmol, 2.315 g), *n*-octane (65 mL), reaction mixture was stirred for 2.5 h, work-up without further

purification. H_2SO_4 (2.0 mL) was added to the obtained mixture of **23** and **24** (3.1 mmol, 1.378 g) in methanol (10 mL), the mixture was stirred for 2 h, work-up according to general procedure 2: eluent pentane/ethyl acetate 90:10; Yield 40% (0.89 g); GC-MS (EI) *m/z* 460 [M^+]; ^{1}H NMR (300 MHz, $CDCl_3$) δ 7.12 (d, *J* = 5.1 Hz, 2H), 6.92 (d, *J* = 4.8 Hz, 1H), 6.92 (d, *J* = 4.8 Hz, 1H), 3.65 (s, 3H), 2.26 (t, *J* = 7.5 Hz, 2H), 1.89 (t, *J* = 5.0 Hz, 2H), 1.83–1.78 (m, 2H), 1.61–1.51 (m, 2H), 1.25–0.83 (m, 19H), 0.75 (t, *J* = 6.8 Hz, 3H), 0.60 (t, *J* = 7.4 Hz, 3H); ^{13}C NMR (75 MHz, $CDCl_3$) δ 174.2 (CO-O), 157.8/157.7, 136.6, 124.3, 121.9, 53.2, 51.4, 41.7, 39.5, 35.2, 34.1, 29.9, 29.2/29.1, 28.6, 27.3, 24.9, 24.3, 22.8, 14.1, 10.7; IR (NaCl, cm^{-1}) ν_{max} 3105/3068 (w, unsaturated C-H), 2953/2928/2855 (s, saturated C-H), 1740 (s, CO-O); UV-vis ($CHCl_3$, nm) λ_{max} (log ε) 250 (3.937), 320 (4.139).

Methyl 9-(2,6-dibromo-4-(2-ethylhexyl)-4*H*-cyclopenta[2,1-*b*:3,4-*b'*]dithiophene-4-yl)nonanoate (26). According to general procedure 3: NBS (1.46 mmol, 0.260 g), methyl 9-(4-(2-ethylhexyl)-4*H*-cyclopenta[2,1-*b*:3,4-*b'*]dithiophene-4-yl)nonanoate (**25**) (0.685 mmol, 0.315 g), degassed DMF (17.56 mL), eluent hexane/ethyl acetate 90:10; Yield 63% (0.266 g); GC-MS (EI) *m/z* 616/620 [M^+]; ^{1}H NMR (300 MHz, $CDCl_3$) δ 6.92 (s, 1H), 6.91 (s, 1H), 3.64 (s, 3H), 2.26 (t, *J* = 7.5 Hz, 2H), 1.83–1.70 (m, 4H), 1.61–1.53 (m, 2H), 1.24–0.84 (m, 19H), 0.77 (t, *J* = 6.9 Hz, 3H), 0.62 (t, *J* = 7.4 Hz, 3H); ^{13}C NMR (75 MHz, $CDCl_3$) δ 174.5 (CO-O), 155.9/155.8, 136.6/136.5, 125.0/124.9, 111.1, 111.0, 55.1, 51.6, 41.7, 39.4, 35.4, 34.2, 34.1, 29.9, 29.31/29.26, 29.2, 28.6, 27.4, 25.0, 24.3, 22.9, 14.2, 10.8; IR (NaCl, cm^{-1}) ν_{max} 3084 (w, unsaturated C-H), 2928/2855 (s, saturated C-H), 1739 (s, CO-O); UV-vis ($CHCl_3$, nm) λ_{max} (log ε) 250 (3.884), 339 (4.297).

Poly[2,6-(4-(2-ethylhexyl)-4-(9-methylnonanoyl)-4*H*-cyclopenta[2,1-*b*:3,4-*b'*]-dithiophene)-*alt*-4,7-(2,1,3-benzothiadiazole)] (PCPDTBT) (P4). Polymerization procedure 2: Methyl 9-(2,6-dibromo-4-(2-ethylhexyl)-4*H*-cyclopenta[2,1-*b*:3,4-*b'*]dithiophene-4-yl)nonanoate (**26**) (0.416 mmol, 0.256 g), 2,1,3-benzothiadiazole-4,7-bis(boronic acid pinacol ester) (**9**) (0.416 mmol, 0.161 g) and CsF (1.66 mmol, 0.253 g) were added to a three-neck flask under nitrogen atmosphere. Subsequently, degassed DME (4.16 mL) and $Pd(PPh_3)_4$ (42 µmol, 0.048 g) were quickly added. The reaction mixture was stirred under an inert atmosphere at 80 °C for 3 days. Subsequently, a toluene solution of phenylboronic acid (0.458 mmol, 0.056 g) was added, followed by

the addition of bromobenzene (0.458 mmol, 0.048 mL), and the mixture was stirred overnight at 80 °C. Work-up and soxhlet extraction according to polymerization procedure 1; Yield 81% (0.200 g); ^{1}H NMR (300 MHz, $CDCl_3$) δ 8.11 (br, 2H), 7.89 (br, 2H), 3.61 (br, 3H), 2.24 (br, 4H), 1.21 (br, 23H), 0.70 (br, 6H); UV-vis (ODCB, nm) λ_{max} 412, 721; UV-vis (film, nm) λ_{max} 420, 740; IR (NaCl, cm^{-1}) ν_{max} 2955/2924/2852 (m, saturated C-H), 1740 (m, CO-O); GPC (THF, PS standards) M_n = 1.4 x 10^4 g/mol, M_w = 5.2 x 10^4 g/mol, PDI = 3.7.

3.5. Acknowledgments

The authors gratefully acknowledge the IWT (Institute for the Promotion of Innovation by Science and Technology in Flanders) for financial support via the SBO-project 060843 ”PolySpec”. We thank dr. A. Hadipour for the solar cell measurements. We also want to thank BELSPO for a post-doc fellowship to dr. A. E. Boyukbayram. Finally we are also grateful to Huguette Penxten for the CV measurements.

3.6. References

(1) (a) Xue, J. *Polym. Rev.*, **2010**, *50*, 411. (b) Deibel, C.; Dyakonov, V. *Rep. Prog. Phys.*, **2010**, *73*, 096401. (c) Chidichimo, G.; Filippelli, L. *Int. J. Photoenergy*, **2010**, 123534. (d) Nielsen, T. D.; Cruickshank, C.; Foged, S.; Thorsen, J.; Krebs, F. C. *Sol. Energy Mater. Sol. Cells*, **2010**, *94*, 1553. (e) Helgesen, M.; Søndergaard, R.; Krebs, F. C. *J. Mater. Chem.*, **2010**, *20*, 36. (f) Bundgaard, E.; Hagemann, O.; Manceau, M.; Jørgensen, M.; Krebs, F. C. *Macromolecules*, **2010**, *43*, 8115. (g) Krebs, F. C. *Polymeric Solar Cells: Material, Design, Manufacture*; DEStech Publications, Inc., Lancaster, Pennsylvania, **2010**. (h) Arias, A. C.; MacKenzie, J. D.; McCulloch, I.; Rivnay, J.; Salleo, A. *Chem. Rev.*, **2010**, *110*, 3. (i) Brabec, C. J.; Gowrisanker, S.; Halls, J. J. M.; Laird, D.; Jia, S.; Williams, S. P. *Adv. Mater.*, **2010**, *22*, 3839. (j) Boudreault, P.-L. T.; Najari, A.; Leclerc, M. *Chem. Mater.*, **2011**, *23*, 456. (k) Teichler, A.; Eckardt, R.; Hoeppener, S.; Friebe, C.; Perelaer, J.; Senes, A.; Morana, M.; Brabec, C. J.; Schubert, U. S. *Adv. Energy Mater.*, **2011**, *1*, 105. (l) Hübler, A.; Trnovec, B.; Zillger, T.; Ali, M.; Wetzold, N.; Mingebach, M.; Wagenpfahl, A.; Deibel, C.; Dyakonov, V. *Adv. Energy Mater.*, **2011**, DOI: 10.1002/aenm.201100394.

(2) (a) Bundgaard, E.; Krebs, F. C. *Sol. Energy Mater. Sol. Cells* **2007**, *91*, 954. (b) Thompson, B. C.; Fréchet, J. M. J. *Angew. Chem. Int. Ed.*, **2008**, *47*, 58. (c) Chen, L.-M.; Hong, Z.; Li, G.; Yang, Y. *Adv. Mater.*, **2009**, *21*, 1434. (d) Heeger, A. J. *Chem. Soc. Rev.*, **2010**, *39*, 2354. (e) Facchetti, A. *Chem. Mater.*, **2011**, *23*, 733. (h) Thompson, B. C.; Khlyabich, P. P.; Burkhart, B.; Aviles, A. E.; Rudenko, A.; Shultz, G. V.; Ng, C. F.; Mangubat, L. B. *Green*, **2011**, *1*, 29.

(3) (a) Ma, W.; Yang, C.; Gong, X.; Lee, K.; Heeger, A. J. *Adv. Funct. Mater.*, **2005**, *15*, 1617. (b) Li, G.; Shrotriya, V.; Huang, J.; Yao, Y.; Moriarty, T.; Emery, K.; Yang, Y. *Nat. Mater.*, **2005**, *4*, 864.

(4) Dang, M. T.; Hirsch, L.; Wantz, G. *Adv. Mater.*, **2011**, *23*, 3597.

(5) (a) Coppo, P.; Cupertino, D. C.; Yeates, S. G.; Turner, M. L. *J. Mater. Chem.*, **2002**, *12*, 2597. (b) Coppo, P.; Cupertino, D. C.; Yeates, S. G.; Turner, M. L. *Macromolecules*, **2003**, *36*, 2705. (c) Coppo, P.; Turner, M. L. *J. Mater. Chem.*, **2005**, *15*, 1123. (d) Horie, M.; Majewski, L. A.; Fearn, M. J.; Yu, C.-Y.; Luo, Y.; Song, A.; Saunders, B. R.; Turner, M. L. *J. Mater. Chem.*, **2010**, *20*, 4347.

(6) (a) Mühlbacher, D.; Scharber, M.; Morana, M.; Zhu, Z.; Waller, D.; Gaudiana, R.; Brabec, C. *Adv. Mater.*, **2006**, *18*, 2884. (b) Zhu, Z.; Waller, D.; Gaudiana, R.; Morana, M.; Mühlbacher, D.; Scharber, M.; Brabec, C. *Macromolecules*, **2007**, *40*, 1981. (c) Soci, C.; Hwang, I.-W., Moses, D.; Zhu, Z.; Waller, D.; Gaudiana, R.; Brabec, C. J.; Heeger, A. J. *Adv. Funct. Mater.*, **2007**, *17*, 632. (d) Zhang, M.; Tsao, H.; Pisula, W.; Yang, C.; Mishra, A. K.; Müllen, K. *J. Am. Chem. Soc.*, **2007**, *129*, 3472. (e) Morana, M.; Wegscheider, M.; Bonanni, A.; Kopidakis, N.; Shaheen, S.; Scharber, M.; Zhu, Z.; Waller, D.; Gaudiana, R.; Brabec, C. *Adv. Funct. Mater.*, **2008**, *18*, 1757. (f) Coffin, R. C.; Peet, J.; Rogers, J.; Bazan, G. C.; *Nat. Chem.*, **2009**, *1*, 657. (g) Bijleveld, J. C.; Shahid, M.; Gilot, J.; Wienk, M. M.; Janssen, R. A. J. *Adv. Funct. Mater.*, **2009**, *19*, 3262. (h) Kettle, J.; Horie, M.; Majewski, L. A.; Saunders, B. R.; Tuladhar, S.; Nelson, J.; Turner, M. L. *Sol. Energy Mater. Sol. Cells*, **2011**, *95*, 2186.

(7) (a) Peet, J.; Kim, J. Y.; Coates, N. E.; Ma, W. L.; Moses, D.; Heeger, A. J.; Bazan, G. C. *Nat. Mater.*, **2007**, *6*, 497. (b) Lee, J. K.; Ma, W. L.; Brabec, C. J.; Yuen, J.; Moon, J. S.; Kim, J. Y.; Lee, K.; Bazan, G. C.; Heeger, A. J. *J. Am. Chem. Soc.*, **2008**, *130*, 3619.

(8) (a) Yang, L.; Zhou, H.; You, W. *J. Phys. Chem. C.*, **2010**, *114*, 16793. (b) Szarko, J. M.; Guo, J.; Liang, Y.; Lee, B.; Rolczynski, B. S.; Strzalka, J.; Xu, T.; Loser, S.; Marks, T. J.; Yu, L.; Chen, L. X. *Adv. Mater.*, **2010**, *22*, 5468. (c) Piliego, C.; Holcombe, T. W.; Douglas, J. D.; Woo, C. H.; Beaujuge, P. M.; Fréchet, J. M. J. *J. Am. Chem. Soc.*, **2010**, *132*, 7595. (d) Subramaniyan, S.; Xin, H.; Kim, F. S.; Shoaee, S.; Durrant, J. R.; Jenekhe, S. A. *Adv. Energy Mater.*, **2011**, *1*, 854. (e) Oosterhout, S. D.; Koster, L. J. A.; van Bavel, S. S.; Loos, J.; Stenzel, O.; Thiedmann, R.; Schmidt, V.; Campo, B.; Cleij, T. J.; Lutsen, L.; Vanderzande, D.; Wienk, M. M.; Janssen, R. A. J. *Adv. Energy Mater.*, **2011**, *1*, 90.

(9) Van Mierloo S.; Adriaensens, P.; Maes, W.; Lutsen, L.; Cleij, T. J.; Botek, E.; Champagne, B.; Vanderzande, D. J. *J. Org. Chem.*, **2010**, *75*, 7202.

(10) Reynolds, J. R.; Brzezinski, J. Z. *Synthesis*, **2002**, *8*, 1053.

(11) Murage, J.; Eddy, J. W.; Zimbalist, J. R.; McIntyre, T. B.; Wagner, Z. R.; Goodson, F. E. *Macromolecules*, **2008**, *41*, 7330.

(12) Chen, C.-H.; Hsieh, C.-H.; Dubosc, M.; Cheng, Y.-J.; Hsu, C.-S. *Macromolecules*, **2010**, *43*, 697.

(13) Kim, D. Y.; Subbiah, J.; Sarasqueta, G.; So, F.; Ding, H.; Gao, I.; Gao, Y. *Appl. Phys. Lett.*, **2009**, *95*, 093304

(14) Miyanishi, S.; Tajima, K.; Hashimoto, K. *Macromolecules*, **2009**, *42*, 1610.

(15) Kim, B. J.; Miyamoto, Y.; Ma, B.; Fréchet, J. M. J. *Adv. Funct. Mater.*, **2009**, *19*, 1.

(16) Babudri, F.; Fiandanese, V.; Marchese, G.; Punzi, A. *Tetrahedron*, **1996**, *52*, 13513.

(17) Moumne, R.; Lavielle, S.; Karoyan, P. *J. Org. Chem.*, **2006**, *71*, 3332.

(18) Wright, S. W.; Hageman, D. L.; McClure, L. D. *J. Org. Chem.*, **1994**, *59*, 6095.

(19) Brookins, R. N.; Schanze, K. S.; Reynolds, J. R. *Macromolecules*, **2007**, *40*, 3524.

(20) Harm, U.; Bürgler, R.; Fürbeth, W.; Mangold, K.-M.; Jüttner, K. *Macromol. Symp.*, **2002**, *187*, 65.

3.7. Supporting Information

Spin-coating conditions varied from 1200 to 2200 rpm (1000 Acc) wih concomitant film thicknesses ranging from 155 to 90 nm.

Table 3.4. Relationship between spin-coating speed and obtained active layer thickness.

Spin-coating speed	Thickness organic layer
1200 rpm	155 nm
1400 rpm	125 nm
1600 rpm	130 nm
1800 rpm	100 nm
2000 rpm	95 nm
2200 rpm	90 nm

Chapter 4

Synthesis, ^{1}H and ^{13}C NMR Assignment and Electrochemical Properties of Novel Thiopene-Thiazolothiazole Oligomers and Polymers[†]

Novel hexyl-substituted bisthiophene compounds containing a thiazolo[5,4-*d*]thiazole unit have been explored. The molecules are soluble in common organic solvents, which would enhance their chance of possible integration in printable electronics. Synthesis and complete elucidation of the chemical structures by detailed 1D/2D NMR spectroscopy are described. This provides interesting input for chemical shift prediction software, since few experimental data on this type of compounds are available. Furthermore, the potential *n*-type character of these derivatives is verified using electrochemical measurements. In addition, the low-bandgap character of conjugated polymers containing the thiazolothiazole unit is demonstrated by performing an electropolymerization.

[†] Van Mierloo, S.; Chambon, S.; Boyukbayram, A. E.; Adriaensens, P.; Lutsen, L.; Cleij, T. J.; Vanderzande, D. *Magn. Reson. Chem.* **2010**, *48*, 362.

4.1. Introduction

Organic field-effect transistors (OFETs)[1] based on organic semiconductors attract considerable attention for applications such as flexible displays, low-cost electronic paper and smart memory/sensor elements. There are many low molecular weight hole-transporting (*p*-type) semiconductors, such as pentacene[2] and oligothiophenes.[3] However, the number of *n*-type organic semiconductors is still limited and the FET performances are not satisfactory. In the literature, a series of small *n*-type bisthiophenes bearing a thiazolo[5,4-*d*]thiazole unit have been reported, which have high charge carrier mobilities.[4] The thiazolothiazole unit has some excellent characteristics for use in electronic applications. First of all, its electron-accepting property is useful to enhance the stability towards oxygen. Consequently, these compounds are stable in ambient atmospheres at room temperature over a period of several months.[5] Secondly, the thiazolothiazole moiety has a rigid planar structure due to the fused ring system, which can lead to efficient intermolecular π-π interactions.[4,6,7] Finally, the 2,5-bissubstituted thiazolothiazole is quite straightforward to prepare, starting from the corresponding aldehyde and dithiooxamide. The interesting parent compound thiazolo[5,4-*d*]thiazole has already been synthesized many years ago in moderate yield, by combining an aldehyde derivative with dithiooxamide at very high temperature.[8,9] Unfortunately, non-alkylsubstituted derivatives are very poorly soluble and require vacuum deposition techniques for device fabrication. Here, alternatively, a series of analogous thiazolothiazole containing molecules are presented, which do not have the above-mentioned disadvantages. To this end, the synthesized molecules, *i.e.* **D1**, **D2** and **D3** (*cf.* Figure 4.1) have been functionalized with two substituted 3-hexylthiophenes. The choice of substitution with alkyl chains leads to a significantly improved solubility in common organic solvents. Hence, functionalization, purification and characterization become more straightforward and the molecules can be utilized in solvent based processing, such as printable electronics. Moreover, the alkyl chains might improve stacking properties and, consequently, positively impact the charge mobilities in OFETs.

In this paper, we report the synthesis, detailed NMR structural elucidation and electrochemical properties of the first series of novel alkylthiophenyl-substituted thiazolothiazole oligomers. Cyclic voltammetry (CV) was employed to verify the

potential *n*-type character of these compounds and to estimate their highest occupied molecular orbital (HOMO) and lowest unoccupied molecular orbital (LUMO) energy levels. In addition, the molecules were used as monomers in an electropolymerization to demonstrate the low-bandgap character of conjugated polymers containing thiazolothiazole units.

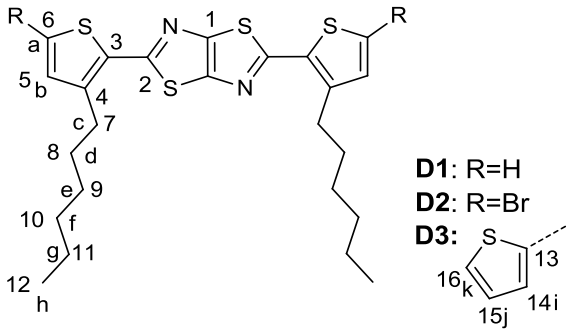

Figure 4.1. Chemical structures of the 2,5-bis(3-hexylthiophen-2-yl)thiazolo[5,4-*d*]thiazole derivatives **D1**, **D2** and **D3**. The different carbon atoms are numbered from C1 to C16 and the different hydrogen atoms are labelled from H-a to H-k.

4.2. Results and Discussion

4.2.1. Synthesis

The first molecule, *i.e.* 2,5-bis(3-hexylthiophene-2-yl)thiazolo[5,4-*d*]thiazole **D1**, was synthesized *via* a condensation reaction between 3-hexylthiophene-2-carbaldehyde and dithiooxamide. 3-Hexylthiophene-2-carbaldehyde was prepared according to a modified literature procedure.[5,10] Instead of iodine activated magnesium turnings, *n*-butyllithium was used to create an anion at the 2-thiophenyl position, followed by a nucleophilic addition on DMF resulting in 3-hexylthiophene-2-carbaldehyde. The resulting compound **D1** was purified by column chromatography and two consecutive recrystallizations from ethanol and acetonitrile. **D1** was obtained as yellow crystals in 47% yield. In order to functionalize compound **D1**, a bromination reaction with NBS was carried out in DMF, giving 2,5-bis(5-bromo-3-hexylthiophene-2-yl)thiazolo[5,4-*d*]thiazole **D2** in 71% yield (Scheme 4.1).

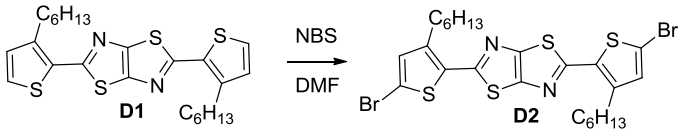

Scheme 4.1. Synthetic route towards **D2**.

Functionalization of **D2** was readily achieved by using a Stille cross coupling with tributyl(thiophen-2-yl) and $Pd(PPh_3)_4$ resulting in 2,5-bis(4-hexyl-2,2'-bithiophene-5-yl)thiazolo[5,4-*d*]thiazole **D3** (Scheme 4.2). This product was also purified by column chromatography followed by recrystallization from ethanol resulting in **D3** in 58% yield. The purity of **D1** and **D3** was further confirmed by HPLC as being higher than 99%.

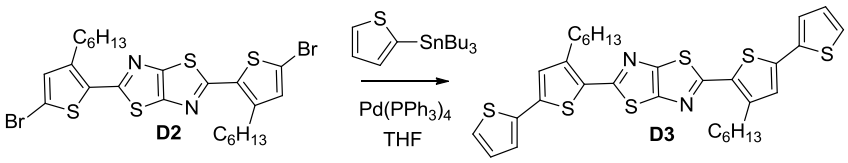

Scheme 4.2. Synthetic route towards **D3**.

Due to the substitution with hexyl side chains, all three compounds **D1**, **D2** and **D3** are soluble in common organic solvents, such as chloroform, dichloromethane and ethers. To confirm the identity of the synthesized structures, complete NMR characterization was performed. To this end, in the following section, the complete structural elucidation of these three synthesized compounds **D1**, **D2** and **D3** will be presented.

4.2.2. NMR Characterization

In order to confirm the structure of the three thiazolothiazole derivatives (**D1**, **D2** and **D3**), they were studied extensively by NMR in order to perform a complete assignment of their ^{13}C and ^{1}H resonances. Table 4.1 presents an overview of all signal assignments. Such a detailed analysis is advantageous, since the obtained chemical shift information can be very useful for implementation in NMR-based prediction software. The chemical structures of all three compounds differ only at the 5-position of the thiophene rings: **D1** bears two hydrogen atoms, **D2** two bromine atoms and **D3** two unsubstituted thiophene rings. Figure 4.1 shows the structures of **D1**, **D2** and **D3**, together with an arbitrary numbering given to their different carbons and hydrogens. APT, DEPT, T_{1C} and short range/long range-HETCOR experiments were performed on

these compounds to obtain a complete chemical shift assignment of the ^{13}C and ^{1}H resonances.

Table 4.1. Chemical shifts (ppm) and assignments of the proton and the carbon atoms in the thiazolothiazole derivatives **D1-D3**. The chemical shift scales are calibrated to TMS at 0 ppm.

	D1 R = H	**D2** R = Br	**D3** R = thien-2-yl		**D1** R = H	**D2** R = Br	**D3** R = thien-2-yl
Carbon				*Protons*			
C1	150.7	150.7	150.7	-	-	-	
C2	162.2	160.9	161.5	-	-	-	
C3	132.5	134.0	131.0	-	-	-	
C4	143.8	144.0	144.5	-	-	-	
C5	131.5	134.1	127.6	H-b	6.97 (d)	6.93 (s)	7.00 (s)
C6	128.0	116.1	137.3	H-a	7.33 (d)	-	-
C7	30.8	30.9	31.1	H-c	2.95 (t)	2.84 (t)	2.88 (t)
C8	30.7	30.4	30.5	H-d	1.70 (q)	1.66 (q)	1.71 (q)
C9	30.0	30.0	30.1	H-e	1.42 (q)	1.42 (q)	1.45 (q)
C10	32.3	32.3	32.3	H-f	1.30 (m)	1.32 (m)	1.34 (m)
C11	23.3	23.3	23.3	H-g	1.30 (m)	1.32 (m)	1.34 (m)
C12	14.8	14.8	14.8	H-h	0.88 (t)	0.89 (t)	0.90 (t)
C13	-	-	139.4		-	-	-
C14	-	-	125.2	H-i	-	-	7.22 (dd)
C15	-	-	128.8	H-j	-	-	7.02 (dd)
C16	-	-	126.0	H-k	-	-	7.24 (dd)

*Assignment of the resonances of the core of **D1** and **D2***

APT, DEPT and short-range HETCOR. The core of the derivatives is formed by 6 different carbons, C1 to C6. For **D2**, it appears that the 160.9, 150.7, 144.0, 134.0 and 116.1 ppm signals are quaternary carbons and only the 134.1 ppm signal is a methine carbon. The latter therefore corresponds to C5. The short-range HETCOR experiment indicates that this 134.1 ppm carbon signal is connected (^1J or direct coupling) to a proton singulet resonance at 6.93, corresponding to H-b.

In **D1**, the 162.2, 150.7, 143.8 and 132.5 ppm signals arise from non-protonated carbons, while the 131.5 and 128.0 ppm signals arise from CH-carbons. The short-range HETCOR indicates that the 131.5 ppm signal is attached to a ^{1}H doublet at 6.96/6.98 ppm and the 128 ppm signal to another ^{1}H doublet at 7.32/7.34 ppm. Based on the results obtained for **D2**, the ^{1}H doublet at 6.96/6.98 ppm can be legitimately attributed to H-b and the 131.5 ppm ^{13}C resonance to C5. By deduction, the 128 ppm resonance can then be attributed to C6 and the ^{1}H doublet at 7.32/7.34 ppm to H-a. Moreover, this assignment is confirmed by the resonance frequency of H-a. Indeed the neighbouring sulphur atom has a deshielding effect on the proton H-a, leading to a resonance signal at lower field as compared to H-b.

Long-range HETCOR. For both derivatives **D1** and **D2**, the signals at 162.2 and 150.7 ppm/160.9 and 150.7 ppm show no coupling with protons. Those signals therefore can be attributed to C2 and C1 (Table 4.1; *vide infra*) since both of them are at least 4 bonds away from a hydrogen atom.[11]

In **D1**, the remaining carbon signals (143.8 and 132.5 ppm) should therefore correspond to C3 and C4. The long range-HETCOR experiment shows that the 132.5 ppm signal correlates only with the 6.96/6.98 ppm ^{1}H doublet while the 143.8 ppm resonance is coupled to both the 7.32/7.34 ppm ^{1}H doublet (H-a) and the triplet centred at 2.86 ppm, corresponding to H-c. The fact that the 143.8 ppm signal is coupled with H-a indicates that it corresponds to C4. Indeed, C3 is to far (4 bonds) from H-a to have a coupling with it. Hence, by deduction the 132.5 ppm signal corresponds to C3.

In **D2**, three quaternary carbon signals have a long range coupling (^2J or ^3J) with protons, *i.e.* 116.1 ppm with H-b, 134.0 ppm with H-b and 144.0 ppm with H-a and H-c. The latter can not correspond to C6 as it is 4 bonds away from H-c. By comparison with its hydrogenated equivalent (**D1**), it is possible to attribute 144.0 ppm to C4 and

134.0 ppm to C3. By elimination, C6 in the brominated sample has a resonance signal at 116.1 ppm.

Concerning the two remaining carbon signals of the core of **D1**, one can observe that the resonance at 162.2 ppm shifts to 160.9 when the thiazolothiazole compound is brominated. On the other hand, the other signal at 150.7 ppm remains unchanged. The latter can be attributed to C1 as it is the carbon most remote from the substituent on C6. Most conclusions can be confirmed by ^{13}C spin-lattice relaxation time (T_{1C}) experiments (Table 4.2). Carbon nuclei mainly relax through space via the surrounding magnetic moments of protons ($1/T_{1C}$ has a $1/r^6$ dependency). These proton magnetic moments induce local oscillating magnetic fields due to molecular motions, the source of T_1 relaxation.[12] As the 150.7 ppm signal has the longest relaxation time, its corresponding carbon atoms indeed should be the most remote from protons. C2, being spatially more close to protons (e.g. H-c), therefore corresponds to the resonance signal at 162.2 in **D1** and 160.9 in **D2**. In addition, the assignment of C3 and C4 in **D1** can be confirmed by means of the T_{1c} relaxation decay times, being clearly longer (less efficient relaxation) for C3. The same holds true for **D2** sharing a decrease in the T_{1C} in going from C3 over C6 to C4.

*Assignment of the resonances of the core of **D3***

The ^1H spectrum presents four resonance patterns corresponding to the four protons of the core: a singulet at 7.00 ppm and three double doublets at 7.02 ppm (^3J=3.7 Hz, ^3J=5.1 Hz), 7.22 ppm (^3J=3.7 Hz, ^4J=1.0 Hz) and 7.24 ppm (^3J=5.1 Hz, ^4J=1.0 Hz). According to the *J*-coupling pattern and literature data,[12] these four signals correspond to H-b, H-j, H-i and H-k, respectively.

Concerning the assignment of the carbons, the assignments for **D1** and **D2** already allow the assignment of the core carbon signals at 161.5, 150.7, 144.5 and 131.0 ppm to C2, C1, C4 and C3, respectively. From the remaining 6 carbons of the core, the ones resonating at 137.3 and 139.4 ppm are quaternary carbons and correspond to C6 and C13. The long-range HETCOR experiment (Figure 4.2) showed that the 139.4 ppm signal couples with H-b, H-i and H-j, while the 137.3 ppm signal has only a small coupling with H-i. This allows to assign the 139.4 ppm signal to C13 as C6 is separated by 4 bonds from H-j. C6 then corresponds to the signal at 137.3 ppm. This attribution is

further confirmed by the T_{1C} relaxation which shows a longer decay time for the 137.3 ppm signal as compared to the 139.4 ppm one (6.1 and 4 s, respectively).

Table 4.2. ^{13}C spin-lattice relaxation decay times (T_{1C}) for all carbon signals of **D1** and **D3**.

D1		**D3**	
^{13}C Resonance frequency (ppm)	T_{1C} (s)	^{13}C Resonance frequency (ppm)	T_{1C} (s)
162.2	14.2	161.5	6.7
150.7	21.1	150.7	9.3
143.8	6.6	144.5	3.3
132.5	15.9	139.4	4.0
131.5	0.66	137.3	6.1
128	0.72	131.0	7.8
32.3	2.01	128.8	0.63
30.8	0.74	127.6	0.40
30.7	1	126.05	0.41
30.0	1.3	125.2	0.63
23.3	2.9	32.3	1.67
14.8	3.2	31.1	0.50
		30.5	0.71
		30.1	1.00
		23.3	2.32
		14.8	3.12

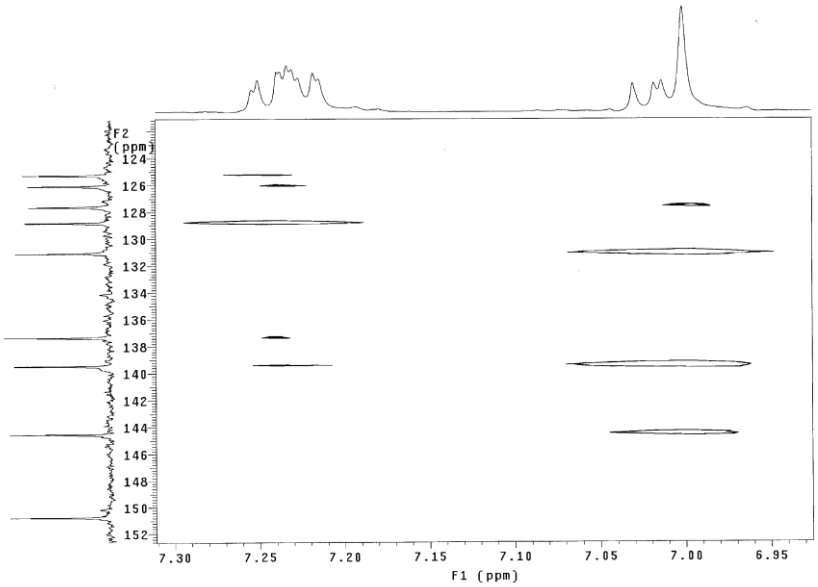

Figure 4.2. Long-range HETCOR (J = 8 Hz) of **D3**.

According to the short-range HETCOR (Figure 4.3), the four remaining signals at 128.8, 126.0, 125.2 and 127.6 ppm are respectively coupled with the double doublets centred at 7.02 (H-j), 7.24 (H-k), 7.22 (H-i) and the singulet at 7.00 (H-b) ppm. They correspond to C15, C16, C14 and C5, respectively.[13]

Alkyl side chain resonance assignment

The attribution of the carbon and proton signals is only described for **D1** as the same procedure holds for **D2** and **D3**.

The chemical shift and *J*-coupling pattern of the 2.95 ppm and 0.88 ppm signals indicate that they correspond to H-c and H-h, respectively. The short-range HETCOR experiment already attributed their corresponding carbon signals to 30.8 and 14.8 ppm, respectively.

In order to assign the 4 remaining side chain carbon signals and their respective protons, ^{13}C spin-lattice relaxation time (T_{1C}) and COSY experiments were performed. Table 4.2 summarises the T_{1C} values for the different carbon signals. For mobile side chains, the closer the carbon is situated towards the side chain end, the longer its relaxation decay time will be due to less restricted conformational motions.[12] This is clear for C7 (30.8 ppm) and C12 (14.8 ppm) which have respectively the shortest and the longest T_{1c} time constant of the alkyl chain carbons. Following this theory we can

attribute the 30.7, 30.0, 32.3 and 23.3 ppm signals to C8, C9, C10 and C11, respectively. The short-range HETCOR spectrum allows the assignment of their respective proton signals and the COSY experiment confirmed these attributions.

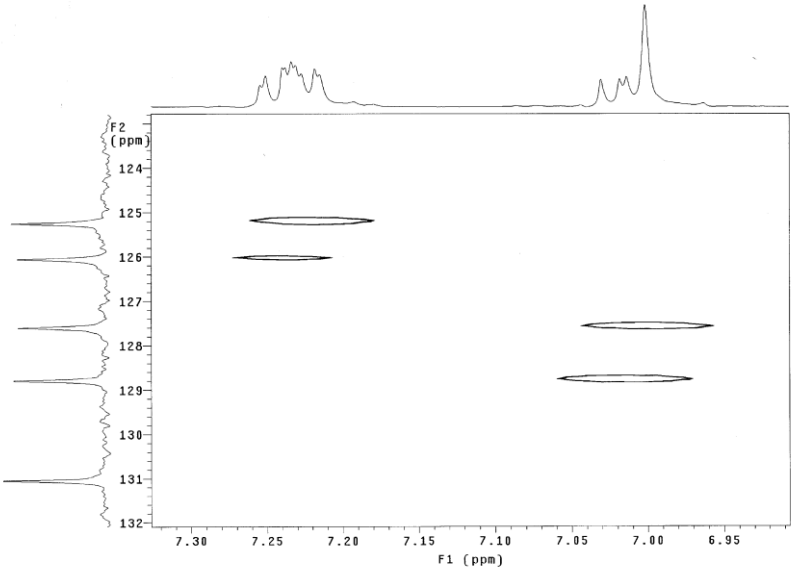

Figure 4.3. Short-range HETCOR (J = 140 Hz) of **D3**.

4.2.3. Electrochemical Characterization

Since NMR has confirmed that compounds **D1** and **D3** were available in excellent purity, the electrochemical properties, which are important towards potential application, can now be investigated. Cyclic voltammetry (CV) was employed to investigate the electrochemical behavior of **D1** and **D3** and to estimate their HOMO and LUMO energy levels. In addition, the compounds were electropolymerized under the same conditions. Upon electropolymerization, a dark red polymer was obtained with **D1** as monomer and a greyish-blue polymer was obtained with **D3** as monomer. The intensity of the color and the film thickness increased with polymerization time. However, after one hour of polymerization, no further increase in the thickness was observed. In addition, for both monomers, no bulk polymer was observed in solution. For the cyclic voltammetry of the polymers, the formed polymer films were first rinsed with CH_3CN, after which a fresh electrolyte solution was added.

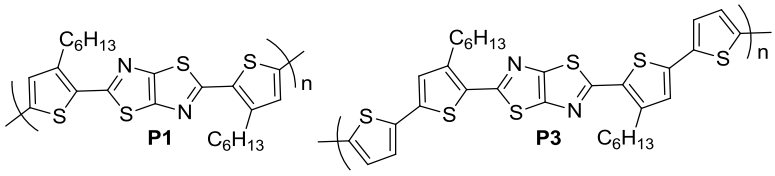

Figure 4.4. Chemical structures of polymers **P1** and **P3**.

The cyclic voltammogram of monomer **D1** displays typical oxidation and reduction processes as shown in Figure 4.5. The HOMO-LUMO gap was calculated at 2.83 eV using the onset values of oxidation and reduction and the corresponding HOMO-LUMO values (Table 4.3). The sharp oxidation peak around 0.670 V in Figure 4.5, which occurs after the first scan, is a result of the formation of an intermediate oligomer. Upon further electropolymerizing **D1** (Figure 4.6), the oxidation peak of the conjugated polymer (**P1**, *cf.* Figure 4.4) appears at *circa* 0.5 V. The final onset values of the oxidation and reduction of **P1** are 0.325 V and -1.505 V, from which the electrochemical energy gap can be estimated at 1.83 eV (Table 4.3). The LUMO of **P1** can be readily determined at -3.43 eV (Table 4.3), which is more accurate than a previously reported value, which was indirectly obtained from the oxidation potential and the optical bandgap.[5]

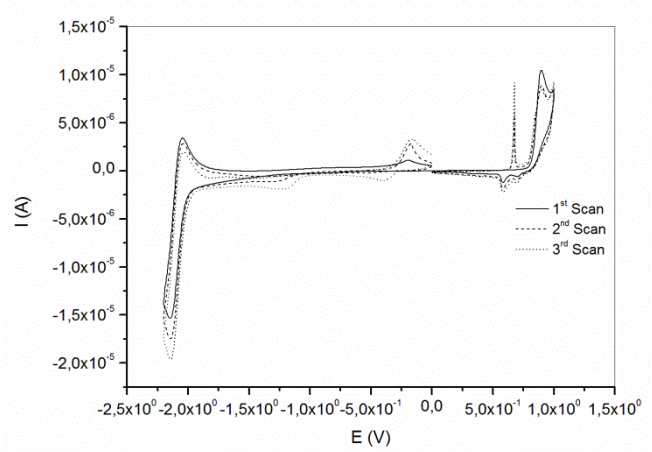

Figure 4.5. Cyclic voltammogram of **D1** (solid: 1st scan; dashed: 2nd scan; dotted: 3rd scan).

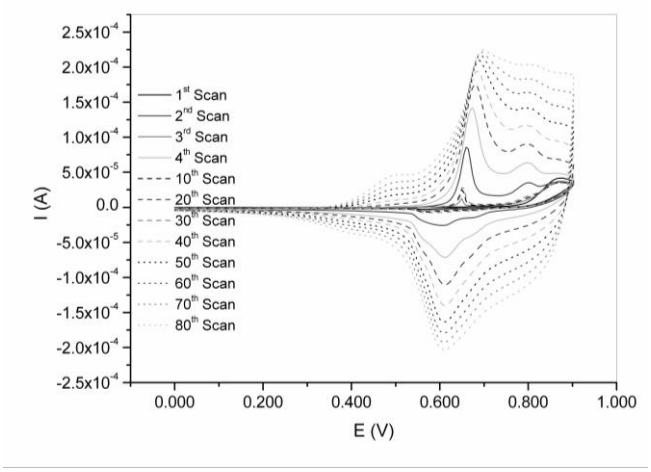

Figure 4.6. Electropolymerization of **D1**. Every tenth of 80 consecutive scans is presented.

The onset of oxidation and reduction for **D3** give an electrochemical HOMO-LUMO gap of 2.40 eV (Figure 4.7). After several scans, the oxidation peak of the corresponding conjugated polymer (**P3**, *cf.* Figure 4.4) appears around 0.6 V (Figure 4.8). The final onset values of the oxidation and reduction of **P3** are 0.315 V and -1.425 V, from which the electrochemical energy gap can be estimated at 1.74 eV (Table 4.3).

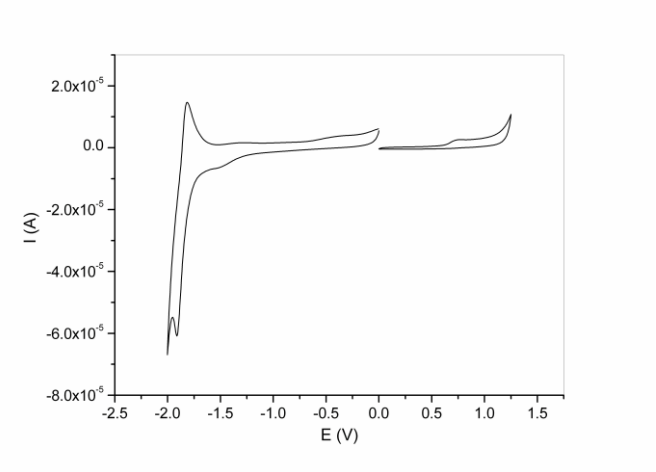

Figure 4.7. Cyclic voltammogram of **D3.**

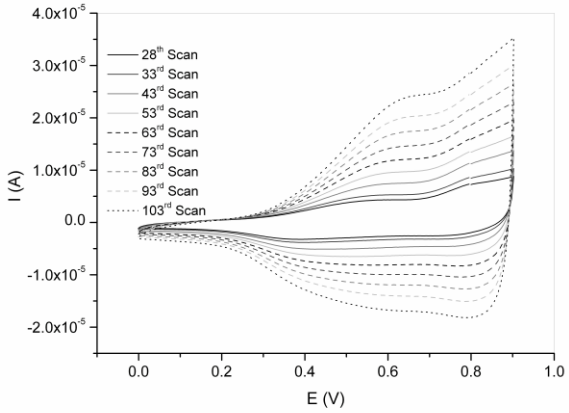

Figure 4.8. Electropolymerization of **D3**. Selective scans of a total of 103 consecutive scans are presented.

It is noteworthy that both **D1** and **D3** exhibit a distinct reversible reduction peak in their cyclic voltammograms. This confirms the potential *n*-type character of these compounds. However a more thorough mobility study has to be performed to confirm the *n*-type character. Furthermore, the HOMO-LUMO energy gap values of both monomers and polymers are in good agreement with their corresponding optical energy gaps (Table 4.3). In addition, the low-bandgap character of conjugated polymers containing thiazolothiazole units is demonstrated by the electrochemical energy gap values observed for **P1** and **P3**, which are both below 2 eV.

Table 4.3. HOMO-LUMO and optical/electrochemical energy gap values of **D1** and **D3** as well as the corresponding electropolymerized conjugated polymers **P1** and **P3**.

	HOMO(eV)	LUMO(eV)	E_g^{EC}(eV)	E_g^{OP}(eV)* (solution)	E_g^{OP}(eV)* (thin film)
D1	-5.74	-2.91	2.83	2.84	
P1	-5.26	-3.43	1.83		1.9
D3	-5.54	-3.14	2.40	2.46	
P3	-5.25	-3.51	1.74		1.7

(*) Determined by means of UV-Vis spectroscopy.

4.3. Conclusions

Substitution of thiopene-thiazolothiazole derivatives **D1**, **D2** and **D3** with hexyl side chains noticeably improved their solubility in common organic solvents. As a result, **D1** and **D2** could readily undergo functionalization reactions to become suitable for printable electronics. The proposed chemical structures of **D1**-**D3** are fully confirmed by NMR spectroscopy. A complete assignment of the proton and carbon resonances was accomplished by means of 1D- and 2D-NMR experiments. Since it concerns rather newly developed compounds, such a complete signal assignment will be highly useful for further progression in NMR prediction software. Cyclic voltammetry was used to estimate the HOMO and LUMO energy levels of **D1** and **D3**. These values, in combination with the reversible character of the reduction processes, indicate that these compounds potentially have *n*-type character. In addition, **D1** and **D3** were used as monomers in an electropolymerization and it was demonstrated that conjugated polymers containing the thiophene-thiazolothiazole core as building block can have a low bandgap character.

4.4. Experimental Section

Synthesis

Tributyl(thiophen-2-yl)stannane was synthesized according to a literature procedure.[14]

3-Hexylthiophene-2-carbaldehyde

A solution of 2-bromo-3-hexylthiophene (5.7 g, 0.023 mol) in THF (150 mL) was cooled down to -78 °C, after which *n*-butyllithium (14 mL, 0.023 mol, 1.6 M in hexane) was slowly added under N_2 atmosphere. After the mixture was stirred for 15 minutes, dry DMF (2.40 mL, 0.031 mol) was added dropwise at the same temperature. Subsequently, the mixture was warmed up to room temperature and stirred for an additional two hours. Afterwards the reaction mixture was treated with a HCl-solution (0.5 M) and extracted with diethyl ether (3 x 50 mL). The combined organic layers were washed with saturated bicarbonate solution and brine, dried over magnesium sulphate and concentrated by evaporation *in vacuo*. The crude product was purified by column chromatography using silica gel (eluent: hexane/ethylacetate 95:5) giving 3.20 g of a viscous yellow oil (71 % yield).

^{1}H NMR ($CDCl_3$): δ = 9.95 (s, 1H), 7.55 (d, *J* = 5.1 Hz, 1H), 6.93 (d, *J* = 5.1 Hz, 1H), 2.88 (t, 2H), 1.58 (m, 2H), 1.21 (m, 6H), 0.80 (t, 3H).

2,5-Bis(3-hexylthiophene-2-yl)thiazolo[5,4-*d*]thiazole D1

A mixture of 3-hexylthiophene-2-carbaldehyde (3.02 g, 0.015 mol) and dithiooxamide (0.29 g, 2.42 mmol) was stirred at 200 °C for two hours. Subsequently, the reaction mixture was cooled down to room temperature and diluted with water (50 mL) and diethyl ether (50 mL). The organic layer was separated and the aqueous layer was extracted with diethyl ether (3 x 50 mL). The combined organic layers were washed with a saturated bicarbonate solution and brine, dried over magnesium sulphate and concentrated by evaporation *in vacuo*. The resulting brown oil was purified by column chromatography using silica gel (eluent: hexane/ethyl acetate 95:5) followed by subsequent recrystallization from acetonitrile and ethanol giving 0.54 g of yellow crystals (47% yield).

^{1}H NMR ($CDCl_3$): δ = 7.33 (d, *J* = 5.1 Hz, 2H), 6.97 (d, *J* = 5.1 Hz, 2H), 2.95 (t, 4H), 1.7 (q, 4H), 1.42 (q, 4H), 1.3 (m, 4H), 1.3 (m, 4H), 0.88 (t, 6H); ^{13}C NMR ($CDCl_3$): δ = 162.2, 150.7, 143.8, 132.5, 131.5, 128.0, 32.3, 30.8, 30.7, 30.0, 23.3, 14.8; MS: m/z= 474 (M^+); UV-Vis (solution chloroform) (λ_{max}) 392 nm, mp = 71°C

2,5-Bis(5-bromo-3-hexylthiophene-2-yl)thiazolo[5,4-*d*]thiazole D2

Protected from light, a solution of NBS (0.61 g, 3.44 mmol) in DMF (50 mL) was added dropwise to a solution of 2,5-bis(3-hexylthiophene-2-yl)thiazolo[5,4-d]thiazole **D1** (0.51 g, 1.08 mmol) in DMF (50 mL), after which the mixture was stirred for 48 hours. Subsequently, the mixture was poured onto ice and extracted with diethyl ether (3 x 50 mL). The combined organic layers were washed with a saturated bicarbonate solution and brine, dried over magnesium sulphate and concentrated by evaporation *in vacuo*. The crude solid was purified by column chromatography using silica gel (eluent: hexane/ethyl acetate 95:5). The compound was obtained as an orange solid (0.48 g, 71% yield).

^{1}H NMR ($CDCl_3$): δ = 6.93 (s, 2H), 2.84 (t, 4H), 1.66 (q, 4H), 1.42 (q, 4H), 1.32 (m, 4H), 1.32 (m, 4H), 0.89 (t, 6H); ^{13}C NMR ($CDCl_3$): δ = 160.9, 150.7, 144.0, 134.1, 134.0, 116.1, 32.3, 30.9, 30.4, 30.0, 23.3, 14.8; MS: m/z = 632(M^+); UV-Vis (solution chloroform) (λ_{max}) 393 nm.

2,5-Bis(4-hexyl-2,2'-bithiophene-5-yl)thiazolo[5,4-*d*]thiazole D3

A solution of tributyl(thiophen-2-yl)stannane (0.47 g, 1.26 mmol) in dry THF (50 mL) was added dropwise to a stirred mixture of 2,5-bis(5-bromo-3-hexylthiophene-2-yl)thiazolo[5,4-*d*]thiazole **D2** (0.32 g, 0.51 mmol) and $Pd(PPh_3)_4$ (0.003 g, 2.60 µmol) in dry THF (50 mL) at ambient temperature. After stirring for 12 h at reflux temperature, the reaction mixture was diluted with water (50 mL). The organic layer was separated and the aqueous layer was extracted with diethyl ether (3 x 50 mL). The combined organic layers were washed with a saturated bicarbonate solution and brine, dried over magnesium sulphate and concentrated by evaporation *in vacuo*. The reaction product was purified by column chromatography (eluent hexane/ethyl acetate 95:5) and recrystallized from ethanol resulting in 0.19 g of red crystals (58% yield).

^{1}H NMR ($CDCl_3$): δ = 7.24 (dd, *J* = 5.1 Hz, *J* = 1.0 Hz, 1H), 7.22 (dd, *J* = 3.7 Hz, *J* = 1.0 Hz, 1H), 7.02 (dd, *J* = 5.1 Hz, *J* = 3.7 Hz, 1H), 7.00 (s, 2H), 2.88 (t, 4H), 1.71 (q, 4H), 1.45 (q, 4H), 1.34 (m, 4H), 1.34 (m, 4H), 0.90 (t, 6H); ^{13}C NMR ($CDCl_3$): δ = 161.5, 150.7, 144.5, 139.4, 137.3, 131.0, 128.8, 127.6, 126.0, 125.2, 32.3, 31.1, 30.5, 30.1, 23.3, 14.8; MS: m/z = 638 (M^+); UV-Vis (solution chloroform) (λ_{max}) 449 nm; mp= 153°C.

Electrochemical Characterization/Electropolymerization

Electrochemical measurements were performed with an Eco Chemie Autolab PGSTAT 30 Potentiostat/Galvanostat using 0.1 M Bu_4NPF_6 in anhydrous CH_3CN as the electrolyte under N_2 atmosphere. A three-electrode microcell was utilized containing an $Ag/AgNO_3$ reference electrode (0.1 M $AgNO_3$ and 0.1 M Bu_4NPF_6 in CH_3CN), a platinum counter electrode and an indium tin oxide (ITO) coated glass substrate as the working electrode. The respective monomers were dissolved to their maximum solubility in the electrolyte solution. Cyclic voltammograms were recorded at a scan rate of 50 mV/s. Oxidative electropolymerization was achieved by scanning between 0 and 0.9 V at the same scan rate for a large number of consecutive scans. For the conversion to eV, all electrochemical potentials have been referenced to a known standard (ferrocene/ferrocenium in CH_3CN, 0.05 V *vs.* $Ag/AgNO_3$), which in acetontrile solution is estimated to have an oxidation potential of -4.98 V *vs.* Vacuum.

UV-Vis spectra were recorded on a Varian CARY 500 UV-Vis-NIR spectrophotometer from 200 to 800 nm at a scan rate of 600 nm min^{-1}.

NMR Characterization

All ^{1}H and ^{13}C liquid-state NMR experiments on **D1**, **D2** and **D3** were performed at room temperature on a Varian Inova 300 spectrometer in a 5 mm four-nucleus PFG probe. Solutions were prepared in $CDCl_3$ with concentrations of 3 mg/mL and 50 mg/mL for the ^{1}H and ^{13}C spectra, respectively. The chemical shift scales are calibrated to TMS at 0 ppm. The proton spectra were acquired with a 90° pulse of 4.3 μs, a spectral width of 4500 Hz, an acquisition time of 3.5 s, a preparation delay of 8 s and 20 accumulations, processed with a linebroadening of 0.2 Hz and a data matrix of 65k. The carbon spectra were acquired with a 90° pulse of 12 μs, a spectral width of 8500 Hz, an acquisition time of 0.8 s, a preparation delay of 60 s and 2500 accumulations, processed with a linebroadening of 3 Hz and a data matrix of 32k.

4.5. Acknowledgments

The authors gratefully acknowledge the EU for the FP6-Marie Curie-RTN "SolarNtype" (MRTN-CT-2006-035533), and the IWT (Institute for the Promotion of Innovation by Science and Technology in Flanders) for the financial support via the SBO-project 060843 "PolySpec". We also want to thank BELSPO in the frame of network IAP P6/27 for a post-doc fellowship (A.E.B.). Furthermore, the support of the Fund for Scientific Research-Flanders (FWO projects G.0161.03N, G.0252.04N and G.0091.07N) is also acknowledged.

4.6. References

(1) H. Klauk, *Organic Electronics: Materials, Manufacturing and Applications*, Wiley: Weinheim, **2006**.

(2) (a) D. J. Gundlach, J. A. Nichols, L. Zhou, T. N. Jackson, *Appl. Phys. Lett.*, **2002**, *80*, 2925. (b) H. Meng, M. Bendikov, G. Mitchell, R. Helgeson, F. Wudl, Z. Bao, T. Siegrist, C. Kloc, C. H. Chen, *Adv. Mater.*, **2003**, *15*, 1090. (c) J. E. Anthony, *Chem. Rev.*, **2006**, *106*, 5028.

(3) M. Halik, H. Klauk, U. Zschieschang, G. Schmid, S. Ponomarenko, S. Kirchmeyer, W. Weber, *Adv. Mater.*, **2003**, *15*, 917.

(4) S. Ando, J.-i. Nishida, H. Tada, Y. Inoue, S. Tokito, Y. Yamashita, *J. Am. Chem. Soc.*, **2005**, *127*, 5336.

(5) Naraso, F. Wudl, *Macromolecules*, **2008**, *41*, 3169.

(6) S. Ando, J.-i. Nishida, Y. Inoue, S. Tokito, Y. Yamashita, *J. Mater. Chem.*, **2004**, *14*, 1787.

(7) S. Ando, D. Kumaki, J.-i. Nishida, H. Tada, Y. Inoue, S. Tokito, Y. Yamashita, *J. Mater. Chem.*, **2007**, *17*, 553.

(8) J. R. Johnson, R. Ketcham, *J. Am. Chem. Soc.*,**1959**, *82*, 2719.

(9) J. R. Johnson, D. H. Rotenberg, R. Ketcham, *J. Am. Chem. Soc.*, **1970**, *92*, 4046.

(10) I. Osaka, G. Sauvé, R. Zhang, T. Kowalewski, R. D. McCullough, *Adv. Mater.*, **2007**, *19*, 4160.

(11) A. Rössler, P. Boldt, *J. Chem. Soc., Perkin Trans.*, **1998**, *1*, 685.

(12) P. J. Adriaensens, F. G. Karssenberg, J. M. Gelan, V. B. F. Mathot, *Polymer*, **2003**, *44*, 3483.

(13) E. Pretsch, P. Bühlmann, C. Affolter, *Structure Determination of Organic Compounds*, Springer-Verlag: New York, **2000**.

(14) T. Pinault, F. Chérioux, B. Therien, G. Süss-Fink, *Heteroatom Chemistry*, **2004**, *15*, 121.

Chapter 5

Functionalized Dithienylthiazolo[5,4-*d*]thiazoles for Solution-Processable Organic Field-Effect Transistors[†]

A series of 5'-aryl-substituted 2,5-bis(3'-hexylthiophen-2'-yl)thiazolo[5,4-*d*]thiazole derivatives was synthesized and these expanded semiconductors were investigated as active materials for solution-processable organic field-effect transistors. Field-effect mobilities up to 10^{-3} cm^2 V^{-1} s^{-1} were obtained, representing the first reasonable FET behavior for highly soluble thiazolo[5,4-*d*]thiazole-based small organic compounds suitable for printable electronics. Thermal and electro-optical material properties were studied by thermogravimetric analysis, differential scanning calorimetry, cyclic voltammetry and UV-vis spectroscopy. Additional X-ray diffraction, atomic force microscopy and scanning electron microscopy studies provided insight in the relationship between the molecular structures, film morphologies and FET performances. The fibrillar microcrystalline structure observed for the best-performing thienyl-substituted material was tentatively linked to the high mobility.

[†] Van Mierloo, S.; Vasseur, K.; Van den Brande, N.; Boyukbayram, A. E.; Ruttens, B.; Rodriguez, S. D.; Botek, E.; Liégeois, V.; D'Haen, J.; Adriaensens, P. J.; Heremans, P.; Champagne, B.; Van Assche, G.; Lutsen, L.; Vanderzande, D.; Maes, W. manuscript submitted to *Chem. Mater*.

5.1. Introduction

Organic semiconductors recently receive significant attention as functional materials applicable in organic field-effect transistors (OFETs),[1] organic light emitting diodes (OLEDs),[2] and organic photovoltaics.[3] Some of the particular features of organic materials render them more attractive than their inorganic counterparts for electronic applications requiring large area coverage, structural flexibility and solution processability. In the design of organic semiconductors, the consideration of molecular properties such as oxidation potentials, electron affinities and intermolecular π-π interactions is a crucial aspect. Several prominent semiconducting materials have been obtained by modification of oligothiophene derivatives and their properties have been tuned by introducing substituents onto the π-conjugated backbone.[4] Among these thiophene-based molecules, a number of materials containing a thiazolo[5,4-*d*]thiazole (TzTz) unit have shown high field-effect mobilities when used as active layers in both *n*- and *p*-type OFET devices. The TzTz fused heterocycle shows some excellent characteristics toward applications in organic electronics. Its electron-accepting character is useful to enhance the stability toward oxygen. TzTz compounds are generally stable under ambient atmosphere at room temperature over a period of several months. Moreover, the TzTz moiety has a rigid planar structure due to the fused bicyclic ring system, which leads to efficient intermolecular π-π interactions.[5–7] Finally, 2,5-disubstituted TzTzs can easily be prepared starting from the corresponding aldehydes and dithiooxamide.[8,9]

The majority of TzTz molecules reported so far is very poorly soluble and requires vacuum deposition techniques for device fabrication. In order to be applicable to printing processes, highly attractive for large area coverage at a reasonable cost, solubilizing groups/side chains have to be appended to the extended π-systems. Such highly soluble TzTz materials are also of particular appeal for integration (as acceptor components) in low bandgap donor-acceptor copolymers toward efficient organic solar cells. The interest in the TzTz structure in this respect has increased spectacularly, noticeably in the last year.[10]

In this paper, a series of highly soluble functionalized TzTz-based semiconductors is presented. Four 2,5-bis(5'-aryl-3'-hexylthiophen-2'-yl)thiazolo[5,4-*d*]thiazole (DTTzTz) molecules, *i.e.* **Th-DTTzTz**, **4-CF_3-Ph-DTTzTz**, **4-F-Ph-DTTzTz** and **4-**

CN-Ph-DTTzTz (Figure 5.1), were synthesized, in which the two 3-hexylthiophene units ensure solvent-based processing.[11] Functionalization, purification and characterization of the molecules are considerably simplified by their high solubility. The correlation between the molecular structures of the synthesized DTTzTz derivatives, their thermal and (photo)physical properties, spin-coated film morphologies and FET performances is thoroughly analyzed.

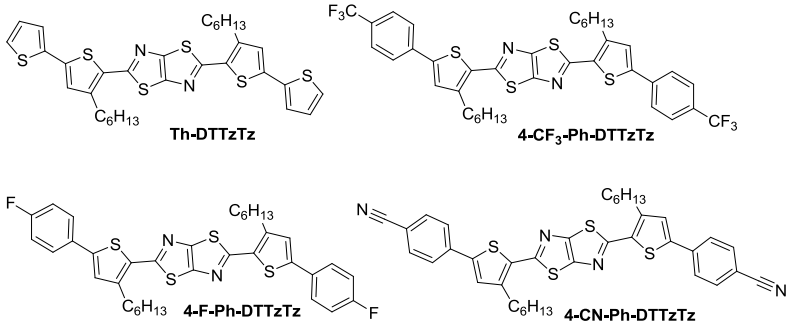

Figure 5.1. Synthesized 2,5-bis(5'-aryl-3'-hexylthiophen-2'-yl)thiazolo[5,4-*d*]thiazole (DTTzTz) derivatives.

5.2. Experimental Section

General Methods

Unless stated otherwise, all reagents and chemicals were obtained from commercial sources and used without further purification. NMR chemical shifts (δ, in ppm) were determined relative to the residual $CHCl_3$ absorption (7.24 ppm) or the ^{13}C resonance shift of $CDCl_3$ (77.7 ppm). Gas chromatography-mass spectrometry (GC-MS) analyses were carried out using Chrompack Cpsil5CB or Cpsil8CB capillary columns. Solution UV-vis absorption measurements were performed at a scan rate of 600 nm min^{-1} in a continuous run from 200 to 800 nm. Infrared spectra were collected with a resolution of 4 cm^{-1} (16 scans) using films drop-casted on a NaCl disk from a $CHCl_3$ solution. The XRD measurements were performed with a Bruker D8 discover diffractometer under θ-2θ conditions. The system works in parafocusing geometry using a Göbel mirror (line focus, mostly $CuK\alpha_1$ and $CuK\alpha_2$ rays). The X-rays are detected by a 1D detector. Electrochemical measurements were performed with an Eco Chemie Autolab PGSTAT 30 potentiostat/galvanostat using 0.1 M Bu_4NPF_6 in anhydrous MeCN as the electrolyte under N_2 atmosphere. A three-electrode microcell was utilized containing an $Ag/AgNO_3$ reference electrode (0.1 M $AgNO_3$ and 0.1 M Bu_4NPF_6 in MeCN), a

platinum counter electrode and an indium tin oxide (ITO) coated glass substrate as the working electrode. The respective monomers were dissolved to their maximum solubility in the electrolyte solution. Cyclic voltammograms were recorded at a scan rate of 50 mV s^{-1}. For the conversion to eV, all electrochemical potentials were referenced to a known standard (ferrocene/ferrocenium in MeCN, 0.05 V vs. $Ag/AgNO_3$), which in MeCN solution is estimated to have an oxidation potential of -4.98 V *vs.* vacuum. DSC measurements were performed at 20 K min^{-1} in aluminum crucibles on a TA Instruments Q2000 Tzero DSC equipped with a refrigerated cooling system (RCS), using nitrogen (50 mL min^{-1}) as a purge gas. TGA experiments were performed at 50 K min^{-1} in platinum crucibles on a TA Instruments Q5000 TGA using nitrogen (50 mL min^{-1}) as a purge gas. FET transistors were made on a highly doped Si n^{++} common gate substrate on which 120 nm SiO_2 was thermally grown. Afterwards, Au source/drain bottom contacts were defined by a lift-off process. The measured transistors had a channel width (W) of 5000 µm and a channel length (L) of 10 µm. Substrate cleaning consisted of subsequent rinsing with detergent, deionized water and acetone, followed by submersion in isopropanol. Finally, a 15 min UV-O_3 treatment was applied prior to depositing the nicely soluble compounds at room temperature by spin-coating. The FET characteristics were then determined inside a glove box under N_2 atmosphere with a Hewlett Packard Agilent 4156. SEM images were recorded with a FEI Quanta 200 FEG scanning electron microscope. The topography of the spin-coated and sublimed films was studied by AFM, using a Picoscan PicoSPM LE scanning probe microscope in tapping mode.

Synthesis

2,5-Bis(5'-bromo-3'-hexylthiophene-2'-yl)thiazolo[5,4-*d*]thiazole (Br-DTTzTz) was synthesized according to a previously reported procedure.[12] Material identity and purity were confirmed by mp, MS, ^1H and ^{13}C NMR.

2,5-Bis(4-hexyl-2,2'-bithiophene-5-yl)thiazolo[5,4-*d*]thiazole (Th-DTTzTz) was synthesized according to a previously reported procedure.[12] Material identity and purity were confirmed by mp, MS, ^1H and ^{13}C NMR.

4,4,5,5-Tetramethyl-2-[4-(trifluoromethyl)phenyl]-1,3,2-dioxaborolane was synthesized according to a literature procedure.[13] Material identity and purity were confirmed by MS and ^{1}H NMR.

2-(4-Fluorophenyl)-4,4,5,5-tetramethyl-1,3,2-dioxaborolane was synthesized according to a literature procedure.[14] Material identity and purity were confirmed by MS and ^{1}H NMR.

4-(4,4,5,5-Tetramethyl-1,3,2-dioxaborolan-2-yl)benzonitrile was synthesized according to a literature procedure.[14] Material identity and purity were confirmed by MS and ^{1}H NMR.

2,5-Bis[5'-(4-fluorophenyl)-3'-hexylthiophen-2'-yl]thiazolo[5,4-*d*]thiazole (4-F-Ph-DTTzTz). General procedure. A solution of 2-(4-fluorophenyl)-4,4,5,5-tetramethyl-1,3,2-dioxaborolane (0.480 g, 1.76 mmol) in DME (15 mL) was added dropwise to a stirring mixture of 2,5-bis(5'-bromo-3'-hexylthiophene-2'-yl)thiazolo[5,4-*d*]thiazole (0.450 g, 0.706 mmol) and $Pd(PPh_3)_4$ (0.033 g, 28.5 μmol) in DME (20 mL) at ambient temperature. Subsequently, a $NaHCO_3$ solution (1 M, 25 mL) was added. After stirring for 24 h at 60 °C under N_2 atmosphere and protected from light, the reaction mixture was diluted with water (50 mL). The organic layer was separated and the aqueous layer was extracted with $CHCl_3$ (3 x 50 mL). The combined organic layers were washed with a saturated $NaHCO_3$ solution and brine, dried over $MgSO_4$ and concentrated by evaporation *in vacuo*. The reaction product was purified by column chromatography (silica, eluent hexane/ethyl acetate 95:5) and recrystallized from ethanol, resulting in red crystals of pure **4-F-Ph-DTTzTz** (0.250 g, 53% yield). Mp = 171 °C; ^{1}H NMR (300 MHz, $CDCl_3$): δ = 7.60 (dd, J = 9/6 Hz, 4H), 7.08 (t, J = 9 Hz, 4H), 7.12 (s, 2H), 2.94 (t, J = 8 Hz, 4H), 1.79–1.69 (m, 4H), 1.49–1.43 (m, 4H), 1.37–1.32 (m, 8H), 0.90 (t, J = 7 Hz, 6H); ^{13}C NMR (75 MHz, $CDCl_3$): δ = 163.6, 161.9, 150.9, 145.2, 144.9, 131.9, 130.7, 128.3 (CH), 127.4 (CH), 116.8 (CH), 32.4 (CH_2), 31.1 (CH_2), 30.7 (CH_2), 30.1 (CH_2), 23.3 (CH_2), 14.8 (CH_3); MS (ESI): m/z = 663 (MH^+); UV-vis ($CHCl_3$, nm): λ_{max} (log ε) = 433 (4.714).

2,5-Bis(3'-hexyl-5'-[4-(trifluoromethyl)phenyl]thiophen-2'-yl)thiazolo[5,4-*d*]thiazole (4-CF_3-Ph-DTTzTz). Synthesis according to the general procedure: 4,4,5,5-tetramethyl-2-[4-(trifluoromethyl)phenyl]-1,3,2-dioxaborolane (1.076 g, 3.96 mmol), 2,5-bis(5'-bromo-3'-hexylthiophene-2'-yl)thiazolo[5,4-*d*]thiazole (1.000 g, 1.58

mmol), $Pd(PPh_3)_4$ (0.073 g, 63.3 μmol), DME (20 + 80 mL), $NaHCO_3$ (1 M, 65 mL); 0.698 g of red crystals (58% yield). Mp = 166 °C; ^{1}H NMR (300 MHz, $CDCl_3$): δ = 7.73 (d, J = 9.0 Hz, 4H), 7.64 (d, J = 9.0 Hz, 4H), 7.27 (s, 2H), 2.97 (t, J = 8.0 Hz, 4H), 1.81–1.71 (m, 4H), 1.49–1.45 (m, 4H), 1.38–1.33 (m, 8H), 0.90 (t, J = 6.9 Hz, 6H); ^{13}C NMR (75 MHz, $CDCl_3$): δ = 161.5, 150.9, 144.7, 143.9, 137.3, 133.0, 130.4, 128.3 (CH), 126.6 (CH), 126.2 (CH), 124.7, 32.3 (CH_2), 31.2 (CH_2), 30.4 (CH_2), 30.1 (CH_2), 23.3 (CH_2), 14.8 (CH_3); MS (ESI): m/z = 763 (MH^+); UV-vis ($CHCl_3$, nm): λ_{max} (log ε) = 434 (4.713).

4,4'-[5,5'-(Thiazolo[5,4-*d*]thiazole-2,5-diyl)-bis(4-hexylthiophene-5,2-diyl)]dibenzonitrile (4-CN-Ph-DTTzTz). Synthesis according to the general procedure: 4-(4,4,5,5-tetramethyl-1,3,2-dioxaborolan-2-yl)benzonitrile (0.420 g, 1.83 mmol), 2,5-bis(5'-bromo-3'-hexylthiophene-2'-yl)thiazolo-[5,4-*d*]thiazole (0.230 g, 0.367 mmol), $Pd(PPh_3)_4$ (0.017 g, 14.7 μmol), DME (20 + 50 mL), K_3PO_4 (0.260 g, 1.25 mmol), eluent hexane/$CHCl_3$ 20:80; 0.159 g of red crystals (64% yield). Mp = 225 °C; ^{1}H NMR (300 MHz, $CDCl_3$): δ = 7.72 (d, J = 9 Hz, 4H), 7.67 (d, J = 9 Hz, 4H), 7.30 (s, 2H), 2.96 (t, J = 7.8 Hz, 4H), 1.80–1.70 (m, 4H), 1.50–1.45 (m, 4H), 1.37–1.32 (m, 8H), 0.90 (t, J = 6.9 Hz, 6H); ^{13}C NMR (75 MHz, $CDCl_3$): δ = 161.6, 151.3, 145.0, 143.5, 138.3, 133.8, 133.5 (CH), 129.2 (CH), 126.6 (CH), 119.3, 112.0, 32.3 (CH_2), 31.1 (CH_2), 30.5 (CH_2), 30.1 (CH_2), 23.3 (CH_2), 14.8 (CH_3); MS (ESI): m/z = 677 (MH^+); UV-vis ($CHCl_3$, nm): λ_{max} (log ε) = 445 (4.776); IR (NaCl, cm^{-1}): ν_{max} = 2956/2925/2855 (s, saturated C-H), 2220 (m, CN).

5.3. Results and Discussion

5.3.1. Synthesis and (Electro-Optical) Characterization

The novel thiazolo[5,4-*d*]thiazole derivatives have been prepared through a convenient three-step synthetic protocol (Scheme 5.1). The backbone unit, 2,5-bis(3'-hexylthiophene-2'-yl)thiazolo[5,4-*d*]thiazole, was synthesized *via* the classical condensation approach, reacting 3-hexylthiophene-2-carbaldehyde and dithiooxamide.[8,9] After that, a bromination reaction with *N*-bromosuccinimide (NBS) was carried out (in DMF), affording 2,5-bis(5'-bromo-3'-hexylthiophene-2'-yl)thiazolo[5,4-*d*]thiazole (**Br-DTTzTz**). 2,5-Bis(4-hexyl-2,2'-bithiophene-5-yl)thiazolo-[5,4-*d*]thiazole (**Th-DTTzTz**) was then obtained through a Stille cross-

coupling reaction with tributyl(thiophen-2-yl)stannane ($Pd(PPh_3)_4$, THF).[12] On the other hand, 4-(trifluoromethyl)phenyl-, 4-fluorophenyl- and 4-cyanophenyl-substituted DTTzTz derivatives (**4-CF_3-Ph-DTTzTz**, **4-F-Ph-DTTzTz** and **4-CN-Ph-DTTzTz**) were synthesized through Suzuki cross-coupling reactions with the respective boronic esters ($Pd(PPh_3)_4$, DME, $NaHCO_3$ or K_3PO_4 base). The use of the K_3PO_4 base provided higher yields for the **4-CN-Ph-DTTzTz** compound. All DTTzTz compounds were purified efficiently by column chromatography and consecutive recrystallizations, and were isolated as red crystals. The materials were found to be stable under ambient atmosphere at room temperature over a period of several months. Due to the substitution with hexyl side chains, all compounds were nicely soluble in common organic solvents, in particular in chlorinated solvents and ethers.

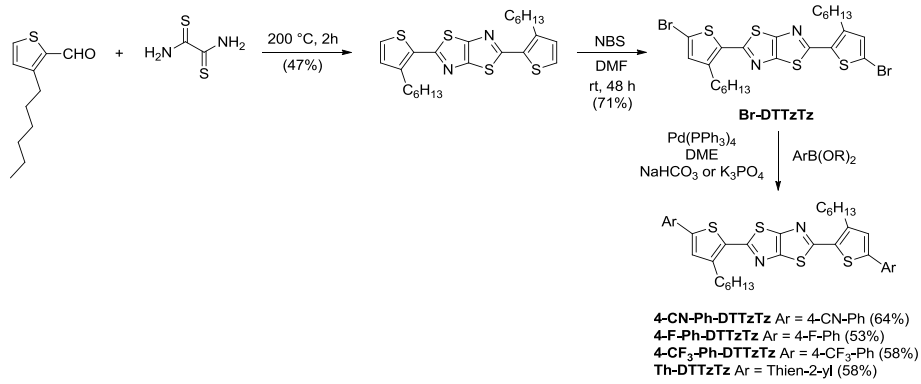

Scheme 5.1. Synthetic pathway toward soluble 2,5-dithienylthiazolo[5,4-*d*]thiazole derivatives.

Experimental UV-vis absorption maxima (in $CHCl_3$) and cyclic voltammetry (CV) data of the DTTzTz derivatives are summarized in Table 5.1. For the phenyl-substituted compounds **4-F-Ph-DTTzTz**, **4-CN-Ph-DTTzTz** and **4-CF_3-Ph-DTTzTz**, the absorption maxima were observed at 433, 445 and 434 nm, respectively, somewhat blue-shifted relative to **Th-DTTzTz** (λ_{max}= 449 nm). On the other hand, CV measurements of **4-F-Ph-DTTzTz**, **4-CN-Ph-DTTzTz** and **4-CF_3-Ph-DTTzTz** revealed oxidation peaks at 0.73, 0.83 and 0.90 V, respectively, notably higher than for **Th-DTTzTz** (0.58 V). These results point to somewhat deeper HOMO levels for the phenyl-substituted materials, suggesting that these compounds might have a higher stability toward oxygen. On the other hand, reduction peaks were found at -1.88, -1.69, -1.89 and -2.01 V for **4-F-Ph-DTTzTz**, **4-CN-Ph-DTTzTz**, **4-CF_3-Ph-DTTzTz** and

Th-DTTzTz, respectively. Similar CV data concerning the incorporation of phenyl substituents have been reported before for TzTz-based semiconductors.[15]

Table 5.1. Optical and electrochemical data for the dithienylthiazolo[5,4-*d*]thiazole derivatives.

	λ_{max} (log ε)[a]	HOMO[b] (eV)	LUMO[b] (eV)	E_g^{EC} (eV)	E_g^{OP}[c] (eV)
Th-DTTzTz[d]	449 (4.768)	-5.51	-2.92	2.59	2.46
4-F-Ph-DTTzTz	433 (4.714)	-5.66	-3.05	2.61	2.52
4-CN-Ph-DTTzTz	445 (4.777)	-5.76	-3.25	2.51	2.44
4-CF_3-Ph-DTTzTz	434 (4.713)	-5.83	-3.04	2.79	2.56

[a] In $CHCl_3$. [b] Evaluated from a CV study in MeCN: 0.1 M Bu_4NPF_6, Pt electrode, scan rate 50 mVs^{-1}. [c] Evaluated from the onset of the absorption spectra in $CHCl_3$. [d] Data taken from previous work.[12]

Density functional theory (DFT) and time-dependent DFT (TDDFT) calculations, summarized in Table 5.2, supported the experimentally observed changes in optical and electrochemical properties upon replacing the thiophene ring of **Th-DTTzTz** by substituted phenyl groups. In general, the calculated data reflect the experimentally observed trends rather well. The impact of the nature of the terminal aryl moiety on the frontier orbitals and optical band gaps was further exemplified by the topology of the HOMO and LUMO, which are delocalized over the whole backbone (Figure 5.2 and S1–S4 in Supporting Info). These differences in optical and electrochemical properties have then been correlated to the Mulliken charge distribution and therefore to the relative electronegativity of the different substituents (Figure 5.3). So, the smaller/larger optical and electrochemical gaps are associated with more/less positive thiophene donor rings (directly linked to the TzTz core) and less/more positive substituted terminal rings, in other words, with a better/smaller distribution of the excess positive charge on the 2+2 external ring units, whereas the central TzTz acceptor moiety bears a negative charge.

Table 5.2. Calculated optical and electrochemical data for the dithienylthiazolo[5,4-*d*]thiazole derivatives as obtained from DFT and TDDFT calculations (in comparison to the phenyl-substituted analogue Ph-DTTzTz).

	λ_{ge} (nm) (f_{ge}[b])	E_g^{OP} (eV)	HOMO (eV)	LUMO (eV)	E_g^{EC} (eV)
Ph-DTTzTz[a]	484 (1.91)	2.56	-5.20	-2.28	2.92
Th-DTTzTz	516 (1.96)	2.40	-5.10	-2.36	2.74
4-F-Ph-DTTzTz	484 (1.91)	2.56	-5.21	-2.30	2.91
4-CN-Ph-DTTzTz	508 (2.17)	2.44	-5.45	-2.65	2.80
4-CF_3-Ph-DTTzTz	492 (2.00)	2.52	-5.36	-2.48	2.88

[a] The Ph-substituted analogue was merely used as a reference compound for the theoretical calculations and was not included in the OFET study. [b] Oscillator Strength.

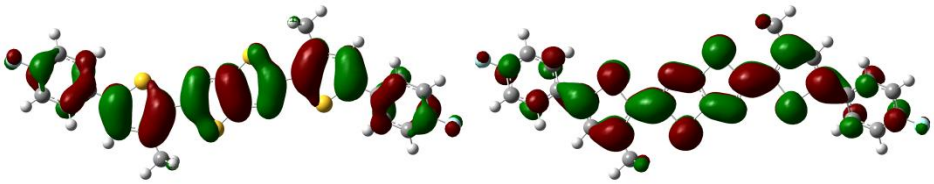

Figure 5.2. Sketch of the HOMO (left) and LUMO (right) of the most stable conformer of **4-F-Ph-DTTzTz** (hexyl side chains were truncated to methyl groups).

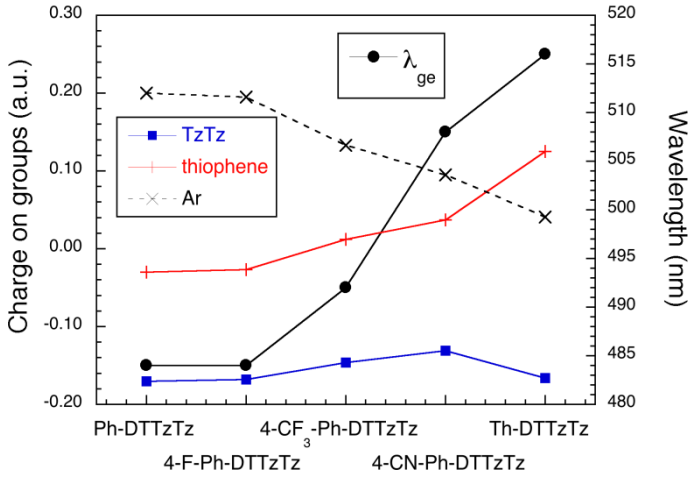

Figure 5.3. Relationship between the wavelength of absorption of the lowest energy optical transition (λ_{ge}) and the charge distribution on the ring moieties.

5.3.2. Thermal Analysis

The DTTzTz moieties were found to be quite thermally stable, as determined by thermogravimetric analysis (TGA), losing less than 1% of their weight on heating up to 400 °C (Figure S5, in Supporting Info). The thermal properties of the synthesized compounds were further investigated by differential scanning calorimetry (DSC). The DSC results are depicted in Figure 5.4. All derivatives displayed pronounced endothermic and exothermic peaks in heating and cooling, ascribed to melting and crystallization, respectively. **Th-DTTzTz** showed indications of thermal degradation or unwanted reactions in the DSC experiments. During cooling, crystallization was seen at about 145 °C in the first cycle. These crystals melted at about 177 °C in the subsequent heating. When this cool-heat process was repeated, the crystallization peak shifted to lower temperatures, while the melting peak remained mostly unchanged, except for a

shoulder appearing at lower temperatures. The results after five cycles can be seen in Figure 5.4 (dashed line). This observation can most likely be explained by a limited amount of undesirable side reactions at more elevated temperatures. For comparison, the non-alkylated analogue showed a single high temperature melting endotherm at 280 °C.[5a] Introduction of a solubilizing alkyl side chain is indeed expected to lower T_m.

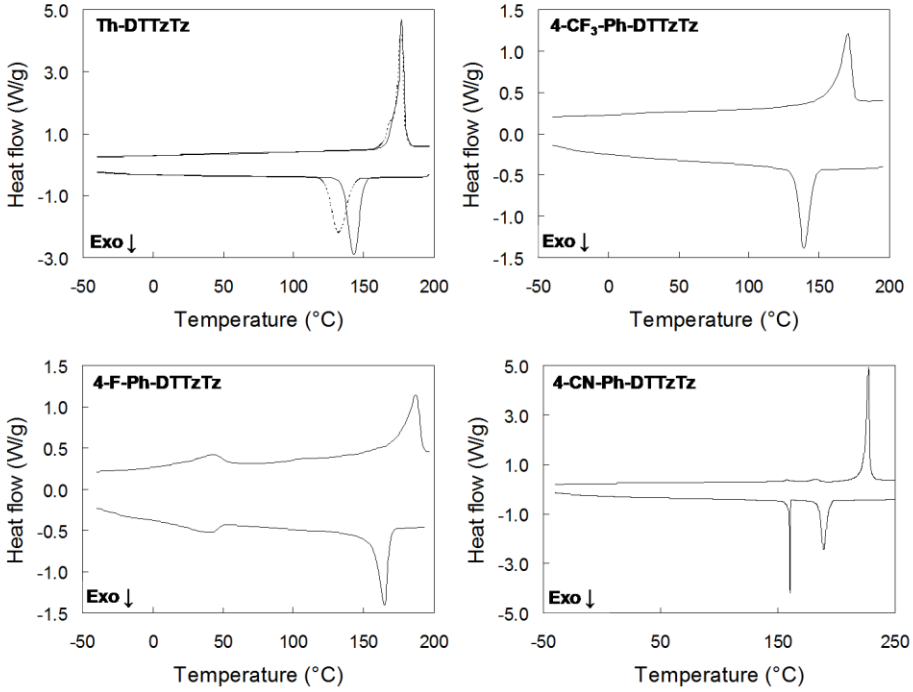

Figure 5.4. DSC thermograms of **Th-DTTzTz**, **4-CF$_3$-Ph-DTTzTz**, **4-F-Ph-DTTzTz** and **4-CN-Ph-DTTzTz** showing heating and cooling cycles at 20 K min^{-1}. The dashed line for **Th-DTTzTz** shows the result after 5 cycles.

The **4-CF$_3$-Ph-DTTzTz** material displayed a melting endotherm at 173 °C, whereas the insoluble non-alkylated analogue showed a sharp melting endotherm at 298 °C.[5c] Introduction of a solubilizing alkyl side chain is indeed expected to lower T_m. For **4-F-Ph-DTTzTz**, in addition to a melting peak at 188 °C and a crystallization peak at 165 °C, a broad endotherm and exotherm were noted between -10 °C and 60 °C, in both heating and cooling. This might be ascribed to a transition between a liquid crystalline and crystalline form. Finally, the **4-CN-Ph-DTTzTz** compound exhibited a sharp exotherm at 161 °C during cooling, in addition to crystallization at 193 °C, adding up to about 54 J g^{-1}. Upon heating, two very small endothermic peaks were followed by a

large melting peak, adding up to 58 J g^{-1}. At a slower cooling rate of 5 K min^{-1}, the exotherm at 161 °C disappeared, but the exothermal enthalpy remained 54 J g^{-1}. The sharp exotherm at 161 °C probably corresponds to the formation of a less stable polymorph that reorganizes to a more stable form upon heating. In summary, although the four synthesized DTTzTz compounds have the same core structure, their crystallization and melting behavior showed significant differences and is complicated by polymorphism and/or liquid crystalline transitions. The considerably higher transition enthalpy in heating for **Th-DTTzTz** (50 kJ mol^{-1}) as compared to the other DTTzTz compounds (22 kJ mol^{-1} for **4-CF_3-Ph-DTTzTz**, 29 kJ mol^{-1} for **4-F-Ph-DTTzTz**, and 39 kJ mol^{-1} for **4-CN-Ph-DTTzTz**) indicates a higher crystallinity for **Th-DTTzTz** (Table S1, in Supporting Info).

5.3.3. Solution-Processed OFET Characteristics

Subsequently, the electronic and morphological properties of solution-casted thin films of the functionalized TzTz semiconducting materials were investigated, with the goal to obtain good OFET characteristics. Transistor performance was mainly evaluated by the thin film hole mobility (μ) extracted in the saturation regime and by the threshold voltage (V_T), which are listed in Table 5.3. For the **4-CN-Ph-DTTzTz** derivative, several spin-coating conditions were tested (with optimization of concentration, solvent, spin-coating speed and acceleration), but unfortunately no suitable layers for OFET measurements could be obtained. Although optimized spin-coating conditions were found for **4-CF_3-Ph-DTTzTz** (5 mg mL^{-1} in 1,2-dichlorobenzene, 3000 rpm, 5000 acc, 60 s), hole mobilities of the films calculated in the saturation regime were found to be only around 2×10^{-6} cm^2 V^{-1} s^{-1}. The **4-F-Ph-DTTzTz** material showed a slightly better performance for the same optimized spin-coating conditions, with a calculated hole mobility of 1×10^{-5} cm^2 V^{-1} s^{-1}. On the other hand, the **Th-DTTzTz** semiconductor afforded a noticeably better FET performance with a hole mobility of 1.58×10^{-3} cm^2 V^{-1} s^{-1} (spin-coating conditions: 5 mg mL^{-1} in 1,2-dichlorobenzene, 3000 rpm, 3000 acc, 60 s). Figure 5.5 shows the obtained transfer characteristics for the **Th-DTTzTz** device, with I_d, V_{DS} and V_{GS} representing the source-drain current, source-drain voltage and gate voltage, respectively. It must be emphasized that, despite the rather poor film-forming characteristics inherent to small molecules, the **Th-DTTzTz**

films showed reasonably high hole mobilities. For the analogous non-alkylated Th-DTTzTz material, processed by vacuum deposition, a mobility of 0.02 $cm^2 V^{-1} s^{-1}$ was reported, *i.e.* one order of magnitude higher.[5e] From a structural point of view, the best result for the **Th-DTTzTz** derivative does not come as a real surprise, as the additional thiophene unit increases the hole affinity. On the other hand, film morphology and crystallinity also have a major impact on device performance, and the noticeable differences in thermal behavior within the DTTzTz series already hint to large differences in crystallization tendencies.

Table 5.3. Organic field-effect transistor characteristics of bottom contact devices made from the DTTzTz derivatives.

	Hole mobility (μ)($cm^2 V^{-1} s^{-1}$)	**I_{on}/I_{off} Ratio**	**Threshold Voltage (V_T)**
Th-DTTzTz	1.58×10^{-3}	10^5	1.4
4-F-Ph-DTTzTz	1×10^{-5}	10^4	-3.4
4-CF_3-Ph-DTTzTz	2×10^{-6}	10^3	-2.2

5.3.4. Morphology Studies

To investigate the molecular organization of the DTTzTz molecules on the transistor surface and evaluate a possible correlation with the observed hole mobilities, XRD, atomic force microscopy (AFM) and scanning electron microscopy (SEM) studies were carried out. The observed XRD diffraction patterns are shown in Figure 5.6. The results were quite similar to earlier reported data for the unsubstituted analogues.[5a,c] The thin films of **Th-DTTzTz** displayed high crystallinity, with a strong primary diffraction peak, pointing to an ordered crystalline structure. This high crystallinity is likely the reason for the high hole mobility observed. On the other hand, the crystallinity of the **4-CF_3-Ph-DTTzTz** and **4-F-Ph-DTTzTz** derivatives was rather poor, whereas the **4-CN-Ph-DTTzTz** film showed even less evidence of a crystalline phase.

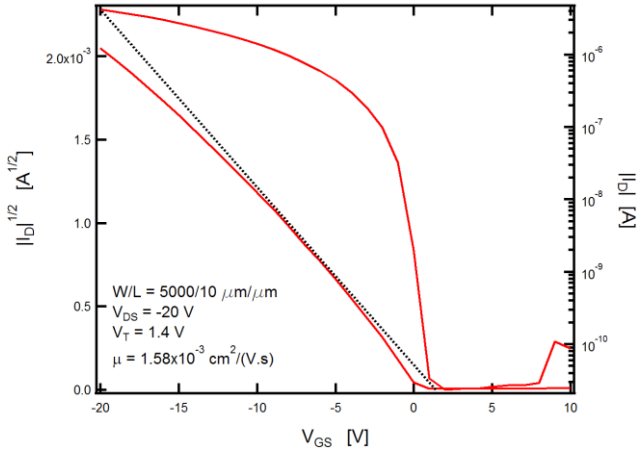

Figure 5.5. FET characteristics of a bottom contact device made from **Th-DTTzTz**: I_d and $I_d^{1/2}$ versus V_{GS} plots at V_{DS} = –20 V.

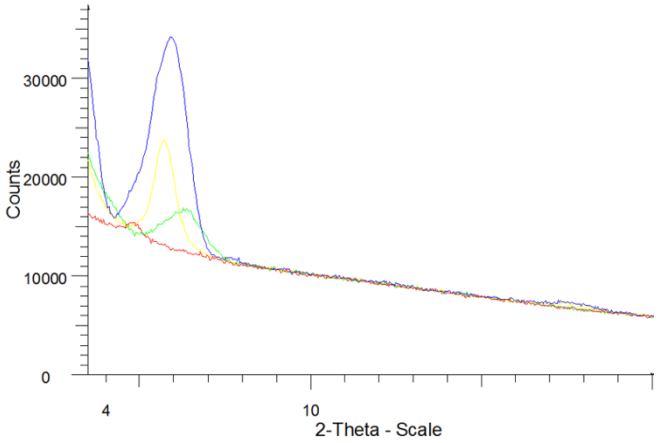

Figure 5.6. XRD patterns of thin films of **4-CN-Ph-DTTzTz** (15.23 nm, red), **4-CF_3-Ph-DTTzTz** (14.25 nm, green), **4-F-Ph-DTTzTz** (25.75 nm, yellow) and **Th-DTTzTz** (23.60 nm, blue).

Figure 5.7 and Figure 5.8 show optical microscope and SEM images obtained for the different spin-coated films, revealing large differences in morphology. The **Th-DTTzTz** films showed an anisotropic fibrillar morphology (Figure 5.7). On the other hand, SEM images of solution-processed thin films of **4-CF_3-Ph-DTTzTz**, **4-F-Ph-DTTzTz** and **4-CN-Ph-DTTzTz** indicated a very different topography, characterized by the presence of partially connected domains, creating a large number of grain boundaries (Figure 5.8). These morphologies are in sharp contrast to the one observed

for **Th-DTTzTz**, and this profound difference was further confirmed by AFM measurements (Figure 5.9). The trend in morphology could clearly be correlated to the electrical characteristics: the **4-CF_3-Ph-DTTzTz**, **4-F-Ph-DTTzTz** and **4-CN-Ph-DTTzTz** films were characterized by the absence of crystals on the micrometer scale and exhibited quite poor hole mobilities, whereas the high mobility **Th-DTTzTz** film showed a fibrillar microcrystalline texture. The significantly higher hole mobility in this case might be related to the presence of intergranular charge transport paths, as boundaries along the fibrils could provide a smaller barrier to charge transport.[16] The thin films were proven to be (oxidatively) stable, as essentially identical SEM images were obtained after storage for two months.

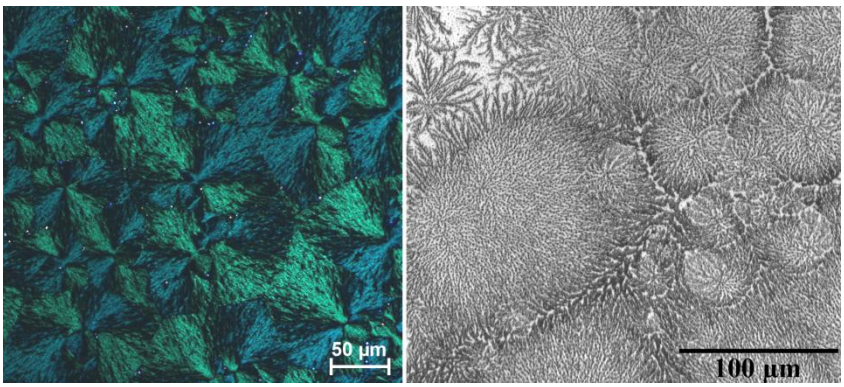

Figure 5.7. Optical microscope (left) and SEM (right) images of spin-coated thin films of **Th-DTTzTz**.

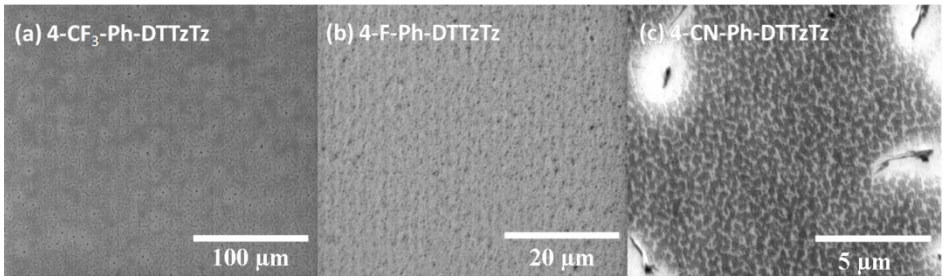

Figure 5.8. SEM images of thin films of **4-CF_3-Ph-DTTzTz, 4-F-Ph-DTTzTz** and **4-CN-Ph-DTTzTz**.

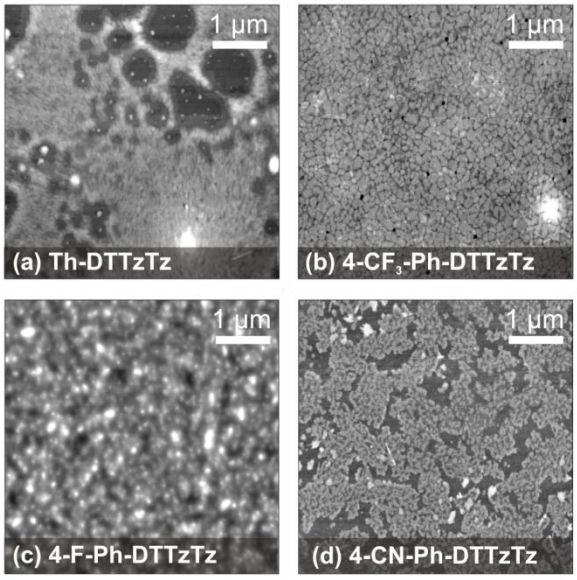

Figure 5.9. AFM images (5 x 5 µm^2) of spin-coated thin films of the DTTzTz derivatives on SiO_2 with a rms roughness of (a) 1.9 nm, (b) 0.8 nm, (c) 3 nm and (d) 1.2 nm.

5.3.5. Vacuum Sublimed OFET

For comparison, the most promising molecule from the series, **Th-DTTzTz**, was also deposited by thermal evaporation in an ultra high vacuum chamber at a base pressure below 5×10^{-8} Torr. The temperature of the evaporation cell varied between 200 and 220 °C. Transistors were fabricated and were subjected to a surface treatment with pentafluorobenzenethiol and deposition of a self-assembling monolayer of phenylethyltrichlorosilane (PETS). The hole mobilities calculated in the saturation regime were found to be 2×10^{-4} cm^2 V^{-1} s^{-1}. Without applying a surface treatment, hole mobilities of only 6×10^{-6} cm^2 V^{-1} s^{-1} were achieved. The hole mobility of 1.58×10^{-3} cm^2 V^{-1} s^{-1} generated in the solution-processed OFETs could hence not be attained by vacuum deposition of the same material. Although XRD studies showed a high degree of crystallinity in the vacuum deposited films (Figure S6, in Supporting Info), the SEM images revealed a high number of grain boundaries due to the presence of a large amount of nanosized domains (Figure 5.10). These nanocrystals probably result in a reduced mobility as compared to the microcrystals obtained after spin-coating. Furthermore, it cannot be excluded that side reactions during vacuum deposition of the

Th-DTTzTz between 200 and 220 °C, as indicated in the DSC experiment (Figure 5.4), might also be correlated to this low mobility.

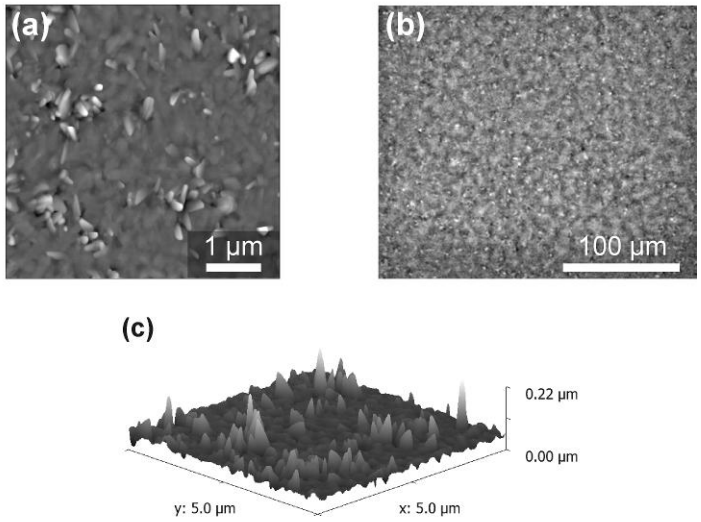

Figure 5.10. Vacuum sublimed **Th-DTTzTz** film imaged by (a) AFM (5 x 5 μm^2), displaying a rms roughness of 14 nm, (b) SEM, (c) 3D AFM.

5.4. Conclusions

Searching for small organic compounds suitable for printable electronics, we have synthesized a family of novel highly soluble 2,5-dithienylthiazolo[5,4-*d*]thiazole semiconducting materials by a convenient three-step protocol, and studied their thermal, optical and electrochemical properties. FET devices were fabricated by spin-coating active TzTz layers from solutions in dichlorobenzene. Despite some difficulties in film formation, the bithiophene-substituted TzTz material (**Th-DTTzTz**) exhibited a fairly high hole mobility of 1.58×10^{-3} cm^2 V^{-1} s^{-1}, making it a first candidate for solution-processable organic field-effect transistors. Moreover, the alkyl-substituted **Th-DTTzTz** showed better self-organization when deposited from solution compared to vacuum deposited layers, resulting in higher hole mobilities. This higher mobility might be linked to the microcrystalline fibrillar structure observed for the solution-cast film, whereas vacuum deposition of the same material afforded nanocrystalline domains.

5.5. Acknowledgments

The authors gratefully acknowledge the IWT (Institute for the Promotion of Innovation by Science and Technology in Flanders) for financial support via the SBO-project 060843 “PolySpec”. We also acknowledge the European ONE-P project for grant agreement n° 212311 which facilitates the IMEC-IMOMEC collaboration. Furthermore, we gratefully thank BELSPO in the frame of the IAP P6/27 network as well as MINCyT and FRS-FNRS for supporting the Buenos Aires-Namur scientific cooperation. The computational calculations were performed on the Interuniversity Scientific Computing Facility (ISCF) installed at the Facultés Universitaires Notre-Dame de la Paix (FUNDP, Namur, Belgium), for which we acknowledge financial support from the FRS-FRFC (Convention No. 2.4.617.07.F) and from the FUNDP. V. L. thanks the FRS-FNRS for his postdoctoral research position. N. VdB. and W. M. thank the FWO (Fund for Scientific Research – Flanders) for a doctoral and postdoctoral research mandate, respectively.

5.6. References

(1) (a) Muccini, M. *Nat. Mater.* **2006**, *5*, 605. (b) Locklin, L.; Roberts, M. E.; Mannsfeld, S. C. B.; Bao, Z. *J. Macromol. Sci., Part C: Polym. Rev.* **2006**, *46*, 79. (c) Di, C.-a.; Yu, G.; Liu, Y.; Zhu, D. *J. Phys. Chem. B* **2007**, *111*, 14083. (d) Braga, D.; Horowitz, G. *Adv. Mater.* **2009**, *21*, 1473. (e) Yamashita, Y. *Sci. Technol. Adv. Mater.* **2009**, *10*, 024313. (f) Serringhaus, H.; Bird, M.; Richards, T.; Zhao, N. *Adv. Mater.* **2010**, *22*, 3893. (g) Wu, W.; Liu, Y.; Zhu, D. *Chem. Soc. Rev.* **2010**, *39*, 1489. (h) Malachowski, M. J.; Zmija, J. *Opto-Electron. Rev.* **2010**, *18*, 121.

(2) (a) Duan, L.; Hou, L.; Lee, T.-W.; Qiao, J.; Zhang, D.; Dong, G.; Wang, L.; Qiu, Y. *J. Mater. Chem.* **2010**, *20*, 6392. (b) Zhong, C.; Duan, C.; Huang, F.; Wu, H.; Cao, Y. *Chem. Mater.* **2011**, *23*, 326.

(3) (a) Ko, H. M.; Choi, H.; Paek, S.; Kim, K.; Song, K.; Lee, J. K.; Ko, J. *J. Mater. Chem.* **2011**, *21*, 7248. (b) Shang, H.; Fan, H.; Liu, Y.; Hu, W.; Li, Y.; Zhan, X. *Adv. Mater.* **2011**, *23*, 1554. (c) Sun, Y.; Welch, G. C.; Leong, W. L.; Takacs, C. J.; Bazan, G. C.; Heeger, A. J. *Nat. Mater.* **2011**, DOI: 10.1038/nmat3160.

(4) (a) Ashizawa, M.; Kato, R.; Takanishi, Y.; Takezoe, H. *Chem. Lett.* **2007**, *36*, 708. (b) Haubner, K.; Jaehne, E.; Adler, H.-J. P.; Koehler, D.; Loppacher, C.; Eng, L. M.; Grenzer, J.; Herasimovich, A.; Scheinert, S. *Phys. Stat. Sol.* **2008**, *205*, 431. (c) Mass-Torrent, M.; Rovira, C. *Chem. Soc. Rev.* **2008**, *37*, 827. (d) Liu, Y.; Yu, G.; Liu, Y. *Sci. China Chem.* **2010**, *53*, 779. (e) Zhang, L.; Di, C.-a.; Yu, G.; Liu, Y. *J. Mater. Chem.* **2010**, *20*, 7059.

(5) (a) Ando, S.; Nishida, J.-i.; Inoue, Y.; Tokito, S.; Yamashita, Y. *J. Mater. Chem.* **2004**, *14*, 1787. (b) Ando, S.; Nishida, J.-i.; Fujiwara, E.; Tada, H.; Inoue, Y.; Tokito, S.; Yamashita, Y. *Chem. Lett.* **2004**, *33*, 1170. (c) Ando, S.; Nishida, J.-i.; Tada, H.; Inoue, Y.; Tokito, S.; Yamashita, Y. *J. Am. Chem. Soc.* **2005**, *127*, 5336. (d) Ando, S.; Nishida, J.-i.; Fujiwara, E.; Tada, H.; Inoue, Y.; Tokito, S.; Yamashita, Y. *Synth. Met.* **2006**, *156*, 327. (e) Ando, S.; Kumaki, D.; Nishida, J.-i.; Tada, H.; Inoue, Y.; Tokito, S.; Yamashita, Y. *J. Mater. Chem.* **2007**, *17*, 553. (f) Kumaki, D.; Ando, S.; Shimono, S.; Yamashita, Y. *Appl. Phys. Lett.* **2007**, *90*, 53506. (g) Mamada, M.; Nishida, J.-i.; Kumaki, D.; Tokito, S.; Yamashita, Y. *Chem. Mater.* **2007**, *19*, 5404. (h) Fujisaki, Y.; Mamada, M.; Kumaki, D.; Tokito, S.; Yamashita, Y. *Jpn. J. Appl. Phys.* **2009**, *48*, 111504.

(6) Naraso; Wudl, F. *Macromolecules* **2008**, *41*, 3169.

(7) (a) Osaka, I.; Sauvé, G.; Zhang, R.; Kowalewski, T.; McCullough, R. D. *Adv. Mater.* **2007**, *19*, 4160. (b) Osaka, I.; Zhang, R.; Sauvé, G.; Smilgies, D.-M.; Kowalewski, T.; McCullough, R. D. *J. Am. Chem. Soc.* **2009**, *131*, 2521. (c) Osaka, I.; Zhang, R.; Liu, J.; Smilgies, D.-M.; Kowalewski, T.; McCullough, R. D. *Chem. Mater.* **2010**, *22*, 4191.

(8) Johnson, J. R.; Ketcham R. *J. Am. Chem. Soc.* **1960**, *82*, 2719.

(9) Johnson, J. R.; Rotenberg, D. H.; Ketcham, R. *J. Am. Chem. Soc.* **1970**, *92*, 4046.

(10) (a) Lee, T. W.; Kang, N. S.; Yu, J. W.; Hoang, M. H.; Kim, K. H.; Jin, J.-L.; Choi, D. H *J. Polym. Sci., Part A: Polym. Chem.* **2010**, *48*, 5921. (b) Jung, I. H.; Yu, J.; Jeong, E.; Kim, J.; Kwon, S.; Kong, H.; Lee, K.; Woo, H. Y.; Shim, H.-K. *Chem. Eur. J.* **2010**, *16*, 3743. (c) Huo, L.; Guo, X.; Zhang, S.; Li, Y.; Hou, J. *Macromolecules* **2011**, *44*, 4035. (d) Lee, S. K.; Cho, J. M.; Goo, Y.; Shin, W. S.; Lee, J.-C.; Lee, W.-H.; Kang, I.-N.; Shim, H.-K.; Moon, S.-J. *Chem. Commun.* **2011**, 1791. (e) Lee, S. K.; Kang, I.-N.; Lee, J.-C.; Shin, W. S.; So, W.-W.; Moon, S.-J. *J. Polym. Sci., Part A: Polym. Chem.* **2011**, *49*, 3129. (f) Lee, T. W.; Kang, N. S.; Yu, J. W.; Hoang, M. H.; Kim, K. H.; Jin, J.-I.; Choi, D. H. *J. Polym. Sci., Part A: Polym. Chem.* **2011**, *49*, 5921. (g) Peet, J.; Wen, L.; Byrne, P.; Rodman, S.; Forberich, K.; Shao, Y.; Drolet, N.; Gaudiana, R; Dennler, G.; Waller, D. *Appl. Phys. Lett.* **2011**, *98*, 043301. (h) Subramaniyan, S.; Xin, H.; Kim, F. S.; Shoaee, S.; Durrant, J. R.; Jenekhe, S. A. *Adv. Energy Mater.* **2011**, *1*, 854. (i) Subramaniyan, S.; Xin, H.; Kim, F. S.; Jenekhe, S. A. *Macromolecules* **2011**, *44*, 6245. (j) Zhang, M.; Guo, X.; Wang, X.; Wang, H.; Li, Y. *Chem. Mater.* **2011**, *23*, 4264. (k) Helgesen, M.; Madsen, M. V.; Andreasen, B.; Tromholt, T.; Andreasen, J. W.; Krebs, F. C. *Polym. Chem.* **2011**, *2*, 2536. (l) Jeong, E.; Kim, G.-h.; Jung, I. H.; Jeong, P.; Kim, J. Y.; Woo, H. Y. *Curr. Appl. Phys.* **2012**, *12*, 11. (m) Van Mierloo, S.; Hadipour, A.; Spijkman, M.-J.; Van den Brande, N.; Ruttens, B.; Kesters, J.; D'Haen, J.; Van Assche, G.; de Leeuw, D. M.; Aernouts, T.; Manca, J.; Lutsen, L.; Vanderzande, D. J.; Maes, W. *Chem. Mater.* **2012**, manuscript accepted.

(11) We have recently reported a combined experimental-theoretical NMR study on a number of 2,5-bis(5'-aryl-3'-hexylthiophen-2'-yl)thiazolo[5,4-*d*]thiazole derivatives: Van Mierloo, S.; Liégeois, V.; Kudrjasova, J.; Botek, E.; Lutsen, L.;

Champagne, B.; Vanderzande, D.; Adriaensens, P.; Maes, W. *Magn. Reson. Chem.* **2012**, manuscript submitted.

(12) Van Mierloo, S.; Chambon, S.; Boyukbayram, A. E.; Adriaensens, P.; Lutsen, L.; Cleij, T. J.; Vanderzande, D. *Magn. Reson. Chem.* **2010**, *48*, 362.

(13) Cremer, J.; Mena-Osteritz, E.; Pschierer, N. G.; Müllen, K.; Bäuerle, P. *Org. Biomol. Chem.* **2005**, *3*, 985.

(14) Ishiyama, T.; Murata, M.; Miyaura, N. *J. Org. Chem.* **1995**, *60*, 7508.

(15) Hong, X. M.; Katz, H. E.; Lovinger, A. J.; Wang, B.-C.; Raghavachari, K. *Chem. Mater.* **2001**, *13*, 4686.

(16) Jimison, L. H.; Toney, M. F.; McCulloch, I.; Heeney, M.; Salleo, A. *Adv. Mater.* **2009**, *21*, 1568.

5.7. Supporting Information

Cyclic voltammograms, and ^{1}H and ^{13}C NMR spectra for all novel thiazolo[5,4-*d*]thiazole derivatives are available via the Internet at http://pubs.acs.org.

Theoretical and Computational Data

The ground state geometries were optimized at the density functional theory (DFT) level of approximation by employing the B3LYP exchange-correlation (XC) functional and the 6-31G(d) basis set. These geometries and wave functions were employed to analyze the shape of the Highest Occupied and Lowest Unoccupied Molecular Orbitals (HOMO and LUMO).

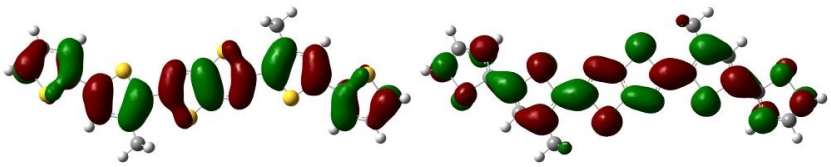

Figure S1. Sketch of the HOMO (left) and LUMO (right) of the most stable conformer of **Th-DTTzTz** (hexyl side chains were truncated to methyl groups).

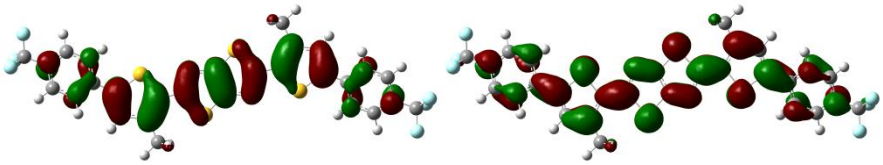

Figure S2. Sketch of the HOMO (left) and LUMO (right) of the most stable conformer of **4-CF_3-Ph-DTTzTz** (hexyl side chains were truncated to methyl groups).

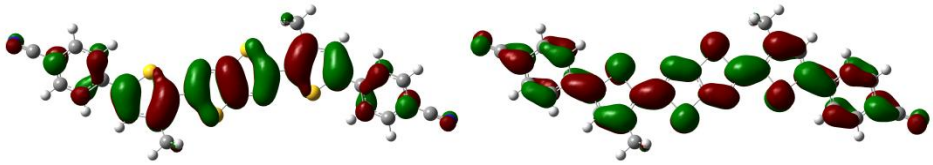

Figure S3. Sketch of the HOMO (left) and LUMO (right) of the most stable conformer of **4-CN-Ph-DTTzTz** (hexyl side chains were truncated to methyl groups).

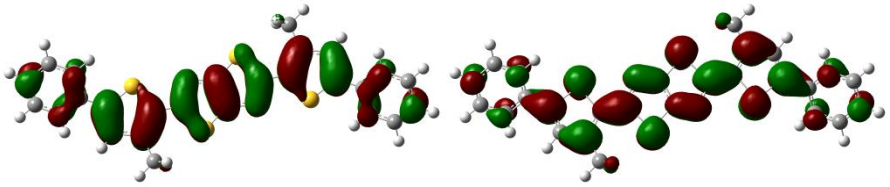

Figure S4. Sketch of the HOMO (left) and LUMO (right) of the most stable conformer of **Ph-DTTzTz** (hexyl side chains were truncated to methyl groups).

The vertical excitation energies ΔE_{ge}, wavelengths λ_{ge}, and associated oscillator strengths f_{ge} were calculated using time-dependent DFT (TDDFT) with the same XC functional containing 20% of HF exchange and the same basis set, which has been shown to be a suitable method for reproducing experimental trends.[1] The effects of the solvent were taken into account within the integral equation formalism of the polarizable continuum model (IEF-PCM)[2] in the geometry optimization as well as to carry out the Mulliken population analysis. All calculations were performed using Gaussian09.[3]

(1) (a) Cavillot, V.; Champagne, B. *Chem. Phys. Lett.* **2002**, *354*, 449. (b) Guillaume, M.; Champagne, B.; Zutterman, F. *J. Phys. Chem. A* **2006**, *110*, 13007. (c) Plaquet, A.; Guillaume, M.; Champagne, B.; Rougier, L.; Mançois, F.; Rodriguez, V.; Pozzo, J.L.; Ducasse, L.; Castet, F. *J. Phys. Chem. C* **2008**, *112*, 5638.
(2) (a) Tomasi, J.; Persico, M.*Chem. Rev.* **1994**, *94*, 2027. (b) Tomasi, J.; Mennucci, B.; Cammi, R. *Chem. Rev.* **2005**, *105*, 2999.
(3) Gaussian 09, Revision A.1, Frisch, M. J.; Trucks, G. W.; Schlegel, H. B.; Scuseria, G. E.; Robb, M. A.; Cheeseman, J. R.; Scalmani, G.; Barone, V.; Mennucci, B.; Petersson, G. A.; Nakatsuji, H.; Caricato, M.; Li, X.; Hratchian, H. P.; Izmaylov, A. F.; Bloino, J.; Zheng, G.; Sonnenberg, J. L.; Hada, M.; Ehara, M.; Toyota, K.; Fukuda, R.; Hasegawa, J.; Ishida, M.; Nakajima, T.; Honda, Y.; Kitao, O.; Nakai, H.; Vreven, T.; Montgomery, Jr. J. A.; Peralta, Jr. J. E.; Ogliaro, F.; Bearpark, M.; Heyd, J. J.; Brothers, E.; Kudin, K. N.; Staroverov, V. N.; Kobayashi, R.; Normand, J.; Raghavachari, K.; Rendell, A.; Burant, J. C.; Iyengar, S. S.; Tomasi, J.; Cossi, M.; Rega, N.; Millam, J. M.; Klene, M.; Knox, J. E.; Cross, J. B.; Bakken, V.; Adamo, C.; Jaramillo, J.; Gomperts, R.; Stratmann, R. E.; Yazyev, O.; Austin, A. J.; Cammi, R.; Pomelli, C.; Ochterski, J. W.; Martin, R. L.; Morokuma, K.; Zakrzewski, V. G.; Voth, G. A.; Salvador, P.; Dannenberg, J. J.; Dapprich, S.; Daniels, A. D.; Farkas, Ö.; Foresman, J. B.; Ortiz, J. V.; Cioslowski, J.; Fox, D. J. Gaussian, Inc., Wallingford CT, **2009**.

Thermal Analysis Data

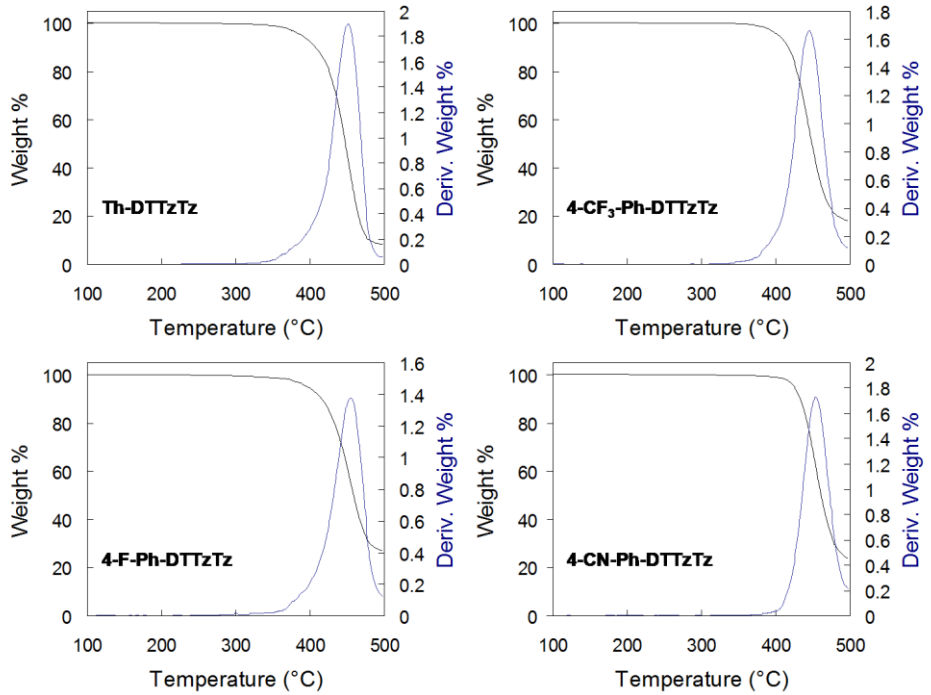

Figure S5. TGA curves of **Th-DTTzTz**, **4-CF_3-Ph-DTTzTz**, **4-F-Ph-DTTzTz** and **4-CN-Ph-DTTzTz** (heating rate 50 K min^{-1}, N_2 atmosphere).

Table S1. Extrapolated onset temperatures and transition enthalpies *ΔH* for the first cool-heat cycles given in Figure 5.4.

		T_{onset} (°C)	ΔH (J g^{-1})	ΔH (kJ mol^{-1})
Th-DTTzTz	cool	149.9	72.6	46.4
	heat	172.9	78.7	50.3
4-CF_3-Ph-DTTzTz	cool	147.7	28.7	21.9
	heat	160.5	29.3	22.4
4-F-Ph-DTTzTz	cool	49.7	11.2	7.4
	cool	169.2	29.6	19.6
	heat	12.2	12.1	8.0
	heat	173.7	31.4	20.8
4-CN-Ph-DTTzTz	cool	161.0	16.7	11.3
	cool	193.0	37.5	25.4
	heat	224.5	58.2	39.4

XRD pattern of the sublimed Th-DTTzTz semiconductor

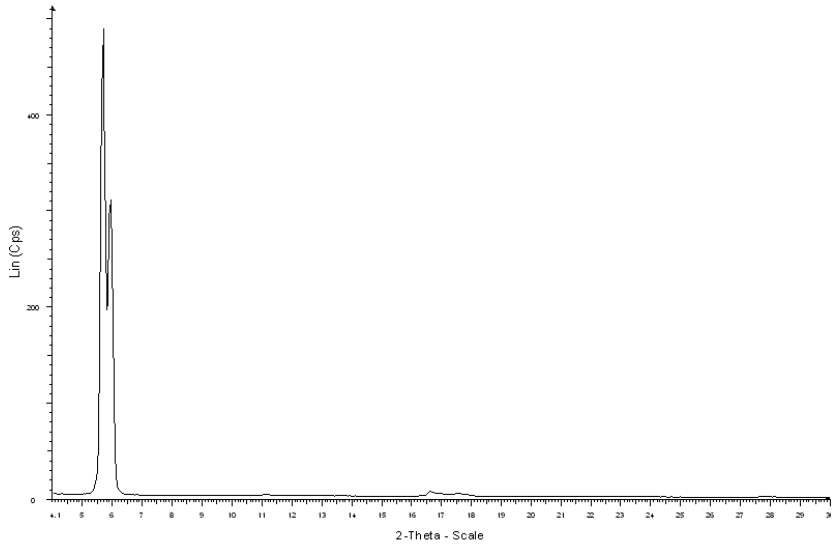

Figure S6. XRD pattern of the sublimed **Th-DTTzTz** material.

Chapter 6

Combined Experimental-Theoretical NMR Study on 2,5-Bis(5-aryl-3-hexylthiophen-2-yl)thiazolo[5,4-*d*]thiazole Derivatives for Printable Electronics[†]

Four 2,5-bis(5-aryl-3-hexylthiophen-2-yl)thiazolo[5,4-*d*]thiazole derivatives have been synthesized and thoroughly characterized. The extended aromatic core of the molecules was designed to enhance the charge transport characteristics and solubilizing hexyl side chains were introduced on the thiophene subunits to enable possible integration of these semiconducting small molecules in printable electronics. Complete elucidation of the chemical structures by detailed 1D/2D NMR spectroscopy is described, providing interesting input for chemical shift prediction software as well, since limited experimental data on these types of compounds are currently available. Furthermore, theoretical calculations have assisted experimental observations – giving support for the chemical shift assignment and providing a springboard for future screening and predictions – demonstrating the benefits of a coordinated theoretical-experimental approach.

[†] Van Mierloo S.; Liégeois, V.; Kudrjasova, J.; Botek, E.; Lutsen, L.; Champagne, B.; Vanderzande, D.; Adriaensens, P.; Maes, W., submitted to *Magn. Reson. Chem.*

6.1. Introduction

The development of organic semiconductors for the active layers of field effect transistors (FETs) has received significant attention during recent years.[1] Carefully designed high performance organic materials are required to achieve high charge carrier mobilities, on/off current ratios, stability, and processability. π-Conjugated small molecules such as thiophene oligomers have been shown to possess excellent charge transport characteristics in FETs. A number of structural modifications have been carried out on such (oligo)thiophene compounds so far.[2] Replacement of some of the thiophene units by thiazolo[5,4-*d*]thiazole (TzTz) fused ring systems is reported to be rather effective, resulting in high charge carrier mobilities.[3] The TzTz moiety possesses some important features toward electronic applications. Thiazolo[5,4-*d*]thiazoles are electron deficient fused heterocycles with a rigid planar structure, which enables efficient intermolecular π-π overlap, and they show enhanced stability toward oxygen.[4,5] Moreover, functionalized TzTz derivatives are easily prepared starting from the corresponding arylcarbaldehydes (e.g. 3-hexylthiophene-2-carbaldehyde) and dithiooxamide.[6,7]

Unfortunately, non-alkylsubstituted TzTz compounds are very poorly soluble and require vacuum deposition techniques for device fabrication. So far, only a few soluble TzTz semiconducting materials have been reported.[4,5] In previous work we have decorated the TzTz core with two 3-hexylthiophene moieties.[8] The substitution with alkyl chains obviously leads to a significantly improved solubility in common organic solvents. Here, an extended series of expanded TzTz chromophores is presented, i.e. **D1**–**D4** (Scheme 6.1). Functionalization, purification and characterization were considerably simplified by the introduction of the solubilizing 3-hexylthiophene subunits and these molecules can hence be utilized in solvent based processing techniques toward printable electronics. Furthermore, such TzTz materials are also of particular appeal for integration (as acceptor components) in low bandgap copolymers toward highly efficient organic solar cells. The interest in the TzTz structure in this respect has increased spectacularly, noticeably in the last year.[9]

In this paper, we report the synthesis, detailed ^{1}H and ^{13}C NMR chemical shift assignment and the correlation of experimental NMR results with theoretical chemical

shift calculations for a number of functionalized 2,5-bis(5-aryl-3-hexylthiophen-2-yl)thiazolo[5,4-*d*]thiazole derivatives.

6.2. Results and Discussion

6.2.1. Synthesis

The common precursor for the reported TzTz semiconductors, 2,5-bis(3-hexylthiophen-2-yl)thiazolo[5,4-*d*]thiazole (**P1**), was synthesized in moderate yield (47%) via a condensation reaction at elevated temperature (200 °C) between dithiooxamide and an excess of 3-hexylthiophene-2-carbaldehyde,[8] prepared according to a modified literature procedure (Scheme 6.1).[6,7] The resulting product mixture required extensive purification (column chromatography and two successive recrystallizations from ethanol and acetonitrile) to convert the black crude residue into pure yellow crystals of **P1**. After subsequent dibromination with *N*-bromosuccinimide (71% yield), the final TzTz derivatives **D1**, **D2**, **D3** and **D4** were obtained through Suzuki cross-coupling reactions with the respective boronic acids or esters (Scheme 6.1).[10] The dithienyl-substituted TzTz counterpart **D0** has previously been prepared by an analogous Stille protocol.[8] The cross-coupling reactions were in general very effective, main product losses occurring during the tedious material purification (by repetitive recrystallization and column chromatography), affording highly pure materials for device applications.

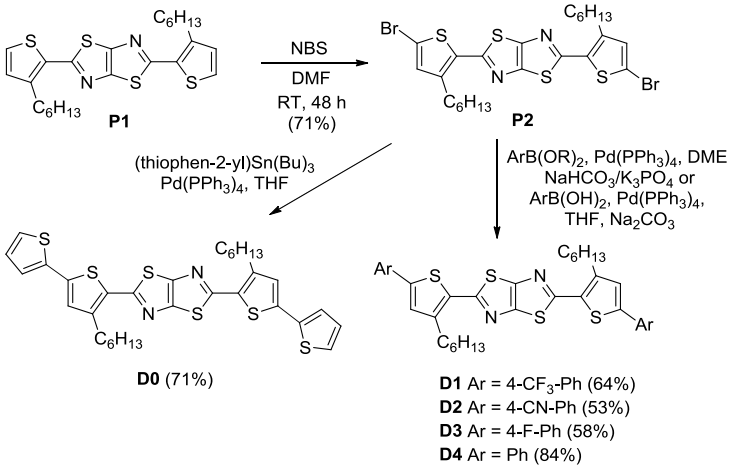

Scheme 6.1. Synthetic procedures toward TzTz derivatives **D0**–**D4**

6.2.2. NMR Characterization

To confirm the identity and purity of the novel thiazolo[5,4-*d*]thiazole derivatives, they were analyzed by mass spectrometry and NMR.[10] NMR spectroscopy confirmed that TzTz's **D0–D4** were obtained in excellent purity. Complete assignment of the ^{1}H and ^{13}C resonances was achieved by a combination of regular ^{1}H and ^{13}C NMR spectra with APT, DEPT, T_{1C}, COSY, and short/long-range HETCOR experiments. Table 6.1 presents an overview of all signal assignments for **D0–D4**. The complete NMR analysis of TzTz **D0** has previously been reported.[8] Such a detailed analysis is useful since the obtained chemical shift information can be helpful in further research on TzTz moieties, for instance by implementation in NMR-based prediction software. To date, experimental NMR data on TzTz compounds, and resonance assignments in particular, are very scarce. The chemical structures of TzTz compounds **D1–D4** differ only in the aryl substituents on the thiophene rings. Figure 6.1 provides an arbitrary numbering scheme for the different carbon and hydrogen atoms of the TzTz derivatives **D0–D4**.

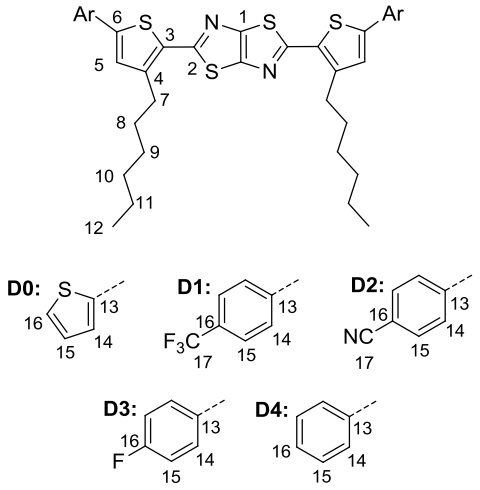

Figure 6.1. Arbitrary numbering scheme for 2,5-bis(5-aryl-3-hexylthiophen-2-yl)thiazolo[5,4-*d*]thiazole derivatives **D0–D4**. The different carbon atoms are numbered from C1 to C17 and the different hydrogen atoms are labelled accordingly from H-5 to H-16.

*Assignment of the resonances of TzTz **D1***

In previous work all ^{1}H and ^{13}C NMR resonances of the precursors **P1** and **P2**, and TzTz derivative **D0** were assigned.[8] This knowledge readily allowed the assignment of the carbon signals of **D1** at 161.5, 150.9, 144.7 and 133.0 ppm to the non-protonated carbon atoms C2, C1, C4 and C3 of the fixed core, respectively. The presence of the three ^{19}F nuclei on the *para*-trifluoromethyl substituent, affording quadruplet ^{13}C resonance patterns under broadband proton-decoupling, was very helpful for further assignments. The non-protonated carbon atom C17 has a chemical shift at 124.7 ppm (split into a quadruplet with lines at 130.1, 126.5, 122.9 and 119.2 ppm due to the direct $^{1}J_{C\text{-}F}$ coupling with coupling constant of 272 Hz). The $^{2}J_{C\text{-}F}$ coupling of 33 Hz was also clearly identifiable in the quadruplet with chemical shift of 130.4 ppm (131.1, 130.6, 130.2 and 129.8 ppm) arising from C16. Finally, a $^{3}J_{C\text{-}F}$ coupling of 3.5 Hz allowed to locate the chemical shift of C15 at 126.6 ppm (Figure 6.2). The proton signal at 7.64 ppm could be assigned to H-15 via a short-range (^{1}J or direct coupling) HETCOR experiment.

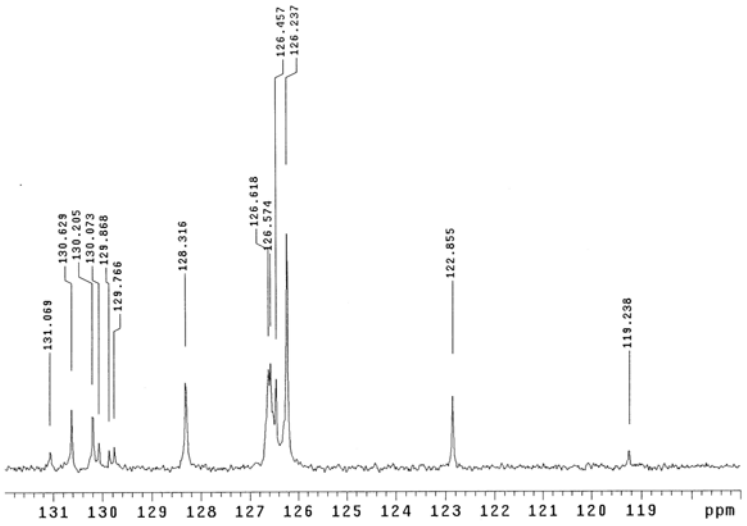

Figure 6.2. Part of the aromatic region of the ^{13}C NMR spectrum of **D1**.

Table 6.1. Chemical shifts (ppm) and assignments of the proton and carbon resonances for thiazolo[5,4-*d*]thiazole derivatives **D0–D4**. The chemical shift scales are calibrated to $CDCl_3$: ^1H = 7.24 ppm and ^{13}C = 77.70 ppm. The assignment of the chemical shifts for TzTz **D0** was retrieved from previous work.[8]

	D0	**D1**	**D2**	**D3**	**D4**		**D0**	**D1**	**D2**	**D3**	**D4**
	Ar = Thien-2-yl	Ar = *p*-CF_3-Ph	Ar = *p*-CN-Ph	Ar = *p*-F-Ph	Ar = Ph		Ar = Thien-2-yl	Ar = *p*-CF_3-Ph	Ar = *p*-CN-Ph	Ar = *p*-F-Ph	Ar = Ph
C1	150.7	150.9	151.3	150.9	150.7		-	-	-	-	-
C2	161.5	161.5	161.6	161.9	161.8		-	-	-	-	-
C3	131.0	133.0	133.8	131.9	131.7		-	-	-	-	-
C4	144.5	144.7	145.0	145.2	144.7		-	-	-	-	-
C5	127.6	128.3	129.2	127.4	127.3	H-5	7.00 (s)	7.27 (s)	7.30 (s)	7.12 (s)	7.20 (s)
C6	137.3	143.9	143.5	144.9	146.1		-	-	-	-	-
C7	31.1	31.2	31.1	31.1	31.2	H-7	2.88 (t)	2.97 (t)	2.96 (t)	2.94 (t)	2.96 (t)
C8	30.5	30.4	30.5	30.7	30.5	H-8	1.71 (p)	1.76 (p)	1.75 (p)	1.74 (p)	1.75 (q)
C9	30.1	30.1	30.1	30.1	30.1	H-9	1.45 (p)	1.48 (p)	1.47 (p)	1.47 (p)	1.47 (q)
C10	32.3	32.3	32.3	32.4	32.3	H-10	1.34 (m)	1.35 (m)	1.35 (m)	1.35 (m)	1.35 (m)
C11	23.3	23.3	23.3	23.3	23.3	H-11	1.34 (m)	1.35 (m)	1.35 (m)	1.35 (m)	1.35(m)
C12	14.8	14.8	14.8	14.8	14.8	H-12	0.90 (t)	0.90 (t)	0.90 (t)	0.90 (t)	0.90 (t)
C13	139.4	137.3	138.3	130.7 (d)	134.1			-	-	-	-
C14	125.2	126.2	126.6	128.3 (d)	126.4	H-14	7.22 (dd)	7.73 (d)	7.72 (d)	7.60 (dd)	7.64 (dd)
C15	128.8	126.6 (q)	133.5	116.8 (d)	129.7	H-15	7.02 (dd)	7.64 (d)	7.67 (d)	7.08 (dd)	7.39 (t)
C16	126.0	130.4 (q)	112.0	163.6 (d)	128.9	H-16	7.24 (dd)	-	-	-	7.31 (t)
C17		124.7 (q)	119.3				-	-	-	-	-

The aromatic region of the ^{1}H NMR spectrum presents three resonance patterns corresponding to the ten aromatic protons of **D1**: an AB-system[11] consisting of H-15 (7.64 ppm) and H-14 (7.73 ppm; ^{3}J = 9.0 Hz) and a singulet resonance at 7.27 ppm from the thiophene protons H-5. A short-range HETCOR experiment than allowed to determine the chemical shifts of C5 (128.3 ppm) and C14 (126.2 ppm). This left only two unidentified chemical shifts (137.3 and 143.9 ppm) for two non-protonated aromatic carbons, C6 and C13. A long-range HETCOR experiment (Figure 6.3) showed a clear correlation between H-15 and the carbon signal at 137.3 ppm which can only arise from the ^{3}J-coupling between H-15 and C13. Indeed, H-15 is too far (four bonds) from C6 to show a correlation.[12] The remaining carbon signal at 143.9 ppm correlates with H-5 and H-14, confirming its assignment to C6. Figure 6.3 shows additional confirmative correlations (e.g. C4-H5, C3-H5, C16-H14, C17-H15) which are not discussed in detail. The assignment of the alkyl side chain carbon atoms was based on COSY and short-range HETCOR experiments as described in our previous paper.[8] Most assignments could be confirmed by ^{13}C spin-lattice relaxation time (T_{1C}) experiments (Table 6.2). Taking the through space dipole-dipole interaction as the main mechanism for relaxation, the T_{1C} relaxation of small molecules in solution (situated in the so-called Extreme Narrowing Region) is mainly determined by the correlation time of motion (τ_c) and the distance to surrounding proton magnetic dipoles ($1/T_{1C}$ has a $1/r^6$ dependency to proton spins). Proton magnetic moments induce, due to molecular motions, local oscillating magnetic fields in the neighbourhood of the carbon atoms, the source of T_{1C} relaxation.[13] Regarding the non-protonated TzTz core carbon atoms (C1, C2, C3, C4 and C6 - with similar τ_c), the decay times are determined by the spatial distance to the nearest protons (a longer distance corresponding to a longer decay time). Regarding the carbon atoms of the mobile hexyl side chains (with a similar distance to protons), the closer the carbon is situated toward the end of the side chain, the longer its relaxation decay time will become due to less restricted conformational motions.[13] This is obvious for C7 and C12 which have the shortest and longest T_{1C} decay time of the side chain carbon atoms, respectively. The short-range HETCOR spectrum allowed the assignment of the proton signals of the bonded protons and this was confirmed by a COSY experiment.

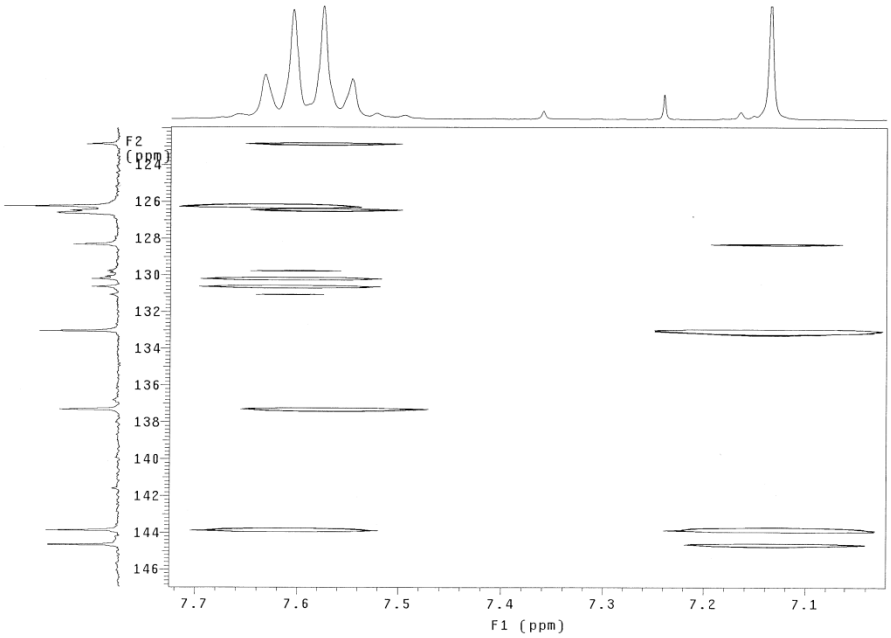

Figure 6.3. Long-range HETCOR (J = 8 Hz) spectrum of **D1**.

*Assignment of the resonances of TzTz **D2***

Carbon peaks at 151.3, 161.6, 133.8 and 145.0 ppm could be assigned to C1, C2, C3 and C4, respectively, based on previous attributions for the precursors **P1** and **P2**, and the TzTz derivative **D0**.[8] The aromatic region of the ^{1}H NMR spectrum again showed three resonance patterns corresponding to the ten aromatic protons of **D2**: an AB-system consisting of H14/H15 (7.72 ppm/7.67 ppm; ^{3}J = 9 Hz) and a singulet resonance at 7.30 ppm for the thiophene protons H-5. A short-range HETCOR experiment allowed to assign the carbon signal at 129.2 ppm to C5 (128.3 ppm). This left six aromatic carbon atoms at 143.5, 138.3, 126.6, 133.5, 112.0 and 119.3 ppm, for which an APT spectrum (and integration) showed that the signals at 126.6 and 133.5 ppm arose from methine carbon atoms. Based on the chemical shift and T_{1C} decay time, the carbon signal at 143.5 ppm could be assigned to C6. Indeed, the long-range HETCOR experiment (Figure 6.4) revealed a ^{3}J coupling between this carbon resonance and the proton resonance at 7.72 ppm, next to a ^{2}J coupling with the proton resonance at 7.30 ppm (H-5). This allowed to assign the proton signal at 7.72 ppm to H-14. Confirmation could be found in C4 (145.0 ppm), which only correlates to H-5

since it is too far (5 bonds) from H-14. The remaining aromatic proton signal at 7.67 ppm could then be assigned to H-15. The carbon signals at 126.6 and 133.5 ppm could be attributed to C14 and C15, respectively, based on a short-range HETCOR experiment. Taking the electron-withdrawing effect of the –CN functional group into account, the reduced electron density at C15 corresponds with its downfield chemical shift (as compared to C14). In the long-range HETCOR experiment, the ^{13}C signal at 112.0 ppm presented a correlation with H14 (7.72 ppm; ^{3}J coupling) and H-15 (7.67 ppm; ^{2}J coupling), and therefore could be assigned to C16 (Figure 6.4). In agreement with previous TzTz derivatives, C13 could be assigned to the carbon signal at 138.3 ppm, while C17 resonates at 119.3 ppm. The latter is fully in agreement with literature.[14] Figure 4 shows additional confirmative correlations (e.g. C17-H15, C14-H14, C15-H15, C3-H5, C13-H5) which are not discussed further in detail. The alkyl side chain assignment was again based on COSY, short-range HETCOR and T_{1C} experiments, as reported above and previously.[8]

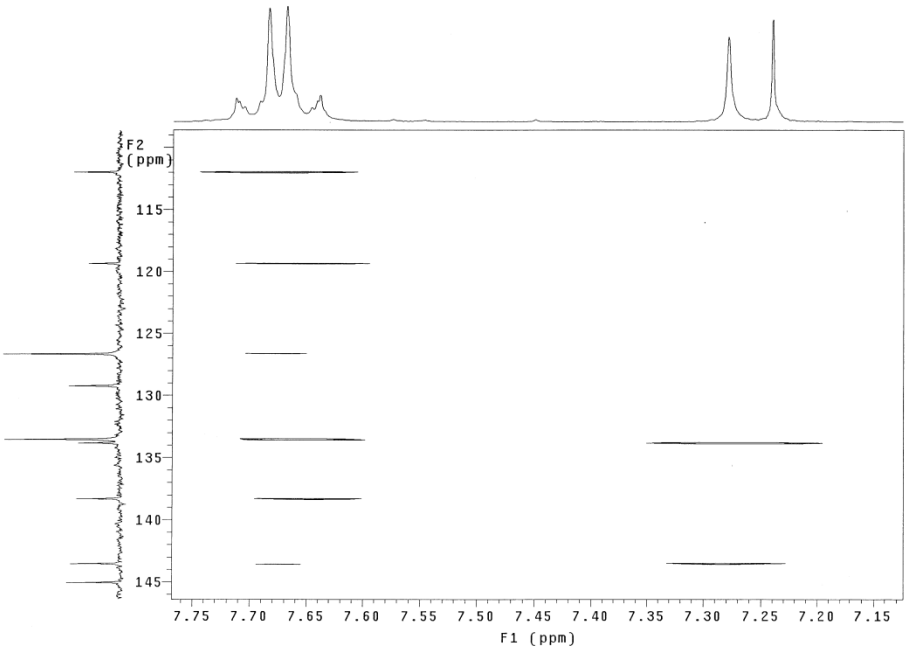

Figure 6.4. Long-range HETCOR (J = 8 Hz) spectrum of **D2**.

Table 6.2. T_{1C} relaxation decay times (s) for the carbon atoms of thiazolo[5,4-*d*]thiazole derivatives **D0**–**D2** and **D4**. T_{1C} data for TzTz **D0** were retrieved from previous work.[8]

	D0 Ar = Thien-2-yl	T_{1C} (s)	**D1** Ar = *p*-CF_3-Ph	T_{1C} (s)	**D2** Ar = *p*-CN-Ph	T_{1C} (s)	**D4** Ar = Ph	T_{1C} (s)
Carbon								
C1	150.7	9.3	150.9	8.55	151.3	11.3	150.7	10.2
C2	161.5	6.7	161.5	6.00	161.6	7.29	161.8	6.81
C3	131.0	7.8	133.0	6.82	133.8	8.67	131.7	8.32
C4	144.5	3.3	144.7	2.74	145.0	3.64	144.7	3.80
C5	127.6	0.40	128.3	0.23	129.2	0.35	127.3	0.43
C6	137.3	6.1	143.9	3.85	143.5	5.48	146.1	4.65
C7	31.1	0.50	31.2	0.39	31.1	0.43	31.2	0.48
C8	30.5	0.71	30.4	0.51	30.5	0.55	30.5	0.69
C9	30.1	1.00	30.1	0.73	30.1	0.86	30.1	0.96
C10	32.3	1.67	32.3	1.24	32.3	1.50	32.3	1.58
C11	23.3	2.32	23.3	1.95	23.3	2.28	23.3	2.35
C12	14.8	3.12	14.8	2.95	14.8	2.97	14.8	2.98
C13	139.4	4.00	137.3	2.51	138.3	4.05	134.1	3.62
C14	125.2	0.63	126.2	0.41	126.6	0.52	126.4	0.76
C15	128.8	0.63	126.6	0.46	133.5	0.46	129.7	0.69
C16	126.0	0.41	130.4	3.42	112.0	3.98	128.9	0.41
C17			124.7	4.26	119.3	1.32		

*Assignment of the resonances of TzTz **D3***

As 4-fluorophenyl-substituted TzTz **D3** was found to be somewhat less soluble in $CDCl_3$, NMR spectra were acquired at a slightly elevated temperature (45 °C). The carbon peaks at 150.9, 161.9, 131.9 and 145.2 ppm could be attributed to the fixed core carbon atoms C1, C2, C3 and C4, respectively, based on the T_{1C} relaxation data (Table 6.2) and previous assignments.[8] The ^{19}F nucleus gave rise to doublet resonance patterns in the proton-decoupled ^{13}C NMR spectrum (Figure 6.5). The non-protonated carbon atom C16 appeared as a doublet (165.2 and 161.9 ppm) with chemical shift centered at 163.6 ppm due to a direct $^{1}J_{C\text{-}F}$ coupling of 248 Hz (remark that the signal of C2 overlaps with the high field line of the doublet). C15 also showed a doublet with chemical shift centered at 116.8 ppm (116.9 and 116.6 ppm) due to a $^{2}J_{C\text{-}F}$ coupling of 22 Hz. Furthermore, C14 and C13 could be attributed to the doublets with chemical shifts at 128.3 and 130.7 ppm, based on their $^{3}J_{C\text{-}F}$ and $^{4}J_{C\text{-}F}$ couplings of 8.5 and 3.4 Hz, respectively (Figure 6.5). Taking the electron-donating effect of the –F functional group into account, the increased electron density at C15 corresponds with its low-frequency chemical shift (as compared to C14). C5 was the only protonated aromatic carbon atom remaining and could hence easily be assigned by DEPT to the signal at 127.4 ppm. A short-range HETCOR correlated C5 to the proton singulet of H-5 at 7.12 ppm.

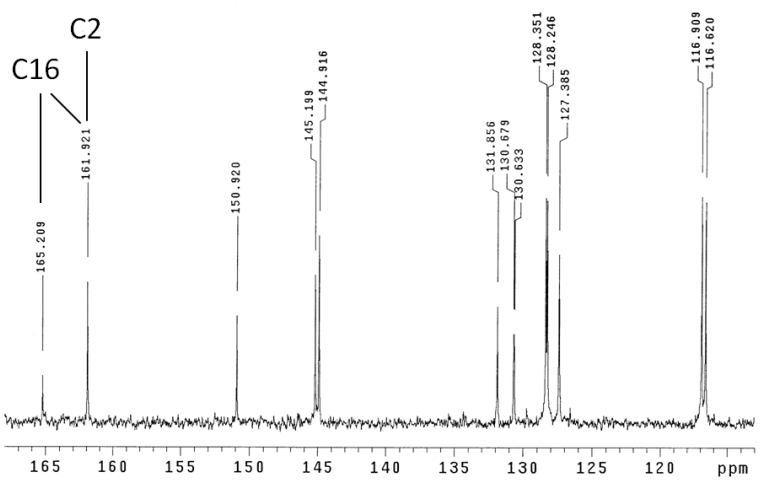

Figure 6.5. Aromatic region of the ^{13}C NMR spectrum of **D3**.

The alkyl side chain assignment was again based on COSY, short-range HETCOR and T_{1C} experiments. The only remaining carbon signal at 144.9 ppm therefore corresponded to C6. Besides the H-5 singulet, the aromatic region of the ^{1}H NMR spectrum showed two additional resonance patterns, originating from the *p*-F-Ph ring protons, which could be assigned based on the *J* coupling patterns: a doublet of doublets at 7.60 ppm ($^{3}J_{H\text{-}H}$ = 9 Hz, $^{4}J_{H\text{-}F}$ = 6 Hz) and an "apparent" triplet at 7.08 ppm ($^{3}J_{H\text{-}H}$ and $^{3}J_{H\text{-}F}$ = 9 Hz; overlap with H-5 at 7.12 ppm). The short-range HETCOR experiment (Figure 6.6) confirmed these assignments: the carbon signal at 116.8 ppm (C15) correlated with the 7.08 ppm "triplet" of H-15, while the 128.3 ppm peak (C14) correlated with the double doublet at 7.60 ppm of H-14.

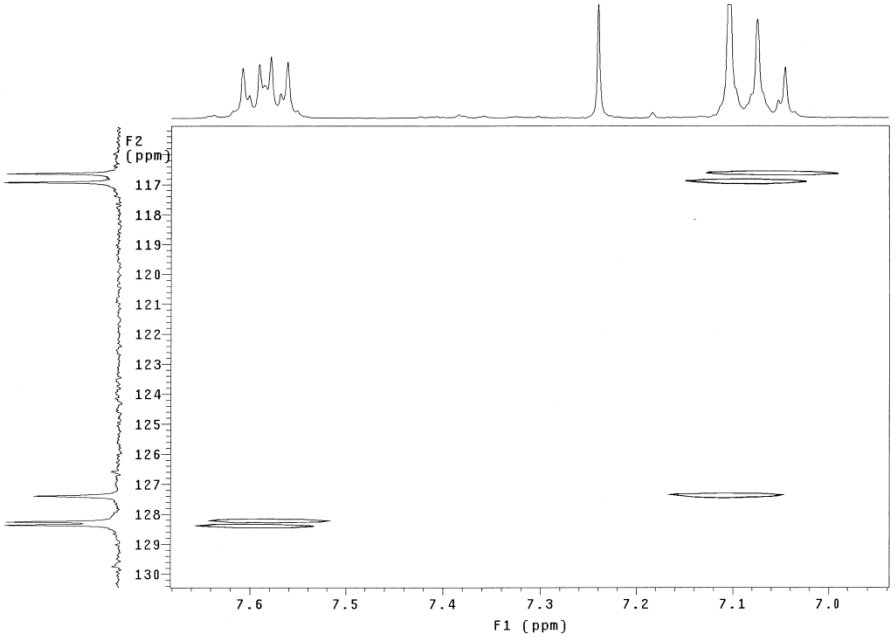

Figure 6.6. Short-range HETCOR (*J* = 140 Hz) spectrum of **D3.**

*Assignment of the resonances of TzTz **D4***

The carbon resonances at 161.8, 150.7, 131.7 and 144.7 ppm are again attributed to the fixed TzTz core carbon atoms C1, C2, C3 and C4, respectively, based on the T_{1C} relaxation data (Table 6.2) and previous assignments for **D0**.[8] The aromatic region of the ^{1}H NMR spectrum showed four resonance patterns originating from the 4 aromatic protons of **D4**, which could easily be interpreted on the basis of *J* coupling patterns and

integration values: the doublet at 7.65/7.62 ppm (^3J = 7.3 Hz, 4H) to H-14, the triplet centered at 7.39 ppm (^3J = 7.3 Hz, 4H) to H-15 and the triplet centered at 7.31 ppm (^3J = 7.3 Hz, 2H) to H-16. The COSY spectrum revealed cross-peaks confirming these assignments. The only remaining aromatic proton signal could be observed as a singulet resonating at 7.20 ppm and corresponded to the thiophene protons (H-5). From the short-range HETCOR experiment (Figure 6.7), it could be derived that the methine carbon signals at 129.7, 128.9, 127.3 and 126.4 ppm belong to C15, C16, C5 and C14, respectively. This left two unassigned aromatic carbon signals at 146.1 and 134.1 ppm. A long-range HETCOR experiment (Figure 6.8) further revealed that the aromatic carbon signal at 146.1 ppm is coupled with both H-14 and H-5, allowing to assign it to C6, as C4 is too remote (5 bonds) from H-14. C4 only correlates to the aromatic proton H-5. The remaining carbon signal at 134.1 ppm could then be attributed to C13. The assignment of the alkyl side chain carbon resonances was based on the same protocol as described above for **D1**–**D3**.

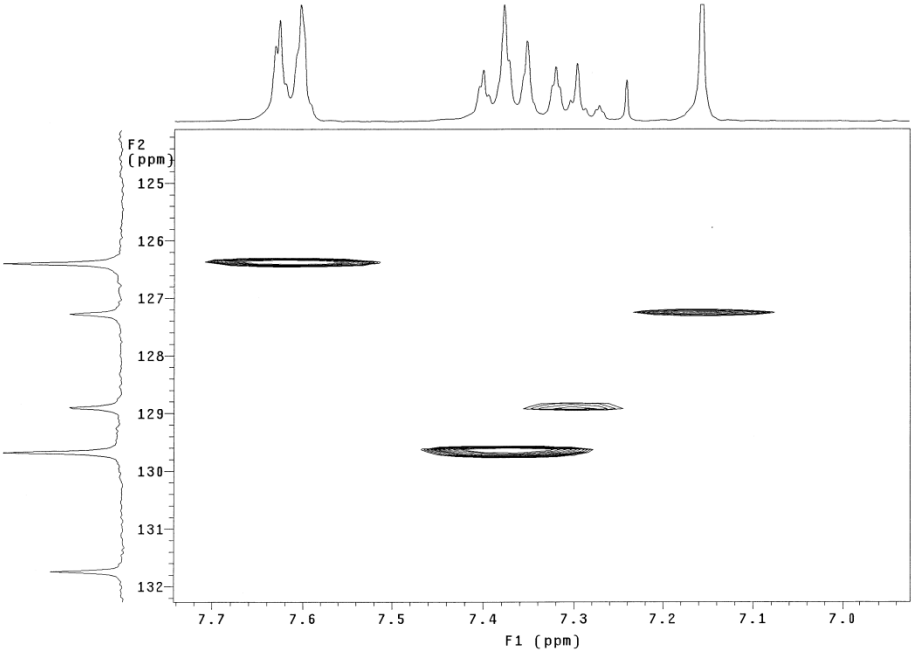

Figure 6.7. Short-range HETCOR (J = 140 Hz) spectrum of **D4**.

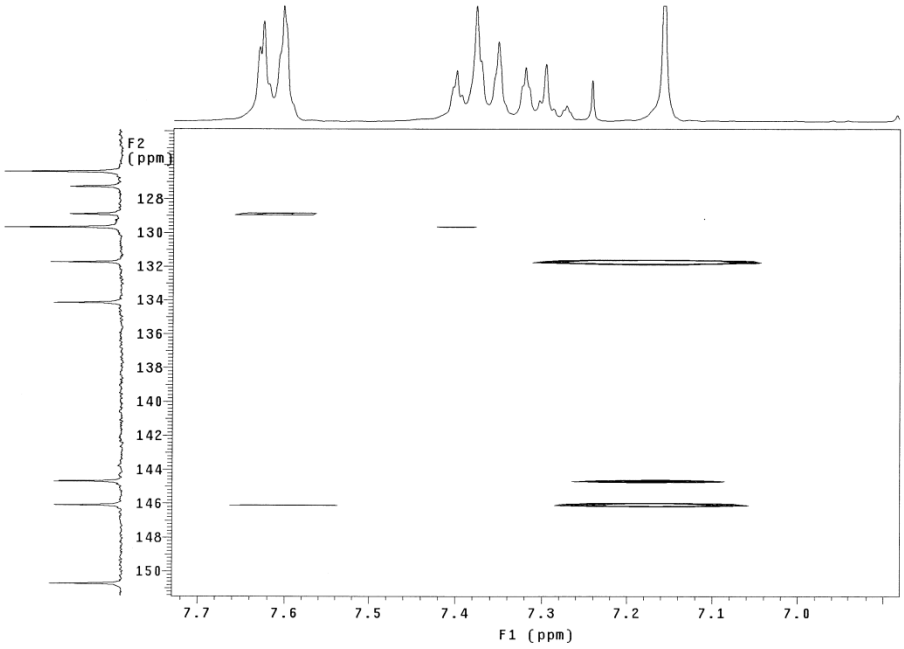

Figure 6.8. Long-range HETCOR (J = 8 Hz) spectrum of **D4**.

In general, only subtle changes in NMR chemical shifts were observed for the TzTz core and hexyl side chain carbon atoms of the differently substituted 2,5-dithienyl-TzTz derivatives **D0**–**D4** (Table 6.1). The most noticeable difference is the deshielding of the thiophene proton for *p*-CF_3-phenyl and *p*-CN-phenyl derivatives **D1** and **D2**, as compared to the reference compound **D4**, and the upfield shift for the *p*-F-phenyl TzTz **D3** (Table 6.1). More pronounced differences were of course observed within the respective aryl substituents, most notably for the *ipso* and *ortho* aromatic carbon resonances, reflecting the nature of the appended functional groups.

Table 6.3. Theoretical chemical shifts (ppm) for thiazolo[5,4-*d*]thiazole derivatives **D0**–**D4**. TMS was taken as a reference and its calculated σ values are 31.31 ppm and 183.33 ppm for ^{1}H and ^{13}C, respectively. All values have been calculated at the IEF-PCM/B3LYP/6-311+G(2d,p) level of theory with $CHCl_3$ as a solvent and have been corrected by the linear regression Eqs.1–4. The differences between the calculated and experimental (Table 6.1) chemical shifts are given in parentheses.

	D0 Ar = Thien-2-yl	**D1** Ar = *p*-CF_3-Ph	**D2** Ar = *p*-CN-	**D3** Ar = *p*-F-Ph	**D4** Ar = Ph		**D0** Ar = Thien-2-yl	**D1** Ar = *p*-CF_3-Ph	**D2** Ar = *p*-CN-Ph	**D3** Ar = *p*-F-Ph	**D4** Ar = Ph
C1	149.8 (-0.9)	150.4 (-0.5)	150.6 (-0.7)	149.8 (-1.1)	149.8 (-0.9)						
C2	158.8 (-2.7)	159.3 (-2.2)	159.3 (-2.3)	159.2 (-2.7)	159.2 (-2.6)						
C3	131.9 (0.9)	135.2 (2.2)	136.0 (2.2)	133.6 (1.7)	133.5 (1.8)						
C4	140.7 (-3.8)	140.1 (-4.6)	140.5 (-4.5)	140.4 (-4.8)	140.6 (-4.1)						
C5	129.1 (1.5)	130.5 (2.2)	131.4 (2.2)	129.4 (2.0)	129.8 (2.5)	H-5	7.11 (0.11)	7.33 (0.06)	7.36 (0.06)	7.16 (0.04)	7.19 (-0.01)
C6	139.4 (2.1)	143.2 (-0.7)	142.7 (-0.8)	144.4 (-0.5)	145.5 (-0.6)						
C13	138.0 (-1.4)	135.3 (-2.0)	135.8 (-2.5)	130.3 (-0.4)	132.5 (-1.6)						
C14	126.4 (1.2)	126.4 (0.2)	126.5 (-0.1)	127.9 (-0.4)	126.9 (0.5)	H-14	7.36 (0.14)	7.74 (0.01)	7.73 (0.01)	7.63 (0.03)	7.64 (0.00)
C15	129.2 (0.4)	126.9 (0.3)	132.2 (-1.3)	119.7 (2.9)	128.4 (-1.3)	H-15	7.03 (0.01)	7.63 (-0.01)	7.69 (0.02)	7.16 (0.08)	7.48 (0.09)
C16	126.5 (0.5)	129.8 (-0.6)	115.9 (3.9)	153.5 (-10.1)	128.1 (-0.8)	H-16	7.31 (0.07)				7.46 (0.15)
C17		129.4 (4.7)	120.6 (1.3)								
CMAE	1.5	1.8	2.0	2.7	1.7		0.08	0.02	0.03	0.05	0.07

Table 6.4. Differences of the theoretical chemical shifts (ppm) between thiazolo[5,4-*d*]thiazole derivatives D1–D3 and D4 (taken as a reference). All values have been calculated at the IEF-PCM/B3LYP/6-311+G(2d,p) level of theory with $CHCl_3$ as a solvent and have been corrected by the linear regression Eqs.1–4. Bold (italic) values represent important deshielding (shielding) effects with respect to the chemical shifts of D4 (Ar = Ph). The corresponding experimental values are given in parentheses.

	D1 Ar = *p*-CF_3-Ph	**D2** Ar = *p*-CN-Ph	**D3** Ar = *p*-F-Ph		**D1** Ar = *p*-CF_3-Ph	**D2** Ar = *p*-CN-Ph	**D3** Ar = *p*-F-Ph
Carbon				*Proton*			
C1	0.6 (0.2)	0.8 (0.6)	0.0 (0.2)				
C2	0.1 (-0.3)	0.1 (-0.2)	0.0 (0.1)				
C3	**1.8 (1.3)**	**2.5 (2.1)**	0.2 (0.2)				
C4	-0.5 (0.0)	-0.1 (0.3)	-0.2 (0.5)				
C5	0.7 (1.0)	**1.6 (1.9)**	-0.4 (0.1)	H-5	**0.14 (0.07)**	**0.18 (0.10)**	-0.03 (-0.08)
C6	*-2.2 (-2.2)*	*-2.8 (-2.6)*	*-1.0 (-1.2)*				
C13	**2.9 (3.2)**	**3.3 (4.2)**	*-2.2 (-3.4)*				
C14	-0.5 (-0.2)	-0.4 (0.2)	**1.1 (1.9)**	H-14	0.09 (0.09)	0.08 (0.08)	-0.02 (-0.04)
C15	*-1.5 (-3.1)*	**3.8 (3.8)**	*-8.7 (-12.9)*	H-15	**0.15 (0.25)**	**0.21 (0.28)**	*-0.33 (-0.31)*
C16	**1.7 (1.5)**	*-12.2 (-16.9)*	**25.4 (34.7)**				

6.2.3. Theoretical Characterization

Table 6.3 presents the calculated chemical shifts as well as the corrected mean absolute errors (CMAE), obtained after using Eqs. 1–4 (see experimental section), with respect to the experimental values given in Table 6.1. The calculated values are in good agreement with the experimental data and confirm the chemical shift assignments. More precisely, when the chemical shifts display a dependence with respect to the substituents (aromatic carbon atoms C5, C6, C13, C14, C15, and C16), the calculations correctly reproduce the chemical shift trends, demonstrating they account for different electron donating and withdrawing effects. This is further illustrated in Table 6.4 where the differences of the calculated chemical shifts for derivatives **D1**–**D3** are reported (the differences between the experimental data are also given in parentheses) with respect to derivative **D4** (Ar = Ph), which is taken as a reference. For instance, C16 becomes more deshielded in derivative **D3** due to the inductive attractor effect of the F atom, while it becomes more shielded in derivative **D2** due to anisotropy of the triple C-N bond. The change of chemical shifts of C15 can be explained by the mesomeric donor (derivative **D3**) and attractor (derivative **D2**) effects. There are also a number of discrepancies but, to a large extent, they can be explained. So, δ (C4) is underestimated, because the hexyl chain is replaced by a methyl group in the calculations. For C16 and C17 the predictions are also of lesser quality as a result of the close proximity to heteroatoms and the fact that our approach has not been fitted specifically for these carbon atoms. However, the CMAE values are smaller than 3.0 ppm for ^{13}C NMR and smaller than 0.1 ppm for ^{1}H NMR, which is a double support for the experimental assignment and the method reliability.

6.3. Conclusions

A series of soluble aryl-substituted 2,5-dithienylthiazolo[5,4-*d*]thiazole semiconductors was efficiently synthesized by Suzuki cross-coupling reactions. Complete NMR chemical shift assignment for these materials was accomplished by means of a number of 1D and 2D NMR experiments. Computational chemistry has been used as an additional tool to confirm the experimental NMR data. The calculated chemical shift trends are generally consistent with the inductive, mesomeric and anisotropic effects imposed by the substituents, and a few signatures were identified enabling

straightforward screening of various (unknown) TzTz compounds in future. The gathered chemical shift data are of relevance for chemical shift prediction software, since limited experimental data on TzTz derivatives are currently available. This will be particularly interesting since a spectacular increase in the application of TzTz semiconducting molecules can be seen from literature in the last year, notably in organic photovoltaics. The acquired knowledge will also strongly support further (ongoing) research within our groups on TzTz-based semiconductors and narrow bandgap copolymers toward applications in organic electronics.

6.4. Experimental Section

Synthesis

Detailed synthetic procedures toward TzTz derivatives **D1**, **D2** and **D3** will be reported elsewhere.[10]

2,5-Bis(3-hexyl-5-phenylthiophen-2-yl)thiazolo[5,4-*d*]thiazole (D4).[15] Under nitrogen atmosphere, a small amount of $Pd(PPh_3)_4$ (6 mg, 5 μmol) was dissolved in THF (4 mL). 2,5-Bis(5-bromo-3-hexylthiophene-2-yl)thiazolo[5,4-*d*]thiazole (**P2**) (100 mg, 158 μmol), a Na_2CO_3 solution (2M, 0.5 mL) and phenylboronic acid (42 mg, 347 μmol) were added to the stirring solution in the mentioned sequence. After heating at reflux temperature for 5 h under nitrogen atmosphere and protected from light, no starting material was observed any more (by TLC analysis). After cooling to RT, the crude reaction mixture was concentrated under reduced pressure and subsequently diluted with water and CH_2Cl_2. The organic layer was separated and the aqueous layer was extracted with CH_2Cl_2 (3 x 50 mL). The combined organic layers were washed with a saturated $NaHCO_3$ solution and brine, dried over $MgSO_4$, filtered and concentrated by evaporation *in vacuo*. The reaction product was purified by gradient column chromatography (silica, eluent CH_2Cl_2 to CH_2Cl_2:MeOH 95:5) and recrystallized from ethyl acetate, resulting in 80 mg (84% yield) of red crystalline needles. GC-MS (EI): *m/z* = 626 (M^+); UV-vis ($CHCl_3$, nm) λ_{max} (log ε) 434 (4.656).

NMR Characterization

All ^{1}H and ^{13}C liquid-state NMR experiments were performed at room temperature on a Varian Inova 300 spectrometer in a 5 mm four-nucleus PFG probe. The chemical shift scales are calibrated to $CDCl_3$: ^{1}H= 7.24 ppm and ^{13}C= 77.70 ppm. The proton spectra were acquired with a 90° pulse of 4.3 μs, a spectral width of 4500 Hz, an acquisition time of 3.5 s, a preparation delay of 8 s and 20 accumulations, processed with a line broadening of 0.2 Hz. The concentration of the samples was ~2 mg/0.7 mL The carbon spectra were acquired with a 90° pulse of 12 μs, a spectral width of 16500 Hz, an acquisition time of 0.8 s, a preparation delay of 60 s and 2500 accumulations, processed with a line broadening of 3 Hz. Higher concentrations were used for the 1D and 2D spectra with ^{13}C detection.

Details on the Computational Procedures

The ground state geometries were optimized at the density functional theory (DFT) level of approximation by employing the B3LYP exchange-correlation (XC) functional and the 6-31G* basis set. For convenience, the *n*-hexyl substituents have been replaced by smaller methyl groups. The chemical shifts (δ) of all systems were calculated as the difference of isotropic shielding constants (σ) with respect to TMS. All σ values were obtained with the B3LYP XC functional and the 6-311+G(2d,p) basis set together with the GIAO method to ensure origin-independence, following the approach that was employed and tested recently for PVC oligomers, fluoroionophores, and poly(thienylene vinylene) (PTV) model compounds.[16] As shown in these previous studies, linear fits between experimental and theoretical δ values of representative model compounds can facilitate the interpretation of the NMR spectra of more complex and larger compounds and can therefore provide a way of correcting the calculated properties from systematic errors. Preliminary investigations on PTV model compounds have been reported before,[16d] and the theoretically estimated δ values were obtained from the calculated values using the following relationships (in ppm):

sp^2 *in* α ^{13}C: $\delta(\text{estimated}) = 0.8099\ \delta[\text{IEF-PCM/B3LYP/6-311+G(2d,p)}] + 15.39$ (1a)

^{1}H: $\delta(\text{estimated}) = 0.8653\ \delta[\text{IEF-PCM/B3LYP/6-311+G(2d,p)}] + 0.67$ (1b)

sp^2 in β	^{13}C: δ(estimated) = 0.7618 δ[IEF-PCM/B3LYP/6-311+G(2d,p)] + 27.61	(2a)
	^{1}H: δ(estimated) = 0.8845 δ[IEF-PCM/B3LYP/6-311+G(2d,p)] + 0.61	(2b)
other sp^2	^{13}C: δ(estimated) = 0.6510 δ[IEF-PCM/B3LYP/6-311+G(2d,p)] + 40.36	(3a)
	^{1}H: δ(estimated) = 0.8911 δ[IEF-PCM/B3LYP/6-311+G(2d,p)] + 0.52	(3b)
other atoms	^{13}C: δ(estimated) = 0.9618 δ[IEF-PCM/B3LYP/6-311+G(2d,p)] – 2.66	(4a)
	^{1}H: δ(estimated) = 0.9451 δ[IEF-PCM/B3LYP/6-311+G(2d,p)] + 0.12	(4b)

All the theoretical chemical shifts reported in this paper have been corrected by one of the linear regression equations. Solvent (here $CHCl_3$) effects were taken into account within the integral equation formalism of the polarizable continuum model (IEF-PCM)[17] for the calculations of the isotropic shielding constants of all compounds (including TMS). The δ[IEF-PCM/B3LYP/6-311+G(2d,p)] values consist in the Maxwell-Boltzmann average chemical shifts over the stable conformers based on the energies calculated at the B3LYP/6-31G* level of theory with the inclusion of solvent effects. Each torsion angle between adjacent rings is characterized by two minima, close to values of 0° and 180°. Therefore, taking into account the molecular symmetry, we end up with 16 conformers for **D0**, but only four for **D1**–**D4**. The Maxwell-Boltzmann weights are given in the supplementary material Table S1. All calculations were performed using Gaussian09.[18]

6.5. Acknowledgments

The authors gratefully acknowledge BELSPO (IAP P6/27 network "Functional Supramolecular Systems"), the IWT (Institute for the Promotion of Innovation by Science and Technology in Flanders) for financial support via the SBO-project 060843 "PolySpec", the European grant agreement n° 212311 of the ONE-P project, and the FWO Vlaanderen (Research Foundation Flanders) for continuous financial support and a postdoctoral fellowship to W.M. V. L. thanks the Fund for Scientific Research (FNRS) for his postdoctoral researcher position. The calculations were performed on

the Interuniversity Scientific Computing Facility (ISCF) installed at the FUNDP, for which we gratefully acknowledge financial support of the FRS-FRFC (Convention No. 2.4.617.07.F), and of the FUNDP.

6.6. References

(1) (a) M. Muccini, *Nat. Mater.* **2006**, *5*, 605; (b) J. Locklin, M. E. Roberts, S. C. B. Mannsfeld, Z. Bao, *J. Macromol. Sci., Part C: Polym. Rev.* **2006**, *46*, 79; (c) C.-a. Di, G. Yu, Y. Liu, D. Zhu, *J. Phys. Chem. B* **2007**, *111*, 14083; (d) D. Braga, G. Horowitz, *Adv. Mater.* **2009**, *21*, 1473; (e) Y. Yamashita, *Sci. Technol. Adv. Mater.* **2009**, *10*, 024313; (f) H. Serringhaus, M. Bird, T. Richards, N. Zhao, *Adv. Mater.* **2010**, *22*, 3893; (g) W. Wu, Y. Liu, D. Zhu, *Chem. Soc. Rev.* **2010**, *39*, 1489; (h) M. J. Malachowski, J. Zmija, *Opto-Electron. Rev.* **2010**, *18*, 121.

(2) (a) M. Ashizawa, R. Kato, Y. Takanishi, H. Takezoe, *Chem. Lett.* **2007**, *36*, 708; (b) K. Haubner, E. Jaehne, H.-J. P. Adler, D. Koehler, C. Loppacher, L. M. Eng, J. Grenzer, A. Herasimovich, S. Scheinert, *Phys. Stat. Sol.* **2008**, *205*, 431; (c) M. Mass-Torrent, C. Rovira, *Chem. Soc. Rev.* **2008**, *37*, 827. (d) Y. Liu, G. Yu, Y. Liu, *Sci. China Chem.* **2010**, *53*, 779; (e) L. Zhang, C.-a. Di, G. Yu, Y. Liu, *J. Mater. Chem.* **2010**, *20*, 7059.

(3) (a) S. Ando., J.-i. Nishida, Y. Inoue, S. Tokito, Y. Yamashita *J. Mater. Chem.* **2004**, *14*, 1787; (b) S. Ando, J.-i. Nishida, E. Fujiwara, H. Tada, Y. Inoue, S. Tokito, Y. Yamashita, *Chem. Lett.* **2004**, *33*, 1170; (c) S. Ando, J.-i. Nishida, H. Tada, Y. Inoue, S. Tokito, Y. Yamashita, *J. Am. Chem. Soc.* **2005**, *127*, 5336; (d) S. Ando, J.-i. Nishida, E. Fujiwara, H. Tada, Y. Inoue, S. Tokito, Y. Yamashita, *Synth. Met.* **2006**, *156*, 327; (e) S. Ando, D. Kumaki, J.-i. Nishida, H. Tada, Y. Inoue, S. Tokito, Y. Yamashita, *J. Mater. Chem.* **2007**, *17*, 553; (f) D. Kumaki, S. Ando, S. Shimono, Y. Yamashita, *Appl. Phys. Lett.* **2007**, *90*, 53506; (g) M. Mamada, J.-i. Nishida, D. Kumaki, S. Tokito, Y. Yamashita, *Chem. Mater.* **2007**, *19*, 5404; (h) Y. Fujisaki, M. Mamada, D. Kumaki, S. Tokito, Y. Yamashita, *Jpn. J. Appl. Phys.* **2009**, *48*, 111504.

(4) Naraso, F. Wudl, *Macromolecules* **2008**, *41*, 3169.

(5) (a) I. Osaka, G. Sauvé, R. Zhang, T. Kowalewski, R. D. McCullough, *Adv. Mater.* **2007**, *19*, 4160; (b) I. Osaka, R. Zhang, G. Sauvé, D.-M. Smilgies, T. Kowalewski, R. D. McCullough, *J. Am. Chem. Soc.* **2009**, *131*, 2521; (c) I. Osaka, R. Zhang, J. Liu, D.-M. Smilgies, T. Kowalewski, R. D. McCullough, *Chem. Mater.* **2010**, *22*, 4191.

(6) J. R. Johnson, R. Ketcham, *J. Am. Chem. Soc.* **1960**, *82*, 2719.

(7) J. R. Johnson, D. H. Rotenberg, R. Ketcham, *J. Am. Chem. Soc.* **1970**, *92*, 4046.

(8) S. Van Mierloo, S. Chambon, A. E. Boyukbayram, P. Adriaensens, L. Lutsen, T. J. Cleij, D. Vanderzande, *Magn. Reson. Chem.* **2010**, *48*, 362.

(9) (a) T. W. Lee, N. S. Kang, J. W. Yu, M. H. Hoang, K. H. Kim, J.-L. Jin, D. H. Choi, *J. Polym. Sci., Part A: Polym. Chem.* **2010**, *48*, 5921; (b) I. H. Jung, J. Yu, E. Jeong, J. Kim, S. Kwon, H. Kong, K. Lee, H. Y. Woo, H.-K. Shim, *Chem. Eur. J.* **2010**, *16*, 3743; (c) L. Huo, X. Guo, S. Zhang, Y. Li, J. Hou, *Macromolecules* **2011**, *44*, 4035; (d) S. K. Lee, J. M. Cho, Y. Goo, W. S. Shin, J.-C. Lee, W.-H. Lee, I.-N. Kang, H.-K. Shim, S.-J. Moon, *Chem. Commun.* **2011**, 1791; (e) S. K. Lee, I.-N. Kang, J.-C. Lee, W. S. Shin, W.-W. So, S.-J. Moon, *J. Polym. Sci., Part A: Polym. Chem.* **2011**, *49*, 3129; (f) T. W. Lee, N. S. Kang, J. W. Yu, M. H. Hoang, K. H. Kim, J.-I. Jin, D. H. Choi, *J. Polym. Sci., Part A: Polym. Chem.* **2011**, *49*, 5921; (g) J. Peet, L. Wen, P. Byrne, S. Rodman, K. Forberich, Y. Shao, N. Drolet, R. Gaudiana, G. Dennler, D. Waller, *Appl. Phys. Lett.* **2011**, *98*, 043301; (h) S. Subramaniyan, H. Xin, F. Sunjoo Kim, S. Shoaee, J. R. Durrant, S. A. Jenekhe, *Adv. Energy Mater.* **2011**, *1*, 854; (i) S. Subramaniyan, H. Xin, F. Sunjoo Kim, S. A. Jenekhe, *Macromolecules* **2011**, *44*, 6245; (j) M. Zhang, X. Guo, X. Wang, H. Wang, Y. Li, *Chem. Mater.* **2011**, *23*, 4264; (k) M. Helgesen, M. V. Madsen, B. Andreasen, T. Tromholt, J. W. Andreasen, F. C. Krebs, *Polym. Chem.* **2011**, *2*, 2536; (l) E. Jeong, G.-h. Kim, I. H. Jung, P. Jeong, J. Y. Kim, H. Y. Woo, *Curr. Appl. Phys.* **2012**, *12*, 11.

(10) S. Van Mierloo, K. Vasseur, N. Van den Brande, A. E. Boyukbayram, B. Ruttens, S. D. Rodriguez, E. Botek, V. Liégeois, J. D'Haen, P. J. Adriaensens, P. Heremans, B. Champagne, G. Van Assche, L. Lutsen, D. Vanderzande, W. Maes "Functionalized dithienylthiazolo[5,4-*d*]thiazoles for solution-processable organic field-effect transistors" *submitted to Chem. Mater.*

(11) H. D. Williams, I. Fleming, *Spectroscopic Methods in Organic Chemistry*, McGraw-Hill Publishing Company, Berkshire, **1995**.

(12) A. Rössler, P. Boldt, *J. Chem. Soc., Perkin Trans.* **1998**, *1*, 685.

(13) P. Adriaensens, F. G. Karssenberg, J. M. Gelan, V. B. F. Mathot, *Polymer* **2003**, *44*, 3483.

(14) H.-o. Kalinowski, S. Berger, S. Braun, *Carbon-13 NMR Spectroscopy*, John Wiley & Sons Ltd., **1998**.

(15) K. Horiba, H. Hirose, A. Imai, T. Agata, K. Sato, *Organic Semiconductor Transistor, Method of Producing the Same, and Electronic Device*, Pat. Appl. US 2010/0243995 A1.

(16) (a) Ph. d'Antuono, E. Botek, B. Champagne, M. Spassova, P. Denkova, *J. Chem. Phys.* **2006**, *125*, 144309; (b) Ph. d'Antuono, E. Botek, B. Champagne, J. Wieme, M. F. Reyniers, G. B. Marin, P. J. Adriaensens, J. Gelan, *J. Phys. Chem. B* **2008**, *112*, 14804; (c) E. Botek, Ph. d'Antuono, A. Jacques, R. Carion, L. Maton, D. Taziaux, J. L. Habib-Jiwan, *Phys. Chem. Chem. Phys.* **2010**, *12*, 14172; (d) H. Diliën, L. Marin, E. Botek, B. Champagne, V. Lemaur, D. Beljonne, R. Lazzaroni, T. J. Cleij, W. Maes, L. Lutsen, D. Vanderzande, P. J. Adriaensens, *J. Phys. Chem. B.* **2011**, *115*, 12040.

(17) (a) J. Tomasi, M. Persico, *Chem. Rev.* **1994**, *94*, 2027; (b) J. Tomasi, B. Mennucci, R. Cammi, *Chem. Rev.* **2005**, *105*, 2999.

(18) Gaussian 09, Revision A.1, M. J. Frisch, G. W. Trucks, H. B. Schlegel, G. E. Scuseria, M. A. Robb, J. R. Cheeseman, G. Scalmani, V. Barone, B. Mennucci, G. A. Petersson, H. Nakatsuji, M. Caricato, X. Li, H. P. Hratchian, A. F. Izmaylov, J. Bloino, G. Zheng, J. L. Sonnenberg, M. Hada, M. Ehara, K. Toyota, R. Fukuda, J. Hasegawa, M. Ishida, T. Nakajima, Y. Honda, O. Kitao, H. Nakai, T. Vreven, Jr. J. A. Montgomery, Jr. J. E. Peralta, F. Ogliaro, M. Bearpark, J. J. Heyd, E. Brothers, K. N. Kudin, V. N. Staroverov, R. Kobayashi, J. Normand, K. Raghavachari, A. Rendell, J. C. Burant, S. S. Iyengar, J. Tomasi, M. Cossi, N. Rega, J. M. Millam, M. Klene, J. E. Knox, J. B. Cross, V. Bakken, C. Adamo, J. Jaramillo, R. Gomperts, R. E. Stratmann, O. Yazyev, A. J. Austin, R. Cammi, C. Pomelli, J. W. Ochterski, R. L. Martin, K. Morokuma, V. G. Zakrzewski, G. A. Voth, P. Salvador, J. J. Dannenberg, S. Dapprich, A. D. Daniels, Ö. Farkas, J. B. Foresman, J. V. Ortiz, J. Cioslowski, D. J. Fox, Gaussian, Inc., Wallingford CT, **2009**.

6.7. Supporting Information

Table S1. Maxwell-Boltzman weights for the different conformers of each thiazolo[5,4-*d*]thiazole derivative **D0**–**D4**. The weights have been evaluated from the IEF-PCM/B3LYP/6-31G* energies with $CHCl_3$ as a solvent.

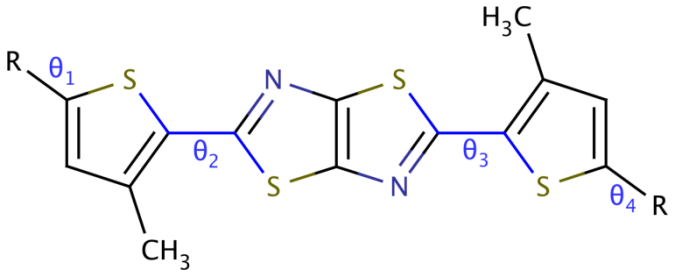

For **D1**–**D4**: θ_2-θ_3 torsion angles.

	180° - 180°	180° - 0°	0° - 180°	0° - 0°
D1 (R = *p*-CF_3-Ph)	79.7%	10.2%	10.2%	0.0%
D2 (R = *p*-CN-Ph)	80.3%	9.3%	9.3%	1.1%
D3 (R = *p*-F-Ph)	78.1%	10.3%	10.3%	1.4%
D4 (R = Ph)	77.2%	11.1%	11.1%	0.7%

For **D0** (R = thien-2-yl): θ_1-θ_2/θ_3-θ_4 torsion angles.

θ_1-θ_2\\θ_3-θ_4	180° - 180°	180° - 0°	0° - 180°	0° - 0°
180°- 180°	48.9%	13.5%	5.8%	1.7%
180° - 0°	5.8%	1.6%	0.6%	0.2%
0° - 180°	13.5%	3.9%	1.6%	0.5%
0° - 0°	1.7%	0.5%	0.2%	0.1%

Chapter 7

Improved Photovoltaic Performance of a Semi-Crystalline Narrow Bandgap Copolymer Based on 4*H*-Cyclopenta[2,1-*b*:3,4-*b*']dithiophene Donor and Thiazolo[5,4-*d*]thiazole Acceptor Units[†]

A solution processable narrow bandgap polymer composed of alternating 2,5-dithienylthiazolo[5,4-*d*]thiazole and asymmetrically alkyl-substituted 4*H*-cyclopenta[2,1-*b*:3,4-*b*']dithiophene units (**PCPDT-DTTzTz**) was synthesized by Suzuki polycondensation and the donor-acceptor copolymer was thoroughly characterized. Thermal analysis and X-ray diffraction studies disclosed the semi-crystalline nature of the material. When blended with $PC_{71}BM$ and integrated in bulk heterojunction organic solar cells, a power conversion efficiency of 4.03% under AM 1.5 G (100 mW/cm^2) was achieved. The purified polymer exhibited a relatively high field-effect carrier mobility of 1.0 x 10^{-3} cm^2/Vs. The active layer morphology was explored by atomic force microscopy and transmission electron microscopy studies, showing phase segregation on the nanometer scale.

[†] Van Mierloo, S.; Hadipour, A.; Spijkman, M.-J.; Van den Brande, N.; Ruttens, B.; Kesters, J.; D'Haen, J.; Van Assche, G.; de Leeuw, D. M.; Aernouts, T.; Manca, J.; Lutsen, L.; Vanderzande, D. J.; Maes, W. *Chem. Mater*. **2012**, manuscript accepted.

7.1. Introduction

Organic (polymer) solar cells (OSCs) offer great opportunities as renewable energy sources, as they combine unique features such as the potential for low cost large-area fabrication, solution processability, aesthetics, light weight and mechanical flexibility.[1] Bulk heterojunction (BHJ) OSCs based on regioregular poly(3-hexylthiophene) (P3HT) and [6,6]-phenyl-C_{61} butyric acid methyl ester ($PC_{61}BM$) as active layer donor and acceptor materials, respectively, have achieved power conversion efficiencies (PCEs) of 4–5%.[1–3] The main problem associated with the P3HT:$PC_{61}BM$ combination is the mismatch between the OSC absorption window and the terrestrial solar spectrum due to the relatively large bandgap of the polythiophene donor polymer and the limited absorption width of the material blend. The most popular approach to obtain lower bandgap structures is based on copolymerization of (heteroaromatic) donor and acceptor moieties.[1] Incorporating alternating electron rich and electron deficient subunits produces a significant decrease in the bandgap (and a concomitant red-shifted absorption) due to intramolecular charge transfer (ICT).

During the last five years, 4*H*-cyclopenta[2,1-*b*:3,4-*b'*]dithiophene (CPDT) has emerged as an attractive building block for organic photovoltaics (OPV), combining good electron-donating properties, a rigid coplanar structure favoring π–π intermolecular interactions, and straightforward side-chain manipulation to influence solubility and processability. Although a standard workhorse material among the high efficiency low bandgap copolymers has not been defined yet, **PCPDTBT**, consisting of alternating CPDT and 2,1,3-benzothiadiazole (BT) units, is undoubtedly the most studied and best defined material within this subclass.[4–15] Bazan and co-workers achieved a break-through result – a noticeable PCE improvement from 2.8 to 5.5% – for this polymer, carrying branched 2-ethylhexyl side chains, in combination with $PC_{71}BM$ ([6,6]-phenyl-C_{71} butyric acid methyl ester) upon processing with 1,8-octanedithiol.[6] On the other hand, ultrahigh mobility (3.3 cm^2/Vs) has very recently been observed for a **PCPDTBT** copolymer bearing long linear alkyl side chains.[11] The crucial influence of the alkyl side chains and the polymer molecular weight, often underestimated in the past, on the opto-electronic properties have clearly been illustrated for this (and other) low bandgap material(s). The electron deficient thiazolo[5,4-*d*]thiazole (TzTz) entity has also been introduced as an interesting

candidate for integration in organic electronics due to its strong electron-withdrawing properties, high oxidative stability, planar and rigid structure and straightforward synthesis.[16–29] In the OPV field, TzTz building blocks have become increasingly popular, noticeably during the last year. A number of donor-acceptor copolymer structures incorporating TzTz moieties as the electron poor units have appeared in literature, showing rather high charge-carrier mobilities and PCEs.[19–29]

Combination of both attractive building blocks in a low bandgap copolymer is evidently a promising approach. Shim *et al.* already reported cyclopentadithiophene-*co*-thiazolothiazole copolymers (**PheCDT-Tz**) with a hole mobility of 1.1 x 10^{-4} cm^2/Vs and an average PCE of 2.23% when blended with $PC_{61}BM$.[19] Based on synthetic experience within the group on both monomeric precursors,[30,31] the design and synthesis of an alternative more performant '**PCPDT-TzTz**' derivative were pursued. Here, we report the synthesis and physicochemical properties of a novel narrow bandgap copolymer, poly([4-(2'-ethylhexyl)-4-octyl-4*H*-cyclopenta[2,1-*b*:3,4-*b'*]dithiophene-2,6-diyl]-*alt*-[2,5-di(3'-hexylthiophen-2'-yl)thiazolo[5,4-*d*]thiazole-5,'5"-diyl]) or **PCPDT-DTTzTz**, composed of asymmetrically dialkylated CPDT units and hexyl-substituted dithienyl-TzTz moieties in an alternating fashion. After blending the polymer with $PC_{71}BM$ as an electron acceptor in a 1:3 w/w ratio, BHJ OSCs were fabricated and the photovoltaic properties of the devices were investigated. The device characteristics are discussed in terms of the molecular structure, polymer purity, charge-carrier mobility, and film morphology of the blend.

7.2. Results and Discussion

7.2.1. Synthesis and Characterization

The cyclopentadithiophene building block was synthesized using a method recently developed in our group (Scheme 7.1).[30] This three-step synthetic protocol allows to synthesize asymmetrically disubstituted CPDT units. As the side chains are of crucial importance for the final opto-electronic features of the low bandgap material,[28,32–34] with a major impact on blend morphology, flexibility in the design of the side chains is of high value. In this procedure, variability is introduced at the stage of the ketone derivative. With the aim of balancing polymer crystallinity (toward high charge-carrier mobility) and solubility/processability (toward optimum blend morphology), a CPDT

building block with a linear octyl and a branched 2-ethylhexyl side chain was prepared. CPDT-bisboronate monomer **1** (Scheme 7.2), required for Suzuki polycondensation,[35] was synthesized by lithiation of the dibrominated CPDT precursor and reaction with 2-isopropoxy-4,4,5,5-tetramethylether-1,3,2-dioxaborolane.

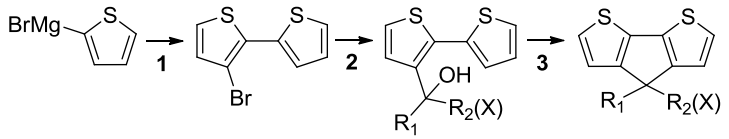

1. 2,3-dibromothiophene, $Pd(dppf)Cl_2$; **2.** *n*-BuLi, ketone; **3.** H_2SO_4

Scheme 7.1. Three-step synthetic approach to asymmetrically functionalized 4*H*-cyclopenta[2,1-*b*:3,4-*b'*]dithiophenes.

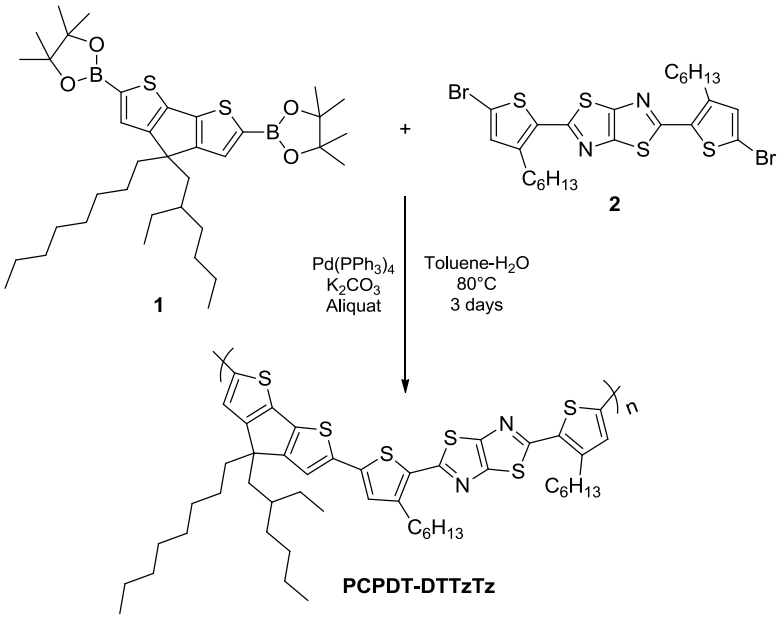

Scheme 7.2. Synthesis of the **PCPDT-DTTzTz** narrow bandgap polymer.

The complementary dibromo-TzTz monomer, 2,5-bis(3'-hexylthiophene-2'-yl)thiazolo[5,4-*d*]thiazole (**2**), was obtained through a condensation reaction between 3-hexylthiophene-2-carbaldehyde and dithiooxamide, and subsequent dibromination with *N*-bromosuccinimide (NBS).[31,36] The additional hexyl side chains on both thienyl constituents were introduced to improve solubility. The **PCPDT-DTTzTz** copolymer was then produced by means of a Suzuki polymerization reaction in toluene (Scheme

7.2).[7,35] End-capping was performed by sequential addition of phenylboronic acid and bromobenzene. The polymer was purified by successive Soxhlet extractions (with methanol, *n*-hexane and $CHCl_3$, respectively) and finally precipitated from methanol as a dark, almost black powder. The material was found soluble in a number of common organic solvents such as chloroform, chlorobenzene and tetrahydrofuran. The number-average molecular weight (M_n) after purification, as determined by analytical size exclusion chromatography (SEC) in tetrahydrofuran, was 1.7 x 10^4 g/mol, with a polydispersity (PDI) of 2.9. Reproducibility of the Suzuki polycondensation reaction was satisfactory, as similar molecular weights and PDI's were observed for two other polymerization trials.

Thermogravimetric analysis (TGA) experiments in inert atmosphere showed degradation sets in at 400 °C (Figure 7.7, Supporting Info). No weight loss was observed up to 350 °C. Differential scanning calorimetry (DSC) experiments from rt up to 300 °C at a heating rate of 20 K/min (after cooling from 300 °C at the same rate) showed a small step in heat capacity around 10 °C (0.05 J/g·K), followed by a broad exotherm (1 J/g) that gradually evolved to a broad endotherm with a peak maximum at 262 °C (11 J/g) (Figure 7.1, Table 7.1). These events can be attributed to a glass transition, cold crystallization and crystal reorganization, and melting of the crystals, respectively. Upon cooling at 20 K/min, a crystallization peak was seen with a maximum at 231 °C (10 J/g). Summarily, DSC experiments indicated the polymer is semi-crystalline, showing a small T_g and a broad melting endotherm. To confirm this semi-crystallinity, XRD analysis of the polymer powder was performed. The XRD spectrum (Figure 7.2) showed the presence of some crystalline phase, as demonstrated by the appearance of several broad peaks. For a series of four alternating CPDT-based copolymers different from the ones synthesized here, Shim *et al.*[19] found glass transition temperatures of 103–107 °C. No indications of the presence of a crystalline phase were mentioned in those cases.

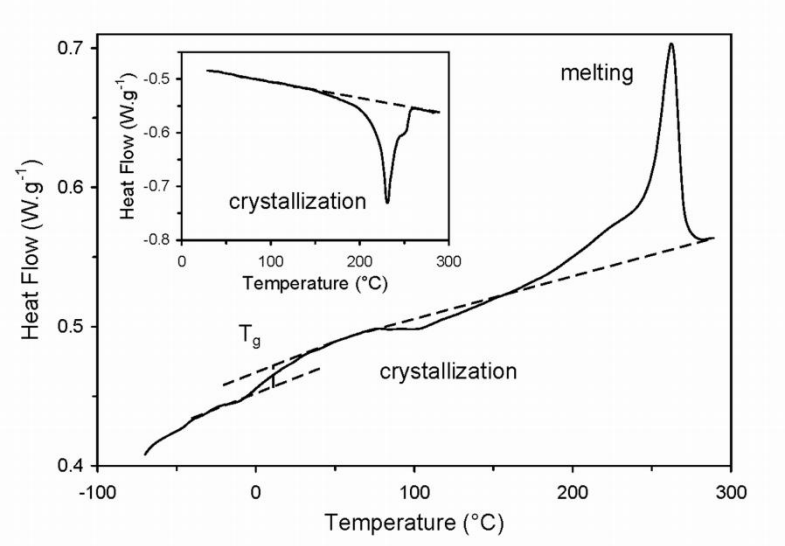

Figure 7.1. Thermal behavior of **PCPDT-DTTzTz** as measured by DSC at 20 K/min (after cooling at the same rate).

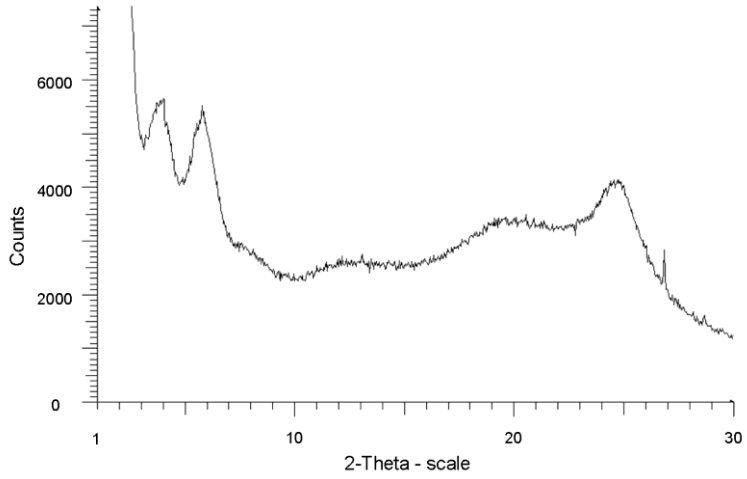

Figure 7.2. XRD pattern for the **PCPDT-DTTzTz** copolymer.

Table 7.1. Thermal, electrochemical and optical properties of **PCPDT-DTTzTz**.

T_g (°C)	T_m (°C)	T_c (°C)	T_d (°C)	HOMO (eV)	LUMO (eV)	E_g^{EC} (eV)	E_g^{OP} (eV)[a]
10	262	231	400	-5.31	-3.51	1.80	1.79

[a] In film.

UV-vis absorption spectra of the polymer in solution ($CHCl_3$) and film are plotted in Figure 7.3. Intramolecular charge transfer between the electron rich CPDT and the electron poor TzTz units in the polymer backbone induces a narrow bandgap and a reasonably broad absorption that covers the 450–700 nm range. In chloroform, the spectrum showed a maximum absorption at 580 nm (with a vibronic shoulder at the low-energy side). In film, the peak bandwidth was broader and a noticeable fine-structure appeared at the high-wavelength side, suggesting local structural order. The optical bandgap in film was determined to be around 1.79 eV (Table 7.1). Compared to the well-known bis(2-ethylhexyl)-substituted **PCPDTBT** donor polymer (E_g 1.46 eV),[6] the optical bandgap is significantly larger and the overlap with the solar spectrum is somewhat reduced, in particular at the near-IR side.

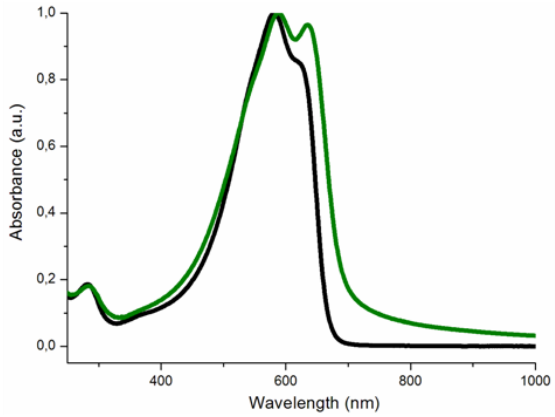

Figure 7.3. UV-vis absorption spectra of **PCPDT-DTTzTz** in chloroform solution (black) and in film (green).

The cyclic voltammogram of a thin film of **PCPDT-DTTzTz** displayed quasi-reversible oxidation and reduction processes during the first potential scan. Upon repeated scanning, the currents associated with these features reduced slowly. The onsets of oxidation and reduction occurred at 0.38 V and -1.42 V *vs.* $Ag/AgNO_3$, respectively. The corresponding energy levels for the highest occupied molecular orbital (HOMO) and the lowest unoccupied molecular orbital (LUMO) are -5.31 eV and -3.51 eV, respectively, very close to the values reported by Brabec *et al.* for **PCPDTBT** (-5.3 and -3.57 eV).[4] The resulting electrochemical bandgap is 1.80 eV. This value is almost identical to the observed optical bandgap (1.79 eV) (Table 7.1).

7.2.2. BHJ Organic Solar Cells

When the **PCPDT-DTTzTz** polymer, as obtained after Soxhlet extraction and precipitation (batch A), was blended with $PC_{71}BM$ in a 1:3 w/w ratio (in chlorobenzene), the resulting solar cell device (ITO:PEDOT/PSS:active layer:Ca-Ag) showed a moderate performance with an open circuit voltage (V_{oc}) of 0.58 V, a fill factor (FF) of 0.47, a short-circuit current density (J_{sc}) of 9.0 mA/cm^2, and a resulting PCE of 2.43% under air mass 1.5 global illumination conditions (AM 1.5G; 100 mW/cm^2) (Table 7.2, Figure 7.4).

Table 7.2. OSC Performances of **PCPDT-DTTzTz**.

Batch	M_n (g/mol)	PDI	V_{oc} (V)	J_{sc} (mA/cm^2)	FF	PCE (%)
A	1.7 x 10^4	2.9	0.58	9.0	0.47	2.43[a]
B	1.7 x 10^4	2.3	0.63	10.33	0.51	3.34[b]
C	1.5 x 10^4	2.2	0.63	10.37	0.54	3.50[b]
D	1.4 x 10^4	2.4	0.67	11.13	0.54	4.03[b,c]

[a] Unpurified polymer. [b] Purification by preparative SEC. [c] Mixture of B and C in 1:2 ratio.

As polymer molecular weight (distribution) and purity are essential parameters influencing the opto-electronic properties and the final solar cell outcome, purification and fractionation of the **PCPDT-DTTzTz** copolymer were pursued by preparative SEC. An additional advantage of this technique is that it can somehow remediate the significant batch-to-batch variations often observed for transition-metal catalyzed polymerization reactions (mainly Suzuki/Stille). Unfortunately, limited solubility of the material (at a concentration of 20 mg/2 mL) in the eluent ($CHCl_3$) somewhat hampered effective fractionation due to polymer aggregation (see Figure 7.8 and Figure 7.9, Supporting Info). Two purified polymer fractions (B and C, Table 7.2) were obtained, with slightly varying M_n and PDI. Solar cell devices constructed from these materials showed a significant increase in PCE of more than 1% (to 3.5% for batch C, Table 7.2), by noticeable improvement of all three parameters (V_{oc}, J_{sc} and FF). Upon mixing both purified batches (batch D = 1:2 ratio of B and C, Table 7.2), mainly affecting the PDI, the solar cell performance was even further improved, showing a PCE of 4.03% (V_{oc} 0.67 V, FF 0.54, J_{sc} 11.13 mA/cm^2) (Table 7.2, Figure 7.4). As the experimentally observed V_{oc} fits rather well with the theoretically expected value, the PCE seems to be

V_{oc} limited for this material.[4,6] The PCE was noticeably higher than for a series of four different **PCDT-X**:$PC_{61}BM$ combinations earlier reported by Shim and co-workers.[19]

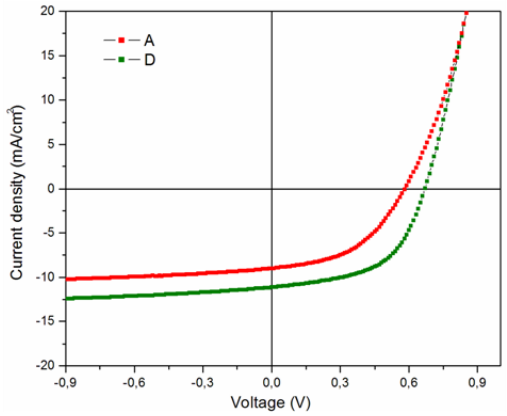

Figure 7.4. *J-V* characteristics of photovoltaic devices fabricated from different batches of **PCPDT-DTTzTz** (blended with $PC_{71}BM$ in a 1:3 w/w ratio).

The thin film morphology of the BHJ mixture was examined by atomic force microscopy (AFM) and transmission electron microscopy (TEM) (Figure 7.5). The purified **PCPDT-DTTzTz** polymer formed homogeneous, well-distributed blend films with $PC_{71}BM$, indicating good miscibility (or compatibility) with phase segregation on the nanometer scale.

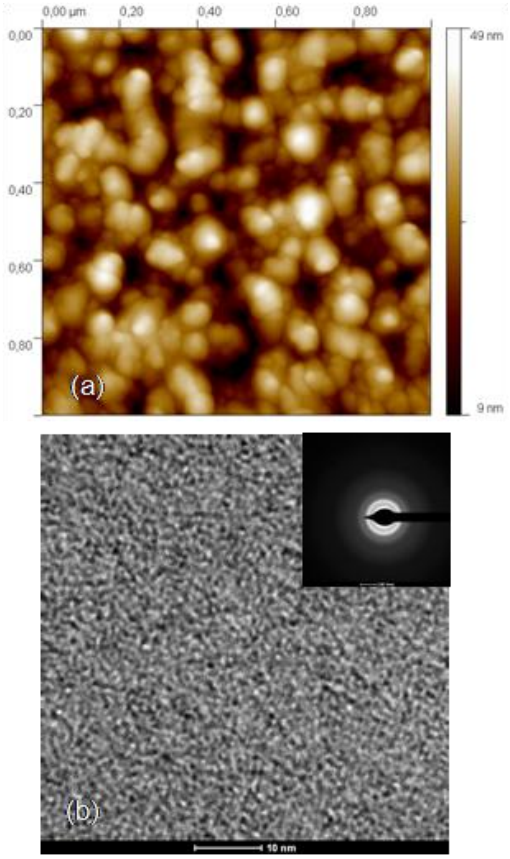

Figure 7.5. Topographic AFM images of spin-coated **PCPDT-DTTzTz**:$PC_{71}BM$ films (measurements on a solar cell device), with a rms roughness value of 7.3 nm (1 µm x 1 µm) (a) and BFTEM-image (with diffraction pattern in inset) of the **PCPDT-DTTzTz**:$PC_{71}BM$ (1:3) film (b).

7.2.3. Thin-Film Transistors (TFTs)

To relate the relatively high short-circuit current density to polymer mobility, thin-film transistors were prepared from the purified polymer batch (D). The **PCPDT-DTTzTz** copolymer exhibited typical *p*-channel TFT characteristics. Output and transfer curves are displayed in Figure 7.6. The field-effect mobility, calculated in the linear regime, was found to be 1.0 x 10^{-3} cm^2/Vs, one order of magnitude higher than reported values in literature for different TzTz-based copolymers,[19] and hence in good agreement with the photovoltaic properties. In addition, the transfer curves of the **PCPDT-DTTzTz** material exhibited a small threshold voltage (V_{th}) around -14 V. The small hysteresis suggests a high degree of purity.

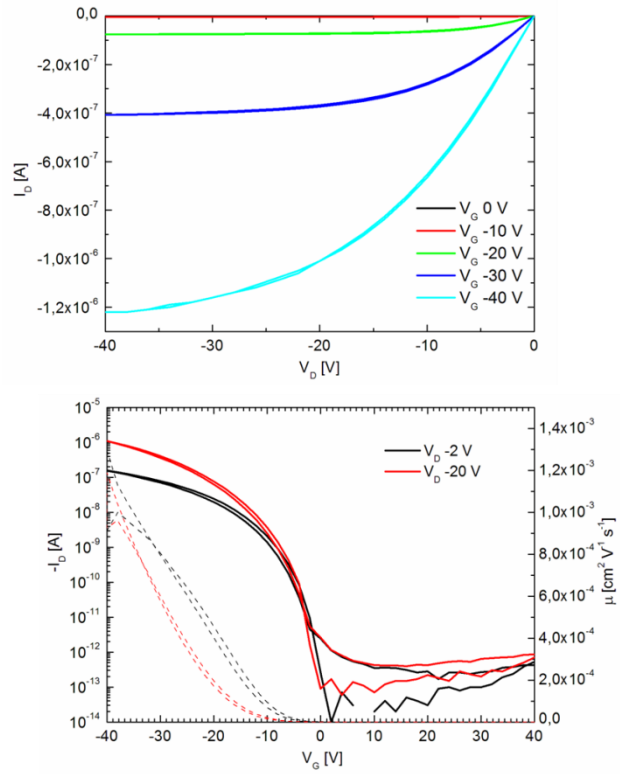

Figure 7.6. (a) Output curves for various gate biases. The gate bias was changed in 10 V steps from 0 V to -40 V. (b) Linear and saturated transfer characteristics of a **PCPDT-DTTzTz** transistor. The channel length and width were 10 and 2500 µm, respectively. The extracted mobilities were around 1.0 x 10^{-3} cm^2/Vs.

7.3. Conclusions

We have synthesized a novel performant poly[(4*H*-cyclopenta[2,1-*b*:3,4-*b'*]dithiophene)-*alt*-(2,5-dithienylthiazolo-[5,4-*d*]thiazole)] narrow bandgap copolymer **PCPDT-DTTzTz**, with asymmetrical alkyl substitution on the CPDT building blocks and additional hexyl side chains on the thienyl subunits of the TzTz constituents. Addition of these extra substituents improved the solubility on one hand, and on the other hand triggered the stacking tendency of the polymer resulting in a semi-crystalline material. After purification by preparative SEC, the polymer showed a hole mobility of 1.0 x 10^{-3} cm^2/Vs and organic solar cells constructed with a **PCPDT-DTTzTz**:$PC_{71}BM$ active layer afforded a photovoltaic power conversion efficiency of 4.03% (without extensive optimization work). A noticeable increase in efficiency of more than 1% was obtained upon purification. The presented results clearly stress the

crucial effects of the (alkyl) functionalization pattern and material purity on the photovoltaic performance of low bandgap polymer materials.

7.4. Experimental Section

Materials and Methods

NMR chemical shifts (δ, in ppm) were determined relative to the residual $CHCl_3$ absorption (7.26 ppm) or the ^{13}C resonance shift of $CDCl_3$ (77.16 ppm). Gas chromatography-mass spectrometry (GC-MS) analyses were carried out applying Chrompack Cpsil5CB or Cpsil8CB capillary columns. Molecular weights and molecular weight distributions were determined relative to polystyrene standards (Polymer Labs) by analytical size exclusion chromatography (SEC). Chromatograms were recorded on a Spectra Series P100 (Spectra Physics) equiped with two mixed-B columns (10 µm, 0.75 cm x 30 cm, Polymer Labs) and a refractive index detector (Shodex) at 40 °C. THF was used as the eluent at a flow rate of 1.0 mL/min. Preparative SEC was performed on JAIGEL *2H* and *2.5H* columns attached to a LC system equipped with a UV detector (path 0.5 mm) and a switch for recycling and collecting the eluent ($CHCl_3$: flow rate 3.5 mL/min and injection volume 1.0 mL).
Solution UV-vis absorption measurements were performed with a scan rate of 600 nm/min in a continuous run from 200 to 800 nm. Thin film electrochemical measurements were performed with an Eco Chemie Autolab PGSTAT 30 Potentiostat/Galvanostat using a conventional three-electrode cell under N_2 atmosphere (electrolyte: 0.1 M $TBAPF_6$ in anhydrous CH_3CN). For the measurements, a $Ag/AgNO_3$ reference electrode (0.01 M $AgNO_3$ and 0.1 M $TBAPF_6$ in anhydrous CH_3CN), a platinum counter electrode and an ITO coated glass substrate as working electrode were used. The polymers were deposited by drop-casting directly onto the ITO substrates. Cyclic voltammograms were recorded at 50 mV/s. From the onset potentials of the oxidation and reduction the position of the energy levels could be estimated. All potentials were referenced using a known standard, ferrocene/ferrocenium, which in CH_3CN solution is estimated to have an oxidation potential of -4.98 eV *vs.* vacuum. DSC measurements were performed at 20 K/min in aluminum crucibles on a TA Instruments Q2000 Tzero DSC equiped with a refrigerated cooling system (RCS), using nitrogen (50 mL/min) as purge gas. TGA

experiments were performed at 50 K/min in platinum crucibles on a TA Instruments Q5000 TGA using nitrogen (50 mL/min) as purge gas. The XRD measurements were performed with a Bruker D8 discover diffractometer under *θ-2θ* conditions. The system worked in parafocussing geometry using a Göbel mirror (line focus, mostly CuKα1 and CuKα2 rays). The X-rays were detected by a 1D detector.

Polymer solar cells were fabricated by spin-coating a **PCPDT-DTTzTz**:$PC_{71}BM$ (Solenne) blend in a 1:3 w/w ratio, sandwiched between a transparent anode and an evaporated metal cathode. The transparent anode was an indium tin oxide (ITO) covered glass substrate which was coated with a 30 nm poly(3,4-ethylenedioxy-thiophene)/poly(styrenesulfonic acid) PEDOT/PSS (CLEVIOS P VP.AI 4083) layer applied by spin-coating. The ITO glass substrate was cleaned by ultrasonification (sequentially) in soap solution, deionized water, acetone and isopropanol. The cathode, a bilayer of 50 nm Ca and 100 nm Ag, was thermally evaporated. **PCPDT-DTTzTz** and $PC_{71}BM$ (1:3 w/w ratio) were dissolved together in chlorobenzene to give an overall 40 mg/mL solution, which was stirred overnight at 80 °C inside a glovebox. Solar cell efficiencies were characterized under simulated 100 mW/cm^2 AM 1.5 G irradiation from a Xe arc lamp with an AM 1.5 global filter. Topography of the solar cells was studied by AFM, using a Picoscan PicoSPM LE scanning probe in tapping mode. The active layer morphology was studied with TEM (FEI Tecnai Spirit using an accelerating voltage of 120 kV).

Transistors were fabricated using heavily doped *n*-type Si wafers as bottom gate electrodes with a 200 nm thermally oxidized SiO_2 layer as the bottom gate dielectric. Au source and drain electrodes were defined by photolithography on a 2 nm Ti adhesion layer. The SiO_2 layer was passivated with hexamethyldisilazane prior to semiconductor deposition. The semiconducting active layer (30 nm) was spin-coated from a 0.5 wt% polymer solution in chlorobenzene. Before measurements, the substrates were annealed in vacuum at 100 °C. The measured transistors had a channel width (W) of 2500 µm and a channel length (L) of 10 µm. Electrical characterization was carried out in vacuum with an Agilent 4155C semiconductor parameter analyzer. Transistor performance was mainly evaluated by the thin film mobility (μ_h) extracted in the linear regime and by the threshold voltage (V_{th}).

Synthesis

Unless stated otherwise, all reagents and chemicals were obtained from commercial sources and used without further purification. 2-Isopropoxy-4,4,5,5-tetramethyl-1,3,2-dioxaborolane was purchased from Acros Organics. THF was dried by distillation from Na/benzophenone. 4-(2'-Ethylhexyl)-4-octyl-4*H*-cyclopenta[2,1-*b*:3,4-*b*']dithiophene and 2,5-bis(5'-bromo-3'-hexylthiophene-2'-yl)thiazolo[5,4-*d*]thiazole (**2**) were synthesized according to previously reported procedures.[30,31] Material identity and purity were confirmed by MS, ^{1}H and ^{13}C NMR.

2,6-Dibromo-4-(2'-ethylhexyl)-4-octyl-4*H*-cyclopenta[2,1-*b*:3,4-*b'*]dithiophene. Protected from light, a solution of NBS (0.94 g, 5.3 mmol) in DMF (50 mL) was added dropwise to a solution of 4-(2'-ethylhexyl)-4-octyl-4*H*-cyclopenta[2,1-*b*:3,4-*b'*]dithiophene (1.00 g, 2.5 mmol) in DMF (65 mL), after which the mixture was stirred overnight at rt. Subsequently, the mixture was poured onto ice and extracted with diethyl ether (3 x 100 mL). The combined organic layers were washed with $NaHCO_3$ (sat) and brine, dried over $MgSO_4$ and concentrated by evaporation *in vacuo*. The crude solid was purified by column chromatography (silica, eluent *n*-hexane). The compound was obtained as a slightly yellow oil (0.91 g, 65%). ^{1}H NMR (300 MHz, $CDCl_3$) δ 6.94 (s, 1H), 6.93 (s, 1H), 1.83 (t, *J* = 4.8 Hz, 2H), 1.78–1.72 (m, 2H), 1.27–0.89 (m, 21H), 0.86 (t, *J* = 7.1 Hz, 3H), 0.79 (t, *J* = 6.9 Hz, 3H), 0.64 (t, *J* = 7.4 Hz, 3H); ^{13}C NMR (75 MHz, $CDCl_3$) δ 155.9/155.8, 136.6/136.5, 125.0/124.9, 111.05/111.0, 55.1, 41.6, 39.4, 35.5, 34.1, 31.9, 30.0, 29.43, 29.40, 28.6, 27.4, 24.4, 22.9, 22.8, 14.3, 14.2, 10.8; GC-MS (EI) *m/z* 558/562 [M^+].

2,2'-[4-(2'-Ethylhexyl)-4-octyl-4*H*-cyclopenta[2,1-*b*:3,4-*b'*]dithiophene-2,6-diyl]-bis(4,4,5,5-tetramethyl-1,3,2-dioxaborolane) (1). A *n*-BuLi solution (1.1 mL, 2.5 M in hexanes) was added at -78 °C to a solution of the dibromo-CPDT precursor (260 mg, 0.46 mmol) in dry THF (20 mL) under inert atmosphere. The mixture was stirred for 30 min at -78 °C, after which 2-isopropoxy-4,4,5,5-tetramethyl-1,3,2-dioxaborolane (0.5 mL, 0.46 g, 2.4 mmol) was added at -78 °C. The reaction was allowed to reach rt overnight. The reaction mixture was then poured out in water and diisopropyl ether, and the organic layer was washed with brine. The solvents were evaporated from the organic layer and the resulting oil was subjected to preparative SEC in $CHCl_3$. This resulted in the isolation of the diboronic ester **1** (0.201 g, 67%) as a slightly yellow

sticky oil. ^{1}H NMR (400 MHz, $CDCl_3$) δ 7.43 (s, 1H), 7.41 (s, 1H), 1.86 (t, *J* = 5.0 Hz, 2H), 1.80–1.76 (m, 2H), 1.35/1.34 (s, 21H), 1.25–0.90 (m, 21H), 0.84 (t, *J* = 7.0 Hz, 3H), 0.73 (t, *J* = 7.0 Hz, 3H), 0.59 (t, *J* = 7.4 Hz, 3H); ^{13}C NMR (75 MHz, $CDCl_3$) δ 161.4/161.2, 144.1/144.0, 131.6/131.5, 130.0, 84.1, 52.8, 41.8, 39.6, 35.4, 33.8, 31.9, 30.1, 29.4, 28.4, 27.5, 24.9, 24.83, 24.75, 24.4, 22.9, 22.7, 14.2, 10.7; MS (CI) *m/z* 655 [MH^+].

Poly([4-(2'-ethylhexyl)-4-octyl-4*H*-cyclopenta[2,1-*b*:3,4-*b'*]dithiophene-2,6-diyl]-*alt*-[2,5-di(3'-hexylthiophen-2'-yl)thiazolo[5,4-*d*]thiazole-5',5''-diyl]) (**PCPDT-DTTzTz**). CPDT monomer **1** (0.049 g, 78 µmol), TzTz monomer **2** (0.051 g, 78 µmol), K_2CO_3 (0.76 mL, 2 M) and 1 drop of Aliquat 336 were gathered in a mixture of toluene (1.5 mL) and water (0.35 mL). The solution was purged with argon for 30 min, and then $Pd(PPh_3)_4$ (0.009 g, 8 µmol, 10 mol%) was added. The reaction was stirred at 80 °C under an inert atmosphere for 3 days. Subsequently, a toluene solution of phenylboronic acid (0.010 g, 85 µmol) was added, followed by the addition of bromobenzene (0.009 mL, 85 µmol), and the mixture was stirred overnight at 80 °C. The resulting mixture was then poured into a mixture of methanol and water (2:1, 200 mL) and stirred overnight. The precipitated dark solid was recovered by filtration, redissolved in $CHCl_3$ (20 mL) and added dropwise to methanol (200 mL). The precipitated solid was filtered off (PTFE membrane 47 mm/0.45 µm) and subjected to successive Soxhlet extractions for 24 h with methanol, *n*-hexane and $CHCl_3$, respectively. After evaporation, the polymer residue was redissolved in $CHCl_3$ and precipitated again from methanol, filtered, washed with methanol and dried, affording **PCPDT-DTTzTz** as a black powder (0.045 g, 64%); ^{1}H NMR (400 MHz, $CDCl_3$) δ 7.16 (br, 2H), 6.79 (br, 2H), 2.95 (br, 2H), 2.80 (br, 2H), 1.43–1.25 (m, 44H), 1.00–0.85 (m, 18H); UV-vis ($CHCl_3$, nm) λ_{max} 580; UV-vis (film, nm) λ_{max} 588/635; SEC (THF, PS standards) M_n = 1.7 x 10^4 g/mol, M_w = 5.0 x 10^4 g/mol, PDI = 2.9.

7.5. Acknowledgments

The authors gratefully acknowledge the IWT (Institute for the Promotion of Innovation by Science and Technology in Flanders) for their financial support via the SBO-project 060843 ”PolySpec”. We also acknowledge the European ONE-P project for grant agreement n° 212311 which facilitates the IMEC-IMOMEC/High Tech Campus Eindhoven collaboration. NVdB and WM thank the FWO (Fund for Scientific Research – Flanders) for a doctoral and postdoctoral research mandate, respectively. Special thanks go out to Huguette Penxten for performing the cyclic voltammetry measurements.

7.6. References

(1) (a) Bundgaard, E.; Krebs, F. C. *Sol. Energy Mater. Sol. Cells* **2007**, *91*, 954. (b) Thompson, B. C.; Fréchet, J. M. J. *Angew. Chem. Int. Ed.* **2008**, *47*, 58. (c) Chen, L.-M.; Hong, Z.; Li, G.; Yang, Y. *Adv. Mater.* **2009**, *21*, 1434. (d) Brabec, C. J.; Gowrisanker, S.; Halls, J. J. M.; Laird, D.; Jia, S.; Williams, S. P. *Adv. Mater.* **2010**, *22*, 3839. (e) Heeger, A. J. *Chem. Soc. Rev.* **2010**, *39*, 2354. (f) Boudreault, P. T.; Najari, A.; Leclerc, M. *Chem. Mater.* **2011**, *23*, 456. (g) Facchetti, A. *Chem. Mater.* **2011**, *23*, 733. (h) Thompson, B. C.; Khlyabich, P. P.; Burkhart, B.; Aviles, A. E.; Rudenko, A.; Shultz, G. V.; Ng, C. F.; Mangubat, L. B. *Green* **2011**, *1*, 29.

(2) (a) Ma, W.; Yang, C.; Gong, X.; Lee, K.; Heeger, A. J. *Adv. Funct. Mater*. **2005**, *15*, 1617. (b) Li, G.; Shrotriya, V.; Huang, J.; Yao, Y.; Moriarty, T.; Emery, K.; Yang, Y. *Nat. Mater.* **2005**, *4*, 864.

(3) Dang, M. T.; Hirsch, L.; Wantz, G. *Adv. Mater.* **2011**, *23*, 3597.

(4) Mühlbacher, D.; Scharber, M.; Morana, M.; Zhu, Z.; Waller, D.; Gaudiana, R.; Brabec, C. *Adv. Mater.* **2006**, *18*, 2884.

(5) Soci, C.; Hwang, I.-W.; Moses, D.; Zhu, Z.; Waller, D.; Gaudiana, R.; Brabec, C.; Heeger, A. J. *Adv. Funct. Mater.* **2007**, *17*, 632.

(6) Peet, J.; Kim, J. Y.; Coates, N. E.; Ma, W. L.; Moses, D.; Heeger, A. J.; Bazan, G. C. *Nat. Mater.* **2007**, *6*, 497.

(7) Zhang, M.; Tsao, H. N.; Pisula, W.; Yang, C.; Mishra, A. K.; Müllen, K. *J. Am. Chem. Soc.* **2007**, *129*, 3472.

(8) Zhu, Z.; Waller, D.; Gaudiana, R.; Morana, M.; Mühlbacher, D.; Scharber, M.; Brabec, C. *Macromolecules* **2007**, *40*, 1981.

(9) Bijleveld, J. C.; Shahid, M.; Gilot, J.; Wienk, M. M.; Janssen, R. A. J. *Adv. Funct. Mater.* **2009**, *19*, 3262.

(10) Coffin, R. C.; Peet, J.; Rogers, J.; Bazan, G. C. *Nat. Chem.* **2009**, *1*, 657.

(11) Tsao, H. N.; Cho, D. M.; Park, I.; Hansen, M. R.; Mavrinskiy, A.; Yoon, D. Y.; Graf, R.; Pisula, W.; Spies, H. W.; Müllen, K. *J. Am. Chem. Soc.* **2011**, *133*, 2605.

(12) Kettle, J.; Horie, M.; Majewski, L. A.; Saunders, B. R.; Tuladhar, S.; Nelson, J.; Turner, M. L. *Sol. Energy Mater. Sol. Cells* **2011**, *95*, 2186.

(13) Lee, U. R.; Lee, T. W.; Hoang, M. H.; Kang, N. S.; Yu, J. W.; Kim, K. H.; Lim, K.-G.; Lee, T.-W.; Jin, J.-I.; Choi, D. H. *Org. Electron.* **2011**, *12*, 269.

(14) Manceau, M.; Bundgaard, E.; Carlé, J. E.; Hagemann, O.; Helgesen, M.; Søndergaard, R.; Jørgensen, M.; Krebs, F. C. *J. Mater. Chem.* **2011**, *21*, 4132.

(15) Dithienosilole and dithienogermole donor moieties, combined with BT or TPD (*N*-alkyl-thienopyrrolodione) acceptor units, have recently afforded even higher PCEs than their carbon analogues. See e.g. Amb, C. M.; Chen, S.; Graham, K. R.; Subbiah, J.; Small, C. E.; So, F.; Reynolds, J. R. *J. Am. Chem. Soc.* **2011**, *133*, 10062.

(16) (a) Ando, S.; Nishida, J.-i.; Inoue, Y.; Tokito, S.; Yamashita, Y. *J. Mater. Chem.* **2004**, *14*, 1787. (b) Ando, S.; Nishida, J.-i.; Tada, H.; Inoue, Y.; Tokito, S.; Yamashita, Y. *J. Am. Chem. Soc.* **2005**, *127*, 5336. (c) Mamada, M.; Nishida, J.-i.; Kumaki, D.; Tokito, S.; Yamashita, Y. *Chem. Mater.* **2007**, *19*, 5404. (d) Fujisaki, Y.; Mamada, M.; Kumaki, D.; Tokito, S.; Yamashita, Y. *Jpn. J. Appl. Phys.* **2009**, *48*, 111504.

(17) Naraso; Wudl, F. *Macromolecules* **2008**, *41*, 3169.

(18) (a) Osaka, I.; Sauvé, G.; Zhang, R.; Kowalewski, T.; McCullough, R. D. *Adv. Mater.* **2007**, *19*, 4160. (b) Osaka, I.; Zhang, R.; Sauvé, G.; Smilgies, D.-M.; Kowalewski, T.; McCullough, R. D. *J. Am. Chem. Soc.* **2009**, *131*, 2521. (c) Osaka, I.; Zhang, R.; Liu, J.; Smilgies, D.-M.; Kowalewski, T.; McCullough, R. D. *Chem. Mater.* **2010**, *22*, 4191.

(19) Jung, I. H.; Yu, J.; Jeong, E.; Kim, J.; Kwon, S.; Kong, H.; Lee, K.; Woo, H. Y.; Shim, H.-K. *Chem. Eur. J.* **2010**, *16*, 3743.

(20) Lee, T. W.; Kang, N. S.; Yu, J. W.; Hoang, M. H.; Kim, K. H.; Jin, J.-L.; Choi, D. H. *J. Polym. Sci., Part A: Polym. Chem.* **2010**, *48*, 5921.

(21) Lee, S. K.; Kang, I.-N.; Lee, J.-C.; Shin, W. S.; So, W.-W.; Moon, S.-J. *J. Polym. Sci., Part A: Polym. Chem.* **2011**, *49*, 3129.

(22) Lee, S. K.; Cho, J. M.; Goo, Y.; Shin, W. S.; Lee, J.-C.; Lee, W.-H.; Kang, I.-N.; Shim, H.-K.; Moon, S.-J. *Chem. Commun.* **2011**, 1791.

(23) (a) Subramaniyan, S.; Xin, H.; Sunjoo Kim, F.; Shoaee, S.; Durrant, J. R.; Jenekhe, S. A. *Adv. Energy Mater.* **2011**, *1*, 854. (b) Subramaniyan, S.; Xin, H.; Sunjoo Kim, F.; Jenekhe, S. A. *Macromolecules* **2011**, *44*, 6245.

(24) Huo, L.; Guo, X.; Zhang, S.; Li, Y.; Hou, J. *Macromolecules* **2011**, *44*, 4035.

(25) Peet, J.; Wen, L.; Byrne, P.; Rodman, S.; Forberich, K.; Shao, Y.; Drolet, N.; Gaudiana, R.; Dennler, G.; Waller, D. *Appl. Phys. Lett.* **2011**, *98*, 043301.

(26) (a) Zhang, M.; Sun, Y.; Guo, X.; Cui, C.; He, Y.; Li, Y. *Macromolecules* **2011**, *44*, 7625. (b) Zhang, M.; Guo, X.; Wang, X.; Wang, H.; Li, Y. *Chem. Mater.* **2011**, *23*, 4264. (c) Zhang, Z.-G.; Min, J.; Zhang, S.; Zhang, J.; Zhang, M.; Li, Y. *Chem. Commun.* **2011**, 9474.

(27) Hwang, Y.-M.; Ohshita, J.; Harima, Y.; Mizumo, T.; Ooyama, Y.; Morihara, Y.; Izawa, T.; Sugioka, T.; Fujita, A. *Polymer* **2011**, *52*, 3912.

(28) Helgesen, M.; Madsen, M. V.; Andreasen, B.; Tromholt, T.; Andreasen, J. W.; Krebs, F. C. *Polym. Chem.* **2011**, *2*, 2536.

(29) Jeong, E.; Kim, G.-h.; Jung, I. H.; Jeong, P.; Kim, J. Y.; Woo, H. Y. *Curr. Appl. Phys.* **2012**, *12*, 11.

(30) Van Mierloo S.; Adriaensens, P.; Maes, W.; Lutsen, L.; Cleij, T. J.; Botek, E.; Champagne, B.; Vanderzande, D. J. *J. Org. Chem.* **2010**, *75*, 7202.

(31) Van Mierloo, S.; Chambon, S.; Boyukbayram, A. E.; Adriaensens, P.; Lutsen, L.; Cleij, T. J.; Vanderzande, D. *Magn. Reson. Chem.* **2010**, *48*, 362.

(32) Yue, W.; Zhao, Y.; Shao, S.; Tian, H.; Xie, Z.; Geng, Y.; Wang, F. *J. Mater. Chem.* **2009**, *19*, 2199.

(33) Yang, L.; Zhou, H.; You, W. *J. Phys. Chem. C* **2010**, *114*, 16793.

(34) Bronstein, H.; Leem, D. S.; Hamilton, R.; Woebkenberg, P.; King, S.; Zhang, W.; Ashraf, R. S.; Heeney, M.; Anthopoulos, T. D.; de Mello, J.; McCulloch, I. *Macromolecules* **2011**, *44*, 6649.

(35) Murage, J.; Eddy, J. W.; Zimbalist, J. R.; McIntyre, T. B.; Wagner, Z. R.; Goodson, F. E. *Macromolecules* **2008**, *41*, 7330.

(36) (a) Johnson, J. R.; Ketcham R. *J. Am. Chem. Soc.* **1960**, *82*, 2719. (b) Johnson, J. R.; Rotenberg, D. H.; Ketcham, R. *J. Am. Chem. Soc.* **1970**, *92*, 4046.

7.7. Supporting Information

Cyclic voltammograms, and ^{1}H and ^{13}C NMR spectra of the **CPDT** and **TzTz** precursors are available via the Internet at http://pubs.acs.org.

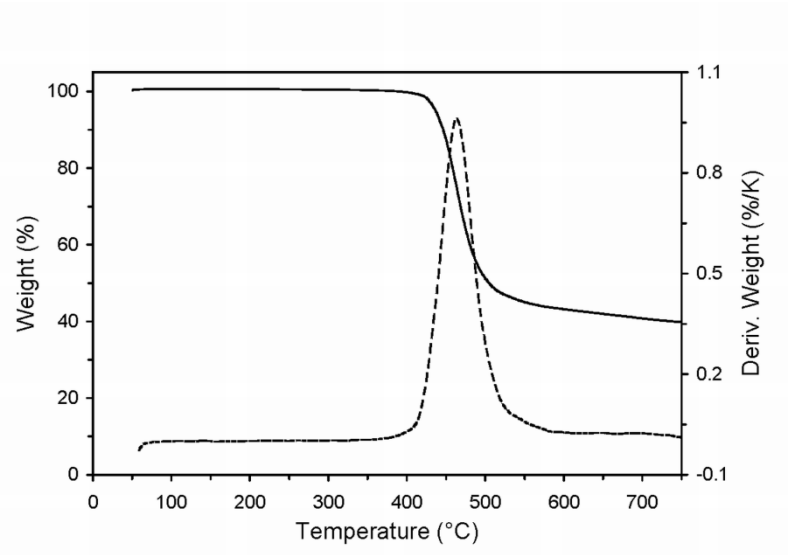

Figure 7.7. TGA curve of the **PCPDT-DTTzTz** copolymer.

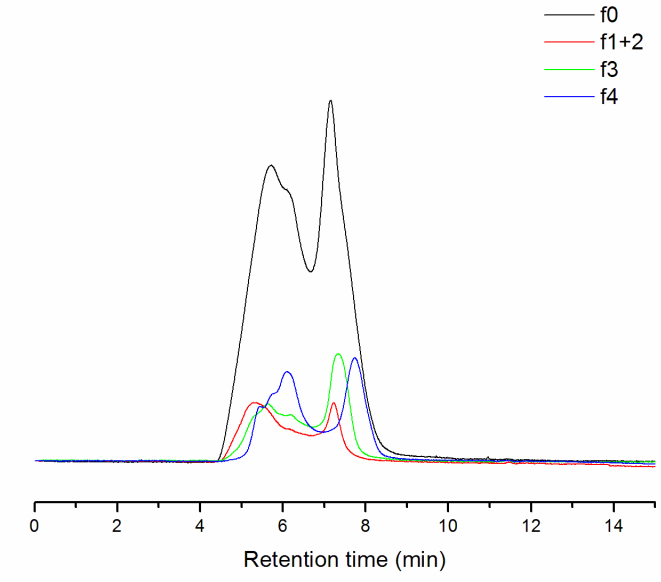

Figure 7.8. Size exclusion chromatograms ($CHCl_3$) of the rough **PCPDT-DTTzTz** copolymer (f0) and fractionated samples (f1–4).

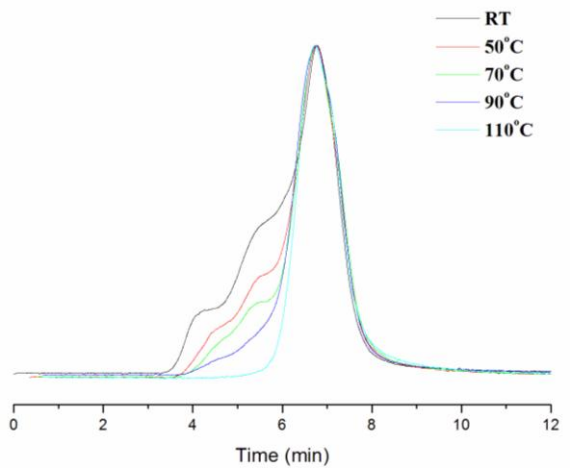

Figure 7.9. HT-size exclusion (chlorobenzene) chromatograms of the **PCPDT-DTTzTz** copolymer at different temperatures, indicating polymer aggregation.

Summary

Over the last decade, organic solar cells – being light-weight, flexible, semi-transparent, printable and rather inexpensive – have evolved in a spectacular way. Several organic compound classes have been explored as active materials for these devices. Low bandgap copolymers composed of alternating donor and acceptor components are currently state-of-the-art, affording power conversion efficiencies of over 7.5% when blended with [6,6]-phenyl-C_{71} butyric acid methyl ester ($PC_{71}BM$) in bulk heterojunction organic solar cells. Although the 10% efficiency boundary is likely to be crossed within a short time, the stability and lifetime of the active layer blend morphology remain critical concerns to allow successful commercialization. The development of novel materials to overcome these stability issues is therefore still required.

This PhD thesis comprises the research work conducted during the last 4 years, mainly focusing on the synthetic chemistry of two material classes, *i.e.* 4*H*-cyclopenta[2,1-*b*:3,4-*b'*]dithiophenes (CPDT's) and thiazolo[5,4-*d*]thiazoles (TzTz's), and their applications in printable electronics.

CPDT has emerged as a potential candidate for integration in low bandgap copolymers due to its fully coplanar, conjugated, electronrich structure and the straightforward introduction of alkyl side chains to improve solubility. A literature study on the synthetic procedures for CPDT's revealed that usually rather laborious multistep tools are applied, affording mostly symmetrically dialkylated compounds. Therefore, we decided to develop a convenient, versatile and efficient three-step pathway suitable for the synthesis of both symmetrically and asymmetrically functionalized CPDT's (**Chapter 2**): i) synthesis of 3-bromo-2,2'-bithiophene through a Kumada coupling, ii) regiospecific formation of the lithio derivative, which was then *in situ* reacted with various dialkyl ketones, affording (a)symmetrically dialkylated tertiary alcohol derivatives, iii) bridging of the two thiophene units by means of a Friedel-Crafts dehydration cyclization in sulfuric acid medium. For the final ring-closing step, a reaction mechanism was proposed, which was supported by NMR spectroscopy and theoretical energy calculations. The choice of the ketone precursor determines the nature of the pendant groups on the methylene bridge of the bithiophene moiety. Upon replacement of the dialkyl ketone by a keto ester, an ester-functionalized CPDT could

be prepared, which represents an attractive precursor material for variously functionalized CPDT compounds.

On a second stage, four of these differently substituted (electron rich) CPDT derivatives were combined with (electron poor) 2,1,3-benzothiadiazole through Suzuki polymerization reactions, affording PCPDTBT-type alternating copolymers (**Chapter 3**). The series consisted of two symmetrical variants, endowed with either two branched 2-ethylhexyl or two linear octyl side chains, one asymmetrical polymer with an octyl and a 2-ethylhexyl side chain, and an asymmetrically ester-functionalized PCPDTBT polymer. Optical and electrochemical features of all polymers were studied, illustrating their intrinsic low bandgap character. Preliminary solar cell measurements afforded 2.71% efficiency (for PCPDTBT:$PC_{71}BM$ active layers), but further performance enhancements should certainly be possible by tedious optimization (taking the effect of the side chains on solubility/processability into account). The ester-functionalized PCPDTBT polymer is applicable as a key intermediate toward a wider collection of functionalized low bandgap materials via straightforward post-polymerization reactions.

The second part of this thesis was focused on thiazolo[5,4-*d*]thiazole-based materials, which also show a few appealing features (high stability, rigidity, planarity and easy accessibility) toward integration in organic electronics. A number of novel hexyl-substituted dithiophene compounds containing a thiazolo[5,4-*d*]thiazole central unit were synthesized. In contrast to most of their literature analogues, these molecules were found to be soluble in common organic solvents, which enables their integration in solution-based printable electronics (avoiding the necessity of expensive vacuum deposition techniques). The dithienyl-TzTz (DTTzTz) core was synthesized *via* a classical condensation reaction between 3-hexylthiophene-2-carbaldehyde and dithiooxamide. After bromination of the DTTzTz core, Stille and Suzuki cross-coupling reactions afforded a series of 5'-aryl-substituted DTTzTz derivatives. Complete elucidation of the chemical structures by detailed 1D/2D NMR spectroscopy was performed (**Chapter 4/6**) and was supported by theoretical chemical shift calculations. Electropolymerization of some of these derivatives illustrated the potential low bandgap character of polymer materials derived from these compounds.

In order to probe the suitability of the novel DTTzTz derivatives for printable electronics, they were investigated as active materials for solution-processable organic

field-effect transistors (OFET's) (**Chapter 5**). Thermal, electrochemical and optical material properties of all derivatives were studied by thermogravimetric analysis, differential scanning calorimetry, cyclic voltammetry and UV-vis spectroscopy. After integration in OFET's, hole mobilities up to 10^{-3} cm^2 V^{-1} s^{-1} were obtained for the thienyl-substituted DTTzTz, while very moderate values of 10^{-5}–10^{-6} cm^2 V^{-1} s^{-1} were achieved for the other materials. Additional X-ray diffraction, atomic force microscopy (AFM) and scanning electron microscopy (SEM) studies revealed a fibrillar microcrystalline morphology for the best-performing thienyl-substituted DTTzTz material (when deposited from solution), whereas nanocrystalline domains were observed for the other derivatives.

In the final part of the thesis, the two material classes previously discussed were combined in low bandgap copolymer materials (**Chapter 7**). A solution-processable narrow bandgap polymer, PCPDT-DTTzTz, composed of alternating DTTzTz acceptor units and asymmetrically alkyl-substituted CPDT donor building blocks, was synthesized through a Suzuki polycondensation protocol. Optical and electrochemical features were studied by UV-vis spectroscopy and cyclic voltammetry. Thermal analysis and X-ray diffraction studies disclosed the semi-crystalline nature of the material. Upon purification by preparative size exclusion chromatography, a reasonable solar cell efficiency of 4.03% (for a PCPDT-DTTzTz:$PC_{71}BM$ blend) could be obtained. Thin-film transistors of the purified polymer displayed a relatively high field-effect carrier mobility of 1.0 x 10^{-3} cm^2 V^{-1} s^{-1}. The active layer morphology was explored by AFM and transmission electron microscopy (TEM) studies, showing phase segregation on the nanometer scale.

Samenvatting

In het afgelopen decennium is er een enorme vooruitgang geboekt binnen het domein van de organische zonnecellen. Dergelijke zonnecellen zijn niet alleen zeer licht, flexibel en semi-transparant, maar ze kunnen ook vrij goedkoop vervaardigd worden op grote oppervlakken, zodat ze een toegevoegde waarde bieden binnen het palet aan fotovoltaïsche systemen. Verschillende klassen van organische halfgeleidende verbindingen werden reeds bestudeerd als actieve componenten van deze zonnecellen. *Low bandgap* copolymeren, opgebouwd uit alternerende donor- en acceptorbouwstenen, behoren momenteel tot de meest performante materialen. Wanneer dergelijke copolymeren gecombineerd worden met fullereenderivaten (bv. $PC_{71}BM$) in *bulk heterojunction* zonnecellen, konden reeds efficiënties boven 7.5% bereikt worden. Hoewel verwacht wordt dat de mijlpaal van 10% efficiëntie binnen afzienbare tijd zal overschreden worden, blijft de lage stabiliteit (en daardoor geringe levensduur) van organische zonnecellen, o.a. te wijten aan de (thermische) instabiliteit van de optimale nanomorfologie van de actieve laag, een prominent probleem. Met het oog op commercialisatie blijft verder onderzoek naar de ontwikkeling van nieuwe materialen dus essentieel.

Het onderzoek beschreven in deze doctoraatsthesis behelst de synthetische exploratie van twee verschillende klassen van materialen, nl. 4*H*-cyclopenta[2,1-*b*:3,4-*b'*]dithiofenen (CPDT's) en thiazolo[5,4-*d*]thiazolen (TzTz's), en toetst tegelijkertijd hun mogelijke toepassingen binnen het domein van de organische elektronica.

Door de gedwongen coplanariteit van de afzonderlijke thiofeeneenheden en de eenvoudige invoer van alkyl-zijketens ter bevordering van de oplosbaarheid vormen CPDT's zeer interessante, elektronenrijke bouwstenen voor integratie in *low bandgap* copolymeren. Het protocol dat meestal gebruikt wordt in de literatuur voor de synthese van gealkyleerde CPDT's is vrij omslachtig en vooral geschikt voor de synthese van symmetrisch digealkyleerde CPDT-derivaten. In dit werk werd allereerst een efficiëntere en meer veelzijdige driestaps-route, toepasbaar voor zowel symmetrisch als asymmetrisch gefunctionaliseerde CPDT's, nagestreefd (**Hoofdstuk 2**): i) vorming van 3-broom-2,2'-bithiofeen via een Kumada-koppeling tussen het Grignard-reagens van 2-broomthiofeen en 2,3-dibroomthiofeen, ii) lithiëring van het monogebromeerd bithiofeen en *in situ* condensatie met een dialkylketon, iii) ringsluiting via een Friedel-

Crafts dehydratatiereactie onder invloed van H_2SO_4. Er werd een reactiemechanisme voorgesteld voor de finale ringsluiting, ondersteund door NMR-spectroscopie en theoretische (energie)berekeningen. Op een relatief eenvoudige manier, nl. door het variëren van het keton, kan de substitutie van de methyleenbrug gevarieerd worden. Anderzijds creëert het gebruik van ketoësters de mogelijkheid om estergroepen te introduceren op de alkylketens, die daarna geconverteerd kunnen worden tot een hele reeks van functionele groepen. De ontwikkelde synthesemethode biedt bijgevolg ruime mogelijkheden voor de opbouw van (a)symmetrisch digealkyleerde of gefunctionaliseerde CPDT-derivaten.

In een volgende fase werden vier digealkyleerde en/of gefunctionaliseerde (elektronenrijke) CPDT-varianten gecombineerd met (het elektronenarme) 2,1,3-benzothiadiazool via Suzuki polymerisaties (**Hoofdstuk 3**). Dit resulteerde in een nieuwe reeks *low bandgap* PCPDTBT-polymeren: symmetrisch gesubstitueerd met twee 2-ethylhexyl- of twee octylzijketens, asymmetrisch gesubstitueerd met één 2-ethylhexyl- en één octylzijketen of asymmetrisch gesubstitueerd met een esterfunctie op één van de zijketens. Na synthetische optimalisatie werden de optische en elektrochemische eigenschappen van deze copolymeren bestudeerd. Initiële *device*-resultaten op basis van deze copolymeren gaven efficiënties van maximaal 2.71% (voor blends met $PC_{71}BM$). Via het verder afstemmen van een reeks parameters, rekening houdend met de aard van de zijketens, is er echter zeker nog ruimte voor verbetering. Finaal werd ook de procedure ter bereiding van het ester-PCPDTBT-copolymeer op punt gesteld. Dit materiaal kan verder aangewend worden voor de synthese van gefunctionaliseerde copolymeren via postpolymerisatiereacties.

In het tweede deel van de thesis werden nieuwe materialen bereid op basis van bicyclische thiazolo[5,4-*d*]thiazool-systemen. TzTz's vormen eveneens aantrekkelijke bouwstenen voor toepassingen in de organische elektronica wegens hun hoge stabiliteit, stijfheid, planariteit en goede synthetische toegankelijkheid. Jammer genoeg zijn de TzTz materialen beschreven in de literatuur weinig of niet oplosbaar, waardoor dure opdamptechnieken vereist zijn voor elektronische toepassingen. De invoer van hexyl-zijketens bevordert de oplosbaarheid aanzienlijk en maakt productverwerking vanuit oplossing mogelijk. 2,5-Bis(3'-hexylthiofen-2'-yl)thiazolo[5,4-*d*]thiazool (DTTzTz) werd gesynthetiseerd via een klassieke condensatiereactie tussen 3-hexylthiofeen-2-carbaldehyde en dithiooxamide. Na dibromering kon via Suzuki en

Stille koppelingsreacties een reeks 5'-aryl-gesubstitueerde DTTzTz derivaten bekomen worden. Deze moleculen werden uitvoerig bestudeerd door middel van 1D/2D NMR spectroscopie, aangevuld en ondersteund met theoretische chemische shift berekeningen (**Hoofdstuk 4/6**). Verder werd het potentiële *low bandgap* karakter van polymeren op basis van deze moleculen aangetoond door middel van elektropolymerisatiereacties.

Om de mogelijkheden van deze verbindingen binnen het domein van de printbare elektronica af te tasten, werden een aantal derivaten getest in *organic field-effect transistors* (OFET's) (**Hoofdstuk 5**). Hun thermische, elektrochemische en optische kenmerken werden bestudeerd door middel van thermogravimetrische analyse, differentiële scanning calorimetrie (DSC), cyclische voltammetrie en UV-vis spectroscopie. Filmen vervaardigd vanuit oplossing gaven goede *hole* mobiliteiten van 10^{-3} cm^2 V^{-1} s^{-1} voor het thiënyl-gesubstitueerde DTTzTz, terwijl de andere derivaten een veel lagere mobiliteit opleverden (10^{-5}–10^{-6} cm^2 V^{-1} s^{-1}). Het verschil in morfologie tussen de filmen werd aangetoond door middel van X-stralen diffractie, AFM (*Atomic Force Microcopy*) en SEM (*Scanning Electron Microscopy*), waarbij vezelachtige, microkristallijne structuren werden waargenomen voor dithiënyl-DTTzTz en veel kleinere, nanokristallijne domeinen voor de andere derivaten. Dergelijke goede mobiliteiten konden niet behaald worden voor opgedampte dithiënyl-DTTzTz filmen, hetgeen het potentieel van dit derivaat voor printbare organische elektronica nog eens extra in de verf zet.

In een finale fase werden de twee bestudeerde materiaalsystemen samen geïntegreerd in een *low bandgap* PCPDT-DTTzTz copolymeer, opgebouwd via Suzuki polycondensatie van de donor- (CPDT) en de acceptorbouwsteen (DTTzTz) (**Hoofdstuk 7**). De optische en elektrochemische eigenschappen van dit nieuwe copolymeer werden bestudeerd met UV-vis spectroscopie en cyclische voltammetrie. De semi-kristalliniteit van het materiaal kon aangetoond worden via X-stralen diffractie en DSC. Zuivering van het polymeer door middel van preparatieve SEC (*Size Exclusion Chromatography*) bleek essentieel om een goede efficiëntie (4.03%) te bekomen in organische zonnecellen gebaseerd op een blend van PCPDT-DTTzTz met $PC_{71}BM$. Via inbouw in *thin-film transistors* konden mobiliteiten van 10^{-3} cm^2 V^{-1} s^{-1} verkregen worden voor dit copolymeer. AFM en TEM (*Transmission Electron*

Microscopy) studies toonden een (actieve laag) morfologie met fasescheiding op nanometerschaal.

List of Publications

- *Synthesis, ^{1}H and ^{13}C NMR assignment and electrochemical properties of novel thiopene-thiazolothiazole oligomers and polymers*

Van Mierloo, S.; Chambon, S.; Boyukbayram, A. E.; Adriaensens, P.; Lutsen, L.; Cleij, T. J.; Vanderzande, D. *Magn. Reson. Chem.* **2010**, *48*, 362.

- *A three-step synthetic approach to asymmetrically functionalized 4H-cyclopenta[2,1-b:3,4-b']dithiophenes*

Van Mierloo, S.; Adriaensens, P. J.; Maes, W.; Lutsen, L.; Cleij, T. J.; Botek, E.; Champagne, B.; Vanderzande, D. J. *J. Org. Chem.* **2010**, *75*, 7202.

- *4,4-Disubstituted 4H-cyclopentadithiophene and methods for synthesizing the same*

Van Mierloo S.; Lutsen, L.; Vanderzande, D. *patent application*.

- *Improved photovoltaic performance of a semi-crystalline narrow bandgap copolymer based on 4H-cyclopenta[2,1-b:3,4-b']dithiophene donor and thiazolo[5,4-d]thiazole acceptor units*

Van Mierloo, S.; Hadipour, A.; Spijkman, M.-J.; Van den Brande, N.; Ruttens, B.; Kesters, J.; D'Haen, J.; Van Assche, G.; de Leeuw, D. M.; Aernouts, T.; Manca, J.; Lutsen, L.; Vanderzande, D. J.; Maes, W. *Chem. Mater.* **2012**, *manuscript accepted*.

- *Combined experimental-theoretical NMR study on 2,5-bis(5-aryl-3-hexylthiophen-2-yl)thiazolo[5,4-d]thiazole derivatives for printable electronics*

Van Mierloo, S.; Liégeois, V.; Kudrjasova, J.; Botek, E.; Lutsen, L.; Champagne, B.; Vanderzande, D.; Adriaensens, P.; Maes, W. *manuscript submitted to Magn. Reson. Chem.*

- *Functionalized dithienylthiazolo[5,4-d]thiazoles for solution-processable organic field-effect transistors*

Van Mierloo, S.; Vasseur, K.; Van den Brande, N.; Boyukbayram, A. E.; Ruttens, B.; Rodriguez, S. D.; Botek, E.; Liégeois, V.; D'Haen, J.; Adriaensens, P. J.; Heremans, P.; Champagne, B.; Van Assche, G.; Lutsen, L.; Vanderzande, D.; Maes, W., *manuscript submitted to Chem. Mater.*

- *Photovoltaic performances of narrow bandgap copolymer derivatives based on 4H-cyclopenta[2,1-b:3,4-b']dithiophene units*

Vanderzande, D.; Van Mierloo, S.; Marin, L.; Verstappen, P.; Lutsen, L.; Maes, W. *Prepr. Pap.-Am. Chem. Soc., Div. Fuel Chem.* **2011**, *55*, XX.

- *Reaction of 4H-cyclopenta[2,1-b:3,4-b']dithiophenes with NBS – a route towards 2H-cyclopenta[2,1-b:3,4-b']dithiophene-2,6(4H)-diones*

Marin, L.; Van Mierloo, S.; Adriaensens, P.; Lutsen, L.; Vanderzande, D.; Maes, W., *manuscript in progress.*

- *Efficient charge transfer in blends of donor polymer poly[2-methoxy-5-(3',7'-dimethyloctyloxy)-1,4-phenylene vinylene] (MDMO-PPV) and acceptor thiazolo[5,4-d]thiazole small molecule for organic photovoltaics*

Nevil, N.; Ling, Y.; Van Mierloo, S.; Vanderzande, D.; Maes, W.; Van Doorslaer, S.; Goovaerts, E., *manuscript in progress (Phys. Chem. Chem. Phys.).*

- *EPR characterization of positive and negative polaron states of thiazolo[5,4-d]thiazole small molecules*

Ling, Y.; Van Mierloo, S.; Vanderzande, D.; Maes, W.; Van Doorslaer, S., *manuscript in progress.*

List of Abbreviations

A	Acceptor
AcOH	Acetic acid
AFM	Atomic Force Microscopy
AM	Air Mass
APT	Attached Proton Test
BELSPO	Belgian Federal Science Policy Office
BF	Bright Field
$BF_3{\cdot}OEt_2$	Borontrifluoride dietherate
BDT	Benzo[1,2-*b*:4,5-*b'*]dithiophene
BHJ	Bulk Heterojunction
BT	2,1,3-Benzothiadiazole
Bu_4NPF_6	Tetrabutylammonium hexafluorophosphate
CB	Chlorobenzene
CdTe	Cadmium-Telluride
$CDCl_3$	Deuterated chloroform
$CHCl_3$	Chloroform
CH_2Cl_2	Dichloromethane
CH_3CN	Acetonitrile
CI	Chemical Ionization
CIGS	Copper-Indium-Gallium-Selenide
CMAE	Corrected Mean Absolute Error
CPDT	4*H*-Cyclopenta[2,1-*b*:3,4-*b'*]dithiophene
CsF	Cesium fluoride
CV	Cyclic Voltammetry
CuBr	Copper bromide
δ	Chemical shift
D	Donor
DEPT	Distortionless Enhancement by Polarization Transfer
DFT	Density Functional Theory
DME	Dimethoxyethane
DMF	Dimethylformamide
DMSO	Dimethylsulfoxide
DNA	Desoxyribonucleic Acid
DSC	Differential Scanning Calorimetry
DTTzTz	2,5-Bis(3'-hexylthiophen-2'-yl)thiazolo[5,4-*d*]thiazole
ε	Extinction coefficient
EC	Electrochemical
E_g	Energy gap/band gap
EI	Electron Impact
EQE	External Quantum Efficiency
ESI	Electrospray Ionization
Et_2O	Diethyl ether
EtOAc	Ethyl acetate
EtOH	Ethanol
eV	Electron volt

FF	Fill Factor
FWO	Fonds Wetenschappelijk Onderzoek
G	Gibbs free energy
GC-MS	Gas Chromatography-Mass Spectrometry
GPC	Gel Permeation Chromatography
HCl	Hydrochloric acid
H_2CrO_4	Chromic acid
HETCOR	Heteronuclear Correlation
HNO_3	Nitric acid
HOMO	Highest Occupied Molecular Orbital
HPLC	High-Performance Liquid Chromatography
H_3PO_4	Phosphoric acid
HRMS	High Resolution Mass Spectrometry
H_2SO_4	Sulfuric acid
HTL	Hole Transport Layer
HT-XRD	High Temperature X-Ray Diffraction
IAP	Interuniversity Attraction Poles
ICT	Intramolecular Charge Transfer
I_d	Source-drain current
IQE	Internal Quantum Efficiency
IR	Infrared
ITO	Indium Tin Oxide
IWT	Agentschap voor Innovatie door Wetenschap en Technologie
J_{max}	Current density at maximum power point
J_{sc}	Short-circuit current density
J-V	Current-Voltage
K_2CO_3	Potassium carbonate
KOH	Potassium hydroxide
K_3PO_4	Potassium phosphate
L	Channel length
λ	Wavelength
LiBr	Lithium bromide
LUMO	Lowest Unoccupied Molecular Orbital
μ	Thin film hole mobility
M	Molar
M^+	Molecular ion
MDMO-PPV	Poly[2-methoxy-5-(3',7'-dimethyloctyloxy)-1,4-phenylene vinylene]
MEH-PPV	Poly[2-methoxy-5-(2'-ethylhexyloxy)-1,4-phenylene vinylene]
MeOH	Methanol
$MgSO_4$	Magnesium sulfate
MHz	MegaHertz
M_n	Number-average molecular weight
MoO_3	Molybdenum trioxide
MP	Möller-Plesset
MPE-PPV	Poly[2-methoxy-5-(2'-phenylethoxy)-1,4-phenylene vinylene]

MS	Mass Spectrometry
M_w	Weight-average molecular weigth
N_2	Nitrogen
NaCl	Sodium chloride
Na_2CO_3	Sodium carbonate
$NaHCO_3$	Sodium bicarbonate/Sodium hydrogen carbonate
NaOH	Sodium hydroxide
NBS	*N*-Bromosuccinimide
n-BuLi	*n*-Butyllithium
NH_4Cl	Ammonium chloride
$Ni(dppp)Cl_2$	[1,3-bis(diphenylphosphino)-propane]dichloronickel(II)
NMR	Nuclear Magnetic Resonance
NOE	Nuclear Overhauser Effect
O_3	Ozone
ODCB	1,2-Dichlorobenzene/*ortho*-dichlorobenzene
ODT	1,8-octanedithiol
OFET	Organic Field-Effect Transistor
OLED	Organic Light-Emitting Diode
OP	Optical
OPV	Organic Photovoltaics
OSC	Organic Solar Cell
$PC_{61}BM$	[6,6]-Phenyl-C_{61}-butyric acid methyl ester
$PC_{71}BM$	[6,6]-Phenyl-C_{71}-butyric acid methyl ester
PCC	Pyridinium chlorochromate
PCDTBT	Poly[(*N*-9-alkyl-2,7-carbazole)-*alt*-5,5-(4',7'-di-2-thienyl-2',1',3'-benzothiadiazole)]
PCE	Power Conversion Efficiency
PCPDTBT	Poly[2,6-(4,4-bis-(alkyl)-4*H*-cyclopenta[2,1-*b*;3,4-*b'*]-dithiophene)-*alt*-(4,7-(2,1,3-benzothiadiazole))]
PCPDT-DTTzTz	Poly([4-(2'-ethylhexyl)-4-octyl-4*H*-cyclopenta[2,1-*b*:3,4-*b'*]dithiophene-2,6-diyl]-*alt*-[2,5-di(3'-hexylthiophen-2'-yl)thiazolo[5,4-*d*]thiazole-5',5''-diyl])
$Pd(dppf)Cl_2$	[1,1'-Bis(diphenylphosphino)ferrocene]-dichloropalladium(II)
PDI	Polydispersity Index
$Pd(PPh_3)_4$	Tetrakis(triphenylphosphino)palladium(0)
P3HT	Poly(3-hexylthiophene)
P3HNT	Poly(3-(5-hexenyl)thiophene)
PEDOT:PSS	Poly(3,4-ethylenedioxy-thiophene):poly(styrenesulfonate)
PETS	Phenylethyltrichlorosilane

PFDTBT	Poly[2,7-(9,9'-dialkylfluorene)-*alt*-5,5-(4',7'-di-2-thienyl-2',1',3'-benzothiadiazole)]
PFG	Pulsed Field Gradient
PGSTAT	Potentiostat/galvanostat
P_{light}	Input light irradiance
P_{max}	Maximum power point value
ppm	Parts per million
PS	Polystyrene
PSBTBT	Poly[(4,4'-bis-(alkyl)-dithieno[3,2-*b*;2',3'-*d*]silole)-2,6-diyl-*alt*-(2,1,3-benzothiadiazole)-4,7-diyl]
PSC	Polymer Solar Cell
PSiFDBT	Poly[(2,7-dialkylsilafluorene)-2,7-diyl-*alt*-(4,7-bis(2-thienyl)-2,1,3-benzothia-diazole)-5,5'-diyl]
PTFE	Polytetrafluoroethylene
$P_{theor\ max}$	Theoretical maximum power point value
p-TsOH	*para*-Toluenesulfonic acid
PTV	Poly(thienylene vinylene)
PV	Photovoltaic
PVC	Polyvinylchloride
RCS	Refrigerated Cooling System
RT/rt	Room temperature
R2R	Roll-to-roll
SBO	Strategisch Basisonderzoek
SEC	Size Exclusion Chromatography
SEM	Scanning Electron Microscopy
SiO_2	Silicon dioxide
σ	Isotropic shielding constants
T_{1C}	^{13}C spin-lattice relaxation time
T_c	Crystallization temperature
T_d	Degradation temperature
TDDFT	Time-Dependent Density Functional Theory
TEM	Transition Electron Microscopy
T_g	Glass transition temperature
TGA	Thermogravimetric Analysis
THF	Tetrahydrofuran
TLC	Thin Layer Chromatography
TMS	Tetramethylsilane
T_m	Melting temperature
TPD	*N*-Alkylthieno[3,4-*c*]pyrrole-4,6-dione
TT	Thieno[3,4-*b*]thiophene
TzTz	Thiazolo[5,4-*d*]thiazole
UV(-vis)	Ultraviolet(visible)
V_{DS}	Source-drain voltage
V_{GS}	Gate voltage
V_{max}	Voltage at maximum power point

V_{oc}	Open circuit voltage
V_{th}	Threshold voltage
W	Channel width
XC	Exchange-Correlation
XRD	X-Ray Diffraction

Dankwoord

Vier jaren doctoreren aan de UHasselt, een leerrijk avontuur met veel herinneringen die waarschijnlijk nog lang zullen bijblijven. Het was een drukke periode met zeer euforische maar ook zenuwslopende, onzekere momenten, meestal parallel lopend met de voortgang van het onderzoek. Een doctoraat maak je zeker niet alleen, het wordt langzaam gevormd door het uitvoeren van vele ideeën in talrijke samenwerkingen. Vandaar wil ik een heel aantal mensen bedanken die allen hebben bijgedragen aan de verwezenlijking van dit onderzoekswerk.

Op de allereerste plaats wil ik mijn promotor Prof. dr. Wouter Maes bedanken. Beste Wouter, we hadden elkaar reeds eerder ontmoet in labo Dehaen, toen al viel je op als een zeer gedreven wetenschapper en wilde iedereen wel stiekem jouw thesisstudent zijn. Het was dan ook heel positief nieuws te vernemen dat je in de UHasselt van start zou gaan. Jouw intensieve begeleiding, doorgedreven motivatie en aanhoudende interesse hebben mijn werk zeer positief beïnvloed. Jouw kritische denken en accuraat handelen hebben mij zeer veel bijgebracht. Dank je wel voor de goede begeleiding in het schrijven van publicaties en het zorgvuldig doornemen van mijn thesis waarbij ik zelf enorm veel heb geleerd. Geen enkel detail ontglipte jou, altijd werden “alle puntjes op de i” gezet! Dank je wel om deel te mogen uitmaken van jouw team!

Mijn co-promotor Prof. dr. Dirk Vanderzande verdient ook een oprecht woord van dank. Dirk, dankzij jou kreeg ik de kans om na twee jaren onderwijs terug in de onderzoekswereld te stappen. Je hielp steeds bij het uitstippelen van de grote lijnen van mijn doctoraat en zorgde ervoor dat we de uiteindelijke doelen niet uit het oog verloren. Het was in mijn eerste doctoraatsjaren soms moeilijk om jou te vinden maar als ik je dan gevonden had, was je steeds bereid mijn syntheseproblemen te bespreken met de nodige tips en nieuwe ideeën. Gedurende onze gesprekjes vaak met vele uitweidingen, heb ik altijd veel bijgeleerd. Bedankt voor het vertrouwen en de grote mate van vrijheid die je mij al die jaren hebt gegeven.

Aussi je voudrais bien remercier mon co-promoteur dr. Laurence Lutsen. Laurence, je voudrais te dire merci pour tous les conseils encourageux pendant le temps de mon doctorat. Merci pour les interventions rapides concernant les commandes de produits et merci surtout pour me faire connaissance avec plusieurs physiciens.

Prof. dr. Peter Adriaensens wil ik als NMR-specialist bedanken voor de begeleiding van alle NMR-werk. Peter, dank je wel voor het altijd zeer zorgvuldig nalezen van artikels en het beantwoorden van al mijn vragen doorheen de vele jaren. Jouw ideeën voor samenwerkingen binnen het IAP- en Polyspec-project betekenden achteraf een meerwaarde voor mijn doctoraat.

Prof. dr. Thomas Cleij voor de vele steun gedurende mijn prille beginperiode, jouw deur stond altijd open en steeds vond je wel een beetje tijd om mijn vragen te beantwoorden. En natuurlijk niet te vergeten, dank je wel voor de overheerlijke etentjes waarop we als labo-groep bij jouw thuis uitgenodigd waren.

Ik zou graag ook de leden van de jury willen bedanken voor hun bereidheid tot het evalueren van dit werk en het IWT voor hun financiële steun via het SBO-project Polyspec.

Vervolgens wil ook al mijn UHasselt-collega's bedanken met wie ik gedurende vier jaren vele uren samen heb doorgebracht.
Eerst een woordje van dank aan de vaste leden van onze groep. Iris, dank je wel voor je luisterend oor in onze vele gesprekjes. Ik zal je missen in mijn verdere loopbaan! Veerle, dank je wel om de labosfeer steeds weer op te fleuren met leuke verhalen en Wibren, dank je wel voor de professionele antwoorden op mijn wetenschappelijke vragen. Huguette, bedankt voor alle cyclische voltammetrie-metingen, Jan de massaman voor de GC/MS metingen, Koen Van Vinckenroye, dank je wel voor het opnemen van alle NMR-analyses aangevraagd via vele papiertjes op jouw bureau;-). Gène en Hilde dank je wel voor het steeds klaarzetten van materiaal en alle hulp bij het organiseren van didactische labo's.
Ook mijn huidige collega's verdienen een grote dank je wel. Lieve Hanne (Hannibal), we hebben de laatste vier jaren heel wat meegemaakt, dank je wel voor alle mooie momenten (haartooi, restaurantjes, autoritjes, …), ook een grote merci voor je behulpzaamheid de laatste maanden, je hebt het hart op de goede plaats! Veel geluk met je nieuwe spruitje binnen enkele maanden! Ans (Ansie Pansie), dank je wel voor alle bekommernis en hulp en je altijd aangename aanwezigheid, hopelijk komen we mekaar nog veel tegen in Opglabbeek. Frederik (Fredje), wat hebben we toch veel gezeverd en gelachen, ik wens je veel geluk in alles wat je doet in je verder leven! Joke, jou ken ik het langst van iedereen, we zaten reeds samen op de banken in de

eerste kandidatuur scheikunde, ik bewonder jouw gedrevenheid en uitstekend organisatievermogen en wens je nog veel succes in je verdere carrière! Lidia, we were spending so many hours together in the lab. During these years, I gotta know you very well and I will really miss you! The first time, I will enter another lab, I will think of you not being there. I liked so much all our talks and jokes. Lidia, your PhD story will also be finished soon and I wish you the best with everything. And remember, once, when I will visit Romania, I will pass by! Gunter, dank je wel voor het zeer actieve samenwerken tijdens de lesvoorbereidingen voor biomedische wetenschappen en de didactische labo's scheikunde. Je straalt zoveel energie uit en hebt een aanstekelijk enthousiasme. Nog veel succes in je verdere loopbaan!
Ook een welverdiende dank je wel aan Inge (zangtalent), Toon (huizenbouwer), Tom (brein vol fantasie), Suleyman (good luck man), Pieter (benzodithiophene rules), Jurgen (merci'tjes voor je mooie figuur), Erik, David, Julija en David (the new thiazolothiazole team), Matthias (thanks for all GPC measurements), Kayte en Rafaël (good luck with your PhDs).
Mijn oud-collega'tjes verdienen ook een bedankje. Bert (mijn favoriete labo-buur), Jan (gaan met de banaan), Wouter (mijn IWT-buddy), Raoul (rode kool met braadworst).
Dank je voor de leuke werksfeer in mijn beginjaren!

Vervolgens wil ik alle mensen die berekeningen en metingen betreffende mijn gesynthetiseerde materialen hebben uitgevoerd ook graag eventjes in de bloemetjes zetten:

Prof. dr. Benoît Champagne (Laboratoire de Chimie Théorique, Namur), merci pour toutes les calculations théoriques qui ont donné une valeur plus importante aux plusieurs articles. Edith, Vincent and Sylvio, merci pour votre collaborations.

Prof. dr. Guy Van Assche van de Vrije Universiteit Brussel, jouw thermische analyses hielpen telkens weer in het iets meer ontrafelen van de eigenschappen van mijn gesynthetiseerde materialen, dank je wel voor jouw waardevolle input en het verbeterwerk van onze twee gezamenlijke publicaties. Ook Niko, dank je wel voor alle metingen op mijn thiazolothiazolen en mijn finale polymeertje, je gastvrijheid om de metingen te mogen meevolgen op jullie afdeling in de VUB, en je vele prutswerk aan mijn figuurtjes.

Prof. dr. Etienne Goovaerts en Prof. dr. Sabine Van Doorslaer van de Universiteit Antwerpen, dank je wel voor het *n*-type karakter van cyanofenyl en trifluoromethylfenyl-gesubstitueerde thiazolothiazolen te achterhalen via talrijke experimenten! Ook dank je wel voor het tot stand brengen van twee publicaties met mijn gesynthetiseerde materialen. Nissy, your persistent work, your critical thinking and your motivation turn you into a good researcher. Your sincerity, kindness and helpfulness were the fundamentals of our good collaboration. Yun Ling, also I wanna thank you for our nice experiment day at Antwerp University.

Ook prof. dr. Dago de Leeuw en dr. Mark-Jan Spijkman van Philips Eindhoven wil ik bedanken voor hun mobiliteitsmetingen op mijn PCPDT-DTTzTz-polymeer. Dank je wel voor mijn hartelijke verwelkoming op Philips Einhoven, ik heb veel kunnen bijleren van jullie zeer uitgebreide FET-expertise.

Thanks to postdoc dr. Elife Boyukbayram for electropolymerizations and many cyclic voltammetry measurements.

Dr. Sylvain Chambon, merci pour tous les bagouts amusants pendant le travail et votre collaboration qui m'a permit de réaliser mon premier article.

Reuzedank je wel aan Joost en Lou van de Technische Universiteit Eindhoven. Dankzij jullie was het mogelijk mijn monomeren te zuiveren en mijn polymeren te fractioneren. Als ik nog eens ooit langskom, breng ik zeker weer een doosje Belgische pralines mee.

Een heel aantal dagen spendeerde ik op de IMEC te Leuven. Een welgemeende dank je wel aan dr. Tom Aernouts, al bij het eerste contact wist ik dat jullie zeer professioneel wilden te werk gaan, dank je wel om mij de mogelijkheid te bieden met een aantal mensen van jouw groep te mogen samenwerken. Griet Uytterhoeven, dank je wel voor de FET-metingen op mijn eerste thiazolothiazool, je was zelf nog maar net op IMEC begonnen maar was onmiddellijk enorm gedreven om mij efficiënt voort te helpen. Karolien, dank je wel voor alle FET-metingen op mijn thiazolothiazolen, alsook de opgenomen AFM-metingen. Dank je wel om het toch aan te durven mijn sterk fluorescerende productjes te zuiveren via jullie sublimatie-apparaat en vervolgens ook nog voor het aanleveren van een FET via vacuümdepositie. Onze vele leuke gesprekjes maakten het werken met jou zeer aangenaam. Naast onze professionele samenwerking,

heb ik je ook leren kennen als mens, je schitterde als bruid op je trouwdag en was een grote steun bij je onverwacht bezoekje in Leuven.
Afshin, dank je wel voor het meten van de 4% zonnecel-efficiëntie! De vele dagen dat we samen zonnecel-devices maakten op IMEC, had ik steeds het gevoel te vertoeven in het gezelschap van een zeer professioneel iemand. Je hebt zoveel ervaring en kennis, dat je gewoon de geknipte figuur bent voor deze job! Maar ook als mens met een zeer rijk verleden heb ik je bij vele koffietjes beter leren kennen, er zijn maar weinigen die in jouw voetsporen zouden kunnen treden en hetzelfde realiseren vanwaar jij gestart bent. Afshin, veel geluk in je verdere leven en carrière. Ik wens je het allerbeste toe!

Ook een dank je wel aan een aantal mensen van IMO fysica. Allereerst dr. Jan D'Haen, jouw XRD-, SEM- en TEM-bijdragen hebben dit werk verrijkt. Bart, dank je wel voor de uitleg en antwoorden op mijn vele vragen, ook een welgemeende dank je wel voor het aanleveren van mijn figuren. Bert Conings, merci voor de altijd zeer uitgebreide antwoorden op mijn fysische vragen en ook voor de hulp met de DEKTAK-metingen van soms toch wel zeer ruwe filmen. Nog veel succes bij het verder afwerken van jouw doctoraat!

Ik heb ook de kans gekregen om gedurende mijn onderzoeksperiode drie bachelorstudenten te mogen begeleiden. Sylvie, dank je wel voor het realiseren van de eerste Suzuki-koppelingen, Bart voor alle moeite om het alkeen-CPDT te maken en Sanne, dank je wel voor al je efficiënte en accurate werk gedurende mijn laatste doctoraatsjaar.

Tenslotte wil ik mijn ouders bedanken voor de kans die ze me ooit gaven om universitaire studies aan te vatten en hun volhardende steun gedurende al deze jaren. Charlotte, ik geniet steeds weer van onze leuke telefoontjes en uitstapjes in vakantieperiodes, ik heb jullie alle drie heel graag!

Het laatste zinnetje van deze thesis is bestemd voor jou, Kristof. Dank je wel voor jouw leven met mij te willen delen, ik zie je supergraag!

Sarah